Characterisation of Aerosols Generated by Pressurised Metered Dose Inhalers

Harang, Marie

Awarding institution:
King's College London

Title: Characterisation of Aerosols Generated by Pressurised Metered Dose Inhalers

Author: Marie Harang

Characterisation of Aerosols Generated by Pressurised Metered Dose Inhalers

Marie Harang

A doctoral thesis submitted in partial fulfilment of the requirements
for the award of
Doctor of Philosophy of King's College London

2013

Abstract

For over half a century, pressurised metered dose inhalers (pMDIs) have been the most sold inhaler devices for the treatment of lung diseases. However, they suffer from significant drug deposition in the mouth and throat, mainly due to the aerosolisation of large and fast-moving droplets. This causes a high occurrence of side effects and is wasteful of drug. They are also affected by a low consistency of dosing and as a result users might not benefit from maximal device efficiencies.

The hypothesis of this work was that the performance of pMDIs is dependent on numerous factors which might alter the characteristics of their particles and their deposition location within the respiratory tract. For example, it was thought that the variations in actuation forces of pMDIs and temperatures at which they are used might contribute to their low consistency.

A one-dimensional Matlab computational model was developed in order to calculate spray properties at the exit of the device where experimental measurements are difficult to conduct. The model simulated the discharge of pure HFA134a formulations and HFA134a-based suspension formulations containing fluticasone propionate; the latter representing a commercially available formulation.

The results showed that the actuation force of a"healthy" adult led to a higher valve opening rate and to the aerosolisation of smaller droplets than the actuation force provided by a "weak" adult. The model also showed that an increase of temperature led to the aerosolisation of smaller droplets. The model was validated using impaction measurements and laser techniques.

The next generation impactor (NGI) experiments revealed the importance of actuation forces on the throat deposition. Automated actuation forces with high valve opening rates led to a lower throat deposition than a manual actuation force with low valve opening rate.

The laser diffraction experiments showed that the automated actuations led to the aerosolisation of smaller droplets than manual actuations, validating the results obtained with the computational model.

The combination of these computational and experimental methods allowed the investigation of the spray along its entire trajectory, providing a deeper insight on the spray properties from the device to the respiratory system.

Acknowledgements

First and foremost, I wish to express my sincere thanks to my research supervisor Dr Lee, who has encouraged me to pursue my PhD degree, and who always showed extreme patience with me. I appreciate the time and effort he spent to help me during all my studies, from the beginning of my bachelor to the last days of my PhD.

I thank Dr Murnane for supervising me in my experimental work at the University of Hertfordshire, Professor Montante and Professor Paglianti for letting me use their PIV equipment and being so nice to me in my multiple stays at the University of Bologna.

I would like to acknowledge Dr Royall and Dr Forbes for welcoming me in the Pharmaceutical Department of King's College London allowing me to pursue my PhD.

I am thankful to Irene Parisini for teaching me the fine art of NGIs and for her camaraderie during my time at the University of Hertfordshire. I would also like to thank Sara Jaffari for her FP particle size measurements, which proved to be very useful.

I am grateful to my family and friends for cheering me up when I was losing motivation, particularly to my parents for providing constant emotional support through good and tough times. I would like to thank my mother for inspiring me and encouraging me in this scientific path.

Finally, my deepest thanks to Anselm, my boyfriend for putting up with me in my darkest moods when my results were going in the wrong direction and continually pushing and motivating me throughout my degree.

Contents

List of Figures

List of Tables

Nomenclature

Roman characters

A	Area	$[\,\mathrm{m}^2\,]$
A'	Specific part of the valve orifice area	$[\,\mathrm{m}^2\,]$
B	Velocity per unit force	$[\,\mathrm{m{\cdot}s^{-1}N^{-1}}\,]$
B'	Specific part of the valve orifice area	$[\,\mathrm{m}^2\,]$
C	Percentage by weight	$[\,-\,]$
C'	Valve orifice opening area	$[\,\mathrm{m}^2\,]$
Cd	Discharge coefficient	$[\,-\,]$
Cp	Specific heat capacity at constant pressure	$[\,\mathrm{kJ{\cdot}kg^{-1}K^{-1}}\,]$
Cpg	Specific heat capacity of gas at constant pressure	$[\,\mathrm{kJ{\cdot}kg^{-1}K^{-1}}\,]$
Cv	Specific heat capacity at constant volume	$[\,\mathrm{kJ{\cdot}kg^{-1}K^{-1}}\,]$
D	Displacement	$[\,\mathrm{m}\,]$
$Diff$	Diffusion coefficient	$[\,\mathrm{m^2{\cdot}s^{-1}}\,]$
D_{10}	10th percentile of the cumulative particle under-size frequency distribution	$[\,\mu\mathrm{m}\,]$
D_{50}	50th percentile of the cumulative particle under-size frequency distribution	$[\,\mu\mathrm{m}\,]$

D_{90}	90th percentile of the cumulative particle under-size frequency distribution	$[\mu\mathrm{m}]$
Dis	Displacement of the particle between two laser pulses	$[\mathrm{m}]$
E	Elastance of the oesophagus	$[\mathrm{cmH_2O{\cdot}min{\cdot}L^{-1}}]$
ERV	Expiratory reserve volume	$[\mathrm{L}]$
F	Force applied to the canister during its actuation	$[\mathrm{N}]$
FEV_1	Forced expiratory volume in the first second	$[\mathrm{L}]$
FPF	Fine particle fraction	$[\%]$
FRC	Functional residual capacity	$[\mathrm{L}]$
FVC	Forced vital capacity	$[\mathrm{L}]$
GSD	Geometric standard deviation	$[\mu\mathrm{m}]$
H	Total enthalpy	$[\mathrm{kJ}]$
Ha	Total enthalpy of air	$[\mathrm{kJ}]$
Hlp	Total enthalpy of liquid propellant	$[\mathrm{kJ}]$
Hp	Total enthalpy of propellant	$[\mathrm{kJ}]$
Hvp	Total enthalpy of vapour propellant	$[\mathrm{kJ}]$
IP	Impaction parameter	$[\mu\mathrm{m^2{\cdot}L{\cdot}min^{-1}}]$
IRV	Inspiratory reserve volume	$[\mathrm{L}]$
K	Boltzmann constant	$[\mathrm{J{\cdot}K^{-1}}]$
L	Length	$[\mathrm{m}]$
LOD	Limit of detection	$[\mu\mathrm{g{\cdot}mL^{-1}}]$
LOQ	Limit of quantification	$[\mu\mathrm{g{\cdot}mL^{-1}}]$

M	Molecular mass	$[\mathrm{kg{\cdot}kmol^{-1}}]$
Ma	Molecular mass of air	$[\mathrm{kg{\cdot}kmol^{-1}}]$
Mp	Molecular mass of propellant	$[\mathrm{kg{\cdot}kmol^{-1}}]$
$MMAD$	Mass median aerodynamic diameter	$[\mu\mathrm{m}]$
MMD	Mass median diameter	$[\mu\mathrm{m}]$
N	Total number of velocity measurements	$[-]$
P	Pressure	$[\mathrm{cmH_2O}, \mathrm{Pa}]$
PM	Picture magnification	$[-]$
Q	Inhalation flow rate	$[\mathrm{L{\cdot}min^{-1}}, \mathrm{m^3{\cdot}s^{-1}}]$
Ra	Ratio	$[-]$
Re	Reynolds number	$[-]$
Res	Resistance of the lungs	$[\mathrm{cmH_2O{\cdot}L^{-1}}]$
Rs	Specific gas constant	$[\mathrm{kJ{\cdot}K^{-1}{\cdot}kg^{-1}}]$
Ru	Universal gas constant	$[\mathrm{kJ{\cdot}K^{-1}{\cdot}kmol^{-1}}]$
RV	Residual volume	$[\mathrm{L}]$
S	Stopping distance of the particle	$[\mathrm{m}]$
Sc	Distance travelled by the canister during its actuation	$[\mathrm{m}]$
Sf	Distance between the fringes	$[\mathrm{m}]$
St	Surface tension	$[\mathrm{kJ{\cdot}m^{-2}}]$
Stk	Stokes number	$[-]$
T	Thermodynamic temperature	$[\mathrm{K}]$
TLC	Total lung capacity	$[\mathrm{L}]$

TV	Tidal volume	$[\,\mathrm{L}\,]$
U	Velocity	$[\,\mathrm{m{\cdot}s^{-1}}\,]$
U'	Turbulence of the spray	$[\,\mathrm{m{\cdot}s^{-1}}\,]$
$\bar{U}$	Mean velocity	$[\,\mathrm{m{\cdot}s^{-1}}\,]$
Ul	Velocity of the liquid phase	$[\,\mathrm{m{\cdot}s^{-1}}\,]$
Uv	Velocity of the vapour phase	$[\,\mathrm{m{\cdot}s^{-1}}\,]$
V	Volume	$[\,\mu\mathrm{L}, \mathrm{mL}, \mathrm{L}, \mathrm{m^3}\,]$
VC	Vital capacity	$[\,\mathrm{L}\,]$
VMD	Volume median diameter	$[\,\mu\mathrm{m}\,]$
Vv	Vapour volume	$[\,\mathrm{m^3}\,]$
$\dot{V}$	Volumetric flow rate	$[\,\mathrm{L{\cdot}min^{-1}}, \mathrm{L{\cdot}s^{-1}}\,]$
Z	Elevation of a point in the flow	$[\,\mathrm{m}\,]$

Lower case

a	Acceleration	$[\,\mathrm{m{\cdot}s^{-2}}\,]$
b	Specific length within the valve orifice	$[\,\mathrm{m}\,]$
c	Constant	$[\,-\,]$
d	Diameter	$[\,\mu\mathrm{m}, \mathrm{mm}, \mathrm{m}\,]$
dt	Time step	$[\,\mathrm{s}\,]$
e	Coefficient	$[\,-\,]$
f	Frequency of oscillations	$[\,\mathrm{Hz}\,]$
g	Gravitational acceleration	$[\,\mathrm{m{\cdot}s^{-2}}\,]$

h	Specific enthalpy	$[\mathrm{kJ{\cdot}kg^{-1}}]$
hlp	Specific enthalpy of liquid propellant	$[\mathrm{kJ{\cdot}kg^{-1}}]$
$hlvp$	Specific enthalpy of propellant vaporisation	$[\mathrm{kJ{\cdot}kg^{-1}}]$
hvp	Specific enthalpy of propellant vapour	$[\mathrm{kJ{\cdot}kg^{-1}}]$
m	Mass	$[\mathrm{kg}]$
ma	Air mass	$[\mathrm{kg}]$
mlp	Liquid propellant mass	$[\mathrm{kg}]$
mp	Propellant mass	$[\mathrm{kg}]$
mvp	Vapour propellant mass	$[\mathrm{kg}]$
$\dot{m}$	Mass flow rate	$[\mathrm{kg{\cdot}s^{-1}}]$
$\dot{m}a$	Mass flow rate of air	$[\mathrm{kg{\cdot}s^{-1}}]$
$\dot{m}l$	Mass flow rate of the liquid phase	$[\mathrm{kg{\cdot}s^{-1}}]$
$\dot{m}p$	Propellant mass flow rate	$[\mathrm{kg{\cdot}s^{-1}}]$
$\dot{m}v$	Mass flow rate of the vapour phase	$[\mathrm{kg{\cdot}s^{-1}}]$
q	Quality	$[-]$
r	Radius	$[\mathrm{m}]$
t	Time	$[\mathrm{s}]$
u	Unknown used to solve the density and enthalpy equations	$[-]$
v	Unknown used to solve the pressure equation	$[-]$
w	Displacement of the canister during actuation	$[\mathrm{m}]$
x	Number of calculated velocity components	$[-]$
y	Number of domain dimensions	$[-]$

z	Determinant of velocity measurements type	$[-]$

Greek characters

α	Angle of the intersecting beams	$[\mathrm{rad}]$
η	Viscosity	$[\mathrm{kg{\cdot}m^{-1}{\cdot}s^{-1}}]$
γ	Propellant vapour heat capacity ratio	$[-]$
λ	Laser wavelength	$[\mathrm{m}]$
μ	Flow dynamic viscosity	$[\mathrm{kg{\cdot}m^{-1}{\cdot}s^{-1}}]$
ρ	Density	$[\mathrm{g{\cdot}cm^{-3}}, \mathrm{kg{\cdot}m^{-3}}]$
$\overline{\rho}$	Average density of propellant	$[\mathrm{kg{\cdot}m^{-3}}]$
ρlp	Propellant liquid density	$[\mathrm{kg{\cdot}m^{-3}}]$
ρvp	Propellant vapour density	$[\mathrm{kg{\cdot}m^{-3}}]$
ρv	Density of the mixture of propellant vapour and air	$[\mathrm{kg{\cdot}m^{-3}}]$
ρ_0	Unit density	$[\mathrm{g{\cdot}cm^{-3}}]$
σ	Random error	$[-]$
θ	Angle	$[\mathrm{rad}]$

Subscripts

a	Air
$aero$	Aerodynamic
amb	Ambiant
atm	Atmospheric
b	Bubble

c	Canister
$crit$	Critical
$Cosol$	Cosolvent
ds	Downstream
ec	Expansion chamber
ED	Emitted dose
$EtOH$	Ethanol
f	Airflow in the airways
$flash$	Flashing
FP	Fluticasone propionate
g	Gas in a bubble
i	Interrogation area
in	Initial
$inter$	Intermediate
l	Liquid
mc	Metering chamber
no	Nozzle orifice
n	Number of the velocity measurement from 1 to n
NV	Non-volatiles
p	Particle
pi	Particle image
re	Residual

RD	Recovered dose
RS	Respiratory system
ts	Terminal settling
us	Upstream
v	Volumetric
vo	Valve orifice
wb	Wet bulb
x	Each component of a formulation

Superscripts

n	New
o	Old

Abbreviations

ACI	Andersen cascade impactor
API	Active pharmaceutical ingredient
APS	Aerodynamic particle sizer
CC	Cross-correlation
CCD	Charged couple device
CFC	Chlorofluorocarbon
CFD	Computational fluid dynamics
COPD	Chronic obstructive pulmonary disease
DIVAS	Droplet imaging velocimeter and sizer

DPI Dry powder inhaler

DPIV Digital particle image velocimetry

DUSA Dosage unit sampling apparatus

FPD Fine particle dose

FP Fluticasone propionate

HCP High capacity pump

HEF HFA134a, ethanol and fluticasone propionate formulation

HEM Homogeneous equilibrium model

HF HFA134a and fluticasone propionate formulation

HFA Hydrofluoroalkane

HPEF HFA134a, ethanol, PEG400 and fluticasone propionate formulation

HPLC High-pressure liquid chromatography

ICH International Conference on Harmonisation

IPACT International Pharmaceutical Aerosol Consortium for Toxicity Testing

LDA Laser Doppler anemometry

LSD Laser speckle velocimetry

LVDT Linear variable differential transformer

NGI Next generation impactor

NIST National Institute of Standards and Technology

NEM Non-homogeneous equilibrium model

ODR Orifice diameter ratio

PDA Phase Doppler anemometry

PDPA Phase Doppler particle analyser

PEG Polyethylene glycol

PET Polyethylene terephthalate

PIPM Particle image pattern matching technique

PIV Particle image velocimetry

pMDI Pressurised metered dose inhaler

PTV Particle tracking velocimetry

RANS Reynolds averaged Navier-Stokes

RMS Root mean square

SD Standard deviation

SFM Separated flow model

SOP Standard operating procedure

UI Uniformity index

Chapter 1

General introduction

1.1 Inhaled drug delivery

1.1.1 History and definition

Delivery of medications by inhalation was invented more than four thousand years ago and was first applied to treat asthma in India two thousand years ago with users smoking herbal preparations (Anderson, 2005). In Egyptian times (around 1500 BC), physicians achieved vaporisation of black henbane using hot bricks so that patients could inhale the vaporised content of the herb (Sanders, 2007). In ancient Greece, Hippocrates used inhalation to deliver vapours distilled in a pot in order to cure airways inflammation (Clarke and Newman, 1984). The pot used by Hippocrates represents the oldest design of inhaler devices and was not modified until the late 18th century when similar devices were still in use (Anderson, 2005).

The word inhaler was first used in 1778 by John Mudge to describe his own design (Anderson, 2005). Several designs followed during the 19th century. In 1899, Helbing developed an inhaler that used the heat of the hand to increase the vapour

pressure of ethyl or methyl chloride inside the canister to develop an aerosol. In the 20th century, the inhalation route became more common as the reproducible creation of aerosols became industrially feasible. However, it was only following the discovery of Freon propellants in the 1930s that aerosols became popular. The first major industrial application of aerosols was as an insecticide designed to combat malaria during Second World War with thirty million units used. In the post-war years aerosols became households products, leading ultimately to the combination of aerosol technology and inhalation therapy to achieve a tremendous commercial success in the 1950s with the first therapeutic aerosol commercialised in 1956 by Riker laboratories (Purewal, 1997). This therapeutic aerosol, the Medihaler, was a pressurised metered dose inhaler (Fradley, 2006).

1.1.2 Medical indications of inhaled drug delivery

In inhaled drug delivery, the active pharmaceutical ingredient (API) is delivered via the respiratory tract. Inhalers can be used to treat a wide range of conditions including infections and diabetes. However, they remain mainly used for the topical treatment of lung disease (the drug is deposited on the target site). There are two major types of lung diseases, the obstructive and restrictive diseases.

Most lung diseases are obstructive diseases. Chronic obstructive pulmonary disease (COPD) is an obstructive disease which generally combines chronic bronchitis and emphysema (Luo *et al.*, 2007). COPD is characterised by an inflammation of the lining of the bronchial tubes, impairing the capacity of the patient to efficiently inhale and exhale. This inflammation may then cause a scarring and thickening of the bronchial airways, increasing the severity of the disease. Symptoms of COPD include excessive production of mucus, cough and shortness of breath. Bronchitis is referred as chronic when the patient suffers cough and shortness of breath for

at least three months a year for two or more consecutive years (Braman, 2006). Emphysema is defined by the destruction of the most distal airways of the lungs. As a result, lungs transfer of oxygen to the systemic circulation is less efficient and may cause a breath shortage.

COPD is the 4th leading cause of mortality worldwide and represents approximately 5% of all deaths globally (Global initiative for chronic obstructive lung diseases, 2011). Approximately 64 million people were affected by COPD in 2004, and more than 3 million people died of the disease in 2005 (Global initiative for chronic obstructive lung diseases, 2011). COPD is closely linked to an ageing population and the majority of the estimated 210 million people worldwide suffering from the disease are long-term smokers and elderly people (Global initiative for chronic obstructive lung diseases, 2011). With an ageing population, the number of deaths due to COPD is forecasted to increase by 30% within 10 years (World Health Organization, 2012).

Asthma is a chronic disease causing obstruction of small and medium-size airways upon contact with irritants. It affects approximately 300 million people worldwide and is more prevalent in pediatric population with 10% of children suffering from the disease (AstraZeneca, 2011).

Inhaled drug delivery is mainly used for the treatment of lung conditions such as COPD, asthma, cystic fibrosis, bacterial infections as well as lung tumours through topical action on the lungs (Kleinstreuer and Zhang, 2011). The fact that inhaled drugs can reach the blood system can be a drawback for lung therapy as it increases the risk of side effects. This is an issue for the delivery of some inhaled APIs such as corticosteroids which increase the risk of osteoporosis in particular for menopausal women (Lipworth, 1999). On the other hand, it can also present an advantage for inhalation therapy on the whole as it allows the delivery of different

proteins targeting the systemic circulation, via the inhalation route. Chemotherapeutic drugs, nicotine, insulin and anti-migraine agents could be produced as inhalable compounds (Laube, 2005). For example, Afrezza is an inhaler for insulin delivery currently developed by MannKind which completed Phase 3 clinical trials (Mannkind Corporation, 2013).

1.1.3 Advantages of inhalation delivery compared to other delivery routes

The main advantage of the inhalation route compared to other delivery methods is its fast onset of action. It can be used to deliver APIs to the target sites much faster than the oral route which is the most common non-invasive delivery route. For example, short-acting bronchodilators such as albuterol start acting within minutes after inhalation (Merck, 2012). This advantage is of particular importance for the relief of asthma crisis where the fast effect of a drug can be vital (Sheffer, 2005). Conversely, orally administered bronchodilators must pass through the digestive system to reach the intestines where they are absorbed into the bloodstream. As a result, the drug has its peak effect between 45 minutes and 90 minutes after absorption (Milner, 1981).

Treatment of lung diseases by inhalation also requires a lower amount of API than other delivery routes. Contrary to orally absorbed drugs, inhaled drugs avoid the first pass metabolism in the liver which destroys small molecules. Big molecules such as proteins are also destroyed by acid and enzymes in the gastrointestinal tract. Systemically delivered drugs are distributed through the entire circulatory system whereas inhaled drugs are administered directly to the site of action in the lungs. As a result, much greater doses of API must be delivered orally in order to obtain the same therapeutic effect as inhaled drugs (Tiddens, 2004). For example,

inhaled salbutamol is therapeutically effective at deliveries of 100 μg to 200 μg per actuation. Conversely, oral salbutamol is administered at a dose of 4 mg to 8 mg with a maximum dose of 32 mg per day in adults (drugs.com, 2009). Delivering low amounts of drugs can lower the costs of a therapy and help reduce side effects.

In the treatment of pulmonary diseases, all drug particles target a specific location in the airways and only a small drug amount is absorbed by the rest of the body. It was shown that anti-inflammatory inhaled steroids cause much fewer side effects than orally administered steroid tablets (van der Molen *et al.*, 2010). The highest risk of side effects for inhaled drugs is caused by the fraction of drug reaching the most distal airways, which are greatly vascularised. The impact of the systemically absorbed fraction of inhaled corticosteroids has been reported. For example, inhaled budesonide has been shown to reduce the growth rate in children at doses of 0.4 mg a day or more (Toogood, 1998). Another survey found that high doses of inhaled budesonide (greater than 1.5 mg a day) increases the risk of exacerbation of glaucomas (Toogood, 1998). The second source of side effects in inhalation therapy is due to drug deposition at oropharynx level which causes conditions such as oral candidiasis, cough or bronchospasm in approximately 5% of patients (Versteeg *et al.*, 2006). To avoid such systemic and local side effects, new types of APIs have been researched. For example, ciclesonide is a new corticosteroid that has low systemic bioavailability, requires bioconversion to the active entity in the lungs and is rapidly eliminated from the body (van der Molen *et al.*, 2010).

There are two methods of inhalation which are nasal and oral inhalations. Oral inhalation is more efficient as a greater proportion of the aerosol can avoid filtration and reach the lungs (Agnew, 1984). For this reason, the industry and academic community focus particularly on the oral inhalation route. The three main types of inhalation devices using the oral inhalation route are the nebulisers, the dry powder inhalers (DPIs) and the pressurised metered dose inhalers (pMDIs).

1.2 Pulmonary anatomy and function

1.2.1 Structure of the respiratory system

The respiratory system comprises the mouth, the pharynx, the trachea and the lungs and extends from the nose or the mouth to the alveoli. The respiratory system is shown in Figure 1.1.

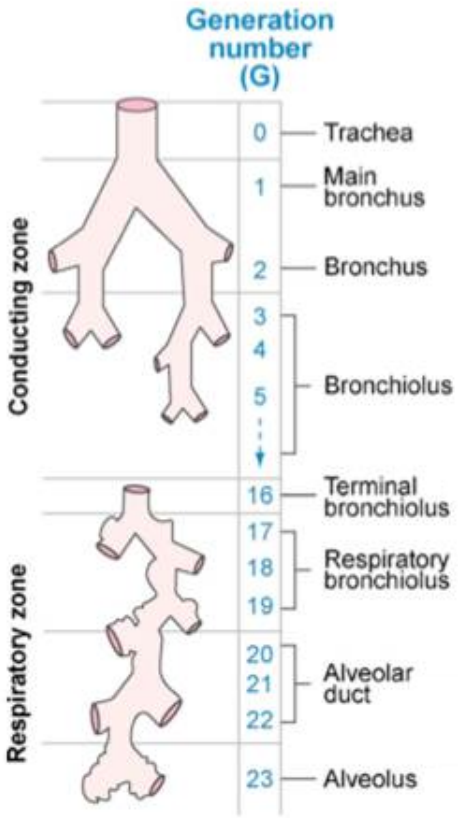

Figure 1.1: Schematic of the human respiratory system (Kleinstreuer *et al.*, 2008).

The lungs are the organs responsible for respiration by letting gas circulate in and outside of the body. Their volume adapts to the volume of air inhaled at a given moment. After being absorbed through the nose, the air goes through the nasopharynx, the oropharynx, the larynx, the trachea, the two main bronchi, the

five lobar bronchi (three on the right lung, two on the left lung) and the bronchioles down to the alveoli. The upper airways are composed of the nose, the mouth and the larynx. The lower respiratory tract has the structure of an inverted tree with two branches departing from the trachea and many branches departing from the bronchi as shown in Figure 1.1.

The respiratory system is divided into the conducting and the respiratory zones. The conducting zone starts at generation 0 with the trachea which has a length of 120 mm to 150 mm and a diameter of 15 mm to 20 mm in an average adult. The first generation consists of the two main bronchi. Each bronchus is then divided into bronchi at generation 2. The bronchi are then divided into bronchioles which have a diameter inferior or equal to 1 mm and are located between generation 3 and 15. At generation 16, the terminal bronchioles are divided into respiratory bronchioles. The conducting zone is shown in Figure 1.2.

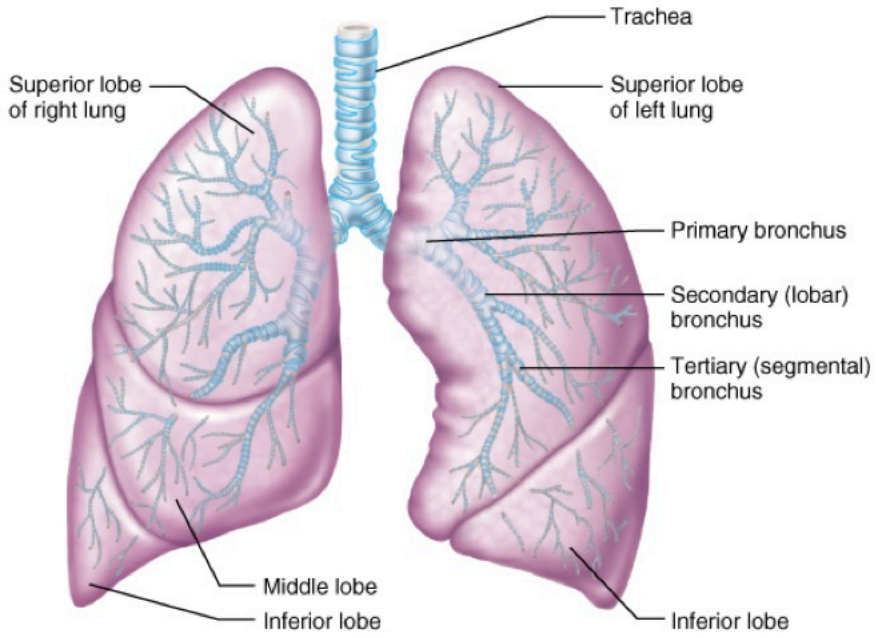

Figure 1.2: Schematic representing the conducting zone (Cumming, 2001).

The respiratory zone consists of the respiratory bronchioles located at generations 17 to 19, the alveolar ducts at generation 20 to 22 and the alveoli at generation

23 (Kleinstreuer and Zhang, 2011). Groups of alveoli form the alveolar sacs. The respiratory zone is shown in Figure 1.3.

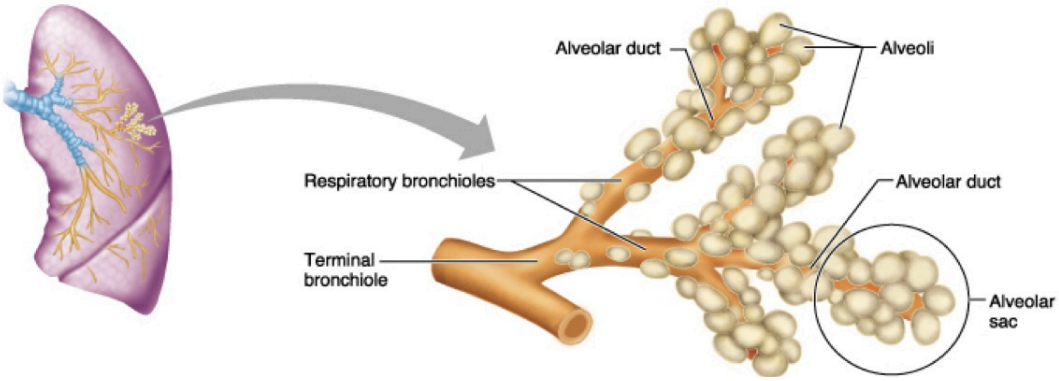

Figure 1.3: Schematic representing the respiratory zone (Cumming, 2001).

When looking at the physiology of the lungs, the potential of inhalation therapy for the delivery of systemic drugs becomes clear. Each alveolus, having an average diameter of 200 μm to 300 μm, is surrounded by a capillary blood vessel located at a distance of between 0.1 μm and 0.2 μm. In comparison, this distance is approximately 30 μm to 40 μm in the bronchial tract (Siekmeier and Scheuch, 2008). The total cross-sectional area at alveoli level is approximately 140 m^2 and represents a significantly bigger surface area than at any other point in the respiratory tract (Siekmeier and Scheuch, 2008). The large surface area of the alveoli as well as the small distance between the alveoli and the capillary blood vessels make the alveolar region an ideal zone of exchange with the systemic circulation. For this reason, inhaled compounds reaching the most distal airways are increasingly used to treat systemic conditions.

In order to maximise the efficiency of inhaled therapeutic agents and minimise their side effects, their deposition location should be as close as possible to their target site in the respiratory system.

1.2.2 Anatomical and physiological modelling of the lungs

Several airway characteristics such as airways segment lengths, diameters and branching angles, angles between airway branches, affect the way APIs deposit in the respiratory system. From the 1930s onwards, scientists started developing lung models helping to predict the deposition site of APIs. As lung function and drug deposition within the respiratory system are complex to simulate, the first anatomical lung models assumed simple lungs structures.

The first anatomical lung model developed by Findeisen in 1935 was a "9 generation" bronchial tree. Landahl (1950), Davies (1961), Weibel and Gomez (1962), Olson *et al* (1970) and Horsfield *et al* (1971) also assumed simple lung structures.

In Weibel's model which is the most famous of those early models, the bronchial tree consists of 24 generations. The 0 generation corresponds to the trachea, the 19th generation corresponds to terminal bronchioles and the 23rd generation corresponds to alveolar sacs. The bronchial tree is composed of successive parallel and semi-rigid tubes connected in series at each bifurcation. The nose and the mouth are treated as flow filters; and the lower respiratory system as an expandable surface where exchanges with the systemic system take place. Table 1.1 shows the geometry and flow rates in the lungs obtained from Weibel and Horsfield's models (as cited by (Ali, 2008)).

Generation number	Number of airways	Length (cm)	Diameter (cm)	Total cross-section (cm^2)	Cumulative volume (cm^3)	Flow, % of Trachea Flow	Reynolds Number
0	1	12.0	1.8	2.54	30.5	100	2213
1	2	4.76	1.22	2.33	41.8	50	1634
2	4	1.90	0.83	2.13	45.8	25	1201
3	8	0.76	0.56	2.00	47.2	12.5	890
4	16	1.27	0.45	2.48	50.7	6.25	554
5	32	1.07	0.35	3.11	54.0	3.125	356
6	64	0.90	0.28	3.96	57.5	1.5625	222
7	128	0.76	0.23	5.10	61.4	0.78125	135
8	256	0.64	0.186	6.95	65.8	0.390625	84
9	512	0.54	0.154	9.56	71.0	0.195312	51
10	1024	0.46	0.130	13.40	77.2	0.097656	30
11	2048	0.39	0.109	19.60	84.8	0.048828	18
12	4096	0.33	0.095	28.80	94.6	0.024414	10
13	8192	0.27	0.082	44.50	106.0	0.012207	6
14	16384	0.23	0.074	69.40	123.4	0.006104	3.29
15	32768	0.20	0.066	113.00	145.1	0.003052	1.84
16	65536	0.165	0.060	180.0	174.8	0.001526	1.01
17	131072	0.141	0.054	300.00	216.6	0.000763	0.56
18	262144	0.117	0.050	534.00	277.7	0.000382	0.30
19	524288	0.099	0.047	944.00	370.9	0.000191	0.16
20	1048576	0.083	0.045	1600.00	510.4	0.000095	0.08
21	2097152	0.070	0.043	3220.00	734.7	0.000048	0.04
22	4194304	0.059	0.041	5880.00	1084.7	0.000024	0.02
23	8388608	0.050	0.041	11800.0	1675.0	0.000012	-

Table 1.1: Dimensions of the symmetric human model designed by Weibel with data on the flow rates within the respiratory tract from Horsfield (Ali, 2008).

The Reynolds number, Re, can be calculated using Equation (1.1)

$$Re = \frac{\rho_a \, U_f \, d_{airways}}{\mu} \tag{1.1}$$

where ρ_a is the density of air in the airways in $\mathrm{kg \cdot m^{-3}}$, U_f is the velocity of the airflow in the airways in $\mathrm{m \cdot s^{-1}}$, $d_{airways}$ is the airways diameter in m and μ is the dynamic viscosity of the airflow in $\mathrm{kg \cdot m^{-1} \cdot s^{-1}}$.

Table 1.1 shows that the Reynolds number is high at the oropharynx compared with the lower airways. This means that the level of turbulence, characterised by significant variations in the flow velocity inside the airways, decreases deeper into the lungs. The decrease of the Reynolds number as a function of the airway generation can be seen in Figure 1.4 which also shows that the level of turbulence in the airways decreases with the flow rate of the patient (Finlay, 2001).

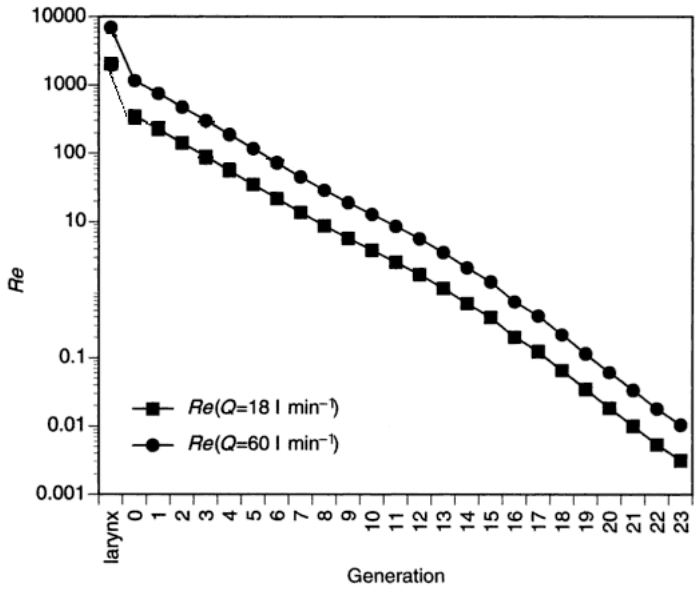

Figure 1.4: Reynolds number Re plotted against generation number of an idealised lung geometry developed by Finlay for two flow rates ($18\,\mathrm{L \cdot min^{-1}}$ and $60\,\mathrm{L \cdot min^{-1}}$) (Finlay, 2001).

Table 1.1 and Figure 1.4 show properties of the airways at varying generations. Those data were gathered using the early lung models such as the ones developed

by Weibel and Horsfield.

Weibel assumes that the respiratory system contains 300 million alveoli, 14 million alveolar ducts and 280 billion capillary segments (Weibel and Gomez, 1962). In more recent studies, the average alveoli number in 6 adult human lungs was found to be 480 million (Ochs *et al.*, 2004). Weibel's model has other limitations such as the assumption of lungs symmetry although in reality, the left lung is slightly bigger than the right one.

These early models remain simple and can only roughly approximate the geometry of the lungs. Anatomical lung models developed from replica casts of the bronchial tree are believed to approximate better the lower part of the respiratory tract (Ferron, 1994).

The Reynolds number of value higher than 2000 calculated by Finlay in the larynx agrees with the values in Table 1.1. All anatomical models describe high levels of turbulence in the upper respiratory tract, which, coupled with airways bifurcations, increase the collision of particles with the airways walls and prevent most particles from reaching the deep lungs.

1.3 Pulmonary ventilation characteristics

1.3.1 Definitions of pulmonary volumes

In order to identify respiratory problems, characteristic lung volumes have been defined. The total lung capacity (TLC) represents the maximum volume to which lungs can expand at maximum inspiratory effort. The TLC has a value of 6 L for an average male adult, 4.2 L for an average female adult and 3 L for a child (Lyons and Tanner, 1962). The tidal volume (TV), which corresponds to the volume of air

of individual breath in quiet breathing is 500 mL for an average adult (Irwin and Rippe, 2008). The inspiratory reserve volume (IRV) corresponds to the volume of air than can be inhaled forcefully after a normal inhalation. It has a value of 3.1 L for an average male adult and 1.9 L for an average female adult. The expiratory reserve volume (ERV) corresponds to the volume of gas than can be exhaled forcefully after a normal exhalation. It has a value of 1.2 L for an average male adult and 0.7 L for an average female adult. The residual volume (RV) is the volume of gas remaining in the lungs after a forced exhalation. It has a value of 1.2 L for an average male adult and 1.1 L for an average female adult (Cumming, 2001). The vital capacity (VC) corresponds to the maximum volume of gas that can be exhaled after a maximum inspiratory effort. It has a value of 4.8 L for an average male adult, 3.1 L for an average female adult and should represent roughly 80% of the TLC. The inspiratory capacity represents the maximum volume of air that can be inhaled after a normal expiration. It has a value of 3.6 L for an average male adult and 2.4 L for an average female adult. The functional residual capacity (FRC) is the volume of gas remaining in the lungs after a normal expiration. It has a value of 2.4 L for an average male adult and 1.8 L for an average female adult (Cumming, 2001).

1.3.2 Ventilation and inspiratory physiology

During inhalation, the diaphragm contracts down and the lungs expand, causing a sub-atmospheric pressure in the airways. Intercostal muscles which allow an increase of the lung volume by raising the ribs and the sternum, are also involved in the expansion of the thorax. The sub-atmospheric pressure resulting from increased lung volume causes air to penetrate into the lungs. During expiration, the intercostal muscles and the diaphragm relax, leading to a reduction of the volume

occupied by the lungs. The pressure inside the lungs becomes higher than atmospheric pressure, causing gas to exit the respiratory system. Between an exhalation and an inhalation, the alveolar pressure equals atmospheric pressure. This is the reason why there is no gas flowing at this stage.

Inhalation is considered to be an active mechanism as it is caused by the contraction of the diaphragm and intercostal muscles. On the contrary, exhalation is a passive mechanism as it is caused by the relaxation of the diaphragm and the intercostal muscles. The pressure difference between the atmosphere and the airways is $-250\,\mathrm{Pa}$ before inhalation and 350 to 800 Pa before expiration. A sufficient pressure gradient between the respiratory airways and the exterior environment is necessary in order to achieve the right volume of gas breathed in and out at each inhalation and expiration. In order to achieve an efficient ventilation process, lungs should be elastic, strong and in overall good shape. Equation (1.2) is used to link the pressure in the lungs to different variables such as the elastance which is the rate of change of pressure related to the change in volume. The elastance can be defined as the ability of an object to resist deformation and to return to its original form (Waechter, 2005), (Ingenito *et al.*, 1998).

$$P_{lungs} = ResV_{RS} + E\dot{V_{RS}} \tag{1.2}$$

where P_{lungs} is the pressure produced by the lungs in $\mathrm{cmH_2O}$, Res is the resistance of the lungs in $\mathrm{cmH_2O{\cdot}L^{-1}}$, V_{RS} is the volume of the respiratory system in L, E is the elastance in $\mathrm{cmH_2O{\cdot}min{\cdot}L^{-1}}$ and $\dot{V_{RS}}$ is the volumetric flow rate in the respiratory system in $\mathrm{L{\cdot}min^{-1}}$. The lung volume increases more steeply at the beginning of a respiratory cycle than at the end when the pressure inside the system is already high (Muramatsu *et al.*, 2001). It can thus be assumed that the elastance of the lungs reduces at the end of the cycle.

Average respiratory rates are 12 to 20 breaths per minute in adults and 15 to 30 breaths per minute in children aged 3 to 10 (Yuan *et al.*, 2013). The average inspiratory flow rate through the trachea in healthy adults is $15\,\mathrm{L{\cdot}min^{-1}}$ (Tobin *et al.*, 1983). The flow rates in other airways are assessed as percentages of the flow rate through the trachea as shown in Table 1.1.

Airway resistance and volumetric flow rate are similar in persons suffering from restrictive diseases as in non-affected persons (Waechter, 2005). However the TLC and elastance vary depending on patient's conditions and can be used as a diagnosis tool for respiratory diseases.

Restrictive diseases such as idiopathic fibrosis, hypersensitivity pneumonitis and sarcoidosis prevent an efficient lung expansion, leading to a reduced TLC and a higher lung elastance. For persons affected by obstructive diseases, the elastance is decreased so that the lungs need to expand to a greater volume to achieve a normal pressure gradient, leading to a higher TLC value (Cumming, 2001).

Obstructive diseases such as COPD and asthma are characterised by narrow airways and prevent efficient airflow in the respiratory system particularly during expiration. In obstructive diseases, the reduced elastance of the respiratory system prevents the lungs to spring back to their original shape. As a result, air remains trapped inside the lungs after expirations, causing hyperinflation of the airways. The FRC is higher in persons suffering from obstructive diseases than in healthy persons due to the reduced elastance of the lungs (O'Donnell and Laveneziana, 2006). On the contrary, as restrictive diseases tend to lead to smaller lung volumes, the FRC tends to be lower in persons affected by those types of diseases. For example, persons affected by emphysema have lower flow rates, particularly in the lower respiratory system as small airways can be destroyed by the disease (Ingenito *et al.*, 1998).

The forced vital capacity (FVC) and the forced expiratory volume in the first second (FEV_1) are powerful tools to diagnose obstructive diseases. The FVC is the maximum volume obtained as one exhales the fastest after a maximum inspiration. The FEV_1 corresponds to the volume obtained during the first second of a forced expiration. The ratio of those two measures is approximately 80% for healthy persons, which means that in one second a healthy person can exhale around 80% of his FVC. When the volume of the respiratory system is smaller, the volume exhaled at the first second and the total volume exhaled are lower but the FEV_1 and the FVC remain proportional. The FEV_1 to FVC ratio is thus normal for patients suffering from restrictive diseases (Waechter, 2005). Obstructive diseases cause the partial blockage or narrowing of airways, leading to a reduction in airway diameters. The expiration therefore takes a longer time, causing the FEV_1 to be small compared to the FVC. As a result, the FEV_1 to FVC ratio is lower in patients suffering from obstructive diseases (Waechter, 2005).

Asthma can be diagnosed by using the tidal expiratory flow rate as most persons suffering from this condition appear to have tidal expiratory limitations. This means that during tidal breathing, flow-limiting segments appear in the airways, preventing the high pressure inside the lungs to result in a high expiratory flow rate (Smaldone *et al.*, 1993). The FEV_1 can therefore be used to diagnose asthmatic persons. Persons with a severe asthma have a $FEV_1 \leq 40\%$ of their personal best and patients with a moderate asthma have a FEV_1 between 40% and 69% of their personal best (Sveum *et al.*, 2012). Table 1.2 summarises the characteristics of obstructive and restrictive diseases (O'Brien, 2012).

Measure	Obstructive diseases	Restrictive diseases
FEV_1/FVC	Decreased	Normal or increased
FEV_1	Decreased	Decreased, normal or increased
FVC	Decreased or normal	Decreased
TLC	Normal or increased	Decreased
FRC	Increased	Decreased

Table 1.2: Characteristics of obstructive and restrictive diseases.

1.4 Lung deposition mechanisms

1.4.1 Target sites within the lungs

Inhalation therapy is ideal for the treatment of respiratory diseases as it is non-invasive and causes fewer systemic side effects than systemically administered drugs. It seems to be promising for the delivery of APIs aiming at the systemic circulation as the inhalation route preserves APIs and provides an excellent exchange platform with the blood system at alveolar level. When particles such as APIs are inhaled, they either deposit at different locations inside the respiratory system or are breathed out during the subsequent exhalation. The main issue associated with inhalation therapy is the poor control over the deposition location of API particles and the amount of API particles reaching the target site.

Each API delivered by inhalation therapy has a specific target site within the lungs. For the treatment of pulmonary diseases, the most commonly prescribed therapeutics include $\beta_2$adrenergic agonists, anticholinergics and corticosteroids. $\beta_2$adrenergic agonists and anticholinergics achieve bronchodilation by relaxing the smooth muscles. The targets of the $\beta_2$adrenergic are the $\beta_2$receptors, which are mainly located in the alveoli although their role at this location remains unknown, as this region does not contain smooth muscles. $\beta_2$adrenergic are most active in the conducting airways which are lined with smooth muscles although the density of $\beta_2$receptors is lower in this region (Labiris and Dolovich, 2003). The targets of

the anticholinergic are the muscarinic receptors which are also located in smooth muscles throughout the airways. However, muscarinic receptors reside mostly in submucosal glands and airway ganglia in the conducting airways which as a consequence represent the ideal target location of anticholinergic drugs (Labiris and Dolovich, 2003). Bronchodilators should therefore be deposited in the conducting airways (Usmani *et al.*, 2003).

Corticosteroids achieve their pharmacological effect on inflammatory cells located in both the airways and the alveoli so should ideally be distributed throughout the lungs (Telko and Hickey, 2005). When deposited in the mouth and throat instead of reaching the lungs, drug particles might cause side effects such as oral candidiasis and dysphonia (Fadl *et al.*, 2010). When deposited in peripheral airways (in the alveoli), the systemic bioavailability of the drug increases, leading to an augmentation of side effects. Certain drugs can cause serious side effects, for example corticosteroids can increase the incidence of osteoporosis when absorbed at high therapeutic dose (Toogood, 1998). This might have been an issue for Qvar, an extrafine corticosteroids formulation. Qvar has the same therapeutic effect as some corticosteroid formulations at half their dose; this may be due to the increased deposition of Qvar in the peripheral airways. As it deposits mainly in the most distal part of the respiratory system, the risk of systemic side effects with Qvar was thought to be higher than with traditional aerosols. However, a long-term study on children revealed that Qvar did not cause adverse effects on growth, bone formation, resorption or adrenal suppression (Schayck and Donnell, 2004).

For the drug delivery of molecules targeting the systemic circulation, the API should be deposited at alveoli level where exchanges with the systemic system are maximised. The performance of aerosols depends on the quantity of drug reaching the target site. There are several particles deposition mechanisms in the human airways, leading to the deposition of drugs at varying locations within the

respiratory system.

1.4.2 Mechanisms of particles deposition in the lungs

In inhaled drug delivery, an aerosol describes the cloud of mist or dry particles formed by different aerosol devices. Once the formulation is propelled out of the device, it is atomised into small particles forming a cloud, which upon inhalation may deposit in the patient's throat. Particles which pass the throat deposit in the respiratory airways according to varying processes which are inertial impaction, sedimentation and diffusion.

Inertial impaction occurs for the biggest particles at oropharynx level and at branching points. Inertial impaction can be explained by Equation (1.3), describing the stopping distance of particles.

$$S = B\, m_p\, U_p \tag{1.3}$$

where S is the stopping distance of particles in m, B is the velocity per unit force in $\mathrm{m{\cdot}s^{-1}{\cdot}N^{-1}}$, m_p is the mass of the particle in kg and U_p is the velocity of the particle in $\mathrm{m{\cdot}s^{-1}}$. Equation (1.3) shows that heavy particles (i.e. particles of high diameter for a given density) achieve longer straight trajectories and therefore have a higher probability of impacting at bifurcations as they cannot easily adapt their trajectory to the airflow inside the respiratory system.

As the main change in direction in the respiratory tract is located at the oropharynx, most of the particles of diameter greater than $10\,\mu$m deposit by inertial impaction in this region. Inertial impaction also occurs in the first 10 generations of the lungs for particles of diameter greater than $5\,\mu$m (Labiris and Dolovich, 2003). Equation (1.3) also shows that inertial impaction increases with particle velocity.

This is due to the fact that a high velocity would also prevent a particle from adapting its trajectory to the airflow inside the respiratory system. The particles deposition pattern is therefore dependent on the inspiratory flow rate as it represents one of the main factors controlling the particles velocity inside the respiratory system.

Sedimentation occurs in the terminal bronchi for smaller particles reaching the lower part of the respiratory tract. The sedimentation process can be described using Equation (1.4).

$$U_{ts} = \frac{(\rho_p - \rho_a)\, {d_p}^2\, g}{18\,\eta} \tag{1.4}$$

where U_{ts} is the particle's terminal settling velocity in $\mathrm{m{\cdot}s^{-1}}$, ρ_p is the particle density in $\mathrm{kg{\cdot}m^{-3}}$, ρ_a is the density of air in $\mathrm{kg{\cdot}m^{-3}}$, d_p is the particle diameter in m, g is the gravitational acceleration in $\mathrm{m{\cdot}s^{-2}}$ and η is the formulation viscosity in $\mathrm{kg{\cdot}m^{-1}{\cdot}s^{-1}}$.

Sedimentation concerns particles with a diameter of $0.5\,\mu$m to $5\,\mu$m (Labiris and Dolovich, 2003). Those particles are sufficiently small to reach the lower respiratory tract but sufficiently heavy to be governed by gravity and sediment in the airways. Sedimentation occurs mainly in the last five to six generations of the airways which correspond to the smaller bronchi and bronchioles (Labiris and Dolovich, 2003).

Diffusion is a process in which particles randomly collide with the airway walls. It is also referred to as Brownian motion. It concerns the smallest particles (primarily particles of diameter less than $0.5\,\mu$m) and occurs mainly in the alveoli (Storey and Ymén, 2011). The diffusion coefficient can be described using Equation (1.5).

$$Dif = \frac{K\,T}{3\,\pi\,\eta\,d_p} \tag{1.5}$$

where Dif is the diffusion coefficient in $\mathrm{m^2{\cdot}s^{-1}}$, K is the Boltzmann constant

in $m^2 \cdot kg \cdot s^{-2} \cdot K^{-1}$ and T is the thermodynamic temperature in K. The diffusion coefficient is inversely related to the size of particles for particles of diameter smaller than $1\,\mu$m (it becomes negligible for particles of higher diameters) (Heyder, 2004).

Particles of diameter between $0.1\,\mu$m and $1\,\mu$m can therefore deposit by sedimentation and diffusion. Submicron particles can also be breathed out without having deposited which can be a problem for the delivery of small particles (Storey and Ymén, 2011).

The last two mechanisms of deposition are of less significance. Interception occurs in peripheral regions where the airways diameter becomes comparable in size to the particles diameter. Electrostatic precipitation concerns charged particles (typically charged during the atomisation process) which deposit on walls with a charge of opposite sign. This process is said to mostly occur for particles of diameter smaller than $1\,\mu$m (Smyth, 2003).

1.4.3 Mucociliary clearance of inhaled particles

The lungs provide a direct access to target sites for the treatment of pulmonary diseases and a direct route to the blood system for the systemic delivery of therapeutic agents, representing an ideal target for drug delivery. As they are exposed to the exterior environment, the lungs need a defence system against foreign bodies. This defence system, composed of mucociliary clearance and alveolar macrophages, represents a barrier reducing the efficiency of inhaled drugs delivery (Labiris and Dolovich, 2003).

Mucus is a substance produced by goblet cells and submucosal glands (Labiris and Dolovich, 2003). It forms a protective layer that prevents airborne foreign bodies from entering the respiratory airways (Rubin, 2002). Mucus contains sodium,

chloride, potassium, calcium ions and glycoproteins which give its slimy consistency (Clarke and Pavia, 1980). Mucociliary clearance is the process in which mucus is transported from the lower respiratory airways to the upper respiratory airways in an escalator like manner. The mucus blanket lies on top of the ciliated epithelium extending from the larynx to the terminal bronchioles (Clarke and Pavia, 1980). Each cilia has a length of approximately 6 μm and a diameter of 0.5 μm (Clarke and Pavia, 1980). The cilia structure moves the mucus layer from the lower airways towards the upper airways. This is done by a whip-like motion in which each cilia has a rate of 700 to 1000 beats per minute. The foreign bodies trapped in the mucus blanket are cleared from the upper airways in less than 6 hours. They are either pushed to the nostrils where they are removed by expiration or to the pharynx where they are digested. In healthy subjects, mucociliary clearance occurs faster in central than in peripheral airways (Smaldone *et al.*, 1993). Clearance from the terminal bronchi is completed in several hours to one day (Clarke and Pavia, 1980).

For the bodies deposited in the alveoli, the clearance takes from one day up to several months (Clarke and Pavia, 1980). The alveoli are not lined with a ciliated structure. At alveolar level, the clearance is realised by macrophage cells known as alveolar macrophages, which engulf the foreign bodies (Clarke and Pavia, 1980).

Other mechanisms such as cough and expiratory flow help to remove foreign bodies from the respiratory airways. Coughing is caused by nerve endings which are stimulated when irritants are present in excess in the airways. As mucociliary clearance is generally impaired in patients affected by lung diseases, coughing replaces it as the main system of airway clearance (Labiris and Dolovich, 2003).

When a drug is deposited in the conducting airways, most of the particles are trapped in the mucus gel and are removed from the airways by mucociliary clear-

ance. Only a fraction is absorbed through the airway epithelium to reach its target site. In the alveolar region, drugs are mostly cleared by alveolar macrophages and only a fraction is absorbed into the systemic circulation (Labiris and Dolovich, 2003). One of the difficulties associated with aerosol therapy is to deliver APIs to the lungs, organs that reject foreign bodies.

1.5 Factors affecting lung deposition

1.5.1 Particle velocity

Particles velocity can influence deposition location by increasing particles momentum as shown in Equation (1.3) earlier in the chapter. Particles velocity might affect the percentage of the spray impacting on the back of the throat by influencing the amount of particles depositing by inertial impaction. This is illustrated in Equation (1.6) developed by Kleinstreuer *et al* (2007).

$$IP = d_p^2 Q \tag{1.6}$$

where IP is the impaction parameter in $\mathrm{m^2{\cdot}L{\cdot}min^{-1}}$ and Q is the inhalation flow rate in $\mathrm{L{\cdot}min^{-1}}$. A higher impaction factor has been shown to increase the deposition of particles in the throat (Kleinstreuer *et al.*, 2007). As the impaction factor is proportional to the flow rate, an increased flow rate is expected to also lead to an increased throat deposition.

Patients flow rates might increase the velocity of particles once they reach the airways. As a result, particles may not be able to adapt their trajectory to the airflow path and might tend to deposit on the airway walls at the biggest bifurcation located in the oropharynx. Numerical modelling work and *in vitro* experiments

using idealised representations of the mouth-throat region are used to simulate the trajectory of particles through this part of the respiratory system. In the respiratory system, air velocity decreases as the air goes deeper into the lungs. This is explained by the fact that the cross sectional area increases from the trachea to the terminal bronchi, leading to a decrease in linear velocity (Clarke and Pavia, 1980). In the first 10 generations of the respiratory system, the airflow is high and turbulent. It is considerably reduced in the terminal bronchi and can be negligible in the alveolar region (Labiris and Dolovich, 2003). At lower airway generations, the airflow decreases linearly with the number of airways and thus impaction does not occur at this level of the respiratory system. The decrease of airflow rate causes the gravitational force to overcome the air resistance and leads to the sedimentation of particles in the terminal bronchi. This implies that lower respiratory flow rates might increase the chance of deposition by sedimentation (Agnew, 1984), (Heyder, 2004).

1.5.2 Size, density, porosity and shape of the particles

The particles size is assessed using several measures such as the aerodynamic diameter d_{aero} and the volumetric diameter d_v. The relationship between those measures is shown in Equation (1.7) (Haynes *et al.*, 2004)).

$$d_{aero} = (\frac{\rho_p}{\rho_0})^{0.5} d_v \tag{1.7}$$

where ρ_p is the density of the particle in $\mathrm{g{\cdot}cm^{-3}}$ and ρ_0 is the unit-density ($1.0\,\mathrm{g{\cdot}cm^{-3}}$). Equation (1.7) assumes that particles are spherical which could be a wrong assumption and lead to errors in the measurements. When quoting particles size, the aerodynamic diameter is more commonly used as it can assess the size of particles of all shapes. The deposition mechanisms of several types of particles within the

respiratory tract are shown in Figure 1.5.

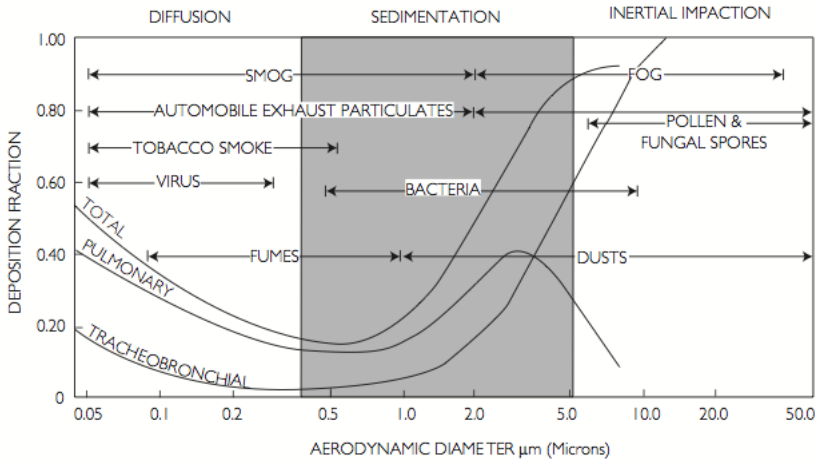

Figure 1.5: Relationship between particles size and lung deposition as printed by Labiris and Dolovich (2003).

Figure 1.5 illustrates the fact that particles with different aerodynamic diameters have different deposition mechanisms.

As particles size is the main factor affecting the deposition mechanisms of particles within the respiratory tract, it also affects their deposition location. For the treatment of lung diseases, particles size should be sufficiently small to avoid deposition in the mouth or in the throat. However they should not be too small in order to avoid being directly breathed out or reaching the bloodstream which may cause side effects.

For the treatment of respiratory diseases, the optimum particle diameter is between $1\,\mu$m and $5\,\mu$m (Storey and Ymén, 2011). For the treatment of systemic conditions, particles with diameters lower than $3\,\mu$m must be delivered (Labiris and Dolovich, 2003). Heyder *et al* (2004) showed the deposition locations of particles in the respiratory system according to their diameter (Figure 1.6). As they developed a model using particles of unit-density, their aerodynamic and geometric diameters are equal.

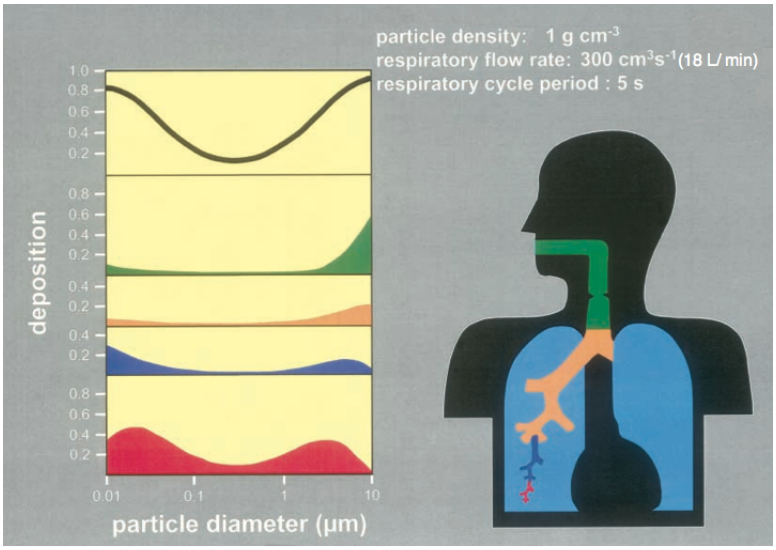

Figure 1.6: Total and regional depositions of unit-density spheres in the human respiratory tract predicted by a deposition model for oral inhalation at rest (Heyder, 2004).

Figure 1.6 shows that the oropharynx is the main deposition location for particles of 10 μm diameter and that alveolar deposition is the main deposition location for particles of diameter smaller than 0.5 μm. As shown in Equation (1.6), an increase in particles diameter leads to an increase in the impaction factor and therefore to an increased throat deposition (Zhang *et al.*, 2003). The shape of the particles also plays a role as it affects their aerodynamics.

1.5.3 Obstruction of the airways

Both COPD and asthma cause inflammation of the lungs, leading to the narrowing and obstruction of the respiratory airways. When studying obstructed and non-obstructed airways, airway geometry is shown to have an effect on particles deposition in particular for particles of diameter larger than 6 μm and for high flow rates (Inthavong *et al.*, 2010). This was observed when comparing a healthy lung model with an asthma lung model. The asthma model had a greater percentage of particle recovery than the healthy model (Inthavong *et al.*, 2010). This means

that drug particles would have more chance to deposit in the airways when inhaled by an asthmatic patient compared with a healthy person. It was also shown that obstructions influence particles deposition process particularly after the obstruction (Luo *et al.*, 2007). The flow rate in the respiratory system is highly dependent on airways diameter. As a result obstruction could significantly influence the airflow rate and subsequently, the deposition pattern of particles. Luo *et al* (2007) developed a model in which particles are at a branch leading to obstructed and unobstructed airways. Their results show that the obstruction prevent many particles from entering the airway and as a result more particles would penetrate in the unobstructed airway. The particles that managed to enter the obstructed airway will tend to deposit on the inflammation due to inertial impaction.

1.5.4 The influence of hygroscopicity on deposition

Hygroscopicity of particles is the process by which particles increase in size due to the effect of humidity. As drug particles are generally hygroscopic, they are expected to grow when entering the lungs which have a relative humidity of approximately 99.5% (Labiris and Dolovich, 2003). The rate of growth depends on the initial size of the particles. Particles of diameter smaller than $1\,\mu$m can increase up to five–fold whereas particles of diameter higher than $2\,\mu$m can increase two to three-fold (Labiris and Dolovich, 2003). This shift in the particle size distribution might result in a more proximal deposition and can be an issue if the drug needs to reach the more distal airways (Barnes and Godfrey, 1998). Xu and Yu for example showed that hygroscopicity could cause particles of $1\,\mu$m diameter to be deposited primarily by impaction instead of sedimentation (Labiris and Dolovich, 2003). However, hygroscopicity is not believed to affect particles issued from pMDIs as much as they affect particles issued from DPIs (Terzano, 1999).

1.6 Performance of inhalation technology

1.6.1 The efficiency of conventional inhaler devices

The performance of inhalers has increased in past years. It is characterised by the percentage of drug reaching the target site which was reported to be approximately 20% of the emitted dose in 2000 compared to 40% to 60% of the emitted dose for some devices in 2005 (Kleinstreuer *et al.*, 2008). However, all inhalers still suffer from the lack of control over the particles deposition location. This prevents aerosols from being used to maximum efficiency in the treatment of many conditions such as local lung tumours or diseases treated systemically via the lungs. The lack of consistency in the deposition location of APIs mainly arise from poor patient technique as well as poor control over the size and velocity of the particles in the aerosol (Kleinstreuer and Zhang, 2011). The factors influencing those aerosol characteristics will be reviewed later in this chapter.

1.6.2 Characterisation of inhaler performance

As seen above, the particle size range of a formulation greatly influences its deposition location in the respiratory system. Different measures help to assess the size of particles in aerosols. The main measure is the mass median aerodynamic diameter (MMAD), a statistical measure of the aerodynamic size of the spray which represents "the aerodynamic diameter that divides the particle size distribution into two halves with respect to mass" (Smyth, 2003). The MMAD is crucial to characterise pMDIs as it influences greatly the sites of particles deposition. The MMAD is more relevant to determine the deposition location of a particle than its geometrical diameter. This is due to the fact that two particles with different shapes, sizes and densities can still behave identically in an airflow and deposit at

the same location. The D_{50} and the MMAD are used depending on the method chosen to measure particles size.

The geometric standard deviation (GSD) is a measure of the spread of particle diameters in the aerosol. An aerosol is considered monodisperse at a GSD value lower than 1.22 and heterodisperse at a GSD value higher than 1.22 (Schuepp *et al.*, 2004). As the GSD controls the spread in the particle size distribution, it directly affects the deposition location of particles and determines the precision with which drug particles deposit at a particular location (Stein and Myrdal, 2004). Monodisperse aerosols should therefore be used to control more accurately the deposition location of the particles. If the size of the particles is appropriately engineered, monodisperse formulations have a greater percentage of drug reaching the target site than heterodisperse formulations and might therefore cause fewer side effects (Usmani *et al.*, 2003). It was shown that using a monodisperse formulation, the amount of drug delivered can be reduced without reducing the efficacy of the treatment (Usmani *et al.*, 2003). However, most commercial aerosols remain heterodisperse (Rubin and Fink, 2003).

The last common measure employed to characterise the particle size range of an aerosol is the fine particle fraction (FPF). It corresponds to the percentage of the total emitted dose that is of a particle size suitable for deposition in the lungs; it is also referred to as the respirable fraction. The FPF represents the percentage of particles with an MMAD$<5\,\mu$m. For the treatment of lung diseases, the target site is the lower respiratory tract. In order to achieve deposition at this location, it was shown that particles should have a diameter between $2\,\mu$m and $4.7\,\mu$m (Berry *et al.*, 2003). Other methods defining the performance of an aerosol spray include spray geometry and spray velocity (Smyth, 2003).

1.7 Inhalation therapies and devices

1.7.1 Nebulisers

Nebulisers were the first inhalation devices to be developed for the treatment of asthma after the early atomisers of the 19th century and were the most common devices in early inhalation technology. The first nebuliser was invented by Dr Auphon Euget-Les Bain in 1849 and the first portable nebuliser was developed by Dr Sales-Girons in 1858 (Anderson, 2005). Glass-bulb nebulisers were commonly developed in the 1930s (e.g. the Parke-Davis Glaseptic) and plastic-bulb nebulisers in the 1940s (e.g. the AsthmaNefrin) (Anderson, 2005). The first compressor nebuliser, the Pneumostat® was designed in Germany in the early 1930s (Anderson, 2005).

As nebulisers can be used during tidal breathing, they are often recommended for patients having problems using pMDIs and DPIs and are suitable for patients of any age and with different diseases severities.

Data from 1995 suggests that nebulisers efficiencies range from 10% to 50% (Clark, 1995). In nebuliser devices, the API is dissolved in water by itself or with the help of a cosolvent such as ethanol or propylene glycol. It can also be suspended in water to form an aqueous suspension formulation (Clarke and Newman, 1984), (O'Riordan, 2002).

Traditional nebulisers use an air compressor which is generally electrically operated (Dhand, 2003). Those devices are composed of three parts which are the face-mask or mouthpiece, the nebuliser chamber and the compressor. The energy of the compressed gas is used to aerosolise the medication into a mist. This principle is somehow similar to the principle behind pMDIs. However, in the case of nebulisers,

the compressed gas is only used to aerosolise the formulation and is not a component of the aerosol as in pMDIs. The mist is then inhaled by the patient through the face-mask or the mouthpiece.

Traditional nebulisers are difficult to transport as they require an electrical or compressed gas source to operate (Dhand, 2003). They are also difficult to maintain as the compressor should ideally be checked every six months and the nebulising chamber should be checked every two months and cleaned daily (Dhand, 2003).

Nebulisers generally deliver coarse droplets which tend to deposit on the throat rather than on the lower respiratory tract (Clark, 1995). More sophisticated nebulisers were invented to resolve this problem. Those nebulisers recirculate the coarse particles and thus deliver smaller particles. However, they are much slower to deliver the medication.

Ultrasonic nebulisers use another operating technology such as the Omron® technology. In those devices, the formulation is aerosolised using high frequency waves generated by piezo-electric crystals. Ultrasonic nebulisers are less bulky than pneumatic ones as they do not require a compressor and can produce fine particles. Other devices such as the Aerogen® aerosol generator are known to have a similar size and drug delivery time to other inhalers (Dhand, 2003). The Aerodose® is a portable nebuliser using the Aerogen® technology. It has approximately the same size as a pMDI but is significantly more expensive. For these reasons, nebulisers are not as popular as DPIs and pMDIs (Clark, 1995).

1.7.2 Dry Powder Inhalers

DPIs are devices that deliver drugs to the lungs in the form of a dry powder. The first DPI was patented in 1864 by Newton in London. The patent outlined that

the powder should be kept dry before being finely propelled out of the device. The first commercial DPI was the Aerohaler® patented by Fields in 1948 and marketed in 1949 by Abbott Laboratories (Clark, 1995). It was used to deliver penicillin.

DPIs are generally composed of one-phase solid particles blends containing the API in micronised form mixed with coarse and large "carrier" particles (Telko and Hickey, 2005). Those particles were originally aimed to dilute the drugs, thus improving the dose-to-dose reproducibility (Bisgaard *et al.*, 1998). After a time it was noticed that they also improved the flow properties as well as the dispersion and de-agglomeration of the particles (Telko and Hickey, 2005).

The first DPIs provided single-dose medication but evolved to provide multi-doses. Multi-dose DPIs can either be pre-metered in blisters or measured in the device in a powder reservoir (Chan *et al.*, 2007).

When a patient inhales through a DPI, an airflow penetrates the static powder bed (on which the API is lying), creating turbulence and shear stress, which fluidizes and entrains the drug-carrier mixture. As they enter the patient's airways, the drug particles are separated from the carrier particles and reach the lungs while the carrier particles impact on the throat (Telko and Hickey, 2005).

Newman suggests that the amount of drug particles depositing in the lungs as a percentage of the metered dose of a DPI ranges from 5% to 40%, depending on the design of the device, its formulation and the patient's inhalation flow rate (Newman and Busse, 2002). Those varying efficiencies can be seen in Table 1.3 gathered by Newman and Busse (2002). DPIs are approximately 2.5 times more expensive to produce than their pMDI equivalents. The cost of recycling is also higher for DPIs than for pMDIs (Covar and Gelfand, 2008). This increased cost is relevant as DPIs do not exhibit a superiority over pMDIs explaining such a price difference.

Device	Drug	Inhalation	Lung deposition (%)
Rotahaler®	Sodium cromoglycate	Slow ($60\,\mathrm{L{\cdot}min^{-1}}$)	6.2
Spinhaler®	Sodium cromoglycate	Fast ($120\,\mathrm{L{\cdot}min^{-1}}$) Slow ($60\,\mathrm{L{\cdot}min^{-1}}$)	13.1 5.5
Diskhaler®	Salbutamol	Not known	12.4
Turbuhaler®	Budesonide	Fast ($58\,\mathrm{L{\cdot}min^{-1}}$) Slow ($36\,\mathrm{L{\cdot}min^{-1}}$)	27.7 14.8
Pulvinal®	Salbutamol	Fast ($46\,\mathrm{L{\cdot}min^{-1}}$) Slow ($28\,\mathrm{L{\cdot}min^{-1}}$)	14.1 11.7
Easyhaler®	Salbutamol	Fast ($60\,\mathrm{L{\cdot}min^{-1}}$)	28.9
Ultrahaler®	Nedocromil sodium	Fast ($75\,\mathrm{L{\cdot}min^{-1}}$) Slow ($42\,\mathrm{L{\cdot}min^{-1}}$)	13.3 9.8
Clickhaler®	Budesonide	$35 - 65\,\mathrm{L{\cdot}min^{-1}}$	30.8
Taifun®	Budesonide	Fast ($36\,\mathrm{L{\cdot}min^{-1}}$) Slow ($21\,\mathrm{L{\cdot}min^{-1}}$)	34.3 29.6
Cyclohaler®	Asthma NCE	Fast ($98\,\mathrm{L{\cdot}min^{-1}}$)	19.1
Spiros®	Budesonide	Slow ($15\,\mathrm{L{\cdot}min^{-1}}$) Fast ($60\,\mathrm{L{\cdot}min^{-1}}$)	40.5 30.4
Novolizer®	Budesonide	Fast ($99\,\mathrm{L{\cdot}min^{-1}}$) Slow ($54\,\mathrm{L{\cdot}min^{-1}}$)	32.1 19.9

Table 1.3: Lung deposition of drugs from various DPIs, as percentages of metered or capsule dose.

The strength of the DPI, (being actuated only upon inhalation) also represents its main weakness. If the patient has a weak flow rate (which is often the case in the treatment of obstructive lung diseases), the force used to aerosolise the drug might not be sufficient to separate the carrier and drug particles, lowering dramatically the device performance. A medium to high inspiratory flow rate is needed to remove the API particles from the dose chamber or capsule and to separate them from the carrier particles (Newman and Busse, 2002).

This is illustrated in Table 1.3 showing increased percentages deposition in the lungs at higher inspiratory flow rates.

For this reason, many patients with lung diseases are unable to effectively generate an aerosol cloud from commercial dry powder inhalers (Burnell *et al.*, 2001).

DPIs are generally not recommended for children under 6, as their inspiratory flow rate tends to be too low to adequately aerosolise the formulation (Bateman and Fitzgerald, 2011). However, some brands are approved for younger children (Turbuhaler® is approved in most countries for 5 year-olds and the Diskus® is approved for 3 year-olds) (Bisgaard *et al.*, 1998). As the efficiency of the devices is dependent on patients inspiratory flow rates, DPIs have low dose uniformity (Telko and Hickey, 2005). In order to overcome this issue, other actuation mechanisms have been added to the patient inspiratory flow rate to aerosolise efficiently the drug-carrier compound. The added component that produces the turbulence can be an electronic vibrator, an impeller or a pneumatic power assisted device (Copley, 2009). Those "active" DPIs produce a sufficient level of turbulence and shear stress to aerosolise efficiently the drug even at low inspiratory flow rates. In those designs, the percentage drug deposition depends less upon patients inspiratory flow rates which could lead to higher efficiencies and dose reproducibilities. However, as those devices are more expensive than the traditional breath-actuated DPIs, they are mainly used for the delivery of expensive systemic drugs such as insulin, for which it is critical to deliver a specific drug amount to a precise deposition site. Exubera®, commercialised in 2006 by Pfizer, was the first inhaler to deliver insulin. It was withdrawn from the market in 2007 due to poor sales. Aspirair® is another active DPI developed in 2007 by Vectura (Furness, 2006).

1.7.3 Inhaled drug delivery market

With an increasing number of people affected by pulmonary diseases, the market for inhaled drug delivery has been constantly growing in the past 20 years (Fadl *et al.*, 2010). In 2011, the markets for the treatment of asthma and COPD achieved sales of respectively 21.6 billion dollars and 12.9 billion dollars worldwide. The

global prescription respiratory market was worth 64.6 billion dollars (AstraZeneca, 2011). As only 20% of people affected with COPD are believed to be diagnosed, and as more patients gain access to treatments, market growth is set to continue. PMDIs are believed to have a global market share of between 60% (Andersen *et al.*, 2010) and 80% (Telko and Hickey, 2005) with annual sales greater than 400 million units (Sanders, 2007). The pMDIs segment generated almost 14.4 billion dollars in 2011 and is forecasted to reach 29.8 billion dollars by 2016 (BBC Research, 2012). However, the number of units sold has slightly decreased between 2002 and 2009 due to the increasing market share of DPIs (Andersen *et al.*, 2010). DPIs became more commercially successful in the past twenty years after regulation caused the decline of pMDIs. DPIs sales reached 14 billion dollars in 2008 and are forecasted to continue increasing in the coming years (Clayborough and Simpson, 2010). DPIs generally have the same price as pMDIs in developed countries. However, they tend to be more expensive than pMDIs in developing countries. This is the reason why although they account for one-third of the inhalation market by sold units, they represent approximately half of the inhalation market in value (Lee, 2011) The market share of DPIs is expected to achieve a higher growth compared with pMDIs in the next few years. This is illustrated by the fact that for more than a decade, the number of patents issued for DPIs devices has outgrown the number of patents issued for pMDIs (Inhalation Report, 2009). However, as they remain more expensive to produce, they are not expected to expand in developing countries (Fink, 2000). The nebuliser market is expected to reach 534.9 million dollars by 2015 (Cassell, 2012).

1.8 Pressurised Metered Dose Inhalers

1.8.1 Device components

pMDIs are devices that use compressed gases as a source of energy to aerosolise drugs. They are composed of disposable and compact canisters containing between 100 and 400 doses (Oliveira *et al.*, 2010). The canister needs to be strong to withstand pressure from 3.5 P_{atm} to 10 P_{atm} but also needs to be light to be easily carried. Therefore, it is often made of aluminium by a deep drawing process (Dunbar *et al.*, 1997). Canisters typically have a volume of 15 mL to 30 mL (Oliveira *et al.*, 2010).

pMDIs also contain a propellant system, a metering valve, an actuator and a mouthpiece. The actuation system is made of the metering chamber, the expansion chamber, and two coupled valves placed on each side of the metering chamber at the level of the interior orifice and the valve orifice (Swarbrick, 2007) as shown in Figure 1.7.

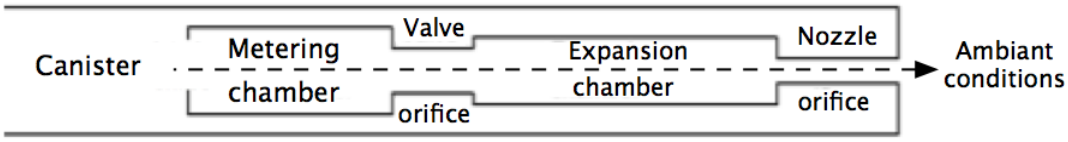

Figure 1.7: Schematic of the interior of a canister.

The metering valve (located at the interior orifice) aims to measure the metered volume accurately and reproducibly. It should also be tightly sealed due to its high pressure content. The metering valve contains a gasket, a ferrule and a valve stem which connects the metering valve to the actuator as shown in Figure 1.8. The expansion chamber represents the area between the valve orifice and the nozzle orifice as seen in Figure 1.7. It is formed of the valve stem and actuator chamber as shown in Figure 1.8.

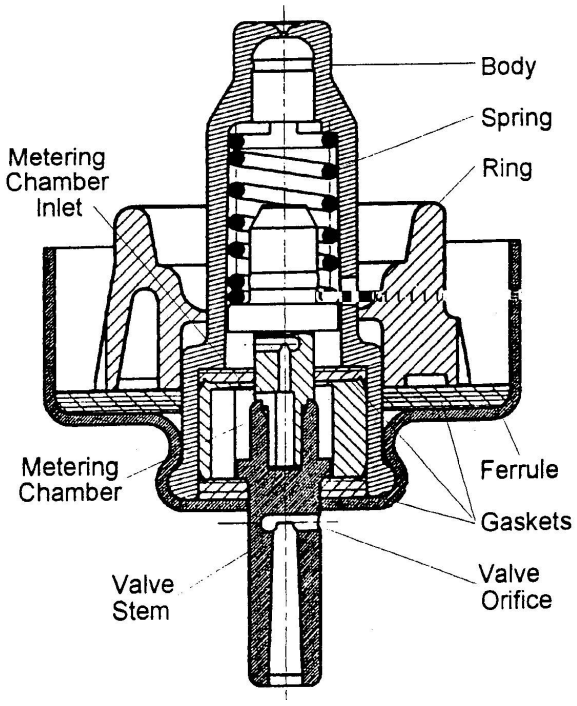

Figure 1.8: Components of a metering valve (Dunbar, 1996).

The expansion chamber's main role is to leave sufficient time for the spray to start atomising before reaching the nozzle orifice so that a liquid and vapour mixture is already formed when exiting the device (Bar-Kohany and Sher, 2004).

Today, most APIs used in pMDIs are bronchodilators, corticosteroids and anti-cholinergic drugs for the treatment of pulmonary diseases. The API represents at most approximately 1% w/w of the total formulation (Fink, 2000) and an upper limit of 2% w/w has been established in order to avoid the clogging of the valve (Smyth, 2003). pMDIs also contain one or several types of substances to make the API suitable for administration. The main component is the propellant.

Propellants are used as the source of energy to propel the formulation out of the canister and aerosolise the flow into small inhalable particles. Propellants generally represent at least 80% w/w of the formulations (Fink, 2000). It was found that formulations containing less than 80% w/w of propellant showed poor spray properties (Ju *et al.*, 2010). pMDIs might contain other substances referred to as

excipients. There are two types of excipients: surfactants and cosolvents.

The surface active agents (surfactants) are often added to pMDIs' formulations in order to lubricate the valves and help stabilise suspension formulations. Cosolvents can also be added to pMDIs formulations. Flavouring agents, stabilising agents, dispersing agents and preservatives are also common components of pMDIs (Fink, 2000). For example, Alupent and Proventil contain respectively sorbitan trioleate and oleic acid as stabilising agents (Berlin and McCarver, 1997).

1.8.2 Advantages of pressurised metered dose inhalers

pMDIs are the most commonly used inhalation devices for the treatment of respiratory diseases due to their low cost, robustness, portability and user-friendly features (Kleinstreuer and Zhang, 2011). Contrary to DPIs, they do not depend on patients' flow rate to de-agglomerate the drug; which allows children younger than 4 years old or patients with low inhalation flow rates to use them (Bateman and Fitzgerald, 2011). They also protect the drug from humidity and other environmental conditions that can damage the API (Keller, 1999).

Their efficiency has improved, with 10% to 20% of the drug particles reaching the lungs for pMDIs designed in the eighties compared to approximately 50% for certain recent designs (Newman, 1985), (Stein and Myrdal, 2006).

1.8.3 Propellants used in pressurised metered dose inhalers

Originally, pMDIs were formulated with chlorofluorocarbon (CFC) propellants. In 1974, Molina and Rowland showed that CFCs cause degradation of the stratospheric ozone layer (Purewal, 1997). In 1987, the Montreal protocol banned CFC

propellants because of their depleting effect on the ozone layer and ordered the complete extinction of CFCs as propellants for aerosols by 2015 (Andersen *et al.*, 2010), (Anderson, 2005). Since Molina and Rowland's discovery, efforts in finding alternative propellant to replace CFCs have been continuous as there was no alternative device as efficient as pMDIs available at the time. However, the effort of finding new ozone-friendly propellants and reformulating each pMDI deterred some industrials who preferred to focus their research on alternatives to pMDIs such as propellant-free liquid methods and DPIs (Smyth, 2003). Because of the time and cost of reformulation (which is believed to have been greater than 1 billion USD (Andersen *et al.*, 2010)), improving the performance of DPIs became more and more appealing to pharmaceutical companies.

Scientists in charge of finding suitable alternative to CFCs analysed the toxicity profile of other propellants, their solubility with APIs and surfactants, their vapour pressure, their density, their taste and their odour. Chlorine free propellants were investigated as chlorine was identified as the component harming the ozone layer.

Dimethyleter was considered but was expensive to manipulate due to its high flammability and was dropped in favour of hydrofluoroalkanes (HFAs) (Swarbrick, 2007). HFA134a and HFA227ea distinguished themselves from other potential propellants and the International Pharmaceutical Aerosol Consortium for Toxicity Testing (IPACT) conducted tests proving their safety and innocuity. Their only side effect was sedation but it occurred at such high concentrations that the sedation was attributed to a lack of oxygen rather than to the HFAs. Some studies also showed that HFA134a and HFA227ea were less likely to cause cardiac adverse effects than some CFCs (Leach, 1995). HFA-based pMDIs proved to have a more constant dosage than CFC-based pMDIs; which could be due to the fact that HFAs are less sensitive to temperature changes (Clark, 1991). In addition, HFAs are not flammable and seem to have similar physical and chemical properties as CFCs.

All IPACT studies led to the conclusion that HFAs were as safe or safer than the CFCs they were meant to replace. The main challenge remained the reformulation of the existing CFC-based pMDIs with HFAs (Leach, 1995). The dissimilarities between CFCs and HFAs that mainly affected the reformulation process were the higher polarity and vapour pressure of the new HFA propellants (Smyth, 2003). When comparing the deposition patterns of CFC and HFA driven pMDIs within the lungs, it was found that HFA was spread more diffusely throughout the airways while CFC remained in the central airways. Leach found that HFA-driven aerosols lead to greater deposition of the aerosol within the lungs while also decreasing the amount depositing at oropharyngeal level (80% to 90% of CFC-based pMDIs deposit in oropharyngeal region whereas HFA-based pMDIs deposit approximately 60% of the aerosol in the central lung region). As a result, a lower amount of drug could be used when using HFA-driven aerosols. Using HFAs rather than CFCs could also decrease the risk of throat inflammation associated with the repeated exposition of the oropharyngeal region to the propellant (Leach, 1995). In his model, Kleinstreuer finds that CFC formulations lead to a lung deposition of 23.2% compared to 46.4% obtained with HFA formulations. Those findings might be due to the fact that HFA propellants produce smaller droplets than CFC propellants (Smyth, 2003). The sprays from HFA-based inhalers are found to be at least twice slower than those of CFC-based inhalers (Hochrainer *et al.*, 2005). It was also found that HFA pMDIs have longer spray durations (0.21 s to 0.36 s for HFA sprays compared with approximately 0.16 s for CFC sprays) (Hochrainer *et al.*, 2005). This could cause CFC-driven aerosols to increase coordination problems compared to their HFA counterparts.

Nowadays, HFA134a and HFA227ea are the most common propellants for pMDIs applications. One study showed that the MMADs of HFA227ea-driven sprays are 0.3 μm to 0.4 μm bigger than the MMADs of HFA134a-driven sprays (Purewal,

1997). Brambilla *et al* (1999) found that the MMAD of a HFA134a formulation was 2.8 μm compared to 3.5 μm for an HFA227ea formulation. This could be explained by the fact that HFA134a has a higher vapour pressure than HFA227ea (at 20°C, HFA134a has a vapour pressure of 570 kPa compared to 390 kPa for HFA227ea). The vapour pressure corresponds to the pressure at which a substance's vapour and liquid phases are in equilibrium. A high vapour pressure will lead to a faster evaporation as the propellant will start evaporating in the metering chamber when the pressure is still relatively high. It is proven that a higher proportion of propellant evaporating in the metering and expansion chambers leads to smaller droplets in the aerosol (Purewal, 1997). This would imply that a high vapour pressure is necessary for aerosol application as smaller droplets decrease the chance of oropharyngeal impaction. However, it was also shown that droplets velocity increases at high vapour pressures (William and Liu, 1998), which could enhance oropharyngeal impaction. The high velocity of pMDIs sprays should be reduced as up to 80% of particles issued from pMDIs impact on the throat (Fink, 2000). In order to reduce the chances of oropharyngeal impaction due to high droplet velocity, HFA134a is often mixed with a solvent of lower vapour pressure. This process is explained later in this chapter.

Although pMDIs do not use CFC propellants anymore, they still have a weaker ecological profile than DPIs as they contain propellants such as hydrofluoroalkanes (HFAs) which exhibit greenhouse gas potential (Leach, 2005).

1.8.4 Pressurised inhalation formulations

Drugs in pMDIs can either be in solution formulations (dissolved in the propellant) or in suspension formulations (drug and propellant are not miscible and stand in two separate phases with drug particles suspended in the propellant). If the inhaler

is a suspension type, the API and the propellant should have a low solubility as partial solubility can induce crystal growth, increasing the risk of variations in particle size and emitted dose (Smyth, 2003).

Suspension may lead to changed quantity of APIs in droplets due to particles aggregation and flocculation (Smyth, 2003). Surfactants are often added to suspension formulations to ensure the chemical stability of the formulation by preventing aggregation of the API. They are also used to lubricate the valves in pMDIs (Smyth, 2003). Those surfactants were generally miscible with CFCs. This is the reason why most CFC-based pMDIs were designed as suspension formulations. Commonly used surfactants such as sorbitan trioleate, oleic acid and lecithin have a much lower solubility with HFAs (0.005% to 0.02% w/v) than with CFCs (0.1% to 2.0% w/v) (Smyth, 2003). The solubility of surfactants in HFAs is not sufficient to ensure the chemical stability of the drug in suspension formulation (Smyth, 2003); (Haynes *et al.*, 2004). It can be increased by adding a cosolvent such as ethanol in the formulation. However, adding a cosolvent to a formulation also increases the solubility of the API in the propellant which must be avoided in suspension formulations. This is the reason why solution type formulations became more popular with the development of HFA-based pMDIs. The main advantage of solution formulations is that a constant quantity of drug is produced at each actuation. However, they do not guarantee the chemical stability of the drug. If the inhaler is a solution formulation, the API should have a sufficient solubility in the propellant so that more API is delivered at each actuation and therapeutic effect is achieved with a few actuations. Solution formulations might thus contain surfactants and/or cosolvents to increase the solubility of the API in HFAs.

In solution formulations, the particle size is mainly governed by the percentage of non-volatile components in the formulation, the vapour pressure of the formulation as well as the device design. On the contrary, the minimum droplet size issued from

suspension formulations is dictated by the size of the drug particles suspended in the formulation. Most suspension formulations are composed of particles with diameter ranging between 2 μm and 5 μm (Smyth, 2003).

1.8.5 The use of cosolvents in pressurised inhalation formulations

Cosolvents are often used in HFA solution formulations to improve the solubility of APIs and surfactants in HFA propellants, leading to the delivery of a greater therapeutic dose by metered volume. They are also used to reduce the vapour pressure of HFA134a leading to the aerosolisation of slower droplets. Adding ethanol to an HFA-based formulation could therefore be thought to decrease oropharyngeal deposition. It is also thought to prevent microbiological contamination (Smyth, 2006). However, studies generally show that the efficiency of HFA solution formulations decreases at high ethanol concentrations. When adding ethanol, the decrease in vapour pressure can have several effects on the aerosolisation process. It might increase the initial droplet mass median diameter and decrease the evaporation rate of the aerosol. As a result, higher ethanol concentrations may lead to bigger initial droplets which evaporate slower. The droplets would thus be bigger when reaching the throat and a larger fraction of the aerosol would possibly impact on the oropharynx (Stein and Myrdal, 2004). Even though high ethanol concentrations lead to a greater amount of drug delivered (due to a greater solubility with HFAs), it is necessary to estimate the net gain of adding ethanol. It was estimated that the benefits of adding ethanol are cancelled when the percentage of ethanol by weight is higher than 10% to 15% of the formulation. At higher concentrations, significant deposition at the oropharynx not only decreases the percentage of drug delivered to the lungs, but also increases the risk of systemic side effects and throat

inflammation (Gupta *et al.*, 2003).

1.8.6 Concentration of drug substance

The mass of API inside the metering chamber can vary from 20 μg to 5000 μg (Oliveira *et al.*, 2010). The MMAD of aerosols was shown to increase with the concentration of API in the formulation. For example, Polli *et al* (1969) investigated two formulations with API concentrations of 0.175 $\mathrm{mg \cdot g^{-1}}$ and 2.86 $\mathrm{mg \cdot g^{-1}}$ and found MMADs of 3.2 μm and 18 μm respectively. When the drug concentration increases, the quantity of propellant relatively decreases. As the propellant represents the source of energy which breaks up the liquid aerosol stream in particles, a lower propellant concentration could result in a lower amount of energy available to aerosolise the flow into small inhalable particles. A greater concentration of drug substance also causes the molecules present in the formulation to be closer to each other, increasing their force of attraction. As a result, when a formulation contains a greater quantity of drug substance, a smaller source of energy is available to break up a greater quantity of concentrate particles strongly bonded together, leading to bigger droplets. The larger particles size could also be explained by the fact that the propellant has the highest vapour pressure of all ingredients in the formulation. Increasing drug substance concentration therefore decreases the vapour pressure of the formulation. As mentioned previously, decreasing the vapour pressure of a formulation results in greater MMAD (as the aerosol undergoes less flashing process (Ashworth *et al.*, 1991)). This may explain why formulations with a higher drug amount have a larger MMAD and a lower FPF (Polli *et al.*, 1969).

1.8.7 Concentration of surfactant

As surfactants are non-volatile, it is also thought that they could be used to modulate the size of residual particles. When comparing a solution containing 1% and 5% w/w of pluronic l81, a study found that the 1% concentration leads to smaller MMAD, higher FPF and deeper lung deposition. This may be due to the reduced evaporative potential of droplets with higher concentration of pluronic l81 caused by the strong hydrogen bond between pluronic l81 and HFA227ea (Saleem and Smyth, 2009). Generally, excipients are used to increase the chemical stability of the drug or to solubilise the drug in the propellant. As excipients are non-volatiles, they will likely increase the size of residual particles and could therefore be used to modify the site of deposition of the drug (Stein and Myrdal, 2004).

1.8.8 Patient-related issues in metered dose inhaler use

It is recognised that pMDIs performance is not consistent and this variability is mainly caused by patient-related factors. Up to 2 out of 3 patients might not use their pMDIs properly, thus reducing their efficiency (Fink, 2000). The handling of the device includes the initialisation of the device and the inhalation technique. Proper device handling can increase pMDIs' performance. Alternatively, inappropriate handling of the device can reduce the treatment's efficacy.

Initialisation of the device

Certain steps in the handling of the device are more critical than others. For example the position of the device can influence the performance of the pMDI but forgetting to prime the device can result in a complete failure of the drug delivery. The initialisation varies from device to device. It generally consists in shaking and priming the device ("firing a few shots") before using it (Keller, 1999). Suspension

type pMDIs need to be shaken prior to use, as the drug is not dispersed in the propellant.

Patient force of actuation

pMDIs' efficiency could also be compromised when patients are not able to apply the required pressure on the pMDI actuator (e.g patient suffering from arthritis). A force between 30 N and 40 N is necessary to overcome the resistance of the device and actuate conventional stem-type metering valves (MacMichael and Hearne, 2002). Those forces might be too high for pediatric and geriatric populations. One study showed that only 29% of the participants could generate a sufficient force to fire all marketed pMDIs with 36% of elderly participants in the study being unable to generate the minimum force to actuate any device (Armitage and Williams, 1988). Another study showed that the patients with the lowest hand strength were unable to properly use pMDIs as they could not coordinate the actuation of the device and the inhalation (Gray *et al.*, 1996). pMDIs are therefore restricted to patients able to actuate the device with sufficient strength.

Patient inhalation technique

One study reveals that 42% of the patients have inadequate inhalation technique when using their pMDIs (Loh *et al.*, 2004). Coordination is the main issue when inhaling a pMDI dose, as the actuation of the device and the inhalation should occur simultaneously. It is estimated that 50% of pMDIs' users encounter coordination problems when using pMDIs (Hickey, 2004). A lack of coordination increases the risk of the actuated dose impacting on the back of the throat and therefore prevents the total dose of drug from reaching the lungs (Marshall, 2010). It results in a greatly decreased efficiency of pMDIs and currently represents their main drawback. To overcome this problem, flow-triggered pMDIs actuated by a user's inspiratory flow rate i.e. breath-actuated pMDIs, were designed. For instance, the Autohaler is

actuated when the flow detected is equal or superior to 30 L.min^{-1}. The Autohaler contains a lever on top of the device that needs to be lifted prior to use. This loads a spring acting against a vane mechanism. Once the flow is superior to 30 L.min^{-1}, the vane moves and causes the canister to be actuated (Fink, 2000). The coordination problem can be solved by using spacer chambers. Those add-on devices have a volume from 20 mL to 750 mL and are attached to the pMDI mouthpiece (Newman, 2005). They delay the penetration of the spray into the mouth by creating a distance between the pMDI and the patient. As a result the need for synchronisation is greatly reduced if not eliminated. However, spacers are bulky and render pMDIs less convenient to transport (Newman, 2005).

As mentioned earlier, it is believed that gravitational sedimentation increases with decreasing airflow rates (Dolovich, 1991). A relatively low airflow rate of 30 L.min^{-1} should be adopted by pMDI users to optimise their device's efficiency (Vincken *et al.*, 2010).

It was also shown that a deep inhalation followed by a breath-hold of 10 s maximises the drug deposition in the lower part of the lungs (Kleinstreuer *et al.*, 2008). As the number of airborne particles subject to gravitational sedimentation decreases exponentially with time, a long inspiration followed by breath-holding might increase the deposition of those particles on the lower airways (Agnew, 1984). Particles depositing by diffusion are also more likely to deposit in the lower airways with breath-holding than when the inhalation is followed immediately by an exhalation as the latter tends to increase the exhalation of those submicron particles (Sanders, 1979). Patients therefore need to practice their inhalation technique adequately in order to maximise their pMDI efficiency.

Positioning of the device during inhalation

The angle at which users hold their pMDI was also found to have an effect on the device's efficiency. The efficiency was shown to be maximised at spray angles of 20° (Fadl *et al.*, 2007). This might be because at a 0° angle, the spray impacts on the tongue and the top of the spray is too far from the mouth ceiling to ensure a sufficient friction to slow it down, leading to an increased throat deposition. At a 20° angle, the spray is at the ideal position, being located equidistantly from the tongue and the mouth ceiling. As a result, shear stress contributed by the tongue and the mouth ceiling can slow down the spray which as a result, does not impact as much on the throat (Fadl *et al.*, 2007).

1.9 Particle sizing methods for inhalation products

As mentioned in the beginning of this chapter, the size of the particles issued from pMDIs determines partly their deposition location. For this reason, particle sizing is of prime importance when designing inhalers. Aerosol particles can be measured using several methods such as microscopy, inertial separation, laser diffraction, image analysis, time-of-flight and phase Doppler analysis.

1.9.1 Laser diffraction analysis

Laser diffraction can be used to assess the size of particles in a flow. Several instruments such as the Malvern 2600®, the Malvern Mastersizer® E and S, the Malvern Spraytec® (Malvern Instruments, Inc., Southborough, MA) and the Sympatec® (Sympatec Inc., Lawrenceville, NJ) employ laser diffraction to assess the size of

particles in different types of sprays. Laser diffraction represents a flow analysis (vaporised formulations in the case of pMDIs) using a laser beam. When entering in contact with a droplet, the laser light splits if the droplet is sufficiently small. The laser diffraction is inversely proportional to the droplet size, allowing the droplet size to be derived from the diffraction angle.

Algorithms used in laser diffraction analysis

In order to solve sprays particle size distributions, laser diffraction instruments can use the Mie or the Fraunhofer scattering theories (Haynes *et al.*, 2004). Fraunhofer theory represents a simplified version of the Mie theory, in which the optical properties of the flow are not needed. It can be applied to opaque and spherical particles of diameters much larger than the laser wavelength. It works best on particles of diameter greater than 25 μm (Mitchell *et al.*, 2006). For particles with smaller diameters such as pMDIs particles, it is recommended to use the Mie scattering theory which takes into account the optical properties of the medium and the spray although the latter might sometimes be difficult to assess (Xu, 2001). Both medium and spray properties are needed as the angular diffraction pattern depends on the ratio of the medium to the particles refractive index.

1.9.2 Inertial impaction analysis

Impactors separate particles according to their inertia. Particles with high inertia deposit by inertial impaction on the impactor location corresponding to the throat. The lowest the inertia of the particles, the further they can travel inside the impactor, to reach locations representing the lower respiratory airways.

The two most common impactors are the Andersen cascade impactor (ACI) and the next generation impactor (NGI). Impactors can generally measure particles

with diameters ranging from 0.5 μm to 35 μm. Impactors are the most commonly used instruments for aerosol particles sizing and are recommended by the United States and the European pharmacopeias (Telko and Hickey, 2005).

One of the many advantages of impactors is that the determination of particle size is aerodynamic so that it can take into account particles density and shape. They can also provide chemical analysis of the particles, which is relevant as it allows the determination of the amount of API of a particular size. Impactors can analyse the whole spray issued from a pMDI and predict the deposition location of particles, as a percentage of the total delivered dose.

However, impaction testing is labour intensive and time consuming. It is also intrusive, as a sample of the spray is needed for the impactor to operate. Underestimation of particles size can occur as small droplets containing only propellant are not filtered by impactors. However, this can be prevented by conducting a chemical analysis following the impaction measurement. The size of the residual particles can be overestimated compared to the size of the initial micronised API when agglomeration of drug particles occurs inside the pMDI.

Michael *et al* (2001) indeed showed that the residual size of salmeterol xinafoate and fluticasone propionate particles was higher than their initial size due to agglomeration. Aggregation is reported to occur more in HFA-based pMDIs than in CFC-based pMDIs (Michael *et al.*, 2001).

Loss of particles on walls and on inter-stage surfaces can also reduce the accuracy of impactor devices. Impactor measurements significantly differ from *in vivo* measurements. This might be due to the fact that the simulation throat used in impactors experiments is not realistic. This problem can be reduced by using anatomic throats (Smyth, 2003).

Laser diffraction and impaction are the two most commonly used methods to measure the size of particles issued from inhalers. Other methods are described below.

1.9.3 Microscopy and particle imaging

The size of particles issued from pMDIs can be determined using microscopy. In this method, the aerosol is fired on a plate treated to maintain the pattern of the droplets. The main issue associated with this technique is that the concentration of droplets should be sufficiently low to ensure that several droplets do not impact at the same location as this would interfere with the size measurements. However, the concentration should be sufficiently high to guarantee statistically significant results (Dunbar, 1996).

1.9.4 Time-of-flight analysis

The time-of-flight analyser is an aerodynamic particle sizer (APS). It assesses the residual size of particles by measuring the spray inside a large reservoir once all its volatile components are evaporated. Time-of-flight analysers measure the time of flight of particles as they travel through two laser beams. Particles velocities are then converted to particles sizes. The APS®3603 from TSI Inc. can measure particles of size ranging from 0.2 μm to 700 μm (Mitchell and Nagel, 2004). The APS®3321, with an operating size range between 0.5 μm and 20 μm, is ideal for the measurement of pMDIs sprays.

Haynes *et al* (2004) reported that time-of-flight analysers suffer from similar particles oversizing problems as the Malvern Spraytec®. These problems may be due to the fact that measurements occur while droplets are not fully evaporated. However, Tiwari *et al.* (1998) showed that the Aerosizer® gave lower particle size distribu-

tions compared to the Malvern 2600® (Haynes *et al.*, 2004). This might be due to the fact that when using the Aerosizer®, the particles were discharged in a 4 L induction port before being measured (which would allow a more complete evaporation of the particles) whereas when using the Malvern 2600®, the particles were measured while still evaporating (Haynes *et al.*, 2004). Mitchell *et al.* (2003) also reported that the APS® tend to undersize particles issued from pMDIs compared with inertial impactors.

In this work, the size of aerosols particles will be measured using cascade impactors and laser diffraction instruments as they remain the most commonly used instruments for the assessment of aerosols particles size (Haynes *et al.*, 2004). However, as each method calculates particles sizes at different times and locations in the aerosolisation process, using varying theories, it is advised not to compare directly the particles size obtained with different apparatus.

1.10 Velocity measurements of emitted aerosols

A high velocity of droplets might increase their chance of inertial impaction and thus reduce their ability to reach the lower respiratory tract (Hochrainer *et al.*, 2005).

However, at higher velocities, droplets might also be able to break up into smaller secondary droplets due to increased aerodynamic forces applied to the spray. This might result in their ability to reach lower parts of the respiratory tract (Finlay, 2001).

Velocity and size are considered the main factors influencing the deposition location of droplets. Several experimental methods discussed below can be used to measure droplets velocity.

1.10.1 High-speed video recording

The velocity of an aerosol can be estimated by recording frames of the developing spray and measuring the distance travelled by the front edge of the spray between 2 frames. Hochrainer *et al* (2005) used this method for HFA-based and CFC-based sprays using a video camera with a 10 ms delay between each frame. The evaporation of the spray enhances its deceleration as it causes particles to shrink and therefore reduces their momentum. Hochrainer *et al* showed that the velocity of HFA-based pMDIs decreased from an initial velocity of $10\,\mathrm{ms}^{-1}$ to $20\,\mathrm{ms}^{-1}$ to a velocity of $2.0\,\mathrm{ms}^{-}$ to $8.4\,\mathrm{ms}^{-1}$ at approximately 10 cm from the nozzle, depending on the device tested.

1.10.2 Particle velocity measurements

Several quantitative methods can be used to measure particles velocity. The first method was invented in the 18th century by the French engineer Henri Pitot. It uses Pitot tubes to derive particles velocity from the pressure of the flow using Equation (1.8) developed by Bernoulli.

$$\frac{U_{flow}^2}{2} + g\,Z + \frac{P_{flow}}{\rho_{flow}} = constant \tag{1.8}$$

where U_{flow} is the flow velocity in $\mathrm{m{\cdot}s^{-1}}$, g is the gravitational acceleration in $\mathrm{m{\cdot}s^{-2}}$, Z is the elevation of the point of measurement in m, P_{flow} is the pressure at the point of measurement in $\mathrm{kg{\cdot}m^{-1}{\cdot}s^{-2}}$ and ρ_{flow} is the density of the flow in $\mathrm{k{\cdot}m^{-3}}$.

In the 1920s, the implementation of hot wire anemometry improved the quality of velocity measurements. Hot wire anemometers contain a fine metal wire at a temperature above ambient temperature. Depending on the flow velocity, the wire

cools to a certain extent, modifying its electrical resistance. The flow velocity can thus be derived from the electrical resistance of the wire. Pitot tubes and wire anemometers disturb the measured flow and can thus modify its behaviour and characteristics (Wernet, 2003).

Laser Doppler anemometry (LDA), invented by Yeh and Cummins (1964), represents the first non-invasive (it does not interact physically with the flow) method to measure 1D, 2D or 3D velocity components of a flow at one point. In LDA, several laser beams are used; their cross-section, referred to as measurement volume, is composed of dark and light fringes. The distance between the fringes is used to calculate particles velocity. Figure 1.9 shows the fringes in the measurement volume.

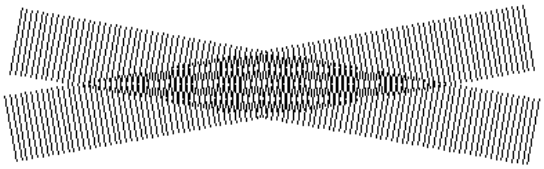

Figure 1.9: Drawing of the measurement volume showing the formation of fringes (Devenport, 2006).

As the flow particles travel through the fringes, they scatter the laser light and generate a modulation of the light intensity referred to as "a Doppler burst". The frequency of this scattering is used to determine the flow velocity. A lens helps to measure the frequency by focusing the fluctuating light on a photodetector transforming the light signals into voltage signals. A signal processor then determines the frequency of this electrical signal which is used to derive the flow velocity using Equations (1.9), (1.10), (1.11) and (1.12).

$$Sf = \frac{\lambda}{2\sin\frac{\alpha}{2}} \tag{1.9}$$

where Sf is the distance between the fringes in m, λ is the wavelength of the laser light in m and α is the angle of the intersecting beams in rad. The relationship between the frequency and the particles velocity is shown in Equations (1.10), (1.11) and (1.12).

$$f = \frac{U_p}{Sf} \tag{1.10}$$

where f is the frequency of oscillations determined by the signal processor in Hz and U_p is the velocity of a particle in $\mathrm{m{\cdot}s^{-1}}$.

$$f = U_p \times \frac{2\sin\frac{\alpha}{2}}{\lambda} \tag{1.11}$$

$$U_p = f \times \frac{\lambda}{2\sin\frac{\alpha}{2}} \tag{1.12}$$

A schematic of a LDA design is shown in Figure 1.10.

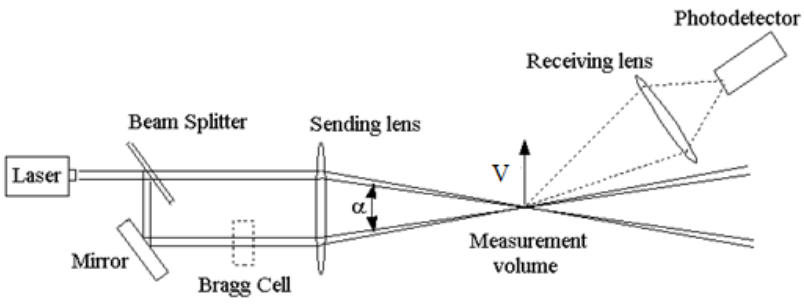

Figure 1.10: Schematic of a single-component dual-beam LDA system (Devenport, 2006).

The two main disadvantages of LDA are that it can only measure particles velocity at one point in the flow and can only assess the size of spherical particles. Particle image velocimetry (PIV) on the contrary can provide particles velocity measurements on one plane. This can be of benefit for the analysis of pMDIs sprays as theoretically all droplets lying on one plane could be inhaled and should therefore be studied.

Pulsed light velocimetry is an umbrella term describing the analysis of particles velocity using pulsed light. Varying laser techniques are used depending on the flow density to be analysed. Laser speckle velocimetry (LSV) is a method designed to measure the velocity of highly dense flows in which overlapping particles form speckles in each interrogation spot (Pust, 2000). Particle tracking velocimetry (PTV) is used to analyse low-density flows by tracking each particle individually. Median density flows are generally measured using high image density PIV mode (Pust, 2000). As sprays issued from pMDIs have a medium to high density depending on the distance from the nozzle orifice at which they are measured, it was thought PIV would be a suitable method to characterise their velocity (Crosland *et al.*, 2009).

1.10.3 Particle image velocimetry measurements

PIV is a technique in which two images are captured in a short lapse of time using laser technology. Particles are recorded on several images and the flow velocity is derived from their displacement during the short lapse of time between the images. PIV can be used to calculate flow velocities ranging from millimetres per second to several hundred meters per second (Adrian, 1991).

PIV is more common than LSV as it is estimated that most flows are not sufficiently dense to produce speckles. It is also thought that the large amount of fine particles needed to induce speckles produce less detectable images than the lower number of larger particles needed for ideal PIV measurements (Adrian, 1991). The two limits of PIV lie between particle tracking velocimetry for low-density flows and high image density PIV for high density flows.

Hinsch classifies PIV methods according to parameters x, y and z where x corresponds to the number of velocity components calculated, y is the number of

dimensions of the domain and z identifies whether the velocity measurements are instantaneous (0) or continuous (1) (Prasad, 2000). The most common type of PIV is of type (2, 2, 0) according to Hinsch's classification. Obtaining 3D velocity components in a 2D domain (3, 2, 1) is achievable with stereoscopic PIV and represents a popular form of PIV (Prasad, 2000). Holographic PIV (3, 3, 0) is difficult and expensive to perform (Prasad, 2000) although cinematic holographic PIV (3, 3, 1) remains the most sophisticated and complex form of PIV. In recent years, the most elaborate PIV techniques have become easier to perform thanks to the development of digital recording (Gharib *et al.*, 2002).

Lasers used in PIV measurements can be continuous wave lasers or pulsed lasers. The laser should have a pulse with a sufficiently high frequency to ensure a good resolution of the measurements. Pulses can be obtained on continuous wave lasers using a chopper or by rapidly sweeping the laser beam over the domain (Prasad, 2000). Pictures recorded with pulses of higher frequency can assess the velocity of faster particles. Pulsed lasers have a shorter pulse than continuous wave lasers (a few nanoseconds for Yag lasers) and can therefore be used to measure the velocity of faster particles (Adrian, 1991). It was thus decided to use a pulsed laser in the PIV experiments conducted in this work.

During PIV measurements, particles in the flow reflect the laser light and this scattered light is focused on a lens placed perpendicularly to the light sheet, before being analysed by a computer. To carry out the velocity analysis, the image is divided into small regions referred to as interrogation spots, the size of which depends on the properties of the studied flow. If the flow velocity is high, the interrogation spot should be of sufficient size to ensure that particles remain in the area from one image to the next. If the flow is highly dense, interrogation spots should be smaller to limit the number of particles in each interrogation zone. Gaseous flows need to be filled with tracer particles in order for the laser light to be

scattered. The tracer particles should ideally follow the flow streamlines without important slip (Prasad, 2000).

Recording methods

The images can be recorded using a charged couple device (CCD) (used in the present work), a film or holographic plates (when the domain studied is a volume) (Gharib *et al.*, 2002).

There are several PIV techniques, each involving different types of frame and pulse recordings. The frames describe the images on which the particles positions are recorded and correspond to the sequence of images captured by the camera or the film. In single frame recordings, one frame is used to record images obtained with several pulses. The term multiframe corresponds to a sequence of images that are used at different time intervals to record particles positions. With this technique, there is a record of particles motion in time.

Laser pulses are used to record an image at different time intervals. The time interval between two pulses determines the maximum velocity that can be measured. The time separation between two pulses can range from $1\,\mu$s to $1\,$ms (Jahanmiri, 2011). The duration of the light pulse determines the sharpness of the picture (Adrian, 1991).

The simplest recording method is the single frame method also referred to as streak photography. This type of recording consists in lighting the particles with a long pulse. It is similar to a certain extent to the single frame/multipulse method as in both methods, the particles trajectories are almost continuous (Adrian, 1991). Although streak photography is efficient for the analysis of two-dimensional flows, the multipulse method is more accurate as it is easier to determine the location of a particle from a dot than from a streak (Adrian, 1991). It is also thought that

the energy of the laser concentrated on short pulses rather than on a long streak leads to more intense scattering of the particles. The multipulse method therefore allows the analysis of smaller particles than streak photography when using lasers of similar power (Adrian, 1991).

The benefits of the multipulse set up are only obtained with pulsed lasers, not with continuous wave lasers. This is due to the fact that continuous lasers have less light intensity than pulsed lasers. Furthermore, their energy decreases as the duration of the pulse decreases. For this reason, the multipulse method with continuous wave lasers is mainly used to analyse slow flows or flows containing large particles (Jahanmiri, 2011).

The single frame/double pulse technique is suitable for flows with low particles density as it cannot deal with particles superposition. This technique also requires a shifting of the image in order to identify the direction of the particles trajectory (Adrian, 1991). As pMDIs flows have a medium to high density, the single frame technique will not be used in the PIV analysis in Chapter 5.

In the multiframe method, the camera exposes particles displacement by producing several shots of the interrogation spot. This technique can be used coupled with single or multipulse laser illumination. The main advantages of multiframe measurements are that the flow direction is determined directly and the time interval between frames can be chosen independently of the time interval between pulses. The lapse of time between pulses can therefore be chosen to satisfy velocity and spatial requirements whereas the time between frames can be chosen to expose the trajectory of the flow as required by the experiment (Adrian, 1991).

Multiframe/single pulse is the simplest type of multiframe techniques. In each frame, the particles are exposed once. This method has several advantages such as the clarity of the images in which particles do not superpose as each of their

positions are exposed on one frame. This allows the particles images to be paired more easily. For this reason, this technique was chosen in Chapter 5. When using this method, the time interval between pulses must be equal or an integral multiple of the time separation between frames.

Applications of different PIV methods

Varying particle imaging techniques, each with several frame and pulse specifications, are used depending on the type of flow to be analysed.

PTV, used for the analysis of low-density flows, is generally combined with single frame/double pulse recordings. In the early age of PIV, the technique consisted in illuminating particles with two pulses and capturing the two images on a single frame. The distance travelled by each particle could then be determined easily by pairing each pair of particles images. Today, the method is digitalised and particle-pairing is computationally executed. The algorithms used must differentiate particles images from noise. This is generally done by removing a certain amount of noise from the picture, ensuring only bright pixels are computed. In order to avoid particles overlapping, PTV should be used on relatively low-density flows such as liquid flows with low seeding particle densities. In these flows, the distance between two neighbouring particles is generally larger than the displacement of one particle between the two laser pulses (Prasad, 2000).

High density PIV is used to analyse flows in which more than one particle is present in each interrogation spot. To ensure the presence of several particles in each interrogation spot, a great care must be taken in the choice of the interrogation spot size.

High image density PIV is the most accurate method for the analysis of particles of diameter equal or smaller to 25 μm corresponding approximately to the size of

particles issued from pMDIs estimated by Dunbar at the nozzle orifice (Adrian, 1991), (Dunbar, 1996). High image density PIV was first used on liquid flows but is also able to measure particles displacement in gaseous flows.

Algorithms

The algorithms used to assess particles displacement in PIV impact the level of errors of the measurements. Several algorithms can be used to solve particles displacement, the most common being the cross-correlation (CC) technique, the auto-correlation technique, the particle tracking technique and particle image pattern matching technique (PIPM) (Huang *et al.*, 1997). The nearest neighbour approach is a simple way to pair particles. It assumes that the nearest neighbour of the particle corresponds to its pair (Adrian, 1991). This method can be made more accurate by taking into account prior displacement of the particle to find its pair (Adrian, 1991).

Correlation algorithms

Correlation algorithms are ideal to analyse particles in dense flows as they do not match pairs of particles but small groups of particles. The algorithm analyses all particles lying on one interrogation spot as one group and finds its match by searching for groups with the most similarities (Adrian, 1991).

Using single frame/double pulse recordings, the auto-correlation algorithm results in three peaks; the auto-correlation peak corresponding to the origin of the displacement, the positive displacement peak corresponding to the correlation of the first image with the second image and the negative displacement peak corresponding to the correlation between the second image and the first image.

As the displacement peaks decrease in amplitude with the flow velocity, the auto-correlation function is not advised for the analysis of high-velocity flows (Prasad,

2000). In order for the method to capture appropriate displacements, the time interval between the two pulses Δt should be calculated according to the flow velocity using Equation (1.13).

$$\Delta t \leq 0.25 \frac{L_i}{PM\, U_{flow}} \tag{1.13}$$

where L_i is the length of the interrogation spot in m, PM is the magnification of the recorded image and U_{flow} is the expected velocity of the measured flow in $\mathrm{m{\cdot}s^{-1}}$ (Prasad, 2000). The following observations can be made from Equation (1.13):

- When the flow velocity increases, the lapse of time between pulses should be shorter as the particles might leave the interrogation spot before the second pulse can record the second picture.
- At high image magnifications, the lapse of time between pulses should be short to ensure that particles remain in the interrogation spot between the two pulses.
- Large time intervals between the two pulses can be used with large interrogation areas as the probability that particles leave the interrogation spot between pulses (referred to as in-plane loss of pairs phenomena) becomes lower.

The accuracy of the auto-correlation algorithm can be improved by using multipulse techniques as they correlate a greater number of pairs, thus providing a larger particles sample. When using single frame/multipulse recording, the lapse of time between the pulses must be reduced to ensure that particles remain in the interrogation area during each of the several pulses.

One of the weaknesses of the auto-correlation technique is that it cannot accurately measure displacements smaller than a particle's diameter as the auto-correlation

peak is too large to recognise small displacements (Bastiaans, 2000). The auto-correlation algorithm is also not advised to solve large displacements as they increase the probability of in-plane loss of pairs. The signal to noise ratio starts decreasing with displacements larger than a fourth of the length of the interrogation spot (Prasad, 2000).

When using the auto-correlation algorithm, peaks smaller than the auto-correlation and displacement peaks are obtained. They correspond to the noise caused by overlapping particles (Adrian, 1991). A noise peak may be larger than the displacement peaks in which case it might be wrongly identified as a displacement peak. In order to avoid this error, a feature specifying that the ratio of the displacement peak to the next peak must exceed a detection threshold can be implemented (Adrian, 1991). It is also possible to look for a displacement peak within a certain region based on neighbouring particles displacements. Post-interrogation techniques in which the obtained displacements are compared with neighbouring particles displacement can also be performed. If some displacements seem not to make sense, the next highest peaks are analysed to determine if, when used, the particles displacement is more in line with the displacement of neighbouring particles.

Another issue of the auto-correlation algorithm is due to the production of the two displacement peaks, making the direct determination of the flow direction impossible (Bastiaans, 2000). Various methods can be employed to resolve this problem. For example, the camera can be translated during the experiments, causing the flow to move at a velocity exceeding the counter flow. The velocity of the translation is subtracted at the end of the experiment to find the real particles velocity. As this method is labour-intensive, the auto-correlation technique should be limited to flows with no reverse flow. As sprays issued from pMDIs are turbulent and contain particles travelling in the opposite direction of the spray, auto-correlation is not anticipated to be suitable in this work (Lee *et al.*, 1991). The double frame/single

pulse recording technique can identify directly the flow direction as both images are stored on two different recording frames. This method leads to the more sophisticated CC technique (Bastiaans, 2000).

CC is used with multiframe/single pulse techniques. As the particles are recorded on at least two frames, the directional ambiguity of auto-correlation algorithms is removed (Bastiaans, 2000). Contrary to auto-correlation, CC only produces one displacement peak.

Errors in digital PIV

The level of error depends on the flow to be analysed, the experimental procedure and the algorithm used. The three main types of errors in digital (DPIV) are outliers, mean-bias and root-mean-square (RMS) errors (Huang *et al.*, 1997).

Some errors are easier to identify than others. For instance, "outliers" which correspond to mismatched particles are generally easy to detect as they are larger than one pixel. The outliers arise from different sources such as three-dimensional motion, large velocity gradients or poor particle seeding (Huang *et al.*, 1997).

Mean-bias errors occur during the determination of particles displacement. They represent the difference between actual and measured displacements and can be due to errors in the determination of the beginning and/or the end of particles displacement. As the reference point corresponds to the centre of the image, mean-bias errors often occur when particles deform or rotate (Adrian, 1991). They can also be due to the fact that particles displacement is not determined with sub-pixel accuracy but always rounded to the nearest pixel integer value. There is no bias error if the particle's displacement corresponds to an integer number of pixels. This type of error referred to as peak locking depends mainly on the size of particles to be analysed. It is accentuated for particles diameter smaller or equal to one pixel

and minimised for particles diameter of approximately two pixels (Pust, 2000).

Bias errors decrease with pixel sizes and with increasing particle size and can be reduced by increasing the image resolution, which leads to a larger particle to pixel ratio.

Velocity bias occurs as faster particles generally have less chance of being identified correctly as they might have left the interrogation area between recordings. This is particularly the case in the presence of high velocity gradients as the PIV system might be set up to record low velocities and might therefore not be able to record big displacements. This might lead to a velocity bias in which small displacements are overestimated (Bastiaans, 2000). This is problematic for low image density DPIV in which the failure of one measurement can be significant due to the small numbers of pairs per interrogation spot (Adrian, 1991). Bias errors decrease with the increasing number of samples and with decreasing particles displacements.

Gradient error is another common type of error due to deformation or rotation within an interrogation area. This can reduce the accuracy of the measurements sometimes leading to false velocity results. However, this problem might be solved by retransforming the images according to their velocity gradients before performing the cross-correlation (Prasad, 2000), (Weng *et al.*, 2010). When gaseous flows are studied, tracking errors can arise due to the inability of the tracer particles to follow the flow without slip (Prasad, 2000). This type of error is not of relevance to this work as tracer particles were not used. Finally, random errors due to noise in the recorded images are unavoidable. Random errors are proportional to the particle image diameter and are given by Equation (1.14) developed by Prasad (2000).

$$\sigma = e\, d_{pi} \tag{1.14}$$

where σ is the random error, e is a coefficient varying between 0.05 to 0.10 depend-

ing on the experimental settings and d_{pi} is the particle image diameter. The size of the interrogation spot also has an effect on the level of measurements errors as small interrogation spots tend to increase spatial resolution but also increase the level of random error as they contain a smaller sample of particles (Fincham and Spedding, 1997).

The camera and its cable might increase the RMS error although this can be reduced using a digital camera as was done in this work (Huang *et al.*, 1997). Even with those error types, PIV remains one of the most accurate methods to determine the velocities of unsteady transient flows such as pMDIs sprays (Weng *et al.*, 2010).

1.10.4 Phase Doppler Anemometry

Phase Doppler anemometry (PDA) is the most comprehensive technique to characterise pMDIs sprays as it can measure the velocity of particles as well as their size and concentration.

In PDA measurements, a laser beam is split and focused around a zone referred to as measurement volume. When the spray reaches the measurement volume, the light scattered by particles is focused on photo-detectors by means of a lens placed between the measurement volume and the photo-detectors. The light scattered by each particle produces a Doppler burst signal used to assess the characteristics of the particle such as size and velocity.

Particles velocity is as important as particles size when determining the efficiency of a pMDI. Particles velocity is difficult to determine at the nozzle orifice using optical measurements as the evaporation of the propellant causes a blur. For this reason, the velocities reported at the nozzle orifice vary tremendously in the literature.

The highest pMDI spray velocities were found by Dunbar (1997) and Kleinstreuer

et al (2007) who reported velocities between $150\,\mathrm{ms}^{-1}$ and $225\,\mathrm{ms}^{-1}$ at the nozzle orifice using computational simulations. The velocity of the liquid spray exiting the pMDI is $15\,\mathrm{ms}^{-1}$ (as cited by Fink (2000)). Hochrainer *et al* (2005) found velocities of $2.0\,\mathrm{ms}^{-1}$ to $8.4\,\mathrm{ms}^{-1}$ when measuring CFC-based and HFA-based pMDIs sprays at a distance of 10 cm from the nozzle orifice using high-speed video recording. They reported higher velocities for CFC-based pMDIs compared to HFA-based pMDIs.

According to Newman *et al* (1982), the initial spray velocity is approximately $30\,\mathrm{ms}^{-1}$ which agrees with the data obtained by Clark (1996) using a phase Doppler particle analyser (PDPA). In their PIV measurements, Crosland *et al* (2009) reported a nozzle orifice velocity of between $50\,\mathrm{ms}^{-1}$ and $60\,\mathrm{ms}^{-1}$. Wigley *et al* (2002) found a peak velocity of $90\,\mathrm{ms}^{-1}$ using PDA.

The large differences observed might be due to the fact that the velocity decays extremely rapidly and might vary significantly if not measured at the exact same moment and at the exact same location. Furthermore, varying measurement techniques use different principles, which might also contribute to those variations in velocity. It is therefore recommended to only compare velocity data obtained using similar experimental techniques and measured at similar times and locations.

1.11 Aims and objectives

pMDIs suffer from inconsistency of the drug deposition location which is mainly due to a poor control over the size and velocity of the aerosolised droplets. The aim of this thesis will therefore be to study those two parameters at several times and locations in the aerosolisation process and identify the factors that might impact them.

Patient-related factors might lead to different aerosol characteristics. As pMDIs perform optimally at low inhalation flow rates, they are commonly recommended for patients who cannot achieve the high inhalation flow rates necessary for DPI use. It is suggested that many of these patients are young children or elderly patients with weak hand strength and might not be able to actuate their pMDI properly. The aim of this work will be to identify the effect of the actuation force on the size and velocity of the particles.

As pMDIs are used globally, the impact of environmental conditions on the aerosol properties is of interest. For this reason, variations in temperature and their effect on the size and velocity of droplets will also be studied.

A one-dimensional Matlab-based model will be developed in order to calculate the size and velocity of the particles at the nozzle orifice where experimental measurements are difficult to obtain.

Residual droplets size of sprays aerosolised under varying experimental conditions will be assessed using a NGI. PIV, Sympatec® and Malvern Spraytec® measurements will be conducted to evaluate the velocity and size of pMDI sprays during their trajectory.

In both the computational and experimental parts of this work, formulation and device design will be modified in order to understand how they can be used to improve the properties of the aerosol in order for the drug particles to reach their target site.

Chapter 2

Development of a computational simulation of pMDI discharge

2.1 Introduction

2.1.1 Actuation mechanisms

The actuation process of pMDIs comprises several steps designed to aerosolise the formulation into fine droplets. Before the actuation of the canister, the valve stem is in a position which allows the formulation to enter and circulate in the metering chamber. The canister is in an inverted position with the inner valve located below the container. This design allows the metering chamber to fill naturally under gravity (Newman, 2005). Because of its fixed volume, only a certain amount of formulation (the metered dose) can enter the metering chamber. When the user actuates the device, the valve stem is pushed inside the metering chamber, sealing it and preventing any more formulation from entering the metering chamber. At the same time, the formulation is released through a valve orifice separating the

metering and expansion chambers into the expansion chamber which consists of the valve stem and the actuator pit (Oliveira *et al.*, 2012). From there, it is aerosolised into droplets when being propelled out of the expansion chamber through the nozzle orifice (Swarbrick, 2007). The actuation mechanism is described in Figure 2.1.

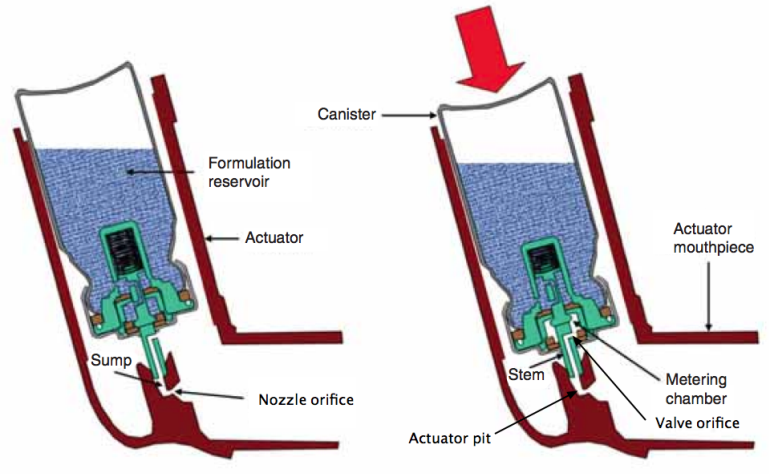

Figure 2.1: Actuation mechanism of a pMDI.
(Lewis, 2007)

In his work on cosmetic aerosols, York defined the spray formation process as the succession of four processes: primary atomisation occurring inside the expansion chamber and at the nozzle orifice, secondary atomisation occurring downstream of the nozzle orifice, evaporation and entrainment (Dunbar, 1996). During the primary atomisation, the formulation breaks into ligaments or large droplets (Versteeg *et al.*, 2006). The droplets then disintegrate into smaller droplets during the secondary atomisation phase. Finally they evaporate and are displaced by the gas phase outside the pMDI.

The aim of this chapter was to develop a model simulating the discharge of the flow issued from a pMDI from the metering chamber to the nozzle orifice, which corresponds to the primary atomisation.

2.1.2 Description of the flow in a pressurised metered dose inhaler

Sequences of the aerosolisation process

Versteeg *et al* (2006) studied the internal flow inside a pMDI using time-resolved laser-based high-speed imaging. Their observations are described below.
Before the actuation of the canister, the metering chamber contains liquid propellant at a certain temperature and at the corresponding saturated vapour pressure. In the first 1 ms to 2 ms of the actuation, the metered dose is forced under pressure into the expansion chamber containing air at atmospheric pressure. When the high-pressured liquid propellant comes in contact with the comparatively low-pressured air, the liquid formulation becomes superheated which causes flash evaporation, producing initially a vapour-only spray.

The flashing of the formulation occurs primarily in the expansion chamber where it is responsible for the initial disintegration of the liquid jet into particles (Sanders, 1979). Flash evaporation represents one of the main processes of primary atomisation (Wigley *et al.*, 2002).

After its initial vapour state in the expansion chamber and at the nozzle orifice, the flow becomes a liquid-rich mixture as the formulation starts filling the expansion chamber (Versteeg *et al.*, 2006).

Simultaneously, the formulation remaining in the metering chamber starts to evaporate to fill the void left by the mass of propellant discharged in the expansion chamber. As a result, the temperature and pressure decrease in the metering chamber. The pressure decrease in the metering chamber combined with the pressure increase in the expansion chamber lead to a decrease in the mass flow rate through the valve orifice (Shaik, 2009).

In the next 5 ms to 10 ms, the expansion chamber is filled with a two-phase foamy mixture. The quality of the formulation (ratio of the total mass of gas, including air, to the total mass of the formulation) therefore increases. The spray exiting the expansion chamber is now a vapour/liquid mixture (Versteeg *et al.*, 2006). This step corresponds to the fully developed phase of the spray and lasts between 60 ms and 70 ms. The spray exiting the pMDI during this phase is dense and composed of very small droplets (Versteeg *et al.*, 2006).

During the terminal 60 ms to 70 ms of the aerosolisation process, the spray density decreases and the size of the droplets emitted increases, particularly at the edges of the nozzle orifice (Versteeg and Hargrave, 2002). This is due to the fact that the mass of propellant decreases, reducing the amount of energy available to break up the droplets forming the spray. At the end of the atomisation, a spring located within the valve returns the actuator to its initial position. The valve orifice is closed and the formulation in the body of the canister can again enter the metering chamber to form a new therapeutic dose.

Flow regimes

Upon actuation, the flow at the valve orifice is critical due to the high pressure gradient between the metering and expansion chambers. This means that the mass flow rate is at its maximal value and cannot be increased further by lowering the pressure in the expansion chamber. The discharge of the propellant from the metering chamber into the expansion chamber, which results in a pressure drop in the metering chamber and a pressure increase in the expansion chamber, causes the flow to become subcritical. The flow is subcritical when Equation (2.1), described later in this chapter, is valid.

$$Ra_{crit} > \frac{P_{ds}}{P_{us}} \tag{2.1}$$

where Ra_{crit} defined later in this chapter is the critical ratio which depends on

thermodynamic properties of the flow, P_{ds} and P_{us} are respectively the pressures downstream and upstream of an orifice in Pa.

At the nozzle orifice, the flow is initially subcritical as there is no pressure gradient between the expansion chamber and the exterior environment (the pressure is atmospheric at both locations). Once the pressure increases in the expansion chamber, the pressure gradient across the nozzle orifice increases to critical ratio, leading to a critical flow. As the metering chamber is depleted of formulation, the pressure in the expansion chamber decreases again, leading to a subcritical flow.

Primary atomisation process

Although little work has been conducted on primary atomisation in pMDIs, research on this subject has been carried in other areas such as the automotive and chemical industries. Diesel injection systems, leaks in "high-pressured" vessels and refrigeration systems are some of the systems that have been extensively researched (Serras-Pereira *et al.*, 2010), (Beychok, 1998), (Gorokhovski and Herrmann, 2008). Those systems can be of help to understand the primary atomisation in a pMDI as they all undergo liquid evaporation due to a sudden pressure drop. This process is referred to as "flash boiling atomisation". Flash boiling atomisation occurs when a liquid is submitted to superheated conditions due to a drop of pressure inside the system. York (1957) assumed that as a result, the liquid would evaporate instantaneously during an adiabatic process corresponding to a mass transfer between the liquid and gas phases (as there would be no time for heat transfer between the two phases during this instantaneous evaporation process) (Dunbar, 1996).

In reality, the liquid evaporation is not instantaneous. As the discharge of the flow from a pMDI is extremely rapid, the liquid starts boiling and parts of it evaporate. When the heat transfer with the exterior environment is negligible, the vapour evaporation energy is taken from the liquid causing the temperature inside the

system to decrease. However, as in many transient processes, the liquid does not have the time to regain equilibrium and remains in a state of instability (Shaik, 2009).

In the expansion chamber, flash boiling atomisation is generally followed by nucleation, fast bubbles growth and liquid atomisation (Sher *et al.*, 2008).
Nucleation defines the formation of vapour nuclei inside a formulation during flash boiling atomisation and the filling of those nuclei by evaporating propellant. Nucleation starts at the valve orifice due to a sudden pressure drop and heterogeneous surface (Sher *et al.*, 2008). In order to grow and not to collapse, the nuclei must have a certain radius, referred to as the critical radius, calculated using Equation (2.2) (Brennen, 2005).

$$r_{crit} = \sqrt{\frac{9\,\gamma\,m_g\,T_b\,Rs}{8\,\pi\,St}} \tag{2.2}$$

Where r_{crit} is the critical radius of the bubble in m, γ is the heat capacity ratio coefficient of the propellant vapour inside the bubble, m_g is the mass of gas in the bubble in kg, T_b is the bubble temperature in K, Rs is the specific gas constant in $K^{-1}{\cdot}kg^{-1}$ and St is the surface tension in $kJ{\cdot}m^{-2}$.

Nucleation can be homogeneous if it occurs in the entire volume of the superheated liquid or heterogeneous if it occurs at the boundaries between the superheated liquid and foreign surfaces such as drug particles or the surface of the canister. In pMDIs, nucleation sites are generally located at the surface of the expansion chamber walls. In suspension formulations, nucleation can also occur at the surface of drug particles (Finlay, 2001).

Dunbar reported that bubble growth does not occur in the expansion chamber as the generated vapour nuclei are continuously destroyed by the incoming flow discharged from the metering chamber and as a result do not reach the critical bubble size. This could be due to the fact that the energy available to develop the

vapour nuclei into bubbles is not sufficiently high (Dunbar, 1997). However, since Dunbar's work, Versteeg *et al* (2006) have proven the existence of bubbles within the expansion chamber through pMDIs visualisations.

Finlay (2001) reported that bubble growth occurs for stable nuclei in the region immediately after the valve orifice where the pressure drop occurs. This region is referred to as "recirculation zone". The boiling flow remains longer in the sub-pressurised recirculation zone than it remains in the non-recirculation region. Due to this increased residence time, the bubbles in the recirculation region become larger. When a pack of bubbles grows, some of them collide and explode; this corresponds to the inception of the flashing process (Shaik, 2009). The growth of the remaining bubbles causes an expansion of the recirculation zone until it obstructs the flow. At this point the recirculation zone is propelled downstream. A new recirculation zone is created and this cycle continues until the end of the atomisation process. The generation and expulsion of the recirculation zone at the nozzle orifice contribute to the oscillating nature of the spray with a frequency between 500 Hz and 800 Hz (Finlay, 2001). Versteeg *et al* (2006) observed dense and lean spray oscillations of frequency between 500 Hz and 1000 Hz in the exiting spray (Figure 2.2).

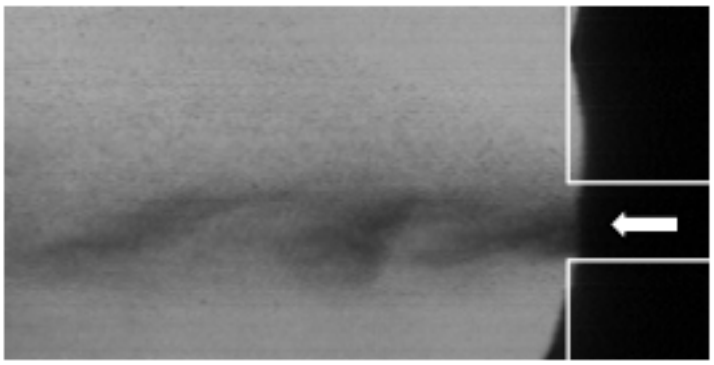

Figure 2.2: Density wave of a spray issued from a pMDI
(Versteeg *et al.*, 2006)

Annular flow regime

In the expansion chamber, most of the liquid propellant is concentrated on the walls; whereas the vapour core is mainly located on an axis aligned with the centre of the nozzle orifice. In the literature, this phenomenon, referred to as "annular flow regime" characterises "the vapour core surrounded by the foamy liquid covering the chamber walls" (Versteeg and Hargrave, 2002). Versteeg *et al* (2006) were able to visualise the annular shape of the flow in a sequence of images of the expansion chamber taken from a high-speed video recording. The annular pattern of the flow caused a slip between the liquid and vapour phases. During the aerosolisation process, the liquid phase observed on the walls of the expansion chamber enters the nozzle orifice where it is elongated into ligaments. Upon contact with stagnant air, the ligaments are broken into droplets which exit the nozzle orifice (Versteeg and Hargrave, 2002). This process, referred to as "shear-thinning" is, with flashing, the other main mechanism of primary atomisation inside pMDIs (Smyth, 2003). As the pressure gradient across the nozzle orifice diminishes towards the end of the aerosolisation process, shear-thinning is reduced and the outer liquid layer forms big droplets at the edges of the spray (Versteeg and Hargrave, 2002).

2.1.3 Previous investigations on flows similar to pMDIs flow

Fraser *et al* (2002) investigated the influence of the flashing location on the mass flow rate of critical flows. They established that the mass flow rate decreased as the flashing location was moved further upstream of the nozzle orifice (as cited by (Shaik, 2009)).

When studying short capillary tubes, systems relatively similar to the design of

pMDIs, Pasqua (1953) observed that the liquid core of the flow diminishes towards the tube exit (Shaik, 2009). When investigating a propellant mixture through twin-orifices, Fletcher (1975) observed a correlation between the mass flow rate and the product of the valve orifice diameter by the nozzle orifice diameter. Fletcher found that the propellant was under metastable conditions in the expansion chamber (as cited by Shaik, (2009)).

Clark (1991) studied experimentally the continuous and metered-dose discharges of propellant through twin-orifices. As his findings were used throughout the numerical simulation, they are summarised later in the chapter.

2.1.4 Models simulating the discharge of turbulent and transient flows

Flows in the expansion chamber are turbulent with a Reynolds number in the range of several hundred thousands (Finlay, 2001). They are also unsteady and multiphase which makes them challenging to model. Several models have been developed to simulate the aerosols issued from inhalers. Models can describe the flow trajectory inside the pMDI, the flow properties at the nozzle orifice, the aerosolisation of the formulation and the deposition of the aerosol inside the respiratory tract. One-dimensional models are generally used to describe the discharge upstream of the nozzle whereas computational fluid dynamics (CFD) models are mainly used to simulate the flow downstream of the nozzle. CFD models simulating the trajectory of aerosols downstream of the nozzle orifice and their deposition in the respiratory airways are not studied in this work which focused on the properties of the spray at the nozzle orifice throughout the aerosolisation process.

Homogeneous equilibrium model

The homogeneous equilibrium model (HEM) was introduced by Strakman *et al* (1964). This approach assumes that there is no slip between the liquid and gaseous phases as the flow is assumed to be a continuous "pseudo-fluid" mixture of liquid and vapour bubbles. In the HEM, the liquid and vapour velocity are therefore equal at one location and they follow the law of a single component system with average properties of liquid and gaseous phases (i.e. a pseudo-fluid). The liquid and vapour phases therefore have the same pressure and temperature and the mixture is assumed to be in thermal equilibrium (Dunbar, 1996), (Shaik, 2009).

Escanes *et al* (1995) and Wongwises *et al* (2001) used the HEM to model transient and steady flows in long capillary tubes and found data matching experimental results (Shaik, 2009). This might be due to the fact that in long tubes, the flow has time to reach the equilibrium conditions assumed in the HEM. However, this approach cannot be adapted to simulate flows in pMDIs as in those transient systems, the flow does not have time to reach equilibrium conditions and therefore remains in a constant state of metastability. The HEM was found to underestimate the choking flow rate in short tubes (Shaik, 2009).

Non-homogeneous equilibrium model

The non-homogeneous equilibrium model (NEM) was developed by Moody in 1965 (Elias and Lellouche, 1994). It resembles the HEM but takes into account the slip between the gas and liquid phases. In the NEM, the vapour phase has a higher velocity than the liquid phase. The NEM assumes adiabatic conditions and thermodynamic equilibrium. This approach simulates more realistically the annular flow inside pMDIs, in which the gaseous core has a higher velocity than the peripheral liquid ring.

Separated flow model

In the separated flow model (SFM), developed by Richter in 1981, varying equations are used to describe the behaviour of each phase within the flow (Elias and Lellouche, 1994). The TFM was used by Yang and Zhang (1995) to describe the behaviour of a two-phase critical propellant flow in short tubes (Shaik, 2009). They assumed different velocities and temperatures for each phase. It was found that the predictions from the SFM for this type of flow were more in line with experimental findings than the HEM which underestimated the mass flow rate by approximately 20 % (Shaik, 2009).

2.1.5 Models simulating the internal flow of a pMDI

Clark was the first to model the behaviour of flows inside pMDIs. His model assessed the velocity, the mass flow rate and the size of the droplets forming the aerosol at the nozzle orifice. Clark calculated droplet diameters ranging from 20 μm to 30 μm and droplet velocities of approximately 30 $\mathrm{m{\cdot}s^{-1}}$ (Clark, 1991). Clark also conducted experimental work and used a Dantec phase Doppler particle analyser (PDPA) to measure particles velocity at a distance of 5 cm from the nozzle orifice and reported a 35 $\mathrm{m{\cdot}s^{-1}}$ velocity. He also measured a volume median diameter between 5 μm and 10 μm at this location using a Malvern laser diffraction system (Clark, 1996). The increasing distance from the nozzle orifice might explain the reduction in droplets sizes assessed computationally and experimentally.

Clark developed two models. In the first model, he studied the discharge of a continuous flow through a twin orifice. The pressure in the metering chamber was therefore assumed to be constant and the flow propelled from the metering chamber was pure liquid during the whole aerosolisation process. This type of flow discharge is composed of four stages.

First, the saturated liquid exits the metering chamber through the valve orifice. This process depends on the pressure gradient between the metering and expansion chambers, the density of the propellant and the geometry of the valve orifice. The flow then undergoes evaporation in the expansion chamber leading to the expansion of the propellant until the propellant vapour fills the expansion chamber.
The two-phase flow then exits the expansion chamber through the nozzle orifice. This stage is more complex as it is influenced by the flow conditions in the expansion chamber (quality, temperature, pressure). The flow is then aerosolised outside the canister.

This model assumes that the flow reaches equilibrium when the mass flow rates at valve and nozzle orifices are equal. It could be applied to simulate the discharge from pMDIs if the volume of the expansion chamber in pMDIs was negligible compared to the volume of the metering chamber. This would be the case in a pressurised canister containing no metering chamber, in which the formulation flows directly from the body of the canister to the expansion chamber. This model has shortcomings as in reality the metering and expansion chambers have comparable volumes. For example, Clark used a canister with a metering chamber volume of $100\,\mu$L and an expansion chamber volume of approximately $125\,\mu$L (Shaik, 2009).

Clark refined his model and took into account the fact that the metering chamber empties during the aerosolisation process. In this second model, a pressure drop occurring inside the constant metering chamber volume simulates the discharge of the pre-metered volume. As soon as the aerosolisation process begins, the pressure in the metering chamber decreases. During the discharge of the formulation, the metering chamber pressure is assumed to drop below the saturated vapour pressure corresponding to the metering chamber temperature. This leads to the discharge of a two-phase flow from the metering chamber (Clark, 1991). The present model was inspired by the second simulation from Clark.

Dunbar (1996) also conducted experimental and theoretical work to characterise the aerosols issued from pMDIs. He developed a model for the discharge of a pure propellant two-phase flow. In his model, Dunbar used a metering chamber volume of 63 μL, an expansion chamber volume of 17.6 μL, a valve orifice diameter of 0.7 mm with a discharge coefficient of 0.61 and a nozzle orifice diameter of 0.5 mm with a discharge coefficient of 0.78. He assumed that the velocities of the gas and liquid phases were equal. He calculated a peak velocity of 225 $\mathrm{m{\cdot}s^{-1}}$ and a mass median diameter between 7.9 μm to 20 μm at the nozzle orifice. He found that the discharged formulation was composed of approximately 80% by weight of liquid (Dunbar *et al.*, 1997).

Ju *et al* (2010) improved Dunbar's model by implementing a feature to simulate a multi-component two-phase flow. Their numerical approach assumed that:

- the aerosolisation duration was divided in small time units referred to as time steps
- the velocity remained constant at both valve and nozzle orifices during each time step
- the liquid phase was incompressible
- the flow was adiabatic (no transfer of heat occurred between the formulation and the device or the atmosphere)
- the conditions in the metering chamber remained saturated during the whole discharge process
- the liquid and gas phases did not have similar velocities
- the discharge coefficients were constant throughout the discharge process

To match Dunbar's experimental setting, Ju *et al* (2010) used a nozzle orifice diameter of 0.5 mm when simulating the discharge of pure HFA134a. They calculated exit velocities of 15 $m \cdot s^{-1}$ to 19 $m \cdot s^{-1}$ at the nozzle orifice depending on the concentration of non-volatile components. Those velocity values are considerably lower than Dunbar's. They calculated spray durations of approximately 0.1 s, which is half of that found by Dunbar. These differences could be due to the fact that Ju *et al* calculated separately the characteristics of the liquid and gas phases whereas Dunbar calculated them using similar equations.

Shaik and Versteeg (2008) developed a model simulating the discharge of a pMDI. They calculated the properties of the flow along the axis of the valve and nozzle orifices. They found that the pressure and temperature across the expansion chamber were constant but decreased across the valve and nozzle orifices as the latter represent sudden constrictions. Their work also showed that the quality of the flow in the expansion chamber slightly increased towards the nozzle orifice compared to the area near the valve orifice. They found that the saturated liquid spray leaving the metering chamber becomes metastable upon entering the expansion chamber due to the extremely transient nature of the discharge and the large pressure drop across the valve orifice. This means that while in the expansion chamber, the formulation is made of a metastable liquid, a saturated liquid and a saturated vapour phases (Vacek and Vins, 2009). Shaik and Versteeg also assumed that the flow was a steady state one-dimensional adiabatic flow and that the velocity of the liquid and vapour phases were equal.

A numerical simulation from Aamir and Watkins (2000) modelled the leak of propane from a high-pressured vessel. As the leak is more likely to occur at a draw off pipe, this scenario was studied. The vessel could be compared to the metering chamber while the pipe could represent the expansion chamber, in the present work.

In their model, Aamir and Watkins (2000) assumed that the discharge coefficient was constant and that the flow was quasi-steady which means that it was steady over the duration of each time step. This system assumed different velocities for the gas and liquid phases. The velocity of subcritical liquid and gas phases was determined using the Bernoulli equation. They found a gas velocity and a liquid velocity of approximately $225\,\mathrm{m{\cdot}s^{-1}}$ and $40\,\mathrm{m{\cdot}s^{-1}}$ respectively and a weighed average of approximately $100\,\mathrm{m{\cdot}s^{-1}}$ at the nozzle orifice. This value compares well with Wigley *et al*'s maximum value of $90\,\mathrm{m{\cdot}s^{-1}}$ at the nozzle orifice using phase Doppler anemometry (PDA) (Wigley *et al.*, 2002). However, it is higher than the maximum values of $60\,\mathrm{m{\cdot}s^{-1}}$ to $70\,\mathrm{m{\cdot}s^{-1}}$ found experimentally by Crosland *et al* (2009) using particle image velocimetry (PIV) at the nozzle orifice.

2.1.6 Models simulating the aerosolisation of sprays downstream of the nozzle orifice

The flow characteristics obtained from the models discussed above can be used as inputs conditions for models simulating the aerosolisation process downstream of the nozzle orifice. The latter information is useful as it is difficult to obtain accurate experimental data at the nozzle orifice.

For example, in order to simulate the aerosolisation of the spray issued from a vessel containing highly pressurised liquid propane, Aamir and Watkins (2000) used the outputs such as the quality and velocity of the flow obtained from their simulation described in Section 2.1.5. They found velocities of approximately $22\,\mathrm{m{\cdot}s^{-1}}$ and mean diameters of $15\,\mu\mathrm{m}$ at a distance of 5 cm from the nozzle orifice. This value is in agreement with the experimental value of $20\,\mathrm{m{\cdot}s^{-1}}$ obtained by Allen when studying propane jets (Aamir and Watkins, 2000).

Stein *et al* (2012) built a model simulating the aerosolisation of suspension formulations. Most of their work focused on the size of the residual droplets from suspension formulations. For example, their model can calculate the effect of drug concentration, size of the suspended drug particles and size of the initial droplets on the residual size of the droplets in suspension formulations. It can also predict the probability of droplets containing zero, one or more drug particles. The model can take into account the geometric standard deviation (GSD) of the formulation and several geometric characteristics of the pMDI such as the volume of the metering chamber and the size of the valve orifice. The limitations of this model are that it uses samples of 10 000 droplets containing drug particles although tens to hundreds of millions are produced in reality. It is also restricted to the simulation of aerosols containing one type of drug.

The inputs needed to run Stein *et al*'s simulation include the properties of the formulation, the size distribution of the micronised drug particles and the size distribution of the initial droplets. Stein *et al* deemed models calculating the initial droplets size too computationally intensive and questioned their accuracy on such volatile formulations. They also judged that experimental measurements would not be sufficiently accurate at the nozzle orifice to calculate the initial droplets size. For those reasons, they developed a semi-empirical model using Equation (2.3) correlating the residual size of droplets obtained experimentally to the size of the initial droplets.

$$MMD_{in} = MMD_{re} \left(\frac{\rho_{in} C_{NV}}{\rho_{re}} \right)^{-\frac{1}{3}} \tag{2.3}$$

where MMD_{in} and MMD_{re} are respectively the mass median diameters of the initial and residual droplets in μm, ρ_{in} and ρ_{re} are respectively the densities of the initial and residual droplets in kg·m^{-3} and C_{NV} is the concentration of non-volatiles (weight fraction). Equation (2.3) fails to account for all elements of secondary atomisation, which could lead to a poor accuracy of the initial droplets size.

Using Equation (2.3) to calculate initial droplet diameters while changing several experimental conditions, Stein *et al* obtained Equation (2.4) correlating the size of the initial droplets to several formulation and design parameters.

$$MMD_{in} = 6.90 + 0.0441 \times V_{mc} + 23.6 \times C_{EtOH} - 63.8 \times C_{EtOH}^2 + 24.7 \times C_{EtOH} \times d_{no} - 0.129 \times C_{EtOH} \times V_{mc} \quad (2.4)$$

where V_{mc} is the volume of the metering chamber in μL, C_{EtOH} is the concentration of ethanol (weight fraction) and d_{no} is the nozzle orifice diameter in mm. Equation (2.4) was initially developed by Stein *et al* (2004) to characterise the initial droplets size of solution formulations. As it was used by Stein *et al* (2012) to assess the initial droplets size of suspension formulations, their determination of the initial droplets size might not be accurate.

2.1.7 Aims and objectives

pMDI flows are complex to study as they involve turbulence, phase changes, density changes as well as pressure fluctuations (Sher *et al.*, 2008). The nozzle orifice is very small with a length of about 1 mm and a diameter smaller than 1 mm, the flow exiting the nozzle has a very high velocity and lasts only a fraction of second. As a result, experimental measurements of the flow properties outside the nozzle orifice are difficult to realise. Experimental measurements of the flow as it exits pMDIs consist mainly of visualisation of the flow inside the expansion chamber and at the nozzle orifice (Versteeg *et al.*, 2006).

Numerical solutions are of great interest as they represent a mean to obtain quantitative information on the flow at the nozzle orifice. Flow characteristics at this location are useful as they can be used as inputs to models describing the aerosoli-

sation of the flow downstream of the nozzle orifice.

The aim of this chapter was to create a computational model simulating the behaviour of the flow inside a pMDI upon actuation of the device. The flow was assumed to be one-dimensional and the flow properties were calculated at the nozzle orifice which was assumed to be two-dimensional. It was thus decided that a three dimensional computational fluid dynamics model was not necessary to simulate the discharge of a pMDI formulation and a one-dimensional Matlab-based simulation was designed.

This simulation could represent a fast and easy way to study the effect of certain parameters on the exit properties of the flow at the nozzle orifice. This chapter outlines the equations used in the simulation. The results and novel features of the model will be shown in the next chapter.

2.2 Assumptions

Some of the assumptions reported in previous work from Clark (1991), Dunbar (1996), Aamir and Watkins (2000) and Ju *et al* (2010) were used in the present model.

- As pMDIs containing solely propellant were studied, a one-component model was used.
- The flow inside the pMDI was assumed to be steady over each time step. This assumption is valid if short time steps are used which was the case in the present model (dt <0.0005 s, where dt is a time step).
- The flow was assumed to be one-dimensional. A 50 μL non-continuous valve from Valois (Valois pharmaceutical division, 780160 Marly Le Roi, France)

was measured with a Mitutoyo Dial Caliper 150 mm with a resolution of 0.01 mm. The length of the expansion chamber was found to be 8.05 mm. As the nozzle orifice of diameter <0.5 mm is relatively small compared to the length of the expansion chamber, the assumption of a one-dimensional flow is reasonable.

- The valve and nozzle orifices were assumed to be two-dimensional. As they have small lengths (<1 mm) compared to the metering and expansion chambers, this assumption was deemed reasonable (Shaik, 2009).

- The Bernoulli equation was assumed valid at the first time step to describe the discharge of the propellant from the metering chamber. This is a valid assumption as the flow is an incompressible liquid at initial conditions.

- The Bernoulli equation was also assumed valid for 2-phase flows at sub-critical conditions. This assumption was also used in the model developed by Aamir and Watkins (2000).

- At each time step, a state of equilibrium was assumed so that the principle of mass and energy conservation could be used in the system.

- In the metering chamber, the two phases were assumed to be in saturated conditions during the whole aerosolisation process.

- The flow properties were assumed to be constant across the expansion chamber. This is not completely accurate as Shaik and Versteeg showed that several properties changed as the flow travelled along the expansion chamber. For example, the quality of the flow increased closer to the nozzle orifice. However, pressure and temperature were evenly distributed across the expansion chamber (Shaik and Versteeg, 2008). As the aim of this chapter was to build a one-dimensional simulation, the variation of properties within the ex-

pansion chamber was not possible to model and was beyond the scope of the current research.

- The pressure in the expansion chamber was calculated by assuming that the gas propellant was an ideal gas.
- The effect of gravity was neglected.

2.3 Initial conditions

- The initial temperature in both the metering and expansion chambers corresponded to ambient temperature.
- The metering chamber was filled with HFA134a at the saturated vapour pressure corresponding to the initial temperature. It follows that as soon as the pressure dropped (due to propellant discharge) the void caused by the emptying of the metering chamber was filled with gaseous propellant. As a result, the flow exiting the metering chamber contained both a gaseous and liquid phases throughout the aerosolisation process except at the onset of the actuation.
- The initial specific enthalpy and density of the propellant in the metering chamber were set to the value of saturated liquid HFA134a enthalpy and density at the specified room temperature.
- At initial conditions, the expansion chamber was filled with air at atmospheric pressure.
- The initial specific enthalpy and density in the expansion chamber were set to the value of air enthalpy and density at the specified room temperature (Rogers and Mayhew, 1995).

2.4 Program outline

The Matlab-based model initiates upon actuation of the device and runs until the pressure in the expansion chamber equals atmospheric pressure (at which point the propellant is no longer propelled out of the device).

At initial conditions, the metering chamber contained pure liquid and became a 2-phase flow system at the subsequent time step. For this reason, a loop was designed that contained all calculations except the calculation of metering chamber properties at initial conditions and mass flow rate at the valve orifice at the onset of the actuation.

Once the mass flow rate at the onset of the actuation was calculated, the program entered the loop that re-iterated calculations until the pressure in the expansion chamber equalled atmospheric pressure. Inside the loop, the program calculated the system's thermodynamic properties in the expansion chamber, then in the metering chamber.

In both chambers the temperature was calculated using energy equations. In the metering chamber, the pressure and other thermodynamic properties were calculated as a function of the temperature as the propellant was assumed to be under saturated conditions. In the expansion chamber, the pressure was calculated as the sum of air pressure and propellant vapour pressure.

The pressure gradient at both orifices was used to determine whether the flow was critical or subcritical (depending on whether the ratio of downstream to upstream pressures was higher or smaller than the critical pressure ratio) at each time step.

The velocities and mass flow rates at both orifices were then determined based on the state of the flow (critical or subcritical), during the time step interval.

Once the loop was finished the program went back into the loop to calculate the thermodynamic properties at the subsequent time step. Those calculations continued until the pressure in the expansion chamber equalled atmospheric pressure.

2.5 Program step by step

2.5.1 Metering and expansion chambers at initial conditions

Figure 2.3 representing a canister, shows specific dimensions used in the simulation.

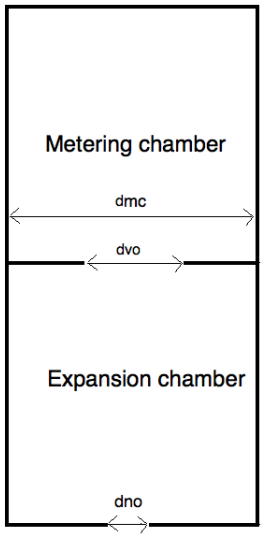

Figure 2.3: Schematic of a canister where d_{mc} is the diameter of the metering chamber in m, d_{vo} is the diameter of the valve orifice in m and d_{no} is the diameter of the nozzle orifice in mm.

The geometrical properties of the pMDI such as the valve and nozzle orifice diameters, the discharge coefficients at both orifices and the metering and expansion chamber volumes were listed at the beginning of the simulation and are presented

in Table 3.1 in Chapter 3.

The properties inside the expansion and metering chambers at initial conditions were defined.

$$T_{ec} = T_{amb} \tag{2.5}$$

where T_{ec} is the temperature in the expansion chamber and T_{amb} is the ambient temperature in K.

$$P_{ec} = P_{atm} \tag{2.6}$$

where P_{ec} is the pressure in the expansion chamber and P_{atm} is the atmospheric pressure in Pa.

Equations (2.7), used to calculate air density, was computed based on thermodynamic tables from Rogers and Mayhew (1995) using Matlab and is listed in the Appendix.

$$\rho_{ec} = \rho_{air} = f(T_{ec}) \tag{2.7}$$

where ρ_{ec} is the density in the expansion chamber and ρ_{air} is the density of air in $\mathrm{kg{\cdot}m^{-3}}$ (Rogers and Mayhew, 1995).

$$h_{ec} = h_{air} = Cp_a\, T_{ec} \tag{2.8}$$

where h_{ec} is the specific enthalpy in the expansion chamber in $\mathrm{kJ{\cdot}kg^{-1}}$, h_{air} is the specific enthalpy of air in $\mathrm{kJ{\cdot}kg^{-1}}$ and Cp_a is the specific heat capacity of air at constant pressure in $\mathrm{kJ{\cdot}kg^{-1}K^{-1}}$. It was assumed that Cp_a was constant which is reasonable as its value varies from $1.0023\,\mathrm{kJ{\cdot}kg^{-1}{\cdot}K^{-1}}$ at 175 K to $1.0063\,\mathrm{kJ{\cdot}kg^{-1}{\cdot}K^{-1}}$ at 325 K (Rogers and Mayhew, 1995).

It was assumed that the metering chamber was entirely filled with HFA134a propellant at saturated conditions. For this reason, the pressure, density and enthalpy

were assumed to be a function of the temperature in the metering chamber as shown in Equations (2.10), (2.11), (2.12).

$$T_{mc} = T_{amb} \tag{2.9}$$

where T_{mc} is the temperature in the metering chamber in K.

$$P_{mc} = f(T_{mc}) \tag{2.10}$$

where P_{mc} is the pressure in the metering chamber in Pa.

$$\rho_{mc} = f(T_{mc}) \tag{2.11}$$

where ρ_{mc} is the density of the propellant in the metering chamber in $\mathrm{kg{\cdot}m^{-3}}$.

$$h_{mc} = f(T_{mc}) \tag{2.12}$$

where h_{mc} is the specific enthalpy of the propellant in the metering chamber in $\mathrm{kJ{\cdot}kg^{-1}}$. Several equations determining thermodynamic properties of HFA134a were studied. For example, for the calculations of the pressure and density of HFA134a, the equations from Tan and Shua (2003) and equations from Dupont's technical report were compared to the Klea134a thermodynamic tables (Dupont, 2004), (Klea134a, 2011). Equations (2.10) to (2.12) are listed in the Appendix.

2.5.2 First time step

At the onset of the actuation, the flow was assumed to be incompressible (single phase fluid). The Bernoulli equation could therefore be applied between the metering and valve orifice to calculate the velocity of the flow at the valve orifice. The

Bernoulli equation as implemented in Matlab is shown in Equation (2.13).

$$P_{mc} + \frac{1}{2}\ \rho lp_{mc}\ U_{mc}^2 = P_{vo} + \frac{1}{2}\ \rho lp_{vo}\ U_{vo}^2 \tag{2.13}$$

where ρlp_{mc} and ρlp_{vo} are respectively the liquid densities of HFA134a in the metering chamber and at the valve orifice in kg·m^{-3}, U_{mc} and U_{vo} are the flow velocities in the metering chamber and at the valve orifice respectively in m·s^{-1} and P_{vo} is the pressure at the valve orifice in Pa. The pressure at the valve orifice was assumed to be equal to the pressure in the expansion chamber so that Equation (2.13) became Equation (2.14). As the valve orifice was assumed to be two-dimensional, this assumption was reasonable.

$$P_{mc} + \frac{1}{2}\ \rho lp_{mc}\ U_{mc}^2 = P_{ec} + \frac{1}{2}\ \rho lp_{vo}\ U_{vo}^2 \tag{2.14}$$

As the mass flow rate was assumed to be constant between the metering chamber and the valve orifice over each time step, Equation (2.15) was assumed valid for metering chambers of circular cross-sections.

$$\rho lp_{mc}\ \frac{\pi}{4}\ {d_{mc}}^2\ U_{mc} = \rho lp_{vo}\ \frac{\pi}{4}\ d_{vo}^2\ U_{vo} \tag{2.15}$$

where d_{mc} is the diameter of the metering chamber and d_{vo} is the diameter of the valve orifice in m (as shown in Figure 2.3). As the flow is incompressible at the onset of the actuation, it was assumed that ρlp_{mc} and ρlp_{vo} were equal. As a result, Equations (2.14) and (2.15) became respectively Equations (2.16) and (2.17).

$$P_{mc} + \frac{1}{2}\ \rho l\ U_{mc}^2 = P_{ec} + \frac{1}{2}\ \rho l\ U_{vo}^2 \tag{2.16}$$

where ρl is the density of the propellant at room temperature in kg·m^{-3}.

$$d_{mc}{}^2 \; U_{mc} = d_{vo}^2 \; U_{vo} \tag{2.17}$$

From Equation (2.17), Equation (2.18) was obtained.

$$U_{mc} = \frac{d_{vo}{}^2}{d_{mc}{}^2} \; U_{vo} \tag{2.18}$$

By substituting Equation (2.18) into Equation (2.16), Equation (2.19) was obtained.

$$P_{mc} + \frac{1}{2} \; \rho l \left(\frac{d_{vo}{}^2}{d_{mc}{}^2} \; U_{vo} \right)^2 = P_{ec} + \frac{1}{2} \; \rho l \; U_{vo}{}^2 \tag{2.19}$$

By simplifying Equation (2.19), Equation (2.20) was obtained.

$$2 \; \frac{(P_{mc} - P_{ec})}{\rho l} = U_{vo}{}^2 \; \left(1 - \frac{d_{vo}{}^4}{d_{mc}{}^4} \right) \tag{2.20}$$

The distances d_{mc} and d_{vo} were measured and were found to have values of respectively 5 mm and 0.55 mm, giving a value of 0.00015 to the ratio $\frac{d_{vo}{}^4}{d_{mc}{}^4}$. As $\frac{d_{vo}{}^4}{d_{mc}{}^4}$ is considerably smaller than the value of 1 to which it is subtracted in Equation (2.20), the term $\frac{d_{vo}{}^4}{d_{mc}{}^4}$ was neglected and Equation (2.21) was obtained.

$$U_{vo} = \sqrt{\frac{2(P_{mc} - P_{ec})}{\rho l}} \tag{2.21}$$

The mass flow rate out of the metering chamber at the onset of the actuation was calculated using Equation (2.22).

$$\dot{m}p_{vo} = \rho l \; U_{vo} \; A_{vo} \tag{2.22}$$

where $\dot{m}p_{vo}$ is the mass flow rate of propellant at the valve orifice in kg·s^{-1} and A_{vo} is the valve orifice area in m^2. By replacing U_{vo} into Equation (2.22) using

Equation (2.21), Equation (2.23) was obtained.

$$\dot{m}p_{vo} = A_{vo}\ \rho l\ \sqrt{\frac{2(P_{mc} - P_{ec})}{\rho l}} \tag{2.23}$$

When simplifying Equation (2.23), Equation (2.24) was obtained.

$$\dot{m}p_{vo} = \sqrt{2\rho l\ (P_{mc} - P_{ec})}\ A_{vo} \tag{2.24}$$

in which $A_{vo} = \frac{\pi}{4}\ {d_{vo}}^2$. When taking the discharge coefficient into account,

$$A_{vo} = \frac{\pi}{4}\ {d_{vo}}^2\ Cd_{vo} \tag{2.25}$$

where Cd_{vo} is the discharge coefficient of the valve orifice. Discharge coefficients are defined by Equation (2.26).

$$Cd = \frac{\dot{m}_{real}}{\dot{m}_{ideal}} \tag{2.26}$$

where $\dot{m}_{real}$ is the real mass flow rate in kg·s^{-1} and $\dot{m}_{ideal}$ is the ideal mass flow rate in kg·s^{-1}. The ideal mass flow rate does not take into account the limit of mass flow due to the vena contracta effect shown in Figure 2.4.

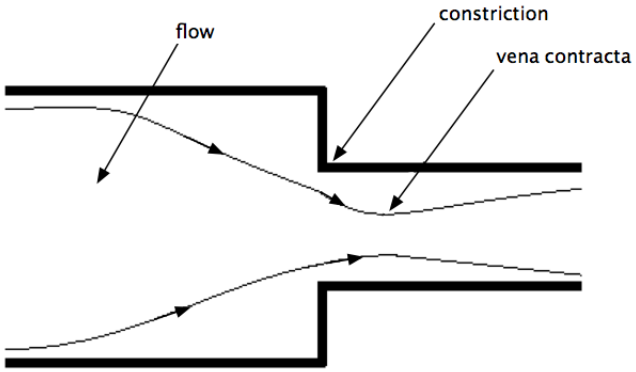

Figure 2.4: Schematic of a flow going through a constriction.

Discharge coefficients are used when a flow passes through a constriction, which is the case between the metering chamber and the expansion chamber.

The difference of pressure after a constriction such as the valve orifice causes the area of the flow to become smaller after the constriction. The point of minimum area is referred to as vena contracta. The size of the vena contracta depends on the velocity, the viscosity and the density of the fluid. In this work, the discharge coefficients enabled the model to take into account the flow constrictions at the valve and nozzle orifices. Discharge coefficients at the valve orifice were shown to range from 0.4 to 0.8 for pMDIs with valve orifice diameters values between 0.259 mm and 1.066 mm (Clark, 1991).

2.5.3 Iterative calculation loop

After the calculation of the liquid propellant velocity at the onset of the actuation from the metering chamber to the expansion chamber, the program enters a loop calculating the conditions in the entire system (i.e. the metering and expansion chambers as well as the valve and nozzle orifices) until the end of the aerosolisation process.

The loop states that:

- the model continues running only if $P_{ec} \geq P_{atm}$
- if $P_{mc} > P_{ec}$ the flow velocity between the metering and expansion chambers must be calculated otherwise it must be set to zero, assuming there is no back flow into the metering chamber.

2.5.3.1 Expansion chamber

After the discharge of the propellant from the metering chamber at the onset of the actuation, the conditions inside the expansion chamber are updated. The mass of each phase (liquid and vapour) in the expansion chamber corresponds to the mass at the previous time step plus the mass coming from the metering chamber minus the mass leaving the expansion chamber in that time step. The masses of the liquid and vapour phases were calculated using Equations (2.27) and (2.28) respectively.

$$mlp_{ec}^{n} = mlp_{ec}^{o} + (\dot{mlp}_{vo}^{o} - \dot{mlp}_{no}^{o})\ dt \tag{2.27}$$

where mlp_{ec} corresponds to the mass of liquid propellant in the expansion chamber in kg, $\dot{mlp}_{vo}$ is the mass flow rate of the liquid phase at the valve orifice in kg·s^{-1}, $\dot{mlp}_{no}$ is the mass flow rate of the liquid phase at the nozzle orifice in kg·s^{-1}, dt corresponds to the time step in s and the superscripts "o" and "n" refer to the previous and current time step values respectively.

$$mvp_{ec}^{n} = mvp_{ec}^{o} + (\dot{mvp}_{vo}^{o} - \dot{mvp}_{no}^{o})\ dt \tag{2.28}$$

where mvp_{ec} corresponds to the mass of propellant vapour in the expansion chamber in kg, $\dot{mvp}_{vo}$ is the mass flow rate of the propellant vapour phase at the valve orifice

in kg·s^{-1} and $\dot{m}vp_{no}$ is the mass flow rate of the propellant vapour phase at the nozzle orifice in kg·s^{-1}.

The mass of air in the expansion chamber was calculated by subtracting the mass of air leaving the expansion chamber from the mass of air at the preceding time step as shown in Equation (2.29).

$$ma_{ec}^{n} = ma_{ec}^{o} - \dot{m}a_{no}\ dt \tag{2.29}$$

where ma_{ec} corresponds to the mass of air in the expansion chamber in kg and $\dot{m}a_{no}$ is the mass flow rate of air at the nozzle orifice in kg·s^{-1}.

The total enthalpy in the expansion chamber is calculated using Equation (2.30).

$$H_{ec}^{n} = H_{ec}^{o} + (\dot{m}p_{vo}\ dt\ h_{mc})^{o} - (\dot{m}_{no}\ dt\ h_{ec})^{o} \tag{2.30}$$

where H_{ec} is the total enthalpy in the expansion chamber in kJ, h_{mc} and h_{ec} are the specific enthalpies in the metering and expansion chambers respectively in kJ·kg^{-1} and $\dot{m}_{no}$ is the total mass flow rate at the nozzle orifice in kg·s^{-1}.

The total enthalpy in the expansion chamber defined in Equation (2.30) is also equal to the sum of liquid propellant, vapour propellant and air enthalpies as shown in Equation (2.31).

$$H_{ec} = Hlp_{ec} + Hvp_{ec} + Ha_{ec} = mlp_{ec}\ hlp_{ec} + mvp_{ec}\ hvp_{ec} + ma_{ec}\ ha_{ec} \tag{2.31}$$

where Hlp_{ec}, Hvp_{ec}, Ha_{ec} are the total enthalpies in the expansion chamber of the propellant liquid phase, propellant vapour phase and of air respectively in kJ and hlp_{ec}, hvp_{ec}, ha_{ec} are the specific enthalpies in the expansion chamber of the propellant liquid phase, propellant vapour phase and of air respectively in kJ·kg^{-1}.

In order to find the temperature and flow characteristics in the expansion chamber at the new time step, the specific enthalpy of the liquid and vapour phases in Equation (2.31) are respectively replaced by Equations (2.32), and (2.33) with unknown constant u from the Mexichem Fluor website (Klea134a, 2011).

$$hlp_{ec} = A_1 + B_1 u + C_1 u^2 + D_1 u^3 + E_1 u^4 \tag{2.32}$$

$$hvp_{ec} = A_2 + B_2 u + C_2 u^2 + D_2 u^3 + E_2 u^4 \tag{2.33}$$

where A_1, B_1, C_1, D_1, E_1, A_2, B_2, C_2, D_2 and E_2 correspond to the coefficients of the specific liquid and vapour enthalpy equations listed in the Appendix and u is related to the expansion chamber temperature through Equation (2.34) (Klea134a, 2011).

$$u = \sqrt[3]{1 - \frac{T_{ec}}{T_{crit}}} \tag{2.34}$$

where T_{crit} corresponds to the critical temperature of the propellant in K.

The thermodynamic properties in the expansion chamber were then calculated based on the new temperature. The density of the liquid propellant in the expansion chamber was calculated using Equation (2.11) listed in the Appendix (Klea134a, 2011).

The volume of the gas phase in the expansion chamber was calculated using Equation (2.35).

$$Vv_{ec} = V_{ec} - \frac{mlp_{ec}}{\rho lp_{ec}} \tag{2.35}$$

where Vv_{ec} is the total volume of the vapour phase (i.e. including air and propellant) in the expansion chamber in m^3, V_{ec} is the volume of the expansion chamber in m^3 and ρlp_{ec} is the density of the liquid phase of the propellant in the expansion chamber in $kg \cdot m^{-3}$. The density of the total vapour phase (taking into account

both gas propellant and air) can be calculated using Equation (2.36).

$$\rho v_{ec} = \frac{mvp_{ec} + ma_{ec}}{Vv_{ec}} \tag{2.36}$$

where ρv_{ec} is the density of the vapour in the expansion chamber in kg·m^{-3}.

The average density in the expansion chamber can then be calculated as shown in Equation (2.37).

$$\overline{\rho_{ec}} = \frac{(mvp_{ec} + ma_{ec} + mlp_{ec})}{V_{ec}} \tag{2.37}$$

where $\overline{\rho_{ec}}$ is the average density inside the expansion chamber in kg·m^{-3}. The quality in the expansion chamber was calculated based on the new masses in the expansion chamber as shown in Equation (2.38).

$$q_{ec} = \frac{mvp_{ec} + ma_{ec}}{mvp_{ec} + ma_{ec} + mlp_{ec}} \tag{2.38}$$

where q_{ec} is the quality of the flow in the expansion chamber. The pressures of the vapour propellant and air phases were calculated by assuming that both propellant vapour and air behaved like perfect gases using Equations (2.39) and (2.40) respectively.

$$Pvp_{ec} = \frac{mvp_{ec}\ \frac{Ru}{M_p}\ T_{ec}}{Vv_{ec}} \tag{2.39}$$

where Pvp_{ec} is the pressure of the propellant vapour in the expansion chamber in Pa, Ru is the universal gas constant in kJ·K^{-1}kmol^{-1} and M_p is the molecular mass of propellant in kg·kmol^{-1}.

$$Pa_{ec} = \frac{ma_{ec}\ \frac{Ru}{Ma}\ T_{ec}}{Vv_{ec}} \tag{2.40}$$

where Pa_{ec} is the pressure of air in the expansion chamber in Pa and Ma is the molar mass of dry air in kg·kmol^{-1} (Rogers and Mayhew, 1995).

The total pressure in the expansion chamber is the sum of the air pressure and vapour propellant pressure and was calculated as shown in Equation (2.41).

$$P_{ec} = Pa_{ec} + Pvp_{ec} \tag{2.41}$$

The flow exiting the expansion chamber can exhibit two behaviours which are critical and subcritical. The equations used to determine the gas and liquid velocities depended on the flow regime which was first calculated at the nozzle orifice using Equation (2.42).

$$Ra_{crit} = \frac{2}{\gamma + 1}^{\frac{\gamma}{\gamma - 1}} \tag{2.42}$$

$\gamma = \frac{Cp_g}{Cp_g - \frac{R}{M_p}}$ where Cp is the specific heat capacity of the vapour phase in $\mathrm{kJ \cdot kg^{-1} \cdot K^{-1}}$ calculated as a function of the new temperature in the expansion chamber. The flow is critical when Equation (2.43) is valid.

$$Ra_{crit} = \frac{P_{ds}}{P_{us}} \tag{2.43}$$

At the nozzle orifice location, Equation (2.43) becomes Equation (2.44).

$$Ra_{crit} = \frac{P_{atm}}{P_{ec}} \tag{2.44}$$

The flow is subcritical when Equation (2.45) defined earlier in this chapter is valid.

$$Ra_{crit} > \frac{P_{ds}}{P_{us}} \tag{2.45}$$

When the flow is subcritical, the Bernoulli equation can be applied and the liquid and gas phase velocities at the nozzle orifice are calculated using Equations (2.46)

and (2.47) respectively.

$$Ul_{no} = \sqrt{\frac{2(P_{ec} - P_{atm})}{\rho l p_{ec}}} \tag{2.46}$$

where Ul_{no} is the velocity of the liquid phase at the nozzle orifice in $\mathrm{m{\cdot}s^{-1}}$.

$$Uv_{no} = \sqrt{\frac{2(P_{ec} - P_{atm})}{\rho v_{ec}}} \tag{2.47}$$

where Uv_{no} is the velocity of the vapour phase at the nozzle orifice in $\mathrm{m{\cdot}s^{-1}}$.

At critical conditions, ($Ra_{crit} \leq \frac{P_{atm}}{P_{ec}}$), the Bernoulli equation cannot be used because the velocity no longer depends on downstream conditions. From Equation (2.44), $P_{atm} = Ra_{crit}\ P_{ec}$, one obtains Equation (2.48) for the calculation of the liquid phase velocity.

$$Ul_{no\,crit} = \sqrt{\frac{2(P_{ec} - P_{ec}Ra_{crit})}{\rho l p_{ec}}} \tag{2.48}$$

Gas velocity at the nozzle orifice is calculated using Equation (2.49).

$$Uv_{no\,crit} = \sqrt{\frac{\gamma P_{ec} Ra_{crit}^{\frac{\gamma-1}{\gamma}}}{\rho v_{ec}}} \tag{2.49}$$

Equations (2.48) and (2.49) were also used by Aamir and Watkins (2000) in their simulation of high-pressured propane leakage.

The liquid and vapour mass flow rates were calculated using Equations (2.50) and (2.51) respectively.

$$\dot{ml}p_{no} = A_{no}\ (1 - q_{ec})\ \overline{\rho_{ec}}\ Ul_{no} \tag{2.50}$$

$$\dot{mv}_{no} = A_{no}\ q_{ec}\ \overline{\rho_{ec}}\ Uv_{no} \tag{2.51}$$

where $\dot{m}v_{no}$ is the total mass flow rate of the vapour phase at the nozzle orifice in kg·s^{-1}. The total mass flow rate at the nozzle orifice was calculated using Equation (2.52).

$$\dot{m}_{no} = \dot{m}lp_{no} + \dot{m}v_{no} \tag{2.52}$$

Clark attempted to correlate the size of particles exiting the nozzle orifice to different factors such as vapour pressures, orifice diameter ratios and surfactant concentrations (Clark, 1991). He measured the residual size of the particle in a large volume holding chamber 5 s after actuating the pMDI. From the residual size of the droplets, he worked back the theoretical initial particle size. He then developed Equation (2.53), correlating the initial particles size to the quality and pressure in the expansion chamber. His correlation matched his experimental data.

$$MMD = \frac{8.02}{q_{ec}^{0.56}(\frac{P_{ec} - P_{atm}}{P_{atm}})^{0.46}} \tag{2.53}$$

where MMD is the mass median diameter of the formulation in μm. This correlation is consistent with experimental results using CFC and HFA134a propellants (Smyth, 2003). However Equation (2.53) cannot be used at the onset and at the end of the discharge process, as when $P_{ec} \rightarrow P_{atm}$, $MMD \rightarrow \infty$. The size of the particles at the nozzle orifice was therefore calculated only during the first half of the spray duration. Equation (2.53) also assumes that the initial size of the droplets is not influenced by the size of the nozzle orifice, which might not be a valid assumption (Berry *et al.*, 2003).

2.5.3.2 Metering chamber

The quality of the flow and other thermodynamic properties were then determined in the metering chamber. The mass of the propellant in the metering chamber

corresponds to the mass of propellant in the metering chamber at the previous time step minus the mass that left the metering chamber as shown in Equation (2.54).

$$mp^{n}_{mc} = mp^{o}_{mc} - \dot{m}p^{o}_{vo}\, dt \tag{2.54}$$

where mp_{mc} is the mass of propellant in the metering chamber in kg. The metering chamber contains a liquid and a vapour phase. The masses of each phase can be calculated using Equations (2.55) and (2.56) respectively.

$$mlp_{mc} = mp_{mc}\ (1 - q_{mc}) \tag{2.55}$$

where mlp_{mc} is the mass of liquid propellant in the metering chamber in kg and q_{mc} is the quality of the propellant in the metering chamber.

$$mvp_{mc} = mp_{mc}\ q_{mc} \tag{2.56}$$

where mvp_{mc} is the mass of vapour propellant in the metering chamber in kg.

The enthalpy at a new time step is calculated in the metering chamber using Equation (2.57).

$$H^{n}_{mc} = H^{o}_{mc} - (\dot{m}p_{vo}\ dt\ h_{mc})^{o} \tag{2.57}$$

where H_{mc} is the total enthalpy in the metering chamber in kJ.

The new total enthalpy in the metering chamber can also be calculated from the specific enthalpies of the propellant as shown in Equation (2.58).

$$H_{mc} = mlp_{mc}\ hlp_{mc} + mvp_{mc}\ hvp_{mc} - (mvp_{mc} - mvp^{o}_{mc})\, hlvp_{mc} \tag{2.58}$$

where hlp_{mc}, hvp_{mc} and $hlvp_{mc}$ are respectively the specific enthalpies of the liquid phase, the vapour phase and the specific enthalpy of vaporisation of the propellant

in the metering chamber in kJ·kg^{-1}.

As in the expansion chamber, the temperature was found by replacing each specific enthalpy by its polynomial form in the energy equation. The program implemented the 4th order equations of state with unknown constant u as shown in Equations (2.59), (2.60) and (2.61).

$$hlp_{mc} = A_1 + B_1 u + C_1 u^2 + D_1 u^3 + E_1 u^4 \tag{2.59}$$

$$hvp_{mc} = A_2 + B_2 u + C_2 u^2 + D_2 u^3 + E_2 u^4 \tag{2.60}$$

$$hlvp_{mc} = A_3 + B_3 u + C_3 u^2 + D_3 u^3 + E_3 u^4 \tag{2.61}$$

$$u = \sqrt[3]{1 - \frac{T_{mc}}{T_{crit}}} \tag{2.62}$$

When Equation (2.58) was implemented in Matlab with each enthalpy term replaced by its approximation equation (Equations (2.59), (2.60) and (2.61)), u was calculated and used to find the new metering chamber temperature.

As the formulation in the metering chamber was assumed to be under saturated conditions, its pressure, its density and its enthalpy could be solved as functions of the temperature using the equations listed in the Appendix.

Equation (2.63) was implemented in Matlab in order to find the quality at the new time step.

$$q_{mc} = \frac{h_{mc} - hlp_{mc}}{hvp_{mc} - hlp_{mc}} \tag{2.63}$$

As in the expansion chamber, the specific heat capacity of the propellant and γ were calculated in order to determine the flow regime at the valve orifice.

Similar types of calculations as for the nozzle orifice were repeated to find the velocities and mass flow rates at the valve orifice. At the valve orifice, Equation (2.43)

became Equation (2.64).

$$Ra_{crit} = \frac{P_{ec}}{P_{mc}} \tag{2.64}$$

The velocities of the gas and liquid phases at the valve orifice at subcritical conditions were calculated using Equations (2.65) and (2.66) respectively.

$$Ul_{vo} = \sqrt{\frac{2(P_{mc} - P_{ec})}{\rho lp_{mc}}} \tag{2.65}$$

where Ul_{vo} is the liquid velocity of the propellant at the valve orifice in $\mathrm{m{\cdot}s^{-1}}$.

$$Uv_{vo} = \sqrt{\frac{2(P_{mc} - P_{ec})}{\rho vp_{mc}}} \tag{2.66}$$

where Uv_{vo} is the velocity of the propellant vapour at the valve orifice in $\mathrm{m{\cdot}s^{-1}}$ and ρvp_{mc} is the propellant vapour density in the metering chamber in $\mathrm{kg{\cdot}m^{-3}}$.

At critical conditions, ($Ra_{crit} \leq \frac{P_{ec}}{P_{mc}}$), Equations (2.67) and (2.68) were used for the calculation of the liquid and gas phase velocities respectively.

$$Ul_{vo\,crit} = \sqrt{\frac{2(P_{mc} - P_{mc}Ra_{crit})}{\rho lp_{mc}}} \tag{2.67}$$

$$Uv_{vo\,crit} = \sqrt{\frac{\gamma P_{mc} Ra_{crit}^{\frac{\gamma-1}{\gamma}}}{\rho vp_{mc}}} \tag{2.68}$$

The liquid and vapour mass flow rates were calculated using Equations (2.69) and (2.70) respectively.

$$\dot{m}l_{vo} = A_{vo}\ (1 - q_{mc})\ \overline{\rho_{mc}}\ Ul_{vo} \tag{2.69}$$

$$\dot{m}v_{vo} = A_{vo}\ q_{mc}\ \overline{\rho_{mc}}\ Uv_{vo} \tag{2.70}$$

The total mass flow rate at the valve orifice was calculated using Equation (2.71).

$$\dot{m}_{vo} = \dot{m}l_{vo} + \dot{m}v_{vo} \tag{2.71}$$

Once the flow characteristics were calculated throughout the system, the simulation went back into the loop until the pressure in the expansion chamber became atmospheric. A flow chart of the model can be seen in Figure 2.5.

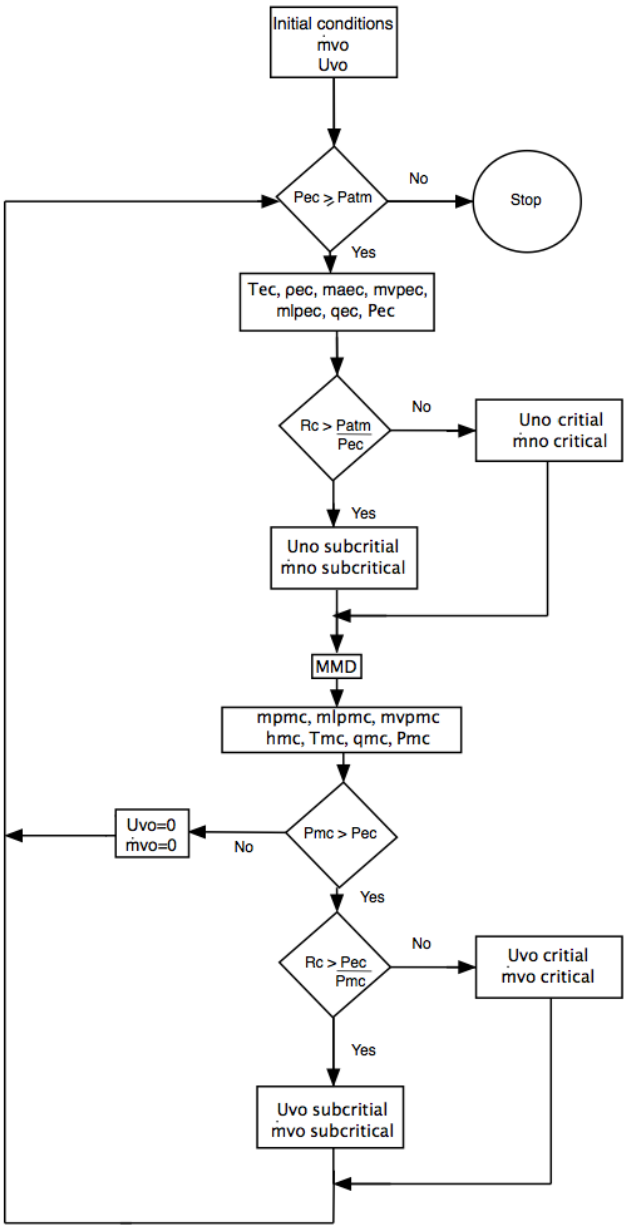

Figure 2.5: Flow chart of the simulation

2.6 Summary

A one-dimensional Matlab model simulating the discharge of a pMDI spray was developed. Since the current model calculates two different flow velocities for the vapour and liquid phases, it may offer greater accuracy than previous simulations. The model was used to calculate spray characteristics such as velocity, mass flow rate and particles size at the nozzle orifice. The results and novel features obtained from the simulation will be discussed in the next chapter.

Chapter 3

Theoretical analysis of metered dose inhaler actuation using a one-dimensional computational model

3.1 Introduction

3.1.1 Effects of different parameters on the properties of pMDIs sprays at the nozzle orifice

In Chapter 1, it was seen that the behaviour of pMDI sprays might be influenced by several factors such as device design, formulation design, exterior conditions and handling of the device. In this chapter, the role of certain parameters on the spray properties was investigated using the model developed in Chapter 2.

Models developed by Clark (1991), Dunbar (1996), Ju *et al* (2010), (2012) simulating the aerosolisation of a pMDI formulation give highly variable results. This might be because the modelling of the discharge from pMDIs is complex and varying assumptions might cause significant differences in the results. The present model was inspired from and compared with those previous models. The parameters studied and their effects on the sprays issued from pMDIs are described below.

Effect of temperature on spray characteristics

When measuring the size of particles issued from pMDIs using a Malvern Spraytec®, Haynes and coworkers (2004) found that an increase in temperature led to the aerosolisation of droplets with a greater initial velocity and with a smaller residual diameter. Pu *et al* (2011) obtained similar findings in their Sympatec® experiments.

In their inertial impaction experiments, Polli *et al* (1969) also reported this trend (albeit with CFC propellants) and observed a dramatic decrease in the MMAD at higher temperatures. The market for pMDIs is expanding in third world countries where temperatures might differ from temperatures in Europe. In some countries, the large differences between outdoor and indoor temperatures could modify the properties of pMDIs sprays. The study of the temperature effect on the spray characteristics is therefore critical. To the best knowledge of the author, the effect of temperature was never incorporated into a simulation although it could be useful in order to develop formulations which behaviours would not be affected by temperature changes. Depending on the formulation, a specific temperature might be required for optimum drug deposition at the target location.

Effect of nozzle and valve orifices diameters on spray characteristics

Nozzle orifice diameters could influence the particle size of aerosols issued from pMDIs. Common nozzle diameters range from 0.2 mm to 0.5 mm (Swarbrick, 2007). Although one might think that smaller orifices might lead to the aerosolisation of smaller droplets, Ashworth *et al* (1991) found that the lung deposition was independent of the nozzle orifice diameter.

Conversely, a study from Berry *et al* (2003) revealed that the amount of fine particles was inversely related to the nozzle orifice diameter. This relationship was also shown by Ganderton *et al* (2003) who plotted the MMAD and the fine particle dose (FPD) obtained using an impactor as functions of the nozzle orifice diameter. They showed that the nozzle orifice had a significant effect on the FPD which decreased from approximately 85 μg to 30 μg as the nozzle orifice diameter increased from 0.22 mm to 0.42 mm. The results of Ganderton *et al* are reproduced in Figure 3.1.

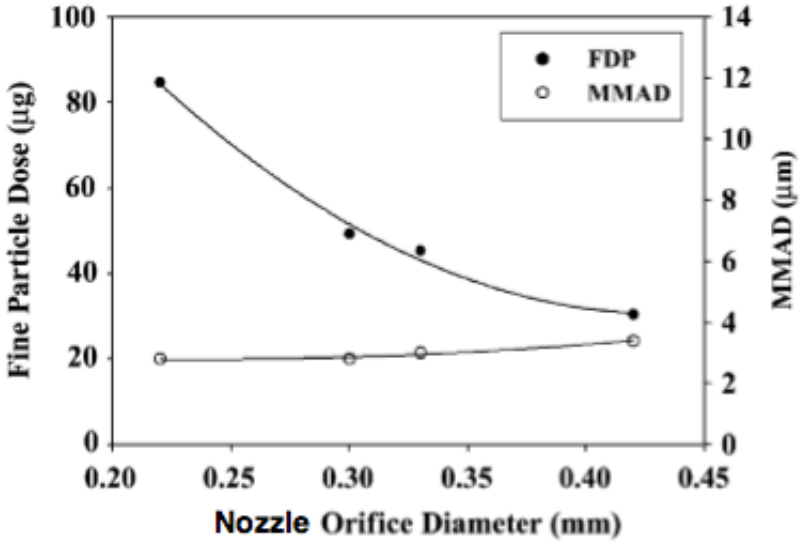

Figure 3.1: Fine particle dose and MMAD plotted as functions of the nozzle orifice diameter (Ganderton *et al.*, 2003).

The results in Figure 3.1 show that the nozzle orifice only has a slight effect on

the size of the particles. This could be due to the fact that small nozzle orifice diameters do not reduce the number of big droplets produced in a spray so that the MMAD remains relatively constant across the range of nozzle orifice diameters tested. However, large nozzle orifice diameters hinder the capacity of the flow to aerosolise into fine droplets so that the FPD value greatly decreases across the range of nozzle orifice diameters tested.

Another explanation for the relatively constant MMAD values could be that the MMAD is only determined from the aerosol reaching the sizing stages of the impactor. As a result, large droplets issued from pMDIs with large nozzle orifices would not reach those stages and the MMAD would not increase significantly.

Another experimental work showed that using a nozzle orifice diameter of 0.25 mm instead of 0.5 mm improved the performance of the inhaler tested (Kleinstreuer *et al.*, 2007). From those results, it would seem beneficial to use nozzle orifices with smaller diameters although they are blocked more frequently than nozzle orifices with bigger diameters (Swarbrick, 2007). The ratio of the nozzle and valve orifices is also important as it might influence the moment in the aerosolisation process when the flow becomes critical and thus affect the exit velocity of the flow.

Effect of force of actuation on spray characteristics

As discussed in Chapter 1, users might have varying actuation forces. The role of the actuation force on the spray characteristics was deemed worth of study, as it was believed to affect the opening rate of the valve orifice. This is illustrated in Equations (3.1) to (3.6).

$$Sc = U_{in\,c}\,t + a_c\,\frac{t^2}{2} \tag{3.1}$$

where Sc is the distance travelled by the canister during its actuation in m, $U_{in\,c}$ is the initial velocity of the canister in $\mathrm{m{\cdot}s^{-1}}$, a_c is the acceleration of the canister

in m·s^{-2} and t is the valve orifice opening time in s. As the initial velocity is 0, Equation (3.1) becomes Equation (3.2).

$$Sc = a_c \frac{t^2}{2} \tag{3.2}$$

Applying Newton's second law on the canister, Equations (3.3) and (3.4) are obtained.

$$F = m_c\, a_c \tag{3.3}$$

$$a_c = \frac{F}{m_c} \tag{3.4}$$

where F is the force applied to the canister in N and m_c is the mass of the canister in kg. When replacing a_c in Equation (3.2) by Equation (3.4), Equation (3.5) is obtained.

$$Sc = \frac{F}{2m_c} t^2 \tag{3.5}$$

which gives Equation (3.6).

$$F = \frac{2Sc\, m_c}{t^2} \tag{3.6}$$

As Sc and m_c are constant, it results that F is proportional to the square of the valve orifice opening rate. To the best knowledge of the author, the role of the actuation force and, consequently, the role of the valve opening rate on the spray properties have not been investigated. It was decided to modify the valve orifice opening rate in the simulation in order to observe its effect on the exit properties of sprays issued from pMDIs.

3.1.2 Aims and objectives

The aim of this chapter was to validate the model by comparing the velocity of the spray, its duration, its quality as well as the particles size at the nozzle orifice with

results obtained from other models and experimental data. After validation of the model, the main objective was to understand the effect of several parameters on the exit properties of the spray.

For example, the effect of the nozzle and valve orifices diameters on the size and velocity of the exiting droplets was studied and helped to validate the model as the results obtained could be compared with the literature.

As mentioned in Chapter 1, the minimum force required to actuate a pMDI might represent an issue for elderly users and other weak users. As the actuating force affects the valve orifice opening rate, the latter was modified in the simulation and its effect on the spray characteristics was assessed.

The model was also modified to simulate the discharge of suspension formulations containing fluticasone propionate (FP). This is relevant as the simulation could thus be used to investigate certain commercial suspension formulations.

Finally, through the monitoring of the spray in the metering and expansion chambers, the aim of the chapter was to investigate the effect of different factors on the evolution of the flow inside the device.

3.2 Methods

The model was developed on Matlab as described in Chapter 2. It was then modified to take into account the velocity of the valve opening orifice and the presence of FP in the formulation.

The default settings of parameters used in the simulation listed in Table 3.1 were set to similar values as previous works in order to enable direct comparisons with these works.

	Present work	Dunbar (1996)	Ju *et al* (2010)
Valve orifice diameter (mm)	0.7	0.7	0.7
Nozzle orifice diameter (mm)	0.5	0.5	0.5
Metering chamber volume (μL)	63	63	63
Expansion chamber volume (μL)	17.6	17.6	17.6
Discharge coefficient at valve orifice	0.61	0.61	0.61
Discharge coefficient at nozzle orifice	0.78	0.78	0.5
Temperature (K)	293	295	293.15

Table 3.1: List of parameters used in the simulation.

3.3 Results

3.3.1 Effect of temperature on spray characteristics

Effect of temperature on velocity

Figures 3.2 and 3.3 respectively show the liquid and vapour phases velocity at the nozzle orifice at several temperatures.

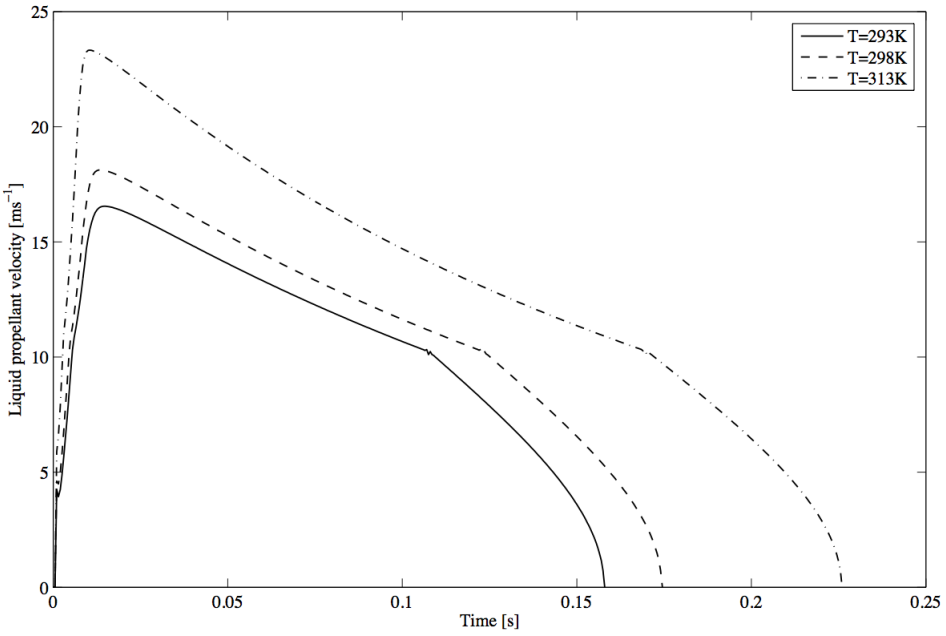

Figure 3.2: Velocity of the liquid phase of the spray at the nozzle orifice at several temperatures.

Figure 3.2 shows that the velocity of the liquid phase increases at higher temperatures. The peak velocity was approximately $17\,\mathrm{m{\cdot}s^{-1}}$ at 293 K compared with a peak of approximately $23\,\mathrm{m{\cdot}s^{-1}}$ at 313 K.

The aerosolisation process had longer durations at higher temperatures (approximately 0.16 s at 293 K, 0.175 s at 298 K and 0.225 s at 313 K).

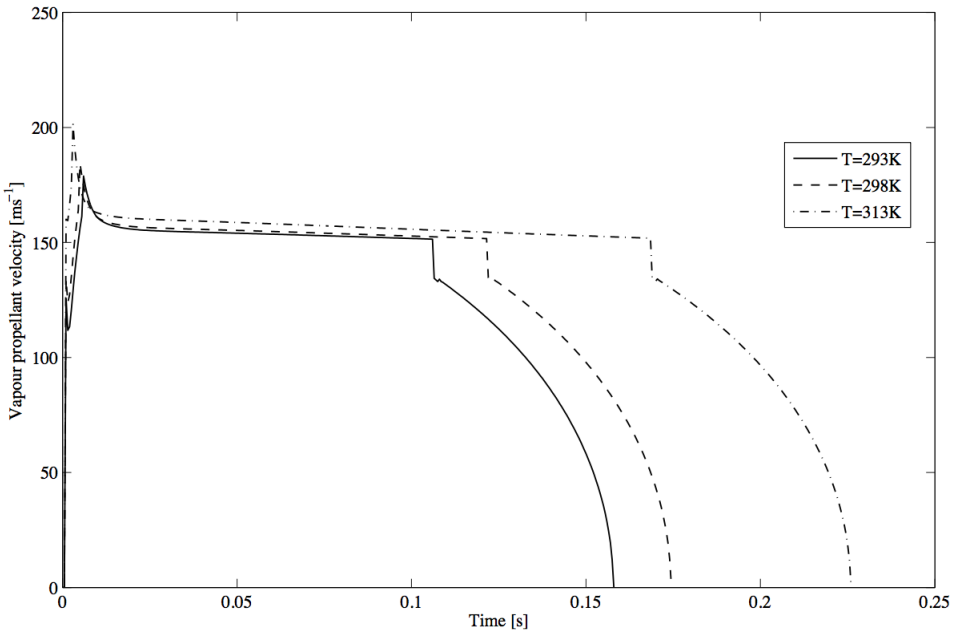

Figure 3.3: Velocity of the vapour phase of the spray at the nozzle orifice at several temperatures.

In Figure 3.3, the initial velocity peak occurs immediately at the onset of the actuation as the spray exits the nozzle orifice. The vapour phase velocity then decreases as more liquid-rich propellant enters the expansion chamber. As the liquid propellant starts evaporating, the flow at the nozzle orifice becomes critical. It remains critical until a sharp drop in the velocity occurs towards the end of the atomisation process due to a lower expansion chamber pressure as the metering chamber becomes depleted of formulation. The velocity then decreases until the end of the discharge process.

Figures 3.2 and 3.3 show that at all temperatures, the vapour phase, with a max-

imum velocity of $200\,\mathrm{m{\cdot}s^{-1}}$ was much faster than the liquid phase which had a maximum velocity of approximately $23\,\mathrm{m{\cdot}s^{-1}}$.

The velocity of the vapour phase also increases at higher temperatures. The peak velocity is approximately $180\,\mathrm{m{\cdot}s^{-1}}$ at $293\,\mathrm{K}$ compared with a peak of approximately $200\,\mathrm{m{\cdot}s^{-1}}$ at $313\,\mathrm{K}$.

The higher velocities observed at higher temperatures could be explained by a higher pressure build up in the expansion chamber at higher temperatures as shown in Figure 3.4.

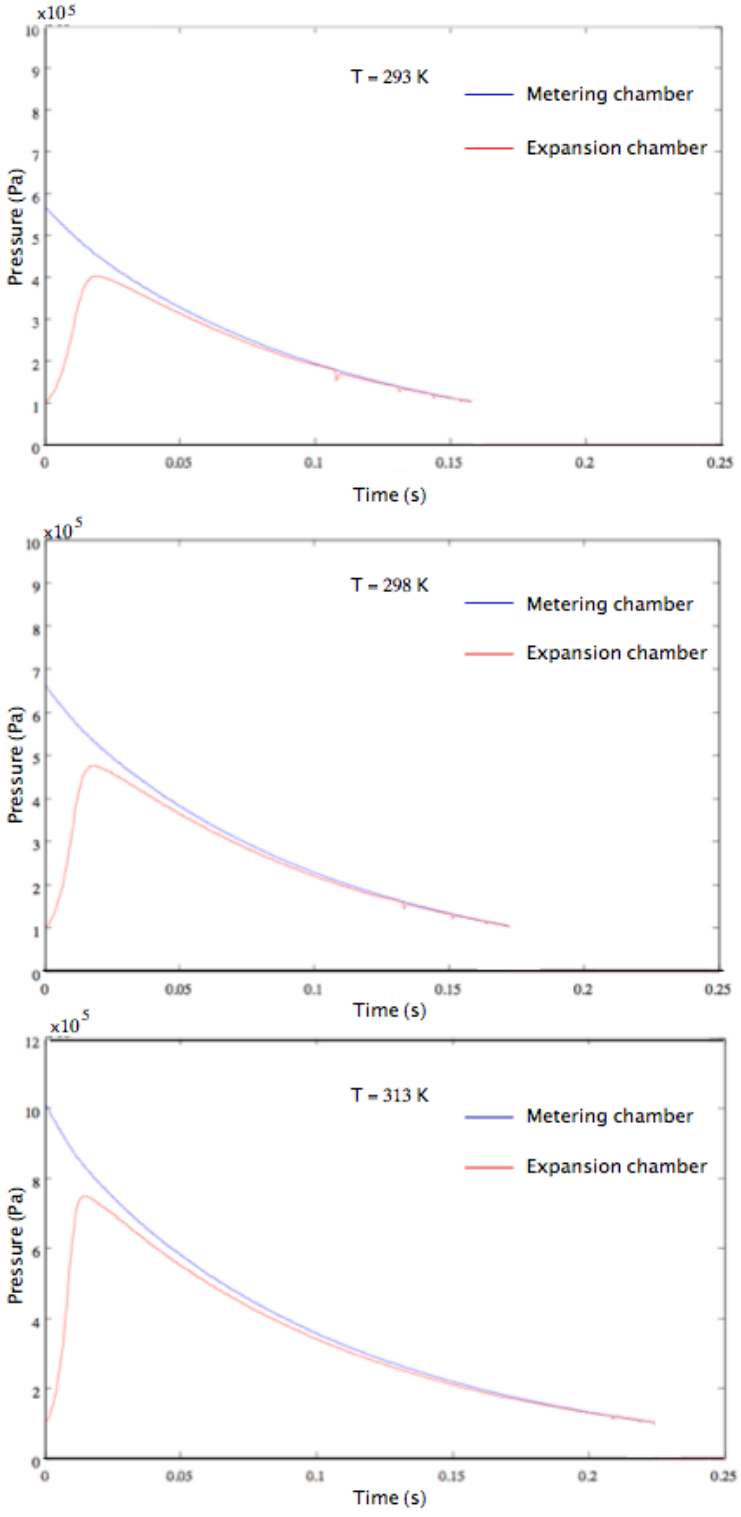

Figure 3.4: Pressure in the metering and expansion chambers when the formulation and the room temperatures are set to 293 K, 298 K and 313 K.

Figure 3.4 shows that the pressure in the metering chamber decreases from the saturated vapour pressure at the specific temperature at which the simulation is run, to atmospheric pressure. The expansion chamber pressure is initially atmospheric before increasing to almost the level of the metering chamber pressure as the propellant is discharged from the metering chamber. Towards the end of the aerosolisation process, the expansion chamber pressure decreases to atmospheric pressure as the formulation is discharged from the device.

Effect of temperature on mass flow rate and residual mass

Figure 3.5 shows the total mass flow rate of the propellant at the nozzle orifice.

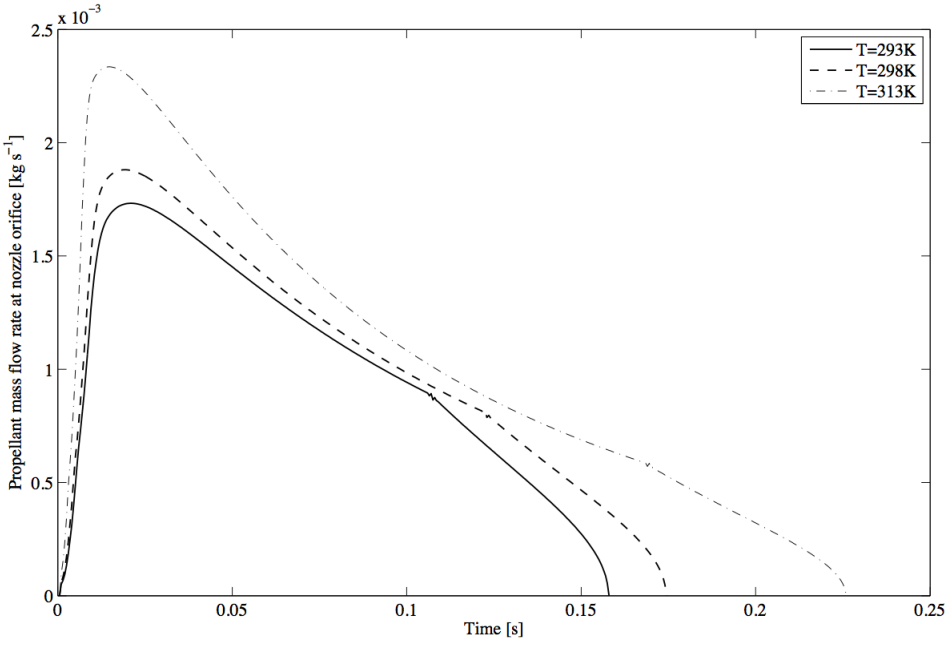

Figure 3.5: Total mass flow rate of the propellant at the nozzle orifice at several temperatures.

The mass flow rate curves follow broadly the expansion chamber pressure curves. The maximum mass flow rate was approximately $2.3\,\mathrm{g{\cdot}s^{-1}}$ at 313 K compared with $1.7\,\mathrm{g{\cdot}s^{-1}}$ at 293 K.

As the mass flow rate was higher and the duration of the spray was longer at

higher temperatures, a greater quantity of propellant would be expected to be discharged. This agrees with Figure 3.6, showing the mass of propellant remaining in the metering chamber when the pMDI was actuated at several temperatures.

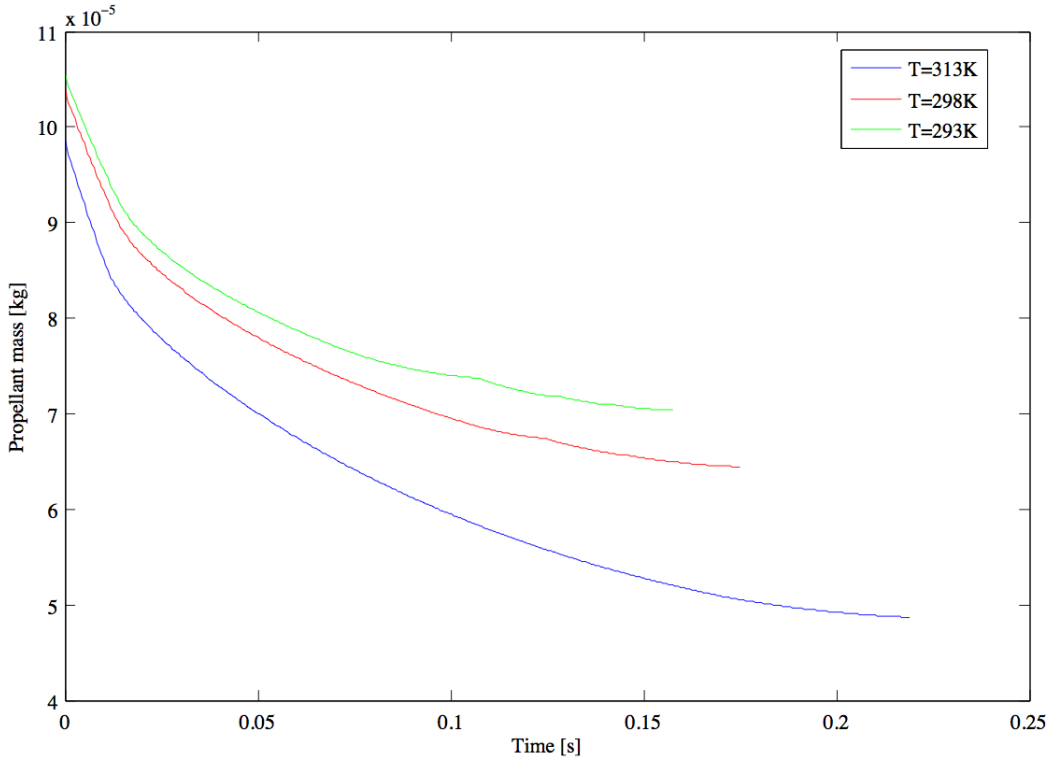

Figure 3.6: Residual mass of propellant in the metering chamber when the formulation and the room temperatures are set to 293 K, 298 K and 313 K.

Figure 3.6 shows that the residual mass inside the metering chamber at the end of the actuation, was lower at higher temperatures as it represented approximately 70% of the initial mass of the metering chamber formulation at 293 K compared to 50% at 313 K.

Effect of temperature on mass flashing and droplet size

Figure 3.7 shows the fraction of the formulation that could potentially evaporate at the nozzle orifice, calculated using Equation (3.7).

$$fraction\, m_{flash} = \frac{hlp_{ec} - hlp_{wb}}{hlvp_{wb}} \tag{3.7}$$

where $fraction\, m_{flash}$ represents the fraction of liquid formulation that could flash at the nozzle orifice, hlp_{ec} is the specific enthalpy of the liquid propellant in the expansion chamber in kJ·kg^{-1}, hlp_{wb} is the specific enthalpy of the liquid propellant at the wet bulb temperature in kJ·kg^{-1} and $hlvp_{wb}$ is the specific enthalpy of vaporisation of the propellant at the wet bulb temperature in kJ·kg^{-1}.

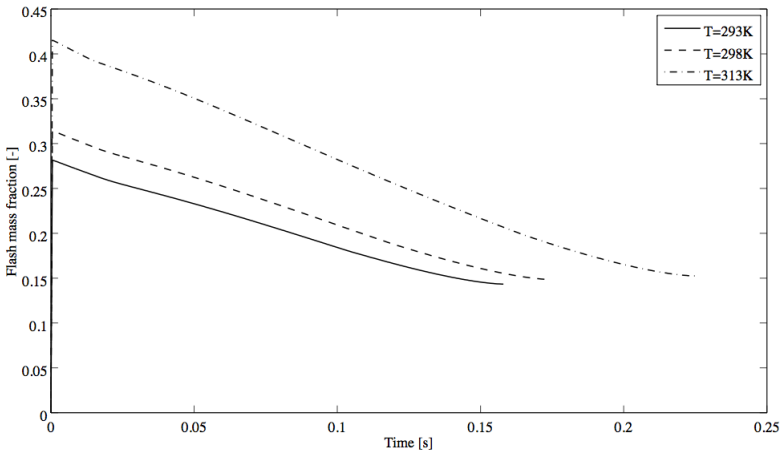

Figure 3.7: Fraction of the formulation that could evaporate at the nozzle orifice at 293 K, 298 K and 313 K.

Figure 3.7 shows that at all temperatures, the fraction of propellant that can evaporate decreases during the actuation process which is expected as the energy available for the evaporation of the propellant and the temperature in the expansion chamber decrease.

The fraction of liquid propellant that can evaporate increases at higher temperatures, potentially leading to the formation of smaller droplets. The effect of temperature on the mass median diameter (MMD) of the droplets emitted at the nozzle orifice is shown in Figure 3.8.

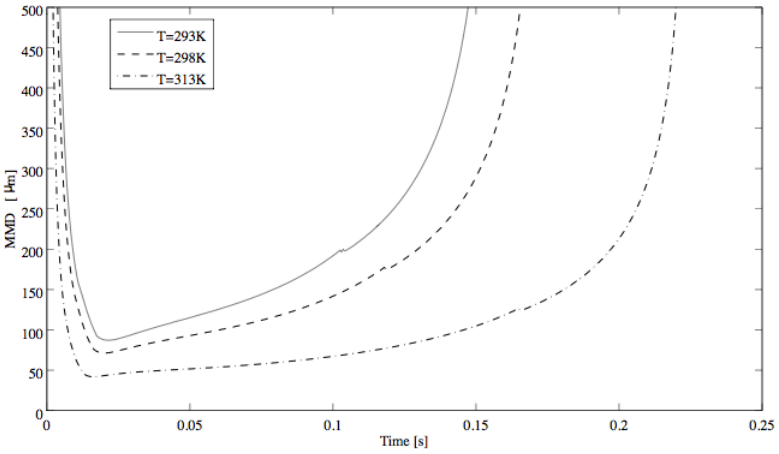

Figure 3.8: MMD of the spray at the nozzle orifice at several temperatures.

In Equation (2.53), developed by Clark and defined in Chapter 2, it can be seen that at the onset and at the end of the actuation, as $P_{ec} \rightarrow P_{atm}$, MMD$\rightarrow \infty$.

$$MMD = \frac{8.02}{q_{ec}^{0.56}\left(\frac{P_{ec}-P_{atm}}{P_{atm}}\right)^{0.46}}$$

For this reason, the value of the MMD at the onset and the end of the actuation were not taken into account in all MMD graphs and the maximum diameter shown was 500 μm as this is the maximum droplet size reported for pMDIs aerosols in the literature (Hochrainer *et al.*, 2005).

The MMD, with a minimum value of approximately 85 μm at 293 K compared to 45 μm at 313 K is seen to greatly decrease at increasing temperatures. From Equation (2.53), lower MMD values could be explained by a higher pressure build up in the expansion chamber or a higher expansion chamber quality. The increasing pressure in the expansion chamber at higher temperatures was shown in Figure 3.4 and the increasing quality at higher temperatures can be seen in Figure 3.9.

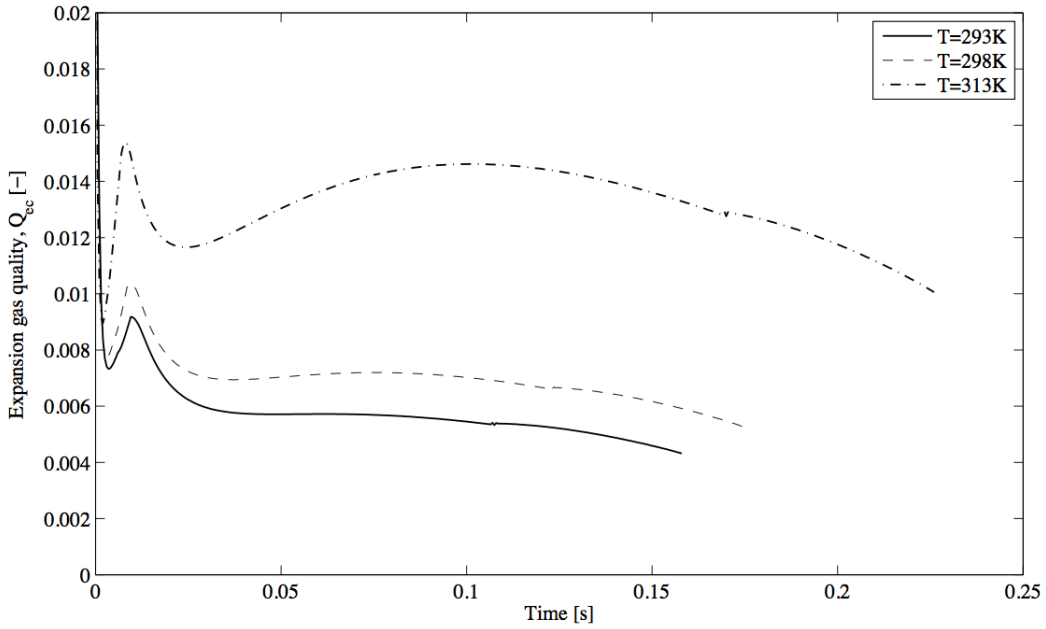

Figure 3.9: Quality in the expansion chamber at 293 K, 298 K and 313 K.

The quality in the expansion chamber has a value of 1 at initial conditions as the expansion chamber is filled with gaseous air. It then decreases due to the replacement of dry air by propellant. As the propellant starts evaporating, the quality increases. It then decreases which could be due to a drop in enthalpy towards the end of the atomisation process as the mass of propellant entering the expansion chamber decreases. This enthalpy decrease would in turn cause a decrease in temperature, resulting in a lower quality.

At 313 K the increasing quality of the propellant in the expansion chamber from approximately 0.03 s to 0.1 s after the onset of actuation might arise from the increasing quality of the propellant coming from the metering chamber. As the metering chamber empties, the quality would indeed increase at a high temperature at which the latent heat of vaporisation is lower than at low temperatures.

3.3.2 Effect of the valve and nozzle orifices diameters on spray characteristics

Effect of nozzle to valve orifices ratios on the pressure build up in the expansion chamber

The ratio of the nozzle orifice to the valve orifice diameters was 0.71 when using the nozzle and valve orifices diameters used by Dunbar (1996) presented in Table 3.1.

The valve orifice diameter of a metering valve and the nozzle orifice diameters from two mouthpieces, employed for experimental work in subsequent chapters, were measured using a travelling microscope.

The valve orifice of a 50 μL non-continuous valve from Valois (Valois pharmaceutical division, 780160 Marly Le Roi, France) was found to have a diameter of 0.55 mm. The nozzle orifice of an Alvesco® mouthpiece (Takeda Pharmaceuticals International GmbH, Zurich, Switzerland) had a diameter of 0.20 mm. The mouthpiece from Flixotide® had a nozzle orifice diameter of 0.50 mm, which is similar to the diameter used by Dunbar (1996). Those two mouthpiece diameters, each combined with the 50 μL non-continuous valve orifice diameter were investigated. Dunbar's valve and nozzle orifices diameter values were also run in the simulation. All the combinations of valve and nozzle orifices diameters studied are listed in Table 3.2 in which the orifice diameter ratio (ODR) corresponds to the ratio of the nozzle orifice to the valve orifice diameters.

	Valve orifice diameter (mm)	Nozzle orifice diameter (mm)	ODR
Dunbar's pMDI	0.70	0.50	0.71
Alvesco® mouthpiece Valois metered valve	0.55	0.20	0.37
Flixotide® mouthpiece Valois metered valve	0.55	0.50	0.91

Table 3.2: List of the combinations of valve and nozzle orifices diameters investigated.

The effect of the nozzle orifice and valve orifice diameters on the expansion chamber pressure can be seen in Figure 3.10.

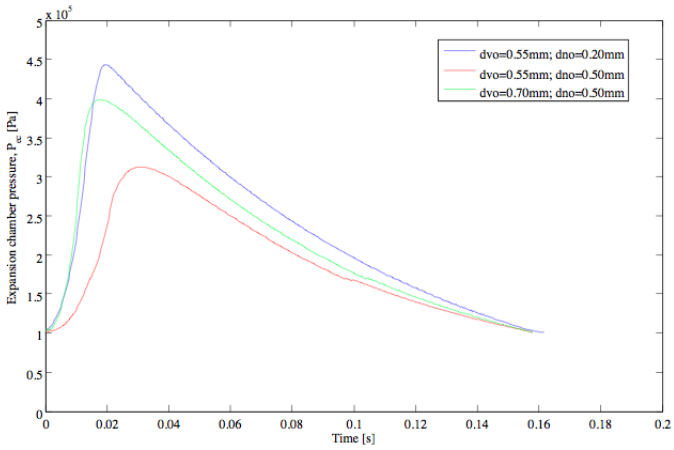

Figure 3.10: Expansion chamber pressures for several nozzle and valve orifices diameter combinations, where d_{vo} and d_{no} are respectively the valve and nozzle orifices diameters in mm.

At a specific valve orifice diameter, a smaller nozzle orifice diameter leads to a greater pressure build up in the expansion chamber. More generally, it shows that when the ODR decreases, the pressure in the expansion chamber increases.

Effect of the nozzle orifice diameter on the discharge duration

When keeping a constant valve orifice diameter and running the simulation at 293 K, the effect of the nozzle orifice diameter on the duration of the discharge process was investigated and is shown in Table 3.3.

Valve orifice diameter (mm)	Nozzle orifice diameter (mm)	Discharge duration (s)
0.7	0.5	0.159
0.7	0.3	0.161
0.7	0.1	0.176

Table 3.3: Effect of the nozzle orifice diameter on the duration of the discharge process.

A smaller nozzle orifice leads to a longer aerosolisation process, which seems logical as a lower amount of formulation could be discharged at each time step.

Effect of the nozzle orifice diameter on the size and velocity of the particles at the nozzle orifice

In Figures 3.11 and 3.12, the valve orifice diameter was kept constant at a value of 0.7 mm, the size of the nozzle orifice was modified and its effect on the size and velocity of the aerosolised particles was investigated.

Figure 3.11 shows that the minimum MMD had a value of approximately 50 μm when a nozzle orifice diameter of 0.2 mm was used compared to a value of approximately 90 μm when a nozzle of orifice diameter of 0.6 mm was used.

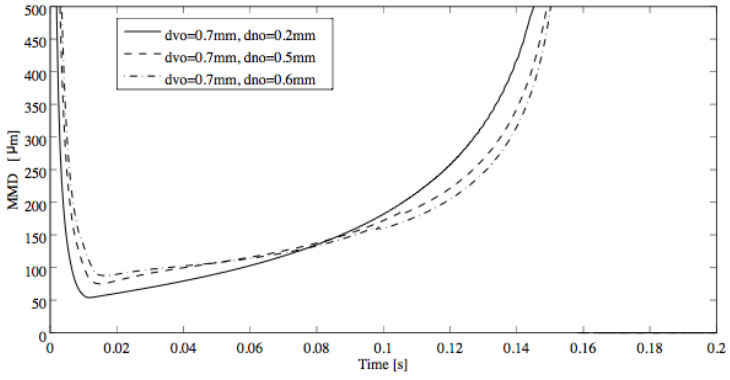

Figure 3.11: MMD values at the nozzle orifice for several nozzle orifice diameters.

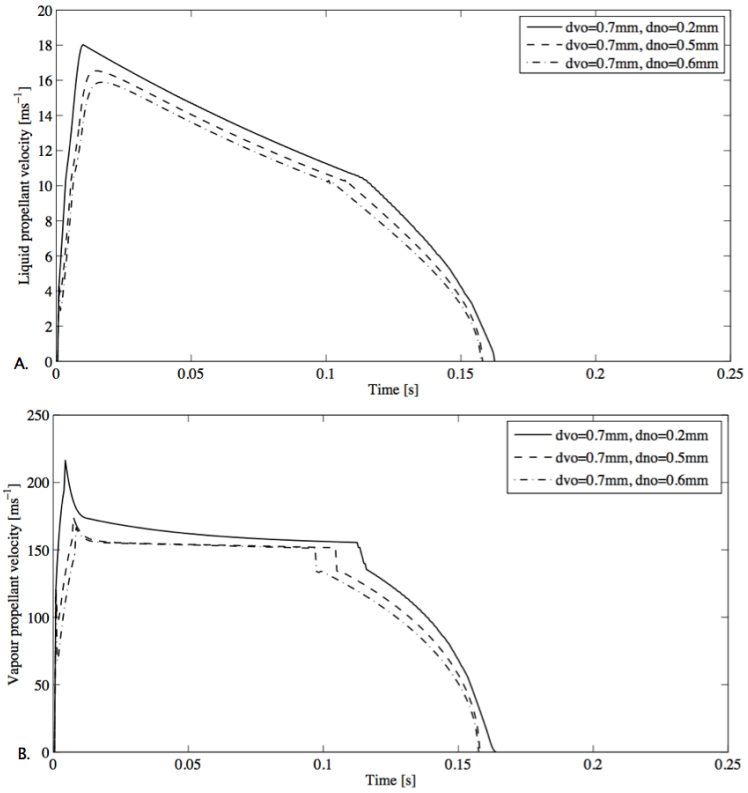

Figure 3.12: A. Velocity of the liquid phase at the nozzle orifice for several nozzle orifice diameters. B. Velocity of the vapour phase at the nozzle orifice for several nozzle orifice diameters.

Figure 3.12 shows that the velocity of the propellant increased at lower nozzle orifice diameters. The liquid phase had a peak velocity of approximately $18\,\mathrm{m{\cdot}s^{-1}}$ at a nozzle orifice diameter of 0.2 mm compared to $16\,\mathrm{m{\cdot}s^{-1}}$ at a nozzle orifice diameter of 0.6 mm. The vapour phase had a peak velocity of approximately $220\,\mathrm{m{\cdot}s^{-1}}$ at a nozzle orifice diameter of 0.2 mm compared to approximately $170\,\mathrm{m{\cdot}s^{-1}}$ at a nozzle orifice diameter of 0.6 mm.

It was believed that the ratio of the maximum expansion chamber pressure to the maximum metering chamber pressure might depend upon the ratio of the nozzle to valve orifices diameters. In order to investigate this relationship, several nozzle orifice diameters were tested for one valve orifice diameter. The nozzle diameters studied varied from 0.1 mm to 0.5 mm in steps of 0.1 mm. This set of simulations was realised for 2 valve orifice diameters (0.55 mm and 0.7 mm) and is shown in

Figure 3.13.

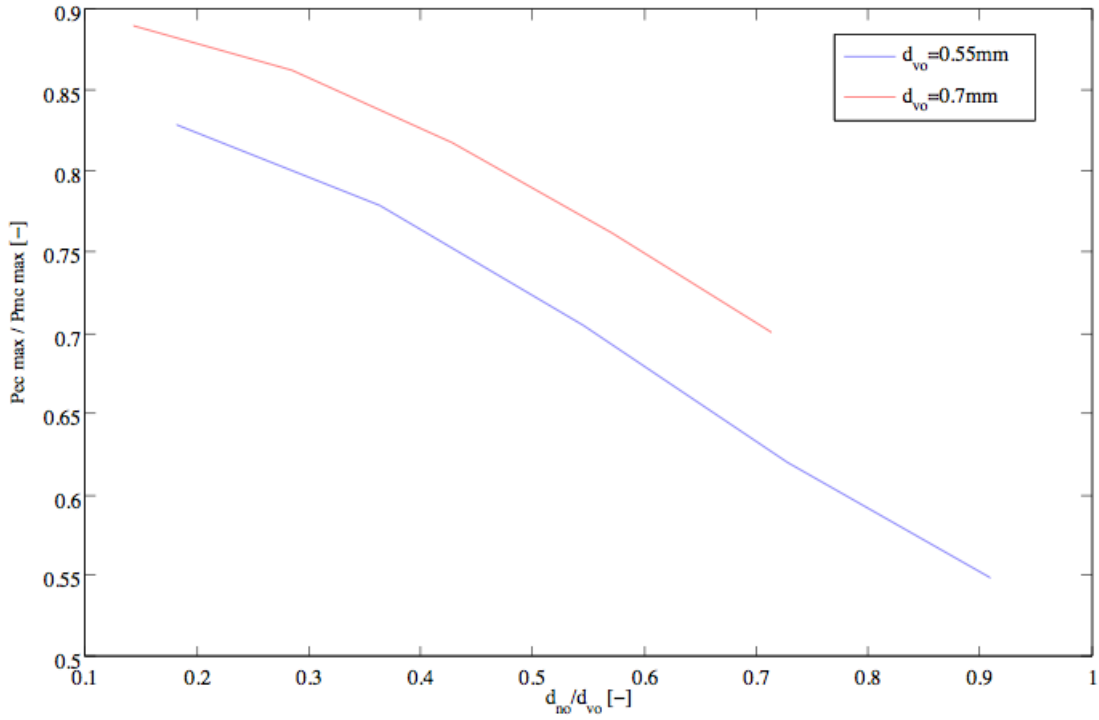

Figure 3.13: Maximum expansion chamber to metering chamber pressure ratios as a function of the nozzle orifice to valve orifice diameter ratios.

Figure 3.13 shows that the maximum expansion to metering chambers pressure ratio decreases almost linearly with the nozzle to valve orifices diameter ratio. The pressure in the expansion chamber can be seen to reach almost 90% of the metering chamber pressure at low nozzle to valve orifices diameter ratios.

3.3.3 Effect of the valve orifice opening rate

Subroutine simulating the opening rate of the valve orifice

In the current work, the valve orifice area was varied in function of time to render the actuation more realistic. Figure 3.14 helps to understand the calculation of the opening of the valve orifice area as a function of the actuation time.

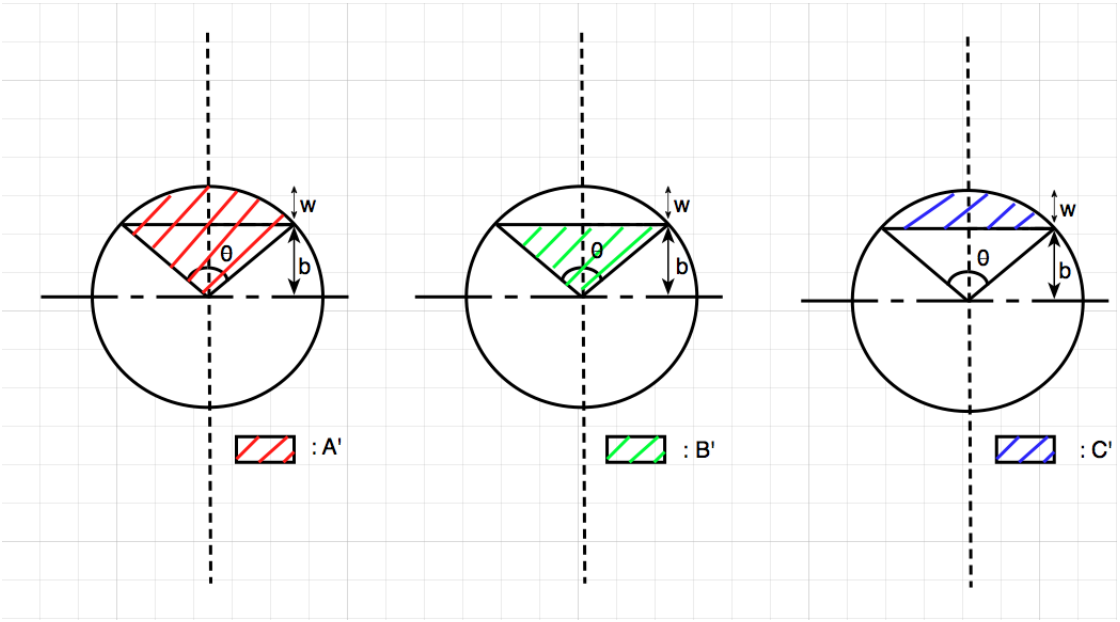

Figure 3.14: Geometry of the valve orifice allowing the calculation of the valve orifice opening as a function of the actuation time where w corresponds to the displacement of the canister in m at a certain time and A', B' and C' refer to the specific hatched areas in m^2, C' being the valve orifice opening area at a certain time.

The subroutine modifying the valve opening area as a function of the actuation time and canister velocity was developed using Equations (3.8) to (3.17).

$$C' = A' - B' \tag{3.8}$$

$$A' = \frac{\pi \, {d_{vo}}^2}{4} . \frac{\theta}{2\pi} \tag{3.9}$$

where d_{vo} represents the diameter of the valve orifice and where θ represents the angle shown in Figure 3.14 in rad, increasing as the valve orifice opens.

$$A' = \frac{{d_{vo}}^2 \theta}{8} \tag{3.10}$$

$$B' = \frac{{d_{vo}}^2}{8} \sin\theta \tag{3.11}$$

$$C' = \frac{{d_{vo}}^2 \theta}{8} - \frac{{d_{vo}}^2}{8} \sin\theta \tag{3.12}$$

$$C' = \frac{{d_{vo}}^2}{8}(\theta - \sin\theta) \tag{3.13}$$

as

$$\theta = 2\arccos\frac{b}{d_{vo}/2} \tag{3.14}$$

where b represents the length depicted in Figure 3.14 and is calculated using Equation (3.15).

$$b = \frac{d_{vo}}{2} - w \tag{3.15}$$

where w corresponds to the displacement of the canister at a specific time t in s as shown in Figure 3.14, and is calculated using Equation (3.16).

$$w = U_c\, t \tag{3.16}$$

where U_c is the velocity of the canister in $\mathrm{m{\cdot}s^{-1}}$.

$$\theta = 2\arccos\left(\frac{d_{vo}/2 - U_c\, t}{d_{vo}/2}\right) \tag{3.17}$$

When replacing θ in Equation (3.9) one obtains Equation (3.18) which was implemented in the simulation.

$$C' = \frac{{d_{vo}}^2}{8}\left[2\arccos\left(\frac{d_{vo}/2 - U_c\, t}{d_{vo}/2}\right) - \sin\left(2\arccos\left(\frac{d_{vo}/2 - U_c\, t}{d_{vo}/2}\right)\right)\right] \tag{3.18}$$

The velocity of a canister actuated by a "healthy" female adult and a "weak" and inexperienced female research team member was studied in order to identify whether diverse actuation types might influence the actuation mechanism and subsequently the spray characteristics.

The velocity of an aluminium canister (Bespak, UK) crimped to a 50 μL non-continuous valve from Valois (Valois pharmaceutical division, 780160 Marly Le

Roi, France) was measured during actuation using a linear variable differential transformer (LVDT). The LVDT output was captured on a computer by means of a USB 6211 analog to digital converter (National Instruments, Berkshire, UK) at a sampling frequency of 1 kHz. The actuation profiles of the "healthy" and the "weak" female users can be seen in Figure 3.15.

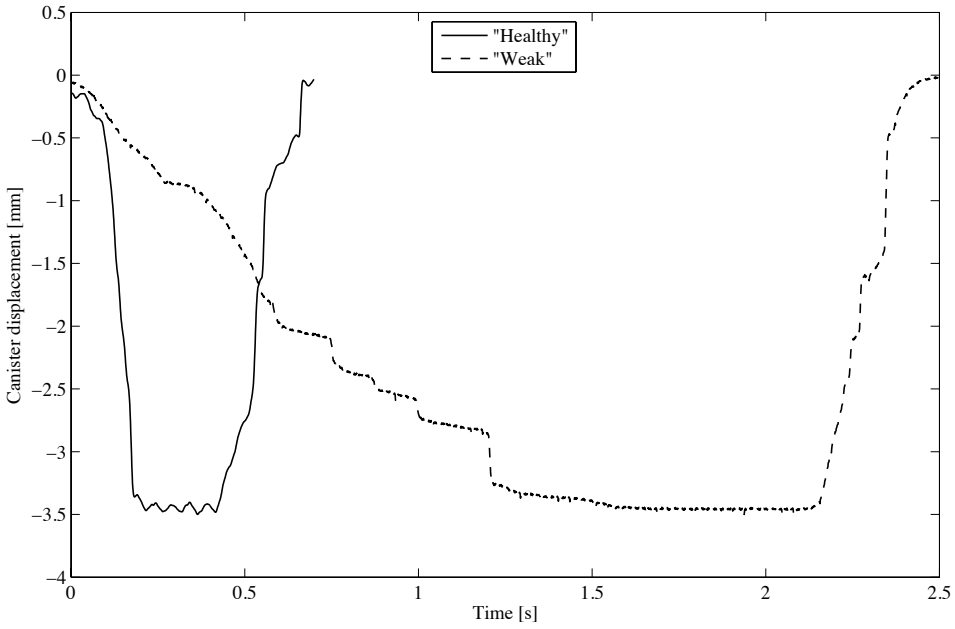

Figure 3.15: Actuation profile of a "healthy" adult female user and a "weak" female user.

The opening rate of the valve orifice for the "weak" inexperienced female user was approximately 1.9 mm·s^{-1}. The actuation velocity varied between 1.7 mm·s^{-1} to 1.9 mm·s^{-1} for five actuations. The opening rate of the valve orifice for the "healthy" female was 21 mm·s^{-1}. The actuation velocity varied between 21 mm·s^{-1} and 27 mm·s^{-1} for five actuations.

Figure 3.15 shows that the "healthy" female and the "weak" inexperienced female have highly different actuation profiles. The time during which the valve orifice is fully open, although it greatly differs between the "healthy" female and the "weak"

female users, is not believed to affect spray characteristics as in both cases, the valve remains open for a longer time than the duration of the discharge process.

In the simulation, it was found that valve opening rates higher than approximately $2\,\mathrm{mm{\cdot}s^{-1}}$ led to similar velocity and MMD results as instantaneous openings of the valve orifice. For this reason, the valve opening rate of the "healthy" female user was not implemented in the simulation. The valve opening rates of the "weak" inexperienced female were tested and compared to the instantaneous opening of the valve orifice. The effect of several valve opening rates on the expansion chamber pressure is shown in Figure 3.16.

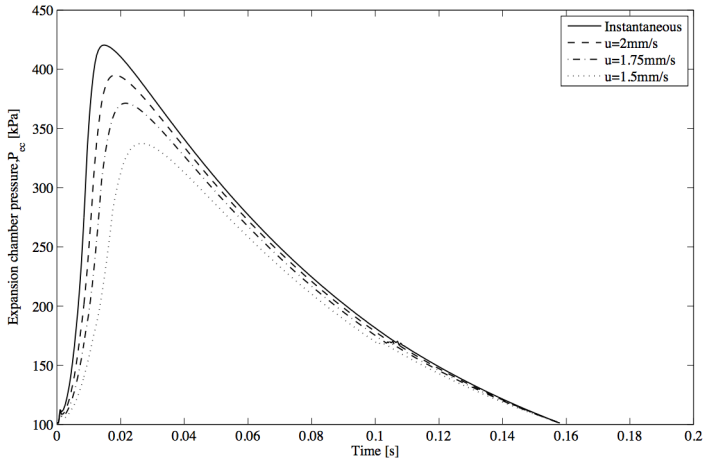

Figure 3.16: Expansion chamber pressure at several valve orifice opening rates.

Figure 3.16 shows that at instantaneous opening of the valve orifice, the pressure in the expansion chamber is higher than at lower valve opening rates. It was believed that a higher pressure build up in the expansion chamber might translate into the aerosolisation of smaller droplets. The MMD values of the spray at various valve opening rates were therefore investigated and are shown in Figure 3.17.

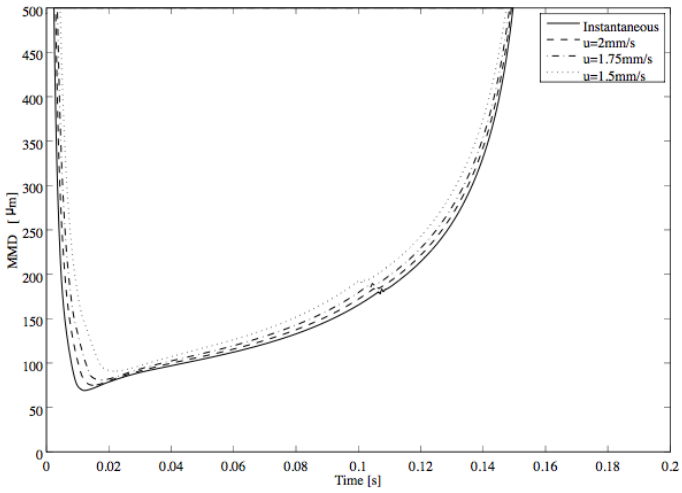

Figure 3.17: MMD at the nozzle orifice at several valve orifice opening rates.

Figure 3.17 shows that the opening rate of the valve orifice has an effect on the MMD of the aerosolised particles. When the valve orifice opens instantaneously, the minimum MMD has a value of approximately 70 μm compared to a value of approximately 90 μm at the lowest tested valve opening rate of 1.5 mm·s^{-1}.

3.3.4 Effect of a suspended drug on spray characteristics

The model was modified to take into account the presence of fluticasone propionate (FP) in the HFA134a formulation. As FP and HFA134a are not soluble and are commonly used as a suspension formulation (e.g. Flixotide®), it was assumed that the drug would not interact with the propellant and would not modify its thermodynamic properties. The properties of FP, found in the Chemical Book website were assumed not to change as a function of temperature (chemicalbook.com, 2008). The FP particles were treated as homogeneously dispersed in the formulation and it was assumed that the same mass of FP was carried by the liquid phase and the vapour phase of the propellant. The model calculated the mass of the drug in the expansion chamber as a percentage of the mass of gas and liquid phases.

The volume of the gas phase in the expansion chamber was calculated after determining the volume occupied by the drug and the liquid phase. The presence of FP therefore decreased the amount of propellant present in the system at each actuation.

It was assumed that the presence of the drug particles did not affect the discharge coefficients of both valve and nozzle orifices. In commercially available pMDIs, a limit of 2% API by weight has been reported in order to avoid blockage of the nozzle orifice (Smyth, 2003). However, concentrations of up to 10% by weight were investigated in the following figures, to better demonstrate the effect of an increased weight concentration of FP on the spray characteristics. Figure 3.18 shows the effect of the drug concentration on the pressure in the expansion chamber.

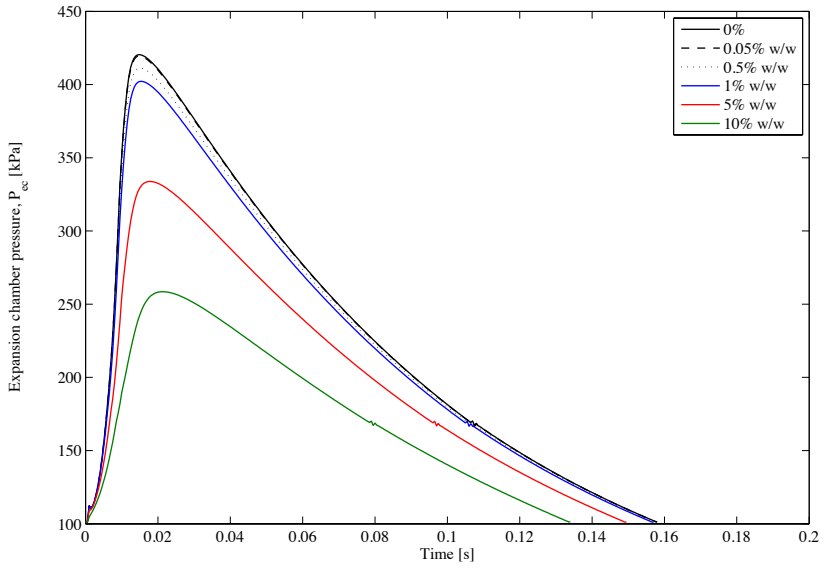

Figure 3.18: Expansion chamber pressure at varying FP concentrations.

The expansion chamber pressure decreases from a peak of 425 kPa at 0% FP to 250 kPa at 10% FP. As the expansion chamber pressure decreases at increasing FP concentrations, the velocity at the nozzle orifice is also expected to decrease. Figures 3.19 and 3.20 respectively show the exit velocity of the liquid and vapour

phases of the formulation at several FP concentrations.

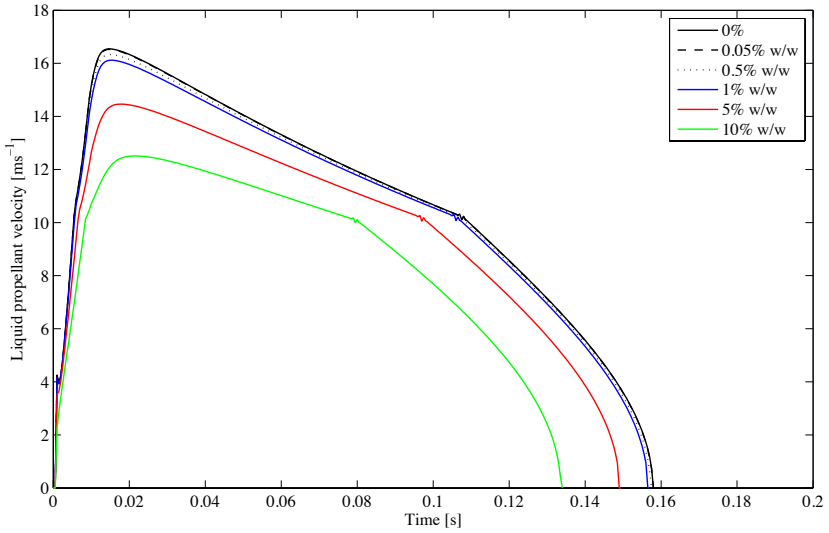

Figure 3.19: Velocity of the liquid phase at the nozzle orifice at varying FP concentrations.

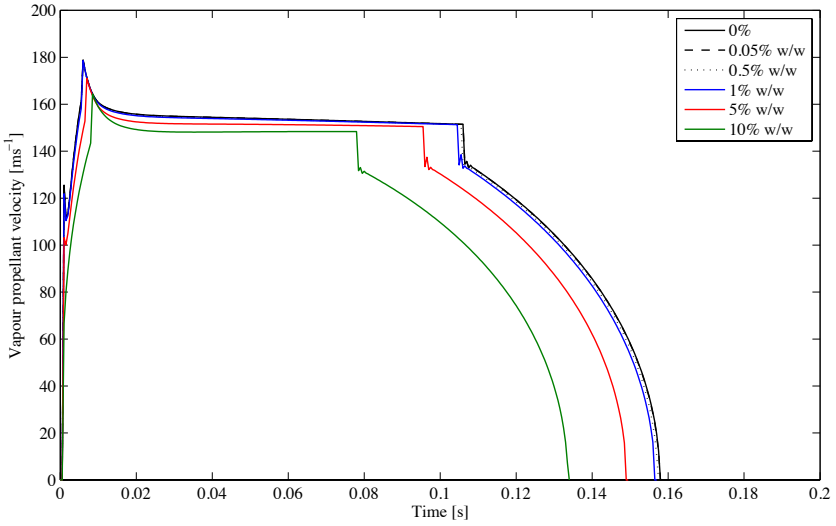

Figure 3.20: Velocity of the vapour phase at the nozzle orifice at varying FP concentrations.

Figures 3.19 and 3.20 show that the velocity of the formulation decreases from approximately 16 m·s^{-1} to 12 m·s^{-1} for the liquid phase and from approximately

180 m·s^{-1} to 165 m·s^{-1} for the gas phase when the FP concentration increases from 0% to 10% by weight.

Figure 3.21 shows the MMD of the formulation at varying FP concentrations.

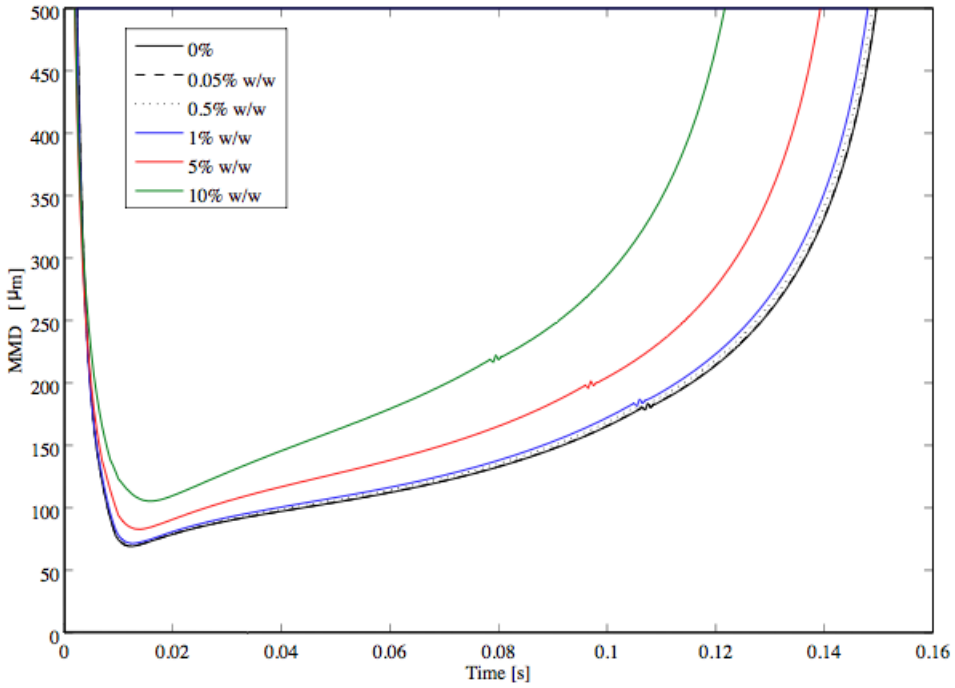

Figure 3.21: MMD of the suspension formulation at varying FP concentrations.

Figure 3.21 shows that the minimum MMD increases from approximately 70 μm to 100 μm as the FP concentration increases from 0% to 10% by weight.

3.4 Discussion

3.4.1 Effect of temperature on spray characteristics

Effect of temperature on velocity

The velocities obtained when the simulation was run at the same temperature as Dunbar and Ju's models were 17 m·s^{-1} and 170 m·s^{-1} for the liquid and vapour

phases respectively (Dunbar, 1996), (Ju *et al.*, 2010).

The model developed by Ju *et al* (2010) calculated a peak velocity of approximately $19\,\mathrm{m{\cdot}s^{-1}}$ for a HFA134a spray although it is not clear if they refer to the liquid or gas phase velocity. It is therefore not possible to compare their velocity values to other work including the present simulation.

In the model of Wigley *et al* (2002), two velocity peaks of approximately $60\,\mathrm{m{\cdot}s^{-1}}$ each were obtained at the nozzle orifice for the mixture of the gas and liquid phases during the actuation of a HFA134a-based pMDI. Wigley's velocity results are shown in Figure 3.22.

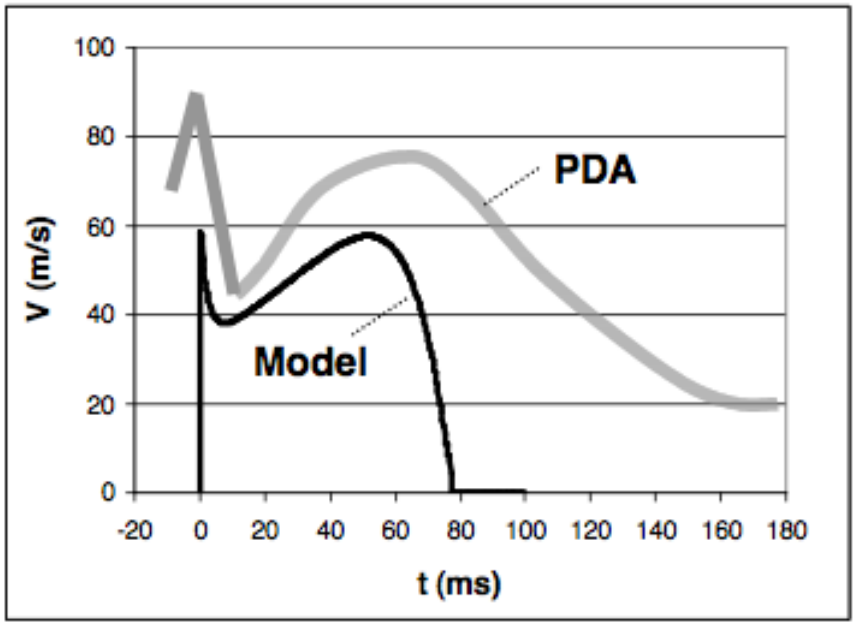

Figure 3.22: Temporal profile of propellant velocity (Wigley *et al.*, 2002).

The first velocity peak in Figure 3.22 is believed to correspond to the high quality flow exiting from the nozzle orifice at the beginning of the discharge. The velocity then reduces due to the fact that the quality of the flow decreases. Towards the end of the spray, the formulation undergoes more intense evaporation due to the emptying of the metering and expansion chambers, leading to the second velocity

peak (Wigley *et al.*, 2002). The present work cannot be directly compared to Wigley's work as the velocity of the liquid and vapour phases were calculated separately.

In his simulation, Dunbar obtained a peak velocity of $225\,\mathrm{m{\cdot}s^{-1}}$ for both the liquid and vapour phases. As velocity values from simulations range from $19\,\mathrm{m{\cdot}s^{-1}}$ to $225\,\mathrm{m{\cdot}s^{-1}}$, it is not possible to validate the current model's velocity profiles using only modelling data so that experimental data were also investigated (Dunbar, 1996), (Ju *et al.*, 2010), (Wigley *et al.*, 2002).

The value of $225\,\mathrm{m{\cdot}s^{-1}}$ reported by Dunbar (1996) for the velocity of both liquid and vapour phases of a HFA134a spray seems very high compared to experimental velocity measurements in the literature. For example, Wigley *et al* (2002) found a maximum velocity of approximately $90\,\mathrm{m{\cdot}s^{-1}}$ in the vicinity of the nozzle orifice when using phase Doppler anemometry (PDA) for HFA134a sprays.

In his PDA measurements, Dunbar measured velocity of approximately $60\,\mathrm{m{\cdot}s^{-1}}$ for a HFA134a spray at a distance of 25 mm from the nozzle orifice. This is in line with the findings of Crosland *et al* (2009) who obtained a maximum velocity of $60\,\mathrm{m{\cdot}s^{-1}}$ in their particle image velocimetry (PIV) measurements of a HFA134a-based pMDI at a location of 1 mm from the extremity of the mouthpiece (approximately 25 mm from the nozzle orifice).

The lower velocity obtained by Dunbar compared to Wigley might be explained by the fact that Wigley measured the velocity of the droplets closer to the nozzle orifice (Dunbar, 1996), (Wigley *et al.*, 2002). However as it is thought that PDA measurements should only be taken at a minimum distance of 10 mm from the nozzle orifice for maximum measurement accuracy due to the high spray concentration closer to the nozzle orifice, Wigley's PDA results (shown in Figure 3.22) might not be as reliable as Dunbar's.

The variations of the spray exit velocity observed from simulations and experimental work might be due to the small size of the nozzle orifice and, as pMDI sprays are extremely transient, turbulent, fast and dense at this location, their properties are difficult to measure or to calculate. However, the velocities found in the present simulation are within the range of velocities quoted from the literature.

The higher velocities observed at higher temperatures might be due to the fact that an increased temperature led to a higher vapour pressure of the formulation, increasing the pressure gradient between the formulation and the atmosphere, thus producing a spray exiting the device at a higher velocity. This was illustrated in Figure 3.4 which showed that the pressure in both the metering and expansion chambers increased at higher temperatures.

Clark (1991) measured the pressure in the metering and expansion chambers of a pMDI containing CFC-12 propellant using a pressure sensor and observed a slightly longer duration of the discharge process compared to the current simulation (0.20 s compared to 0.16 s in the current work). As both CFC-12 and HFA134a have approximately similar vapour pressures, the type of propellant is not believed to be responsible for the durations difference (Smyth and Hickey, 2011). The longer duration in Clark's work could be attributed to the fact that they used a bigger metering chamber (100 μL compared to 63 μL in the current simulation). Clark's experimental measurements shown in Figure 3.23 reveal a similar shape of the pressure curves in the metering and expansion chambers compared to the curves obtained in Figure 3.4.

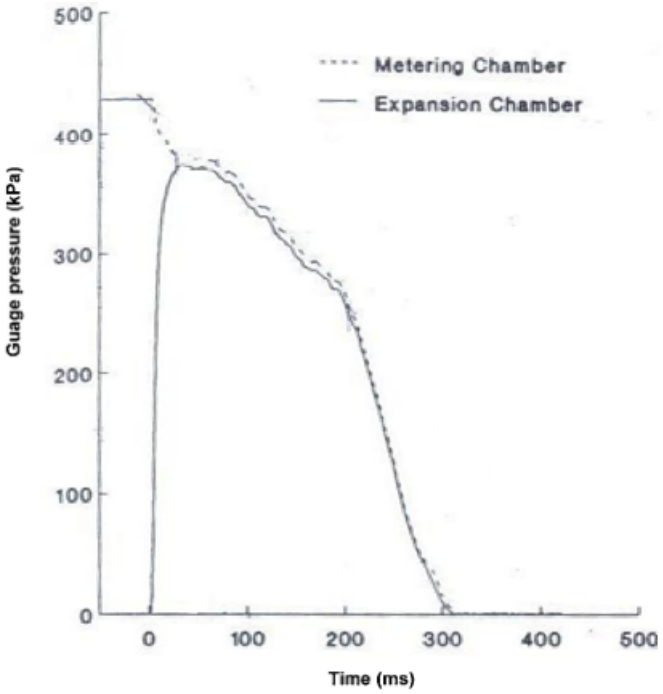

Figure 3.23: Measured pressure inside the metering and expansion chambers for a CFC-12 spray (Clark, 1991).

The similarity between Clark's measured pressure profiles and those simulated in this work (Figure 3.4) provides some evidence towards the validation of the velocity profiles obtained in Figures 3.2 and 3.3.

Effect of temperature on mass flow rate, residual mass and spray duration

Figure 3.4 also provides an explanation for the varying durations obtained at different temperatures. The long discharge processes observed at high temperatures could indeed be due to the fact that the metering chamber containing high pressure formulation might take a longer time to reach atmospheric pressure.

The model developed by Wigley *et al* stops after 0.08 s (Wigley *et al.*, 2002). However, when measuring pMDIs sprays using PDA, they observed an aerosolisation duration of between 0.15 s and 0.20 s. This is to be expected as the PDA set up measures particles moving or standing in the air until they evaporate whereas

simulation models stop running as soon as the pressure in the device becomes atmospheric.

However, Dunbar (1996) calculated an actuation duration of 0.215 s when using his simulation of a HFA134a-based pMDI which is in the same range as the duration of 0.195 s obtained from his PDA measurements (Dunbar, 1996). Dunbar's values are comparable to the duration of approximately 0.16 s obtained in the current work with similar room temperature and nozzle orifice diameter.

When using similar initial conditions, Ju *et al* (2010) found a discharge of approximately 0.1 s with both their numerical simulation and experimental results obtained with the dual laser beam method. The difference in duration between Ju *et al* and Dunbar is attributed to the calculation of a significantly higher mass flow rate in Ju's model compared to Dunbar's model. The mass flow rates from both works are shown in Figure 3.24.

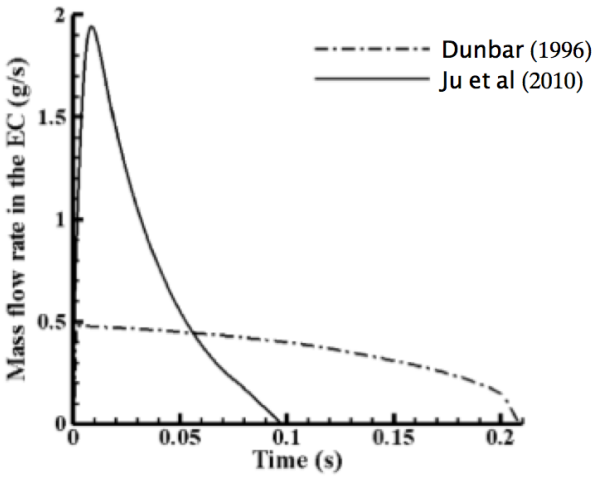

Figure 3.24: Total mass flow rates at nozzle orifice as a function of time (Ju *et al.*, 2010).

The peak mass flow rate of $2\,g{\cdot}s^{-1}$ obtained by Ju *et al* is 4 times greater than the maximum mass flow rate of $0.5\,g{\cdot}s^{-1}$ obtained by Dunbar (1996) although both simulations used similar device geometries. This difference might be due to the fact

that Ju *et al* assumed different velocities for the vapour and liquid phases whereas Dunbar assumed both phases had a similar velocity.

In this work, when the simulation was run at 293 K, the maximum mass flow rate was $1.7\,g{\cdot}s^{-1}$ which is relatively similar to Ju *et al*'s value although the duration is twice as long as Ju *et al*'s duration. As the current simulation uses the same metering chamber volume and propellant as Ju *et al* and Dunbar's simulations, it is believed that the simulations of Ju *et al* and Dunbar are not suitable to describe the entire discharge process in their models, as a significant proportion of the formulation is not discharged. It is expected that the residual mass of formulation remaining in the device in Ju *et al* and Dunbar's simulations would be higher than any of the residual masses shown in Figure 3.6.

The residual mass was shown to decrease at increasing temperatures. This might be due to the fact that at low temperatures, the vapour pressure of the propellant is too low to provide a sufficient amount of energy to discharge the entire metered dose. This is of interest as patients using their pMDIs in different environments could obtain varying amount of drug per metered dose. This might affect the efficacy of pMDIs treatments and might hinder the potential of pMDIs for the delivery of certain drugs such as insulin, for which the amount of drug delivered must be accurate.

The residual mass in the simulation might seem high (up to 70% at 293 K). However, the simulation does not take into account the heat transfer from the surroundings. If the user maintained the pMDI in the actuated position and therefore the valve orifice open, evaporation of the metering chamber formulation would take place due to heat transfer with the surroundings. As a result, the pressure in the metering chamber would increase, causing a prolonged discharge of the formulation and, therefore, a lower residual mass of the formulation in the metering chamber.

Effect of temperature on mass flashing and droplet size

Reports on droplets size at the nozzle orifice in the literature vary tremendously. Morén and Andersson (1980) estimated that the particles at the nozzle orifice have a diameter of approximately 35 μm using holographic microscopy. High-speed photography measurements from Wigley *et al* (2002) showed that large droplets of 30 μm to 60 μm diameters are issued from pMDIs at the beginning of the actuation. Hochrainer *et al* (2005) reported sizes in the range of the nozzle orifice diameter (approximately 200 μm to 500 μm). In the present simulation, one can only quote the minimum MMD as, when using Equation (2.53) developed by Clark (1991), the MMD $\rightarrow \infty$ at the beginning and at the end of the discharge process.

When using Equation (2.53), Dunbar (1996) obtained a minimum MMD of 8 μm compared to approximately 85 μm in the present simulation when using similar experimental parameters. Dunbar's value seems low compared to data in the literature.

In Equation (2.53), MMD values depend solely on the pressure and quality in the expansion chamber (respectively P_{ec} and q_{ec}). In order to understand the difference between the MMDs in the present work and Dunbar's values, the pressure and quality obtained from the current simulation and from Dunbar's simulation were compared. The pressure and quality calculated by Dunbar and Ju *et al* in the expansion chamber are shown in Figure 3.25.

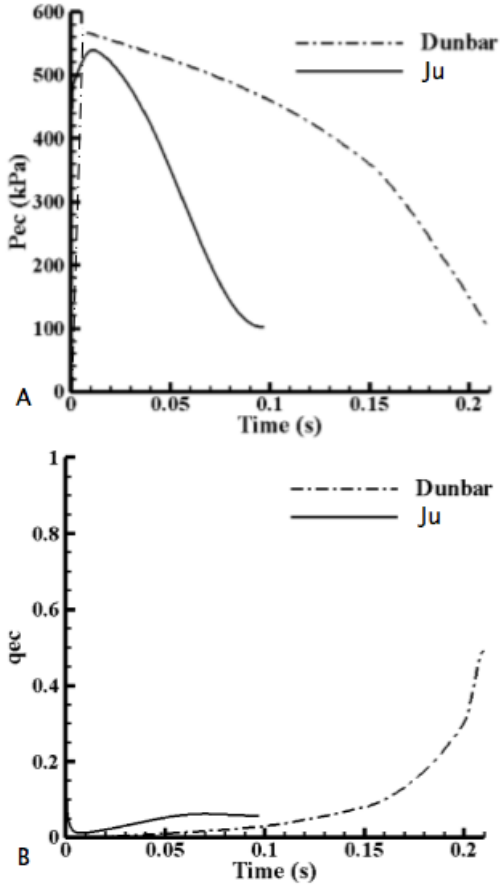

Figure 3.25: A. Pressure in the expansion chamber. B. Quality of the propellant in the expansion chamber (Ju *et al.*, 2010).

Dunbar's expansion chamber pressure is similar to the curve obtained at 293 K in Figure 3.4 although the sharp edge of the pressure peak is not present in the pressure graph in the current work. The experimental pressure measurements from Clark (1991) shown in Figure 3.23 and the pressure calculations from Ju *et al*'s simulation shown in Figure 3.25 did not reveal such a sharp pressure rise at the beginning of the actuation which would suggest that the present simulation is more in line with literature findings.

The quality in the expansion chamber shown in Figure 3.9 greatly differs from Dunbar's quality shown in Figure 3.25.

The quality in the expansion chamber in Ju *et al*'s model is below 0.1 at the end

of the actuation compared to a value of 0.5 calculated by Dunbar and 0.009 in the present simulation. The quality in the expansion chamber in the current work shown in Figure 3.9 has a lower magnitude compared to Ju's simulation. However, the shape of the quality plot in Ju *et al*'s simulation is more similar to the quality plot in Figure 3.9 than to Dunbar's quality plot which has an exponential shape.

The value of the expansion chamber quality in the present simulation is more similar to the quality value in the simulation of the discharge of a HFA134a spray by Shaik (2009). Shaik obtained a q_{ec} smaller than 0.02 in the expansion chamber when using a pMDI with a valve orifice diameter of 0.42 mm and a nozzle orifice diameter of 0.48 mm compared to a valve orifice diameter of 0.7 mm and a nozzle orifice diameter of 0.5 mm in the present simulation. The bigger valve orifice diameter in the present work might explain the lower quality values compared to Shaik's results as a bigger valve orifice area would allow a higher mass of wet propellant to be discharged from the metering chamber in the expansion chamber.

Dunbar (1996) calculates a quality of 0 at the onset of actuation in the expansion chamber when using Equation (3.19).

$$q_{ec} = \frac{mvp + ma}{mvp + mlp + ma} \tag{3.19}$$

where q_{ec} is the quality in the expansion chamber, mvp is the mass of vapour propellant in kg, mlp is the mass of liquid propellant in kg and ma is the mass of air in kg. As at initial conditions the expansion chamber is filled with air and contains no propellant, the quality in the expansion chamber should be 1. It is therefore not clear how Dunbar obtained a value of 0 for the quality in the expansion chamber at initial conditions.

Dunbar's low MMD value of 8 μm could be due to his extremely high expansion chamber quality calculations. As the quality and pressure plots in the present

simulation are more similar in magnitude and shape to other works, the MMD values obtained from the model developed in Chapter 2 might be more reliable.

Figure 3.7 shows that at higher temperatures, a higher proportion of the formulation could evaporate at the nozzle orifice. This is expected as, when the formulation is heated at increased temperatures, the propellant would have more energy to evaporate and because the surrounding air would also be at a high temperature, less energy of evaporation would be required. A temperature increase should also lead to a greater formulation pressure inside the device, leading to the aerosolisation of smaller droplets. This was illustrated in Figure 3.8.

3.4.2 Effect of the valve and nozzle orifices diameters on spray characteristics

Effect of nozzle to valve orifices ratios on the pressure build up in the expansion chamber

Figure 3.10 showed there was a greater expansion chamber pressure build up at lower nozzle orifice to valve orifice diameter ratios which is to be expected as more formulation would enter the expansion chamber and a lower amount of formulation would be discharged from the expansion chamber.

Figure 3.12 showed that the velocity of the propellant increased at lower nozzle orifice diameters. As one of the roles of the expansion chamber is to reduce the speed of the spray in order to reduce the risk of drug particles impacting on the back of the user's throat, small nozzle orifices might not be optimal for an efficient pMDI drug delivery. However, Figure 3.11 also showed that smaller nozzle orifices promote the formation of smaller droplets which impact less on the throat and penetrate more efficiently into the lungs (Finlay, 2001).

Smaller nozzle orifice diameters were shown to lead to the aerosolisation of smaller and faster droplets, which was due to a higher expansion chamber pressure build up. This finding is in agreement with Berry *et al* (2003) who showed that the amount of fine particles was inversely related to the nozzle orifice diameter.

Several valve orifice diameter plots could be added to Figure 3.13 and could be used when choosing the valve and nozzle orifices diameters of the pMDI according to the expansion chamber pressure build up to be achieved.

As the ratio of the twin orifice diameters was shown to affect the velocity of the spray, it is of importance to remind pMDI users that mouthpieces are not interchangeable and cannot be coupled with any canister.

Effect of the nozzle orifice on the aerosolisation duration

In their simulation, Ju *et al* (2010) calculated a discharge of approximately 0.1 s to 0.28 s depending on the formulation and nozzle orifice used. The shortest duration was obtained with a 0.5 mm nozzle orifice diameter when simulating the discharge of pure HFA134a (similar to the nozzle orifice in the current work and Dunbar's work). The longest duration was obtained with a 0.3 mm nozzle orifice diameter when simulating the discharge of multi-component formulations. This agrees with Lewis (2007), who showed that the duration of a spray decreased when mouthpieces with higher nozzle diameters were used.

In the present work, the duration of the discharge process also decreased at increasing nozzle orifice diameters as was shown in Table 3.3.

However the difference observed across the range of most commercially available nozzle orifice diameters was relatively small (0.017s) (Swarbrick, 2007). As a result, it is believed that smaller nozzle orifices could not be used to improve users coordination process by providing a longer spray discharge.

3.4.3 Effect of the opening rate of the valve orifice on spray characteristics

In the work of Clark (1991), Dunbar (1996), Aamir and Watkins (2000) and Ju *et al* (2010), the valve orifice area was assumed constant throughout the actuation process. This assumption is unrealistic as the valve orifice does not open instantaneously and the simulation showed that the time it takes to fully open might affect the MMD of the particles at the nozzle orifice.

The opening rate of several users was measured. The opening rate of a "weak" inexperienced female user resulted in a lower pressure build up in the expansion chamber, leading to higher MMD values compared with instantaneous openings of the valve orifice. This can be explained by the fact that when the valve opens slower, the area of the valve which is available for discharge is smaller for a longer time, allowing a lower amount of propellant to enter the expansion chamber, which in turn would comparatively reduce the expansion chamber pressure. As the valve orifice opening rate is related to the force of actuation, this finding might mean that pMDI users with low actuation forces would aerosolise larger droplets than users with high actuation forces.

In order to resolve this issue, a smaller valve orifice diameter could be used in order to reduce the time needed to open the valve orifice fully for users with low rates of valve orifice opening. Figure 3.13 could also be used in order to determine the optimal nozzle orifice diameter to be combined with a small valve orifice diameter in order to provide the necessary expansion chamber pressure to produce desirable MMD values.

3.4.4 Effect of a suspended drug on spray characteristics

The lower vapour pressure calculated at high drug concentrations can be attributed to the lower mass of propellant discharged from the metering chamber to the expansion chamber. As the propellant mass is smaller, the enthalpy in the expansion chamber decreases, leading to a lower expansion chamber temperature and thus to a decrease in the expansion chamber pressure. The lower expansion chamber pressure, in turn, leads to a decrease in the velocities of both the liquid and vapour phases of the spray.

In their simulation of suspension formulations, Ju *et al* (2010) obtained similar velocity profiles when simulating several formulations containing varying amount of non-volatile components and HFA134a. They calculated velocities decreasing from $19\,\mathrm{m{\cdot}s^{-1}}$ at 100% HFA134a to $18\,\mathrm{m{\cdot}s^{-1}}$ at 90% HFA134a.

The increase in MMD values calculated at increasing FP concentrations was due to the lower expansion chamber pressure but also to a lower quality in the expansion chamber that would be expected as FP is a non-volatile and would therefore reduce the proportion of vapour phase forming in the device. Those results are in line with Polli *et al*'s experimental data as they found that the MMD of formulations increased with the concentration of API (Polli *et al.*, 1969).

However in the present simulation, Equation (2.53) only takes into account the pressure and quality in the expansion chamber to calculate the MMD at the nozzle orifice whereas, in reality, the size of aerosolised droplets would also increase with the size of the drug particles present in the formulation and with their tendency to aggregate (Smyth, 2003), (Murnane *et al.*, 2008). As Equation (2.53) fails to account for those phenomena, it cannot be used to accurately calculate the MMD of suspension formulations.

3.5 Summary

The simulation presented in Chapter 2 was validated by comparing the results to diverse experimental work and simulations (Clark, 1991), (Dunbar, 1996), (Wigley *et al.*, 2002) and (Ju *et al.*, 2010).

The main findings from the model were that the force of actuation might affect the size of the aerosolised particles, which means that weaker patients would potentially aerosolise larger droplets and would therefore risk having a lower amount of drug particles reaching their lungs.

High nozzle to valve orifices diameter ratios were found to lead to a smaller pressure build up in the expansion chamber and consequently to the formation of larger droplets of lower velocity at the nozzle orifice. Higher temperatures were found to increase the initial velocity and reduce the MMD of the discharged sprays, which would translate into a varying performance of pMDIs when exposed to diverse environments. Higher temperatures were also found to reduce the mass of propellant remaining in the metering chamber after the discharge process.

When studying the effect of FP particles on the characteristics of the spray, it was found that increasing the concentration of FP led to a reduced initial velocity and higher MMD values which is in line with the literature.

After comparing the model to the literature, it was found that some of the results from the present simulation might give more accurate predictions than previous models.

Chapter 4

Experimental studies on the actuation of metered dose inhalers

4.1 Introduction

The aerosolisation process is divided into two distinctive phases. The primary atomisation, which is the process involved in the transformation of the liquid formulation into discrete droplets, occurs in the pMDI. Once the spray exits from the nozzle orifice, the secondary atomisation begins. Secondary atomisation describes the behaviour and the transportation of the droplets downstream of the nozzle orifice. The aim of the numerical model was to simulate the behaviour of the flow from the metering chamber to the nozzle orifice, which corresponds to the primary atomisation of the spray. In this chapter, the droplets size was measured during their secondary atomisation downstream of the nozzle orifice.

Secondary atomisation represents the evaporation of the spray occurring outside the pMDI. This atomisation is thought to be a 2-phase gas/liquid process in which the liquid ligaments attached to the gaseous propellant are teared apart by aero-

dynamic forces, causing the aerosolisation of the liquid phase of the spray. The evaporation of the spray starts during the flashing phase of the propellant during the primary atomisation and continues during the transportation of the spray, leading to the reduction of droplets size.

The size of particles has been shown to influence their deposition profiles within the respiratory tract. In *in vivo* studies by Leach *et al* (2002), a HFA-based formulation containing beclamethasone dipropionate with a mass median aerodynamic diameter (MMAD) of 0.9 μm was compared to a CFC-based formulation containing beclamethasone dipropionate with a MMAD of 3.5 μm. The oropharyngeal deposition obtained when testing the CFC formulation was 4 times higher and the total lung deposition was more than 10 times lower than the values obtained for the HFA-based formulation. When testing another CFC-based formulation with a MMAD of 2 μm, the oropharyngeal deposition was lower and the lung deposition was higher than the values obtained with the CFC-based formulation with a MMAD of 3.5 μm (Leach *et al.*, 2002). This shows that particles size significantly influences the spray deposition pattern.

Due to the transient and metastable nature of the flow inside the device, the droplets size and velocity vary during the actuation of the pMDI as was shown in the mathematical simulation in Chapter 3. The droplets velocity also decreases during their trajectory as the spray loses kinetic energy. The size of droplets issued from pMDIs decreases during their trajectory between the nozzle orifice and the oropharynx due to the volatile nature of their propellant. Once the volatile components have completely evaporated, the particles reach their residual size. The size of particles issued from pMDIs can be measured using several experimental techniques such as laser diffraction and impaction techniques described in Chapter 1. Impaction is currently the preferred technique for both the industry and academia as it is the only method directly measuring the active pharmaceutical ingredient

(API) mass-weighted size distribution and the fraction of the spray depositing by impaction on the back of the throat. It also provides consistent results (Mitchell and Nagel, 2004).

The mechanism of impaction can be illustrated by the Stokes number described in Equation (4.1) (Lambert *et al.*, 2011).

$$Stk = \frac{\rho_p \, {d_p}^2 U_p}{18 \, \eta \, r} \tag{4.1}$$

where Stk is the Stokes number, ρ_p is the density of the particle in kg·m^{-3}, d_p is the particle diameter in m, U_p is the velocity of the particle in m·s^{-1}, η is the air viscosity in kg·m^{-1}·s^{-1} and r is the airway radius in m. The Stokes number can be defined as the ratio of the stopping distance of the particle to the diameter of the obstacle. When the Stokes number increases, the particles have greater inertia and are more likely to impact on the oropharynx or on other points of bifurcation in the airways (Clark, 2009).

The inertia of a particle is proportional to its velocity and to the square of its diameter (Dunbar, 1996). As a result, large and fast particles tend to deposit more at the biggest bifurcation of the respiratory tract, which is located at the throat. The high size and velocity of particles therefore affect the efficiency of pMDIs as they reduce the amount of drug that can reach the lungs. The velocity of the particle increases with the inhalation flow rate of the patient. pMDI users with high inhalation flow rates might therefore have a higher throat deposition than users with low inhalation flow rates. Impaction apparatus are able to simulate the effect of inhalation flow rate on throat deposition which is an advantage compared to laser techniques.

Impaction measurements separate particles according to their inertia by making them follow an airflow through various impaction stages. Each stage plate con-

tains jets with different cut-off diameters which depend upon the flow rate drawn through the device. The particles with the largest aerodynamic diameter have a higher inertia. As a result, they are not able to adapt their trajectory to the sinuous airways and impact on the first plates. The smallest particles, which do not impact on the first plates, reach stages with smaller cut-off diameter jets. The first stages represent the upper respiratory tract whereas the last stages represent the lower respiratory tract. Impactors designs may vary with different number of stages, number of jets per stages and jet dimensions. The next generation impactor (NGI) has 7 stages with cut off diameters of 11.72 μm, 6.40 μm, 3.99 μm, 2.30 μm, 1.36 μm, 0.83 μm and 0.54 μm respectively when operating at a flow rate of 30 $\mathrm{L{\cdot}mn^{-1}}$ (Copley, 2012). A picture of a NGI can be seen in Figure 4.1.

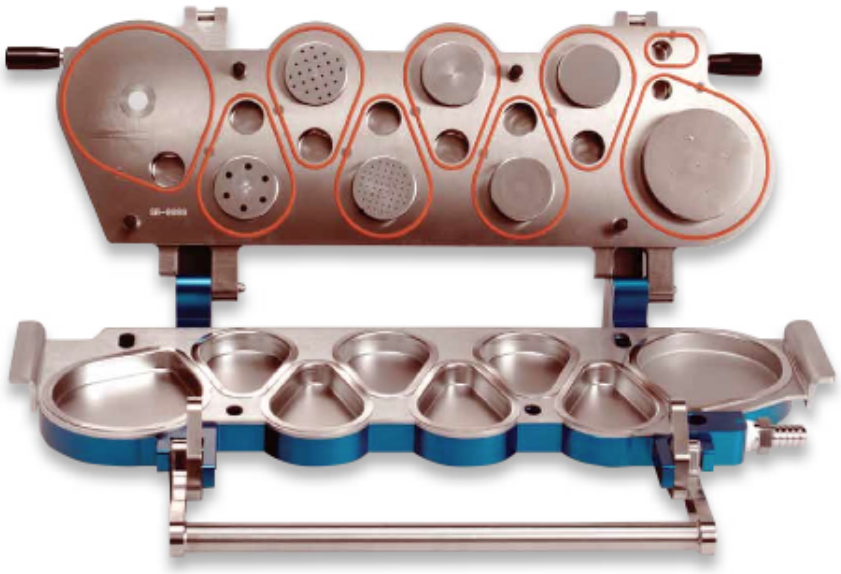

Figure 4.1: Open view of a NGI showing nozzles and collection cups (Copley, 2012).

The efficiency of pMDIs is defined as the percentage of drug delivered to the lungs. It can be assessed using several measures such as the percentage of particles reaching the lungs for each actuation. It can also be defined using the fine particles fraction (FPF) discussed in Chapter 1. The efficiency of pMDIs depends on many factors such as the formulation design, the device design and the way the device is

handled (e.g. users often have difficulties to coordinate the actuation of the device with the inhalation of the spray). Those parameters have an effect on the deposition location within the respiratory tract. Variations in one or several of those parameters will therefore influence the quantity of particles reaching the lungs.

4.1.1 Literature review of factors determining aerosol size distribution

Many articles have focused on the effect of parameters such as formulation and device designs on the deposition patterns of particles in the respiratory tract. For example, Polli *et al* (1969) investigated the effect of drug particles size inside the formulation, drug and surfactant concentration, propellant vapour pressure, propellant temperature and nozzle orifice diameter on particles residual size.

Pu *et al* (2011) compared the particle size measurements using a Sympatec® and an Andersen cascade impactor (ACI). They found that both methods give similar fine particle fractions and mean diameter values for formulations containing a low concentration of non-volatiles. They showed that the residual size of aerosol droplets increased for suspension formulations containing drug particles compared to pure propellant formulations. They also found that the size of residual particles increased with the size of the API used in the formulation.

For their investigation, Pu *et al* (2011) automatically actuated the pMDIs using a Sprayer device from Sympatec®. This device can be used to control the acceleration, velocity, stroke length or force of the actuation piston (Sympatec, 2010). They did not control the force of the piston but its actuation velocity.

Other systems have been used to provide the automatic actuations of canisters such as the SprayVIEW MDx automated actuator (Proveris Scientific Corporation,

Marlborough, MA), controlled by Proveris Viota software (Version 5.2.1) used by Liu *et al* (2012). However, the effect of those actuations have not, to the best knowledge of the author, been investigated or compared with manual actuations.

Murnane *et al* (2008) studied the behaviour of drugs in suspension formulations. They noticed that in suspension formulations, certain drugs such as fluticasone propionate (FP) were prone to aggregation and as a result, did not disperse efficiently in the propellant.

Aggregates forming in suspension formulations can be retrieved in the residual droplets, after all propellant has evaporated. Michael *et al* (2001) showed that the size of the aggregates increased with the concentration of the API. This phenomenon is shown for FP particles in HFA134a in Figure 4.2.

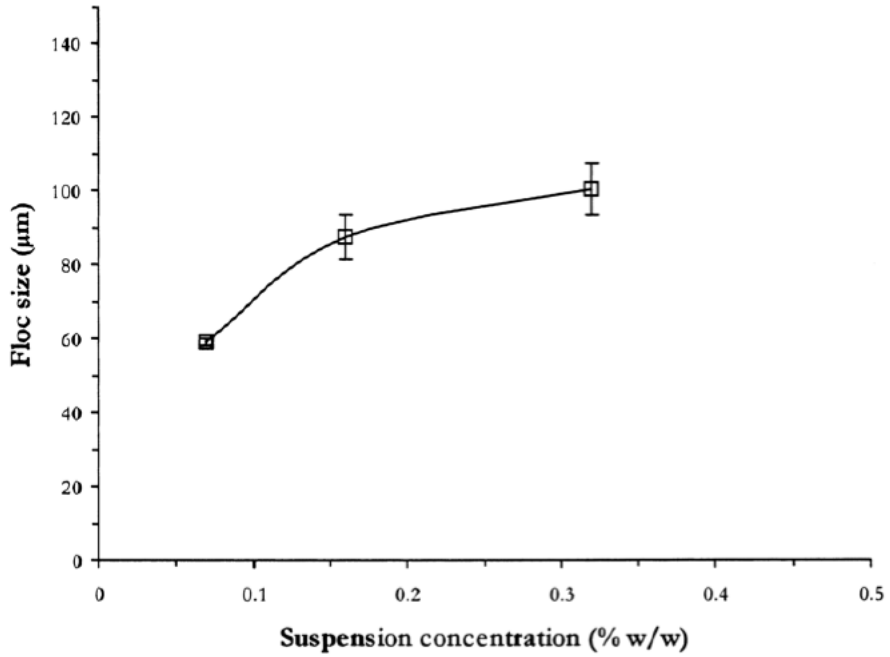

Figure 4.2: Effect of increasing suspension concentrations on average aggregates size of fluticasone propionate in HFA134a (Michael *et al.*, 2001).

As the size of residual particles issued from suspension formulations corresponds to the size of the aggregates, aggregation of drug particles could reduce the FPF

of suspension formulation (Murnane *et al.*, 2008).

Pu *et al* (2011) also found that the FPF of formulations decreased with the increasing size of the API particles.

Brambilla *et al* (1999) investigated the effect of non-volatiles concentration on the residual particles size. They showed that adding non-volatile components increased significantly the size of the particles issued from pMDIs.

Lewis (2007) reported that pMDIs with small nozzle orifices led to a higher FPF than pMDIs with large nozzle orifices. Later in this chapter, those findings are compared to the NGI results in order to determine the influence of the pMDI design on the pattern of the aerosolised sprays.

Stein *et al* (2012) studied the evaporation mechanisms of aerosols issued from pMDIs. They also showed that residual droplets size increased at higher drug concentrations and that the initial particles size increased with the diameter of the nozzle orifice, the metering chamber volume and the concentration of non-volatiles in the formulation.

Haynes *et al* (2004) compared the particle size measurements using a Malvern Spraytec® and an ACI. They found that the Malvern Spraytec® overestimated the size of HFA-based aerosols compared to the ACI. This might be due to the fact that the sprays are not fully evaporated when measured by the Malvern Spraytec®. They showed that it was possible to obtain comparable results with both methods for a solution formulation when placing a 20 cm simulation throat between the pMDI and the Malvern Spraytec® measurement zone as it would allow a more complete evaporation of the aerosol before its measurement. They also noticed that particles size decreased at high temperatures. Their results on FPF and D_{50} obtained with the Spraytec® are in line with the measurements of Pu *et al* (2011)

with the Sympatec®.

4.1.2 Aims and objectives

As the actuation force is not constant among different types of populations and might influence the behaviour of the spray, it was decided to investigate the impact of varying forces on the velocity and size of particles issued from pMDIs. The aim of this study was to identify whether the actuation force affected the deposition pattern of several formulations and if so, for which formulation it had a stronger impact. The influence of the actuation force on the API fraction depositing in the throat was assessed. This work has, to the best knowledge of the author never been conducted before. In order to identify the potential effect of actuation force on spray characteristics, the performance of each formulation under normal adult actuation was studied. A method was also developed to allow the automated actuation of the cylinder under several actuation forces.

This chapter studies the deposition pattern of a suspension and two solution formulations aerosolised using two mouthpieces of varying nozzle orifice diameters. The suspension and solution formulations contained similar FP concentrations. The two solution formulations contained varying excipients at similar concentrations. This has, to the best knowledge of the author never been studied before.

It has been shown in Chapter 3 that varying nozzle orifice diameters, formulation designs and valve opening rates may affect the velocity and size of initial particles at the nozzle orifice. In this chapter, the role of formulation design, mouthpiece design, and actuation force on particles deposition patterns was investigated using the NGI.

4.2 Materials and methods

4.2.1 Materials and equipment

- Solkane® 134 (inhalation grade) (Solvay Florides Inc., Hanover, Germany)
- polyethylene glycol 400 (PEG400) (pharmacopoeial quality) from Fluka (Sigma-Aldrich Chemie GmbH, Industriestrasse 25 CH-9471 Buchs SG Switzerland).
- ethanol (pharmacopoeial quality) (Fisher Scientific, Loughborough, UK)
- fluticasone propionate (pharmacopoeial quality) (LGM Pharma, Boca Raton, Florida, USA); (Batch number 458763)
- aluminium canisters (Bespak, Norfolk, UK)
- transparent polyethylene terephthalate (PET) canisters
- a filling crimping machine (Pamasol, Switzerland)
- 50 μL non-continuous valves from Valois (Valois pharmaceutical division, 780160 Marly Le Roi, France)
- a high-pressure liquid chromatography (HPLC) apparatus Agilent 1260 Infinity chromatograph (S/N DEAAV01717) (Agilent Technologies UK lTD., Edinburgh, UK)
- a Kinetex 2.6 μm particle size reversed-phase column (XB-C18 - 50 mm x 30 mm (Serial 557858.3, Phenomenex, Macclesfield, UK))
- HPLC grade methanol for the preparation of mobile phase and washing solution (Fisher Scientific, Loughborough, UK)
- Hipersolv® grade ammonium acetate for the preparation of the mobile phase and washing solution (Lab3 Ltd, Bristol, UK)

- water from a laboratory water purification unit (Purite, GDF-Suez, France)
- analar grade methanol for washing (Fisher Scientific, Loughborough, UK)
- a dosage unit sampling apparatus (DUSA) for pMDIs (Copley Scientific, Nottingham, UK)
- glass fibre filters to prevent drug particles from escaping the DUSA (Whatman, Kent, UK)
- a DFM3 Flow Controller (Copley Scientific, Nottingham, UK)
- a high capacity pump Model HCP5 (Copley Scientific, Nottingham, UK)
- a critical flow controller Model TPK (Copley Scientific, Nottingham, UK)
- a NGI containing a throat, 7 stages and a micro-orifice collector (Copley Scientific, Nottingham, UK)
- a rotary mixer (Sandrest, East Sussex, England)
- a silicone device/NGI adaptor, manufactured in-house
- a Flixotide® mouthpiece (Allen and Hanburys Ltd, Middlesex, UK)
- an Alvesco® mouthpiece (Takeda Pharmaceuticals International GmbH, Zurich, Switzerland)
- an experimental aluminium rig connected to a switch providing automated actuation of the canisters (built and designed in-house from De Montfort University)
- a pneumatic cylinder (SMC CD85N12-10S-B) (SMC, Buckinghamshire, UK)
- a drying oven Type VT6 (Thermo Fisher Scientific, MA, United States)

4.2.2 Manufacture of test formulations

Size measurements of FP particles using liquid dispersion laser diffraction (Jaffari *et al.*, 2013)

The size measurements of the FP particles were conducted by Jaffari. Her method and findings are reported below.

Laser diffraction particle sizing was carried out using a Malvern Mastersizer® X (Malvern Instruments Ltd, UK) fitted with a 100 mm focal length lens (0.5 μm to 180 μm) and an MS7 magnetically stirred cell. Saturated solvent dispersants were sonicated for 30 mn and stirred overnight. Approximately 1 mg of powder was added to 2 mL filtered dispersant (0.2 μm cellulose acetate syringe ffilter, Gema Medical S.L., Spain) and sonicated (Sonicleaner, DAWE, Ultrasonics Ltd, USA). A background reading was taken and the suspension was added to the sample cell until obscuration was between 10% and 30%. Following equilibration (30 s to 60 s), ten individual measurements were taken for n=3 samples to obtain particle size measurements (Dv_{10}, Dv_{50}, Dv_{90}, volume mean diameter; VMD) calculated using Fraunhofer theory.

The size characteristics of the FP particles are shown in Table 4.1.

Powder	Dv_{10} (μm)	Dv_{50} (μm)	Dv_{90} (μm)	VMD (μm)	Span
FP	1.09±0.02	2.76±0.03	4.97±0.11	2.94±0.04	1.41

Table 4.1: Size characteristics of the FP particles.

Manufacture of solution formulations

Solvents are often added to HFA-based formulations in order to better dissolve the APIs in HFA134a. In this work, one solution formulation contained ethanol and the other solution formulation contained both ethanol and PEG400.

It has been shown that the efficiency of a pMDI decreased at ethanol concentrations

greater than 15% w/w (Gupta *et al.*, 2003). It was thus decided to put 15% w/w of ethanol in the formulation.

In order to determine the solubility of FP in the HFA134a and ethanol solution, the formulations were manufactured in clear PET canisters. FP was first weighed and disposed in the transparent canister. Ethanol was added at the end in order to avoid its evaporation. A magnetic stirrer of 8 mm was added before crimping the canisters using the filling crimping machine (Pamasol, Switzerland). HFA134a was forced under pressure in the canisters until they contained 15 g of formulation. The formulations were stirred overnight on a platform shaker at 150 rpm.

Several concentrations of FP were tested until the final concentration of 0.05% w/w allowed the complete dissolution of FP in the formulation. The final formulation therefore contained 0.05% w/w of FP, 15% w/w of ethanol and approximately 85% w/w of HFA134a. This formulation is referred to as HEF. Several metal canisters containing the HEF formulation were prepared from a large batch of FP+ethanol in order to improve the accuracy of the process. Ethanol was added before closing the recipient. The recipient was then plunged into an ultrasound bath until the drug was dissolved in the ethanol. The canisters were filled from the batch and crimped immediately using the filling crimping machine in order to prevent ethanol evaporation. HFA134a was then forced under pressure in the canisters.

PEG400 is a hydrophilic cosolvent helping APIs to dissolve in propellants. PEG400 was used in the second solution formulation. The same type of procedure was undertaken for the manufacture of this formulation containing 0.05% w/w of FP, 10% w/w of ethanol, 5% w/w of PEG400 and approximately 85% w/w of HFA134a. This formulation is referred to as HPEF. The HEF and HPEF formulations contained similar FP and cosolvents concentrations in order to allow direct comparisons between those two formulations. However, the filling crimping machine could not

force the exact same mass of propellant into each canister, resulting in slightly different compositions between canisters for each formulation. The four canisters with the most similar compositions were chosen for each formulation.

Manufacture of a suspension formulation

FP is often used in HFA134a-based suspension formulations such as Flixotide by Allen and Hanburys Ltd and Flovent by Glaxosmithkline (Murnane *et al.*, 2008). For this reason, a FP suspension containing HFA134a and 0.05% w/w FP formulation was investigated in this work. The 0.05% w/w FP concentration was chosen to allow direct comparisons with the HEF and HPEF formulations. This formulation is referred to as HF. To manufacture this formulation, the drug was weighed and deposited into the canisters which were then crimped and filled with approximately 15 g of HFA134a using the filling crimping machine. However, the filling crimping machine could not force the exact same mass of propellant into each canister, resulting in slightly different compositions between canisters. The three canisters with the most similar compositions were chosen for the study of the HF formulation.

The composition of the three formulations studied are summarised in Table 4.2.

	Names of the formulations		
	HF	HEF	HPEF
FP	0.05%	0.05%	0.05%
HFA134a	$\simeq$ 99.95%	$\simeq$ 84.95%	$\simeq$ 84.95%
Ethanol	-	15%	10%
PEG400	-	-	5%

Table 4.2: Composition of the studied formulations.

Table 4.3 shows an inventory of the formulations manufactured.

	Formulation crimped with a Valois 50 μL valve	Number of canisters
Solution formulations	HEF HPEF	26 35
Suspension formulation	HF	5

Table 4.3: Inventory of the manufactured formulations.

4.2.3 Device dimension characterisation

For the suspension formulation, a Flixotide® mouthpiece with a length of 25 mm and a nozzle orifice diameter of 0.50 mm was used. The Flixotide® mouthpiece was chosen as it is designed for a commercial suspension formulation.

For the two solution formulations, an Alvesco® mouthpiece with a length of 37 mm and a nozzle orifice diameter of 0.20 mm was used. The Alvesco® mouthpiece was chosen as it is designed for a commercial solution formulation.
The solution formulations were also aerosolised with the Flixotide® mouthpiece for comparative purposes. Both nozzle diameters were determined using a travelling microscope.

4.2.4 High performance liquid chromatography analysis

HPLC was used to determine the concentration of FP depositing at each stage of the NGI.

Mobile phase

The mobile phase used in this experiment had the following composition:

- 65% methanol

- 35% ammonium acetate 0.6% (w/v)(aq.)

The washing solution had the following composition:

- 75% methanol
- 25% ammonium acetate 0.6% (w/v)(aq.)

The mobile phase and the washing solution were manufactured using a similar procedure. Purite water was used as impurities can affect the results of HPLC measurements. After 0.6% (w/v) aqueous ammonium acetate solution was mixed with the methanol, the mixture was degassed using a sonicator for approximately 60 s. It was then filtered in a vacuum filtration device using filters of cutoff diameter 2.5 μm (Whatman, Kent, UK) before being sonicated again for 30 mn.

Calibration standards

HPLC vials with several known concentrations of FP were analysed to obtain a calibration curve. The nominal concentrations of FP in mobile phase for the calibration curves were 50 μg·mL^{-1}, 25 μg·mL^{-1}, 10 μg·mL^{-1}, 5 μg·mL^{-1}, 1 μg·mL^{-1} and 0.5 μg·mL^{-1}.

A stock solution was prepared by accurately weighing 2.5 mg of FP with a weighing scale (Mettler Toledo, UK), transferring it into a 50 mL volumetric flask and bringing the solution to volume with mobile phase.

The stock solution was used to prepare a calibration series by pipetting the volumes shown in Table 4.4.

Theoretical concentration (μg·mL^{-1})	Volume of stock solution (mL)	Final volume (mL)
25	10	20
10	5	25
5	1	10
1	1	50
0.5	5 (of the 1 μg·mL^{-1} solution prepared above)	10

Table 4.4: Volume of stock solution required to prepare a calibration series range of 0.5 μg·mL^{-1} to 50 μg·mL^{-1}.

The above solutions were transferred into HPLC vials for analysis by HPLC. A linear regression analysis was conducted, using the LINEST function on Microsoft Excel, to establish the relationship between the peak area determined by the HPLC analysis and the drug concentration in the HPLC vials.

Sensitivity

The limit of area detection (LOD_{area}) and limit of area quantification (LOQ_{area}), both in mAU·s^{-1}, were calculated using Equations (4.2) and (4.3).

$$LOD_{area} = Y_{intercept} + 3SD \tag{4.2}$$

$$LOQ_{area} = Y_{intercept} + 10SD \tag{4.3}$$

where SD is the standard deviation of the $Y_{intercept}$ from the linear regression analysis in mAU·s^{-1}.

The limit of concentration detection ($LOD_{concentration}$) and limit of concentration quantification ($LOQ_{concentration}$), both in μg·mL^{-1}, were calculated using Equations (4.4) and (4.5).

$$LOD_{concentration} = \frac{LOD_{area} - Y_{intercept}}{slope} \tag{4.4}$$

$$LOQ_{concentration} = \frac{LOQ_{area} - Y_{intercept}}{slope} \tag{4.5}$$

Chromatographic conditions

In the experiments below, the mobile phase flow rate was $0.5\,\mathrm{mL{\cdot}mn^{-1}}$ and the temperature of the column was set to $40\,^{\circ}\mathrm{C}$. A UV wavelength of 240 nm was used to detect the FP. Under those conditions, the retention time for FP was approximately 3 mn.

Precision

The precision of the machine was assessed using the standard deviation of several injections of the same vial. The standard deviation of three injections of $20\,\mu\mathrm{L}$ was calculated for each vial and, as it always laid below 2% of the mean, it was considered that three injections were sufficient to ensure an acceptable precision level.

Repeatability

In order to check the accuracy and repeatability of the method above, 5 accuracy standards of concentration $10\,\mu\mathrm{g{\cdot}mL^{-1}}$ were prepared for each calibration curve. For each standard, 2 mg of FP was weighed accurately into a 20 mL volumetric flask. Mobile phase was added until the level of the liquid almost reached the volume mark on the flask. The flask was then sonicated for a few minutes before being finally brought to volume. The final solution was transferred into a HPLC vial for analysis by HPLC. The amount of FP was then calculated using the calibration curve. This process was repeated five times for each calibration curve.

The percentage recovery was calculated using Equation (4.6).

$$\%\,\mathrm{Recovery} = \frac{\text{Calculated concentration}}{\text{Theoretical concentration}} \tag{4.6}$$

4.2.5 Emitted dose analysis of formulations

The dose content of each canister for each formulation was determined using a dosage unit sampling apparatus (DUSA) of the British Pharmacopoeia (2007 261 /id). Four doses determinations were performed for each canister used in the experiments. An airflow of 30 $L \cdot mn^{-1}$ was drawn through the DUSA using a vacuum pump in order to simulate an inhalation of 3.25 L and lasting 6.5 s (Copley Scientific, Nottingham, UK).

The DUSA was branched to the mouthpiece on one side and a rubber fitting helped to form a tight seal between them. On the other side the DUSA was branched to the vacuum pump and the connection was sealed using Parafilm M flexible film. A glass fibre filter by Whatman was inserted inside the apparatus to avoid drug particles escaping on the side of the DUSA branched to the vacuum pump.

The airflow was adjusted to 30 $L \cdot mn^{-1}$ using the DFM3 flowmeter (Copley Scientific, Nottingham, UK) before each experiment. The canister was placed inside a mouthpiece and was shaken for 5 s with one shot fired to waste before inserting the mouthpiece in the rubber fitting. The pump was activated for 5 s prior to pMDI discharge. Each formulation was actuated 4 times into the DUSA, allowing a sufficient amount of drug to be quantified by the HPLC method (Section 4.2.4). Between each actuation, the mouthpiece was removed and the canister was shaken. There was a pause of approximately 10 s between each discharge.

After the 4 actuations, the DUSA was opened and the glass fibre filter was placed in a 50 mL beaker. Approximately 40 mL of the washing solution prepared in Section 4.2.4 were transferred into the beaker. The beaker was then sonicated for a couple of minutes in order to dissolve the drug particles deposited on the glass fibre filter. The content of the beaker was transferred to a 50 mL volumetric flask and brought

to volume with washing solution.

After each use, the DUSA, mouthpiece, canister and rubber fitting were first washed with water then with methanol prior to further testing. The dose content analysis was realised for the three formulations and for a commercial Flixotide® formulation.

4.2.6 Inertial impactor testing of emitted aerosol dose

The NGI was connected to a vacuum pump set at $30\,\mathrm{L{\cdot}mn^{-1}}$. The connection was sealed using Parafilm M flexible film. The flow rate through the NGI was monitored using the DFM3 Flow Controller (Copley Scientific, Nottingham, NG4 2JY). The throat was fitted with a silicone mouthpiece adaptor to form a tight seal around the mouthpiece. Prior to each run, all stages of the NGI were rinsed with 100% (v/v) methanol followed by 100% purite water and dried in an oven at 40 °C. Before each NGI run, the vacuum pump was switched on for approximately 5 s and the canister was shaken for around 10 s and fired once. For each NGI test, the canister was actuated 8 times into the NGI. Between each actuation, there was a pause of 10 s during which the pMDI was shaken for 5 s.

After the experiment, the device (including the mouthpiece, the stem of the canister and the mouthpiece adaptor) was washed with the washing solution then transferred into a 20 mL volumetric flask. It was then sonicated before being brought to volume.

The throat was washed with the washing solution then transferred into a 50 mL volumetric flask. It was then sonicated before being brought up to volume.

Volumes of washing solution of 10 mL were measured with a pipette and transferred into each of the first 5 stages of the NGI. Volumes of washing solution of 5 mL were measured with a pipette and transferred into each of the last 3 stages of the NGI.

All stages were placed on a rocker for approximately 5 mn in order for the FP to dissolve completely in the washing solution.

The device volumetric flask, throat volumetric flask and the 8 stages were each transferred into separate HPLC vials. The concentration of FP in the different parts of the NGI was determined by HPLC using the linear regression discussed in Section 4.2.4. The amount of drug deposited on each stage was subsequently calculated (i.e. $m_{FP} = FP$ concentration $\times$ Volume of washing solution).

4.2.7 Experimental implementation of varying actuation forces

As the actuation force is inversely related to the valve orifice opening time as seen in Equation (3.6) in Chapter 3, it was of interest to investigate the effect of several actuation forces on spray deposition patterns. An aluminium rig shown in Figures 4.3 and 4.4 was designed to this effect. A pneumatic piston with an aluminium "thumb" provided the actuation. The "thumb" always stayed in contact with the pMDI in order to avoid any shock with the canister. The pneumatic piston, located on the upper part of the rig, was connected to an automated switch designed to send a signal to activate the piston.

In order to assess the force needed to actuate the 50 μL valve from Valois used in this work, different forces were applied to the canisters until actuation. The 50 μL valve required approximately 30 N to be actuated which is in line with the minimum forces of 30 N to 40 N reported in the literature for the actuation of stem-type metering valves (MacMichael and Hearne, 2002). Forces of 30 N and 50 N were applied to the canister by modifying the pressure in the pneumatic piston and their effect on spray characteristics were investigated using a NGI.

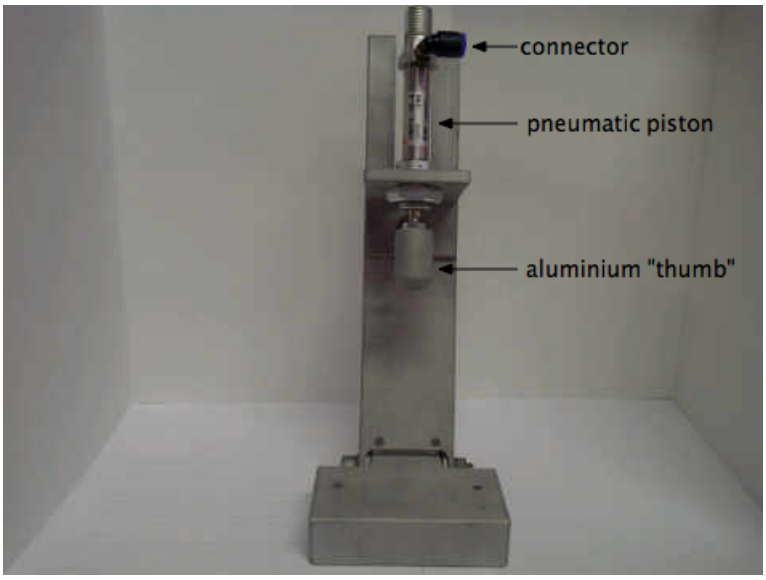

Figure 4.3: Front view of the experimental rig.

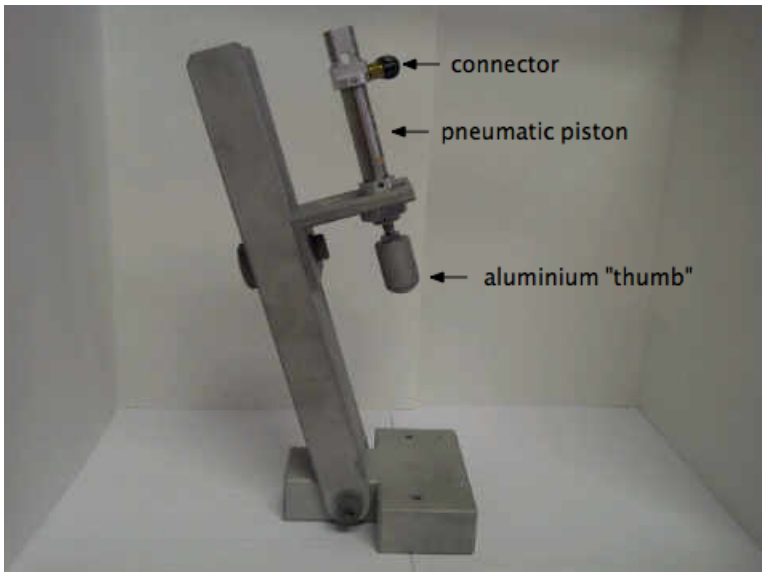

Figure 4.4: Side view of the experimental rig.

4.2.8 Statistical analysis

The significance of all data obtained in this work was determined using a one-way analysis of variance by Tuckey's comparison test. The statistical analysis was conducted using the software SPSS Statistics 20. The results were considered significantly different based upon 95% probability values ($p<0.05$).

4.3 Mathematical prediction of dose performance

4.3.1 Emitted mass calculation

The theoretical mass of FP delivered per actuation with the Flixotide device is known and could therefore be compared to the mass retrieved using the DUSA. For the other formulations, the theoretical mass of FP delivered per actuation had to be calculated using the density of the formulation and the volume of the metered valve. The density of the HF suspension formulation was assumed to be equal to the density of a pure HFA134a formulation as the content of FP was non-significant (0.05% w/w). The density of each solution formulation was calculated using Equation (4.7) determining the densities of mixtures.

$$\rho_{formulation} = \sum C_x \, \rho_x \tag{4.7}$$

where $\rho_{formulation}$ is the density of the formulation in g·mL^{-1}, C_x is the percentage by weight of each component of the formulation and ρ_x is the density of each component of the formulation in g·mL^{-1}. The mass of formulation in each actuation of the 50 μL valve was calculated using Equation (4.8).

$$m_{formulation} = V_{mc} \times \rho_{formulation} \tag{4.8}$$

where $m_{formulation}$ is the mass of formulation delivered per actuation in g and V_{mc} is the metering chamber volume in mL. The mass of FP delivered per actuation was calculated using Equation (4.9).

$$m_{FP} = m_{formulation} C_{FP} \tag{4.9}$$

where m_{FP} is the mass of FP delivered per actuation in g, and C_{FP} is percentage by weight of FP in each formulation.

In this chapter, the amount of drug recovered on each stage was expressed as a percentage of the total recovery. This was decided as the total mass delivered varied from one NGI test to another. This was particularly the case in the section comparing different actuation forces. In this part of the experimental work, the pneumatic piston was used to simulate several forces and the actuation was sometimes not achieved properly. As there was no mean to determine whether the metered dose was discharged completely in the NGI, more actuations were conducted to ensure a sufficient amount of drug would be deposited on each stage of the NGI to allow quantification by the HPLC instrument.

4.3.2 Droplet size distribution calculation

Stein *et al* (2012) found a relationship between the initial and residual size of particles issued from pMDIs. It can be seen in Equation (4.10).

$$MMD_{in} = MMD_{re} \left(\frac{\rho_{in} \times C_{NV}}{\rho_{re}} \right)^{-\frac{1}{3}} \tag{4.10}$$

where MMD_{in} and MMD_{re} are the mass median diameters of initial and residual particles respectively in μm, ρ_{in} and ρ_{re} are the densities of the initial and residual droplets respectively in kg·m^{-3} and C_{NV} is the weight fraction of non-volatiles.

They also showed that the initial size of particles issued from pMDIs increased with the diameter of the nozzle orifice, the metering chamber volume and the concentration of ethanol in the formulation.

This is illustrated in Equation (4.11) (presented in Chapter 2) which is valid for HFA134a-based solution formulations containing ethanol.

$$MMD_{in} = 6.90 + 0.0441 \times V_{mc} + 23.6 \times C_{EtOH} - 63.8 \times C_{EtOH}^2 + 24.7 \times C_{EtOH} \times d_{no} - 0.129 \times C_{EtOH} \times V_{mc} \quad (4.11)$$

where V_{mc} is the volume of the metering chamber in μL, C_{EtOH} is the weight fraction of ethanol and d_{no} is the nozzle orifice diameter in mm.
Lewis (2007) developed Equation (4.12), illustrating that for HFA-based solution formulations, the MMAD is primarily influenced by the concentration of non-volatiles in the formulation.

$$MMAD = 2.31 \times C_{NV}^{\frac{1}{3}} \quad (4.12)$$

where C_{NV} is the weight fraction of non-volatiles in the formulation.

4.3.3 Respirable dose calculation

Lewis (2007) developed Equation (4.13) that calculates the emitted FPF of HFA134a solution formulations containing ethanol according to certain mouthpiece characteristics.

$$FPF_{ED} \leq 5 = 2.1 \times 10^{-5}\, {d_{no}}^{-1.5}\, {V_{mc}}^{-0.25}\, {C_{HFA134a}}^{3} \quad (4.13)$$

where $FPF_{ED} \leq 5$ corresponds to the amount of particle with a diameter smaller than 5 μm expressed as a percentage of the emitted dose, d_{no} is the nozzle orifice diameter in mm, V_{mc} is the metering chamber volume in μL and $C_{HFA134a}$ is the

weight fraction of HFA134a.

4.4 Results

4.4.1 HPLC assay of fluticasone propionate

Linearity

The relationship between the concentration of FP and the peak area obtained for each of the three calibration curves can be seen in Equations (4.14), (4.15) and (4.16).

$$y = 87.303\,x - 26.040 \qquad R^2 = 0.99989 \tag{4.14}$$

$$y = 92.989\,x - 17.744 \qquad R^2 = 0.99973 \tag{4.15}$$

$$y = 92.087\,x - 2.223 \qquad R^2 = 0.99999 \tag{4.16}$$

Equation (4.16) was chosen as it had the highest linearity and when x=0, y had the closest value to zero of Equations (4.14), (4.15), (4.16).

Towards the end of the experimental work, a new Kinetix 2.6 micro (50 X 3.0 mm) column was used and a new calibration curve was produced. Equation (4.17) corresponds to this calibration curve.

$$y = 88.171\,x + 3.786 \qquad R^2 = 0.99997 \tag{4.17}$$

The calibration curve represented by Equation (4.17) can be seen in Figure 4.5.

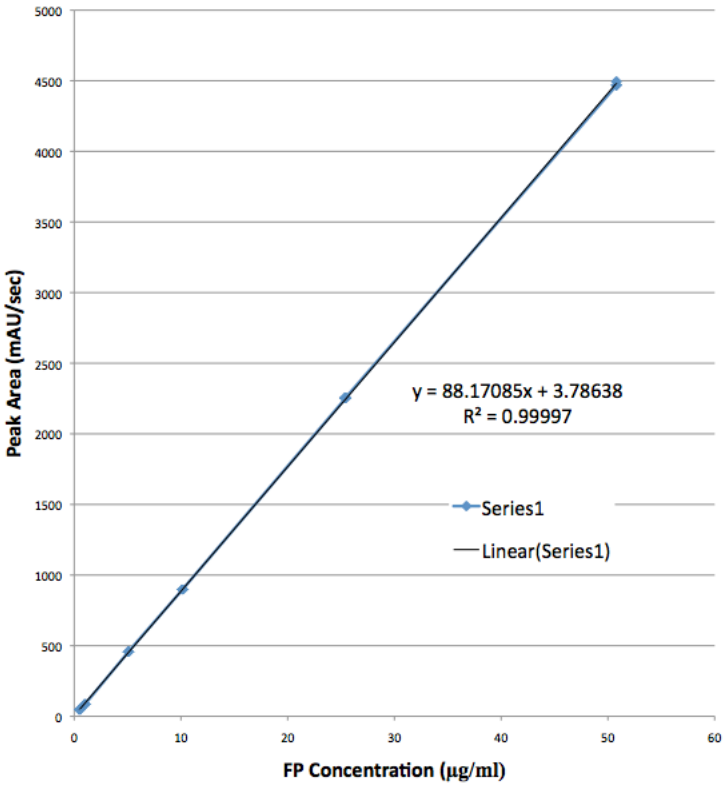

Figure 4.5: Peak area ($\text{mAU}\cdot\text{s}^{-1}$) as a function of concentration of FP ($\mu\text{g}\cdot\text{mL}^{-1}$).

Precision

For Equation (4.16), the $\text{LOD}_{\text{concentration}}$ was $0.04\,\mu\text{g}\cdot\text{mL}^{-1}$ and the $\text{LOQ}_{\text{concentration}}$ was $0.13\,\mu\text{g}\cdot\text{mL}^{-1}$.

For Equation (4.17), the $\text{LOD}_{\text{concentration}}$ was $0.09\,\mu\text{g}\cdot\text{mL}^{-1}$ and the $\text{LOQ}_{\text{concentration}}$ was $0.3\,\mu\text{g}\cdot\text{mL}^{-1}$. These low values indicate a high-sensitivity of the method at low concentrations of FP.

Accuracy

In order to determine whether the experimental method allowed the recovery of a satisfactory percentage of the drug, a commercial formulation of known FP dosage was analysed. The formulation used was Flixotide®125 which is a suspension

formulation containing HFA134a and FP at a dose of 125 μg per metered dose. The aerosolisation of Flixotide®125 in the NGI was performed as discussed in Section 4.2.6.

All the NGI tests reported in this section were performed on the same Flixotide®125 canister. As Flixotide® delivers 125 μg per actuation and 5 actuations were fired for each NGI, the theoretical recovery dose used to calculate the percentage recovery was 625 μg. The results of the NGIs are shown in Table 4.5.

	Mean±SD
Device (μg)	22.98±4.20
Throat (μg)	187.89±25.57
S1 (μg)	15.89±3.97
S2 (μg)	20.34±7.37
S3 (μg)	58.05±33.05
S4 (μg)	106.92±18.73
S5 (μg)	84.28±9.12
S6 (μg)	27.32±1.93
S7 (μg)	8.10±1.56
S8 (μg)	5.33±0.75
Total recovery (μg)	537.11±77.52
Percentage recovery (%)	85.94 ±12.40

Table 4.5: Amount of FP recovered for a mean of 4 NGIs performed on one Flixotide® canister.

4.4.2 Emitted dose analysis

The theoretical dose content per actuation of each formulation determined in Section 4.3.1 were used to calculate the percentages recovery of FP for the 4 DUSA tests realised for each formulation as described in Section 4.2.5. The results are presented in Table 4.6.

Formulation	HF	HEF	HPEF
Theoretical dose content per actuation	30.15μg	28.59μg	29.01 μg
Dose content per actuation Canister 1 (n=4)	35.36±7.20μg	23.27±0.32μg	25.62±0.65μg
Dose content per actuation Canister 2 (n=4)	33.93±3.82μg	24.28±2.03μg	26.32±5.73μg
Dose content per actuation Canister 3 (n=4)	33.53±3.75μg	24.45±0.69μg	28.90±5.69μg
Dose content per actuation Canister 4 (n=4)	na	25.09±0.26μg	32.21±2.11μg
Between canister Mean±SD	34.27±0.96μg	24.27±0.83μg	28.26±2.57μg
Mean percentage recovery	113.68±3.20%	84.90±2.63%	97.43±10.30%

Table 4.6: Percentages of FP recovered for 4 DUSA tests performed on the three formulations.

4.4.3 Aerosolisation of fluticasone propionate suspensions

The MMAD and FPFs calculated as a percentage of the emitted dose and recovered dose were derived from the deposition of the aerosol on the stages of the NGI. The recovered dose of FP represents the total amount recovered on all stages of the NGI, on the throat and on the device whereas the emitted dose of FP corresponds to the total amount of FP recovered from the NGI, excluding the amount of FP recovered from the device. As both measures are used in the literature, the amount of fine particles with a diameter smaller than 5 μm was expressed both as a percentage of the recovered dose (FPF_{RD} $\leq$5 (%)) and as a percentage of the emitted dose (FPF_{ED} $\leq$5 (%)) (Brambilla *et al.*, 1999), (Lewis, 2007). Those data are shown for the Flixotide® and HF formulations using the Flixotide® mouthpiece, in Table 4.7.

	Formulation	
	Flixotide®	HF
	Mean±SD	Mean±SD
Device (%)	4.31±0.74	7.19±1.55
Throat (%)	35.37±4.97	38.69±2.50
FPF_{ED} ≤5 (%)	48.04±2.74	50.54±2.03
FPF_{RD} ≤5 (%)	45.96±2.57	46.90±1.71
FPF_{ED} ≤2.5 (%)	26.74±0.68	34.49±1.59
MMAD (μm)	2.89±0.16	2.09±0.07

Table 4.7: Deposition and size characteristics of the Flixotide® and HF formulations using the Flixotide® mouthpiece. Mean of n≥4 determinations for each formulation.

The MMAD of the Flixotide® formulation was significantly higher than the MMAD of the HF formulation ($p<0.05$). The FPF_{ED} ≤2.5 (%) of Flixotide® was significantly lower than the FPF_{ED} ≤2.5 (%) of the HF formulation ($p<0.05$). The other characteristics were similar for both formulations ($p>0.05$).

The FPF values of the Flixotide® and HF formulations in this work are in line with the results of Feddah *et al.* (2000) obtained on a Flixotide®250 formulation. The FPF_{RD} ≤5 of 45.96% obtained on Flixotide®125 in this work is higher than the FPF_{RD} ≤4 of 32.67±2.1% measured by Feddah *et al* (2000); these data are expected as the percentage of particles smaller than 4 μm should be lower than the percentage of particles smaller than 5 μm. It could also be due to the fact that Feddah *et al* (2000) analysed a formulation containing twice as much FP in the metering chamber compared with the Flixotide®125 in this work. This could accentuate aggregation of the FP particles in the canister and ultimately lead to the aerosolisation of bigger particles (Murnane *et al.*, 2008).

The FPF_{RD} ≤5 of 46.9±1.7% found in Table 4.7 is higher than the value of Pu *et al* (2011). They obtained a FPF_{RD} ≤4.7 of 38.0±2.0% when testing a suspension formulation containing an API of particle diameter of 1.77 μm. This difference could be attributed to the use of an ACI by Pu *et al* instead of a NGI in this work.

It could also be due to the fact that they measured a FPF_{RD} $\leq$4.7 instead of a FPF_{RD} $\leq$5.

Although in Europe, the FPF represents the fraction of particles with a diameter $\leq 5\,\mu$m, the value of $4.7\,\mu$m is also quoted as the upper size limit for FPF as it corresponds to the cut-off diameter of the 3rd stage of the ACI (Mitchell and Nagel, 2004).

The 38% throat deposition obtained with the HF formulation is in line with the findings of Gabrio *et al* (1999). They measured a throat deposition of 42% for a HFA134a and beclamethasone dipropionate formulation with a mouthpiece of similar nozzle orifice diameter (0.50 mm).

4.4.4 Effect of formulations on aerosolisation

The characteristics of the HF, HEF and HPEF formulations using the Flixotide® mouthpiece are shown in Table 4.8. The aerosolisation data of the Flixotide® and HF formulations previously presented are again reported.

	Formulation			
	Flixotide®	HF	HEF	HPEF
	Mean±SD	Mean±SD	Mean±SD	Mean±SD
Device (%)	4.31±0.74	7.19±1.55	6.23±0.85	5.07±1.50
Throat (%)	35.37±4.97	38.69±2.50	77.04±3.17	86.38±1.02
FPF_{ED} $\leq$5 (%)	48.04±2.74	50.54±2.03	14.43±2.64	5.15±0.42
FPF_{RD} $\leq$5 (%)	45.96±2.57	46.90±1.71	13.51±2.47	4.90±0.45
FPF_{ED} $\leq$2.5 (%)	26.74±0.68	34.49±1.59	11.86±2.11	2.90±0.26
MMAD (μ m)	2.89±0.16	2.09±0.07	1.29±0.22	4.12±0.37

Table 4.8: Deposition and size characteristics of the Flixotide®, HF, HEF and HPEF formulations using the Flixotide® mouthpiece. Mean of n$\geq$6 determinations for each formulation.

The deposition of the three formulations in the NGI using the Flixotide® mouthpiece is shown in Figure 4.6.

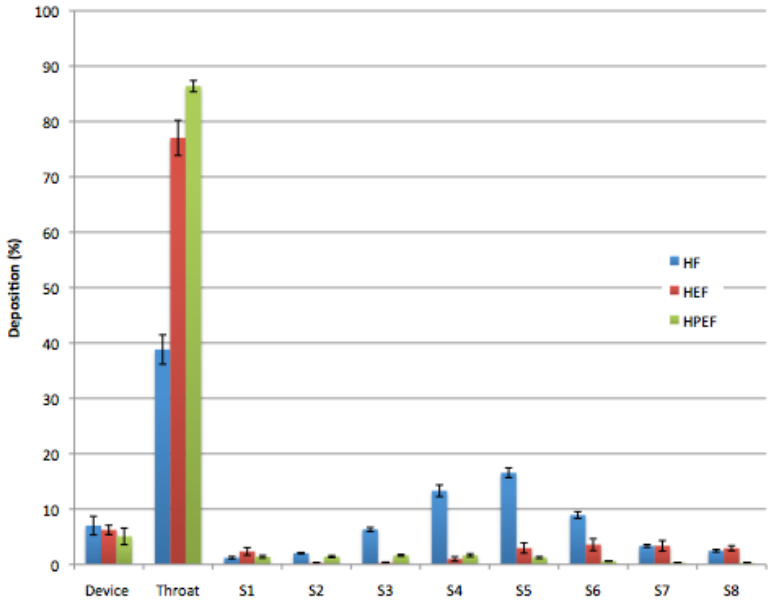

Figure 4.6: *In vitro* deposition profile of the three formulations using the Flixotide® mouthpiece. Mean of n=6 determinations for the FP formulation and mean of n=7 determinations for the HEF and HPEF formulations.

Table 4.8 and Figure 4.6 show that the deposition pattern of particles varies according to the formulation tested. The throat deposition, fine particle fraction and MMAD differ significantly for each formulation ($p<0.05$).

The throat deposition was 38.69±2.50% for the HF formulation compared to 77.04±3.17% for the HEF formulation and 86.38±1.02% for the HPEF formulation.

The MMAD of the suspension formulation was 2.09±0.07 μm compared to 1.29±0.22 μm for the HEF formulation and 4.12±0.37 μm for the HPEF formulation.

4.4.5 Effect of mouthpiece design on aerosolisation

NGI results of the HEF and HPEF formulations with two mouthpiece designs

In the previous experiments, all formulations were tested with the Flixotide® mouthpiece, designed for a FP suspension formulation. In this set of experiments, both solution formulations were tested with the Alvesco® mouthpiece, designed for a solution formulation.

The Flixotide® mouthpiece has a length of 25 mm and a nozzle orifice diameter of 0.50 mm. In comparison the Alvesco® mouthpiece has a length of 37 mm and a nozzle orifice diameter of 0.20 mm. The depositions of the HEF and HPEF solution formulations using the two mouthpieces are shown in Figures 4.7 and 4.8 respectively.

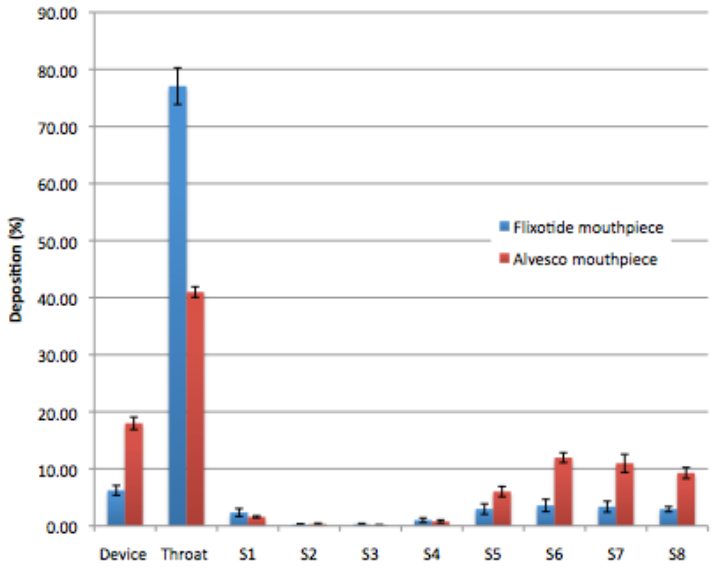

Figure 4.7: *In vitro* deposition profile of the HEF formulation using the Alvesco® and Flixotide® mouthpieces. Mean of n=7 determinations for the Flixotide® mouthpiece and mean of n=4 determinations for the Alvesco® mouthpiece.

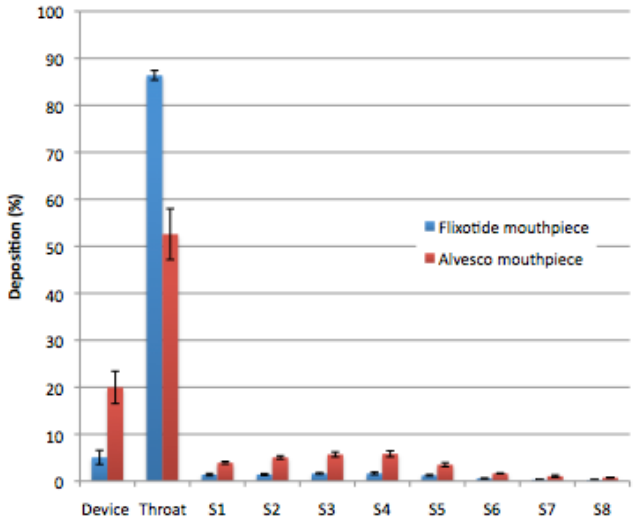

Figure 4.8: *In vitro* deposition profile of the HPEF formulation using the Alvesco® and Flixotide® mouthpieces. Mean of n=7 determinations for the Flixotide® mouthpiece and mean of n=4 determinations for the Alvesco® mouthpiece.

The characteristics of the HEF and HPEF formulations with the two mouthpieces are presented in Table 4.9.

	HEF		HPEF	
Mouthpiece	Flixotide®	Alvesco®	Flixotide®	Alvesco®
	Mean±SD	Mean±SD	Mean±SD	Mean±SD
Device (%)	6.23±0.85	17.97±1.09	5.07±1.50	19.96±3.44
Throat (%)	77.07±3.21	40.98±0.92	86.38±1.02	52.58±5.42
FPF_{ED} ≤5 (%)	14.41±2.66	46.98±1.28	5.15±0.42	19.72±2.98
FPF_{RD} ≤5 (%)	13.51±2.47	38.54±1.43	4.90±0.45	15.71±1.66
FPF_{ED} ≤2.5 (%)	11.85 ± 2.11	41.91±1.00	2.90±0.26	10.76±1.74
MMAD (μm)	1.29±0.22	0.74±0.05	4.12±0.37	4.16±0.19

Table 4.9: Summary of the deposition and size characteristics for the HEF and HPEF formulations with the Flixotide® and Alvesco® mouthpieces. Mean of n=7 determinations for the Flixotide® mouthpiece and mean of n=4 determinations for the Alvesco® mouthpiece.

For the HEF formulation, the FPF_{ED} ≤5 was 46.98±1.28% with the Alvesco® mouthpiece compared to 14.41±2.66% with the Flixotide® mouthpiece ($p<0.05$). The throat deposition was 40.98±0.92% with the Alvesco® mouthpiece compared to 77.07±3.21% with the Flixotide® mouthpiece. The MMAD was 0.74±0.05 μm

with the Alvesco® mouthpiece compared to 1.29±0.22 μm with the Flixotide® mouthpiece ($p<0.05$).

For the HPEF formulation, the FPF_{ED} ≤5 was 19.72±2.98% with the Alvesco® mouthpiece compared to 5.15±0.42% with the Flixotide® mouthpiece ($p<0.05$). The throat deposition was 52.58±5.42% with the Alvesco® mouthpiece compared to 86.38±1.02% with the Flixotide® mouthpiece.

The Alvesco® mouthpiece seemed to be more suitable for the delivery of both solution formulations as it increased the fraction of fine particles and greatly reduced the throat deposition. This could help to reduce the inflammations and side effects observed when the throat is repeatedly exposed to the API.
It was therefore decided to use the Alvesco® mouthpiece to test the HEF and HPEF formulations.

4.4.6 Effect of actuation forces on aerosolisation

In this set of experiments, the size of particles issued from the HF, HEF and HPEF formulations was studied with different actuation forces. One actuation force was provided by a "healthy" female user and two forces of 30 N and 50 N were automated with the use of a pneumatic piston. For each formulation, the three forces were tested. The Flixotide® mouthpiece was used for the suspension formulation and the Alvesco® mouthpiece was used for the two solution formulations.

Effect of the actuation force on the size distribution of the suspension formulation containing HFA134a and FP

The deposition profile of the suspension formulation according to the type of actuation force is shown in Figure 4.9. The NGI tests conducted at 30 N were repeated more than 7 times because of the high variability of the results. The latter could

be due to the fact that in some NGI tests, the canisters were not fully actuated at this low actuation force.

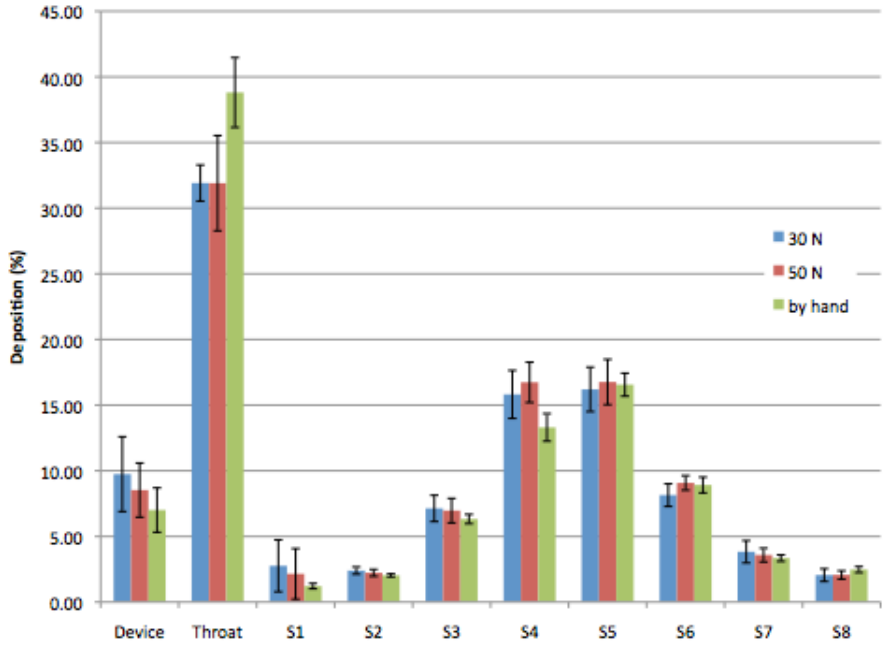

Figure 4.9: *In vitro* deposition profile of the suspension formulation using three types of actuation forces. n=8 for the 30 N actuation, n=5 for the 50 N actuation and n=4 for the manual actuation provided by a "healthy" female user.

Figure 4.9 showed that the 30 N and 50 N actuation forces did not lead to any changes in the deposition pattern of the HF sprays. However, the throat deposition was increased significantly when the pMDI was actuated manually ($p<0.05$).

The spray characteristics of the suspension formulation when the pMDI was actuated with the two piston forces and manually by a "healthy" female user, are summarised in Table 4.10.

	30 N	50 N	by hand
	Mean±SD	Mean±SD	Mean±SD
Device(%)	9.74±2.85	8.53±2.06	7.19±1.55
Throat (%)	31.91±1.38	31.90±3.62	38.69±2.50
FPF_{ED} ≤5 (%)	53.04±3.65	54.92±5.07	50.54±2.03
FPF_{ED} ≤2.5 (%)	34.55±3.24	36.19±3.86	34.49±1.59
MMAD (μm)	2.35±0.24	2.26±0.19	2.09±0.07

Table 4.10: Summary of the deposition and size characteristics of the suspension formulation when the pMDI was actuated at 30 N, 50 N and manually. n=8 for the 30 N actuation, n=5 for the 50 N actuation and n=4 for the manual actuation.

Table 4.10 reveals that the three types of forces used did not have a significant effect ($p>0.05$) on any of the metrics except throat deposition which increased significantly with the manual actuation ($p<0.05$).

Effect of the actuation force on the size distribution of the formulation containing HFA134a, ethanol and FP

The deposition profiles of the HEF formulation according to the type of actuation, presented in Figure 4.10, show that the automated actuations are associated with a higher variability than the manual actuations. One can also observe that the manual actuations of the "healthy" female user resulted in higher throat depositions than the automated actuations at 30 N and 50 N. However, as the automated actuations resulted in highly variable results, this difference was not significant ($p>0.05$). The overall profiles obtained with both automated forces were comparable.

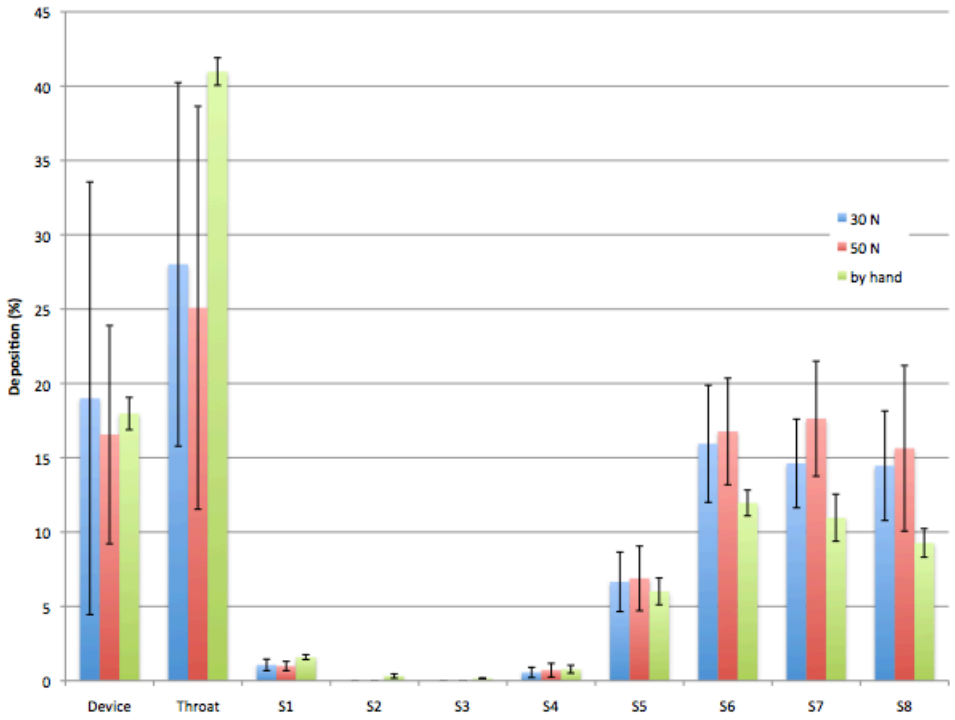

Figure 4.10: *In vitro* deposition profile of the HEF solution formulation using three types of actuation; n=7 for the 30 N actuation, n=4 for the 50 N actuation and n=4 for the manual actuation provided by a "healthy" female user.

The characteristics of the HEF spray when the pMDI was actuated with the two piston forces and manually are presented in Table 4.11.

	30 N	50 N	by hand
	Mean±SD	Mean±SD	Mean±SD
Device(%)	19.00±14.56	16.54±7.35	17.97±1.09
Throat (%)	28.01±12.23	25.05±13.54	40.98±0.92
FPF_{ED} ≤5 (%)	64.93±12.37	68.32±16.21	46.98±1.28
FPF_{ED} ≤2.5 (%)	60.57±12.09	63.76±15.86	41.91±1.00
MMAD (μm)	0.58±0.09	0.58±0.06	0.74±0.05

Table 4.11: Summary of the deposition and size characteristics of the HEF formulation when the pMDI was actuated at 30 N, 50 N and manually; n=7 for the 30 N actuation, n=4 for the 50 N actuation and n=4 for the manual actuation.

Table 4.11 shows that the FPF values decreased significantly when the pMDI was actuated manually compared with the automated actuations at 30 N or 50 N ($p<0.05$).

The device deposition was not significantly altered by any type of actuation. The throat deposition and MMAD increased when the formulation was actuated manually. However, these differences were not significant due to large variations in the results obtained with the pneumatic piston.

Effect of the actuation force on the size distribution of the formulation containing HFA134a, ethanol, PEG400 and FP

The deposition profile of the HPEF formulation according to the type of actuation is shown in Figure 4.11.

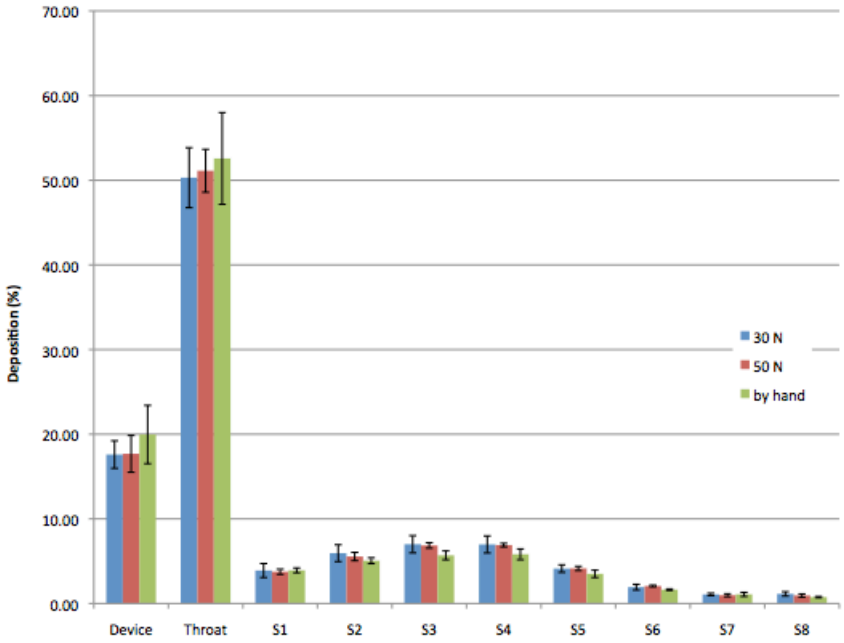

Figure 4.11: *In vitro* deposition profile of the HPEF solution formulation when the pMDI was actuated at 30 N, 50 N and manually; n=6 for the 30 N actuation, n=5 for the 50 N actuation and n=4 for the manual actuation.

Figure 4.11 shows that the percentage of FP deposited on each stage was not altered by any type of actuation ($p>0.05$).

The characteristics of the HPEF spray when the pMDI was actuated with two different piston forces and manually is presented in Table 4.12.

	30 N	50 N	by hand
	Mean±SD	Mean±SD	Mean±SD
Device (%)	17.60±1.63	17.68±2.17	19.96±3.44
Throat (%)	50.30±3.54	51.12±2.53	52.58±5.42
FPF_{ED} ≤5 (%)	23.04±2.63	22.59±0.52	19.72±2.98
FPF_{ED} ≤2.5 (%)	12.80±1.44	12.34±0.44	10.76±1.74
MMAD (μm)	3.94±0.28	3.93±0.15	4.16±0.19

Table 4.12: Summary of the deposition and size characteristics of the HPEF formulation when the pMDI was actuated at 30 N, 50 N and manually; n=6 for the 30 N actuation, n=5 for the 50 N actuation and n=4 for the manual actuation.

It can be seen from Table 4.12 that the device deposition, throat deposition, FPFs and MMAD were not affected by the type of actuation ($p>0.05$). There was no statistical difference between the three types of actuation forces for any parameters listed in Table 4.12 ($p>0.05$).

4.5 Discussion

4.5.1 Suitability of the HPLC assay

The HPLC assay characteristics such as linearity, accuracy, repeatability and sensitivity were in line with the International Conference on Harmonisation (ICH) guidelines (ICH, 2005).

The linearity was determined using 5 concentrations as stated in the ICH guidelines and the R^2 values were greater than 0.999 for both Equations (4.16) and (4.17) presented in Section 4.4.1. This indicates a good linearity for concentrations of FP in the range of 0.5 μg·mL^{-1} to 50 μg·mL^{-1}.

The percentage recovery of FP for each accuracy standard, calculated using Equation (4.6), always laid between 90% and 110%. This shows a good repeatability of the experimental procedure.

The values of the drug recovery as a percentage of the theoretical dose content per actuation shown in Table 4.6 were all within the 80% to 120% range specified in the ICH guidelines which indicates a good accuracy level.

The limit of quantification (LOQ) of FP was calculated using Equation (4.5) given by the ICH guidelines. The LOQ was sufficiently low to allow the accurate quantification of the drug depositing on each stage of the NGI for all NGI tests.

4.5.2 Effect of formulation design on spray characteristics

The fact that the HF formulation had a significantly lower MMAD and higher FPF values than the Flixotide® formulation can be explained by different FP concentrations in the two formulations ($p<0.05$). The Flixotide® pMDI delivers 125 μg FP per metered dose compared to approximately 30 μg FP for the HF formulation. At higher drug concentrations, drug particles tend to aggregate more and might form bigger clusters leading to higher MMAD values and lower FPF values (Michael *et al.*, 2001). Cripps *et al.* (2000) found similar results when comparing a 125 μg and a 250 μg Flixotide® formulations. The MMAD of the 125 μg Flixotide® formulation was 2.4 μm compared to 2.6 μm for the 250 μg Flixotide® formulation. The fact that Cripps *et al* (2000) found a 2.4 μm MMAD compared to the 2.89 μm MMAD in this work might be explained by the use of an ACI in their measurements instead of a NGI in this work.

The MMAD of 1.29±0.22 μm for the HEF formulation was in the same range as the 1.1±0.1 μm MMAD obtained by Brambilla *et al* (1999) when testing a similar formulation. The FPF_{RD} ≤5 is approximately 34% for Brambilla *et al* which is much higher than the FPF_{RD} ≤5 of 13.51± 2.47% found in this work. The higher FPF value obtained by Brambilla could be explained by the smaller nozzle orifice diameter he used (0.33 mm compared to 0.50 mm in this work).

The MMAD of 4.12±0.37 μm for the HPEF formulation is in line with the MMAD obtained by Brambilla *et al* (1999) when testing a comparable formulation. They found a MMAD of 4.4 μm when using a pMDI with a nozzle orifice diameter of 0.33 mm. The slightly lower MMAD in this work could be explained by the fact that the formulation used by Brambilla *et al* contained 21% w/w of semi-volatile and non-volatile components compared with 15% w/w in this work.

The FPF_{RD} $\leq$5 is approximately 12% for Brambilla *et al* (1999), which is much higher than the 4.90% in this work. This could be be due to the use of different nozzle orifice diameters (0.33 mm in Brambilla *et al*'s work compared to 0.50 mm in this work). However, the higher nozzle orifice diameter in this work should theoretically also lead to a high MMAD. This discrepancy between the MMAD and FPF values might be explained by the way the MMAD is calculated.

The MMAD only takes into account particles depositing on stages 1 to 8 of the NGI and therefore does not include the biggest particles depositing in the device and on the throat. It is possible that the HPEF spray contained a large fraction of big particles (which would explain the low FPF value). However those large particles would tend to remain trapped in the device or to deposit on the throat. As a result they would not be taken into account in the MMAD which would remain low.

The MMAD of the HPEF formulation is also comparable to the value of 3.82±0.09 μm obtained by Haynes *et al* (2004) when they tested a solution formulation containing 0.1% w/w nimesulide, 5%w/w PEG and 15%w/w ethanol using an ACI. The smaller MMAD found by Haynes *et al* might be due to different pMDIs designs. As there is no mention of device parameters in Haynes *et al* work, it is difficult to elaborate on the difference observed.

Table 4.8 and Figure 4.6 showed that the particles deposition pattern varied according to the formulation tested. The throat deposition was significantly lower

for the HF formulation compared with the HEF and HPEF formulations ($p<0.05$). This could be explained by the fact that the HEF and HPEF formulations had evaporated less than the HF formulation upon reaching the throat. As a result they had more momentum and therefore impacted more on the back of the throat. The HPEF formulation which was the less volatile formulation had therefore the highest throat deposition of all formulations ($p<0.05$).

Although the throat deposition of the HEF formulation was significantly higher than the HF formulation, the MMAD of the HF formulation was higher than the MMAD of the HEF formulation. This could be explained by the fact that in impaction testing, the MMAD only refers to the fraction of formulation which gets past the throat. As a result, a formulation might have a low MMAD (as the HEF formulation had in this work) and still have a high throat deposition.

The MMAD of the HF formulation might be higher than the MMAD of the HEF formulation because the API is not dissolved in suspension formulations. As a result, the residual droplets cannot be smaller than the diameter of the API particles initially used to manufacture the formulation. In solution formulations, the API is dissolved so the minimum residual size is not limited by the size of the micronised drug used in the formulation (Michael *et al.*, 2001).

The D_{50} of the micronised FP used to manufacture the suspension formulation and measured using a Malvern Mastersizer X as described in Section 4.2.2, was $2.76\pm0.03\,\mu$m. This value should theoretically correspond to the residual size of the FP particles once all propellant has evaporated. However, the MMAD of the HF formulation was $2.09\pm0.07\,\mu$m.

This difference could be attributed to the fact that the size of the micronised FP was evaluated using a laser diffraction instrument (Malvern Mastersizer X) whereas the size of the residual particles was measured with a NGI. The fact that LDA and

impaction methods never measure exactly the same particles size can explain the difference obtained between the size of the initial micronised drug particles and the residual drug particles (Haynes *et al.*, 2004).

The formulation having the highest MMAD was the HPEF formulation containing PEG400, which is agreement with Haynes *et al* (2004). When increasing the PEG concentration from 0.5% to 20%, they found that the MMAD increased from 1.95±0.05 μm to 4.09±0.15 μm, respectively. This might be due to the fact that at increased concentrations of PEG, the formulations become less volatile, leading to a lower evaporation and higher size of residual droplets.

The formulation design significantly altered the FPF_{ED} ≤5 for each formulation ($p<0.05$). It had a value of 50.54±2.03% for the HF formulation compared to 14.43±2.64% for the HEF formulation and 5.15±0.42% for the HPEF formulation.

These findings would suggest that a higher concentration of semi-volatile and non-volatile components increases the size of particles and leads to a higher throat deposition and a lower FPF, which is in agreement with the findings of Brambilla *et al* (1999) and Haynes *et al* (2004).

4.5.3 Effect of mouthpiece design on spray characteristics

The type of mouthpiece used influenced significantly the deposition pattern of the aerosol for both solution formulations ($p<0.05$). Device deposition was higher, throat deposition was lower and all FPF values were higher with the Alvesco® mouthpiece compared with the Flixotide® mouthpiece ($p<0.05$).

The higher device deposition obtained for both solution formulations with the Alvesco® mouthpiece could be due to the fact that it is longer (37 mm compared to 25 mm for the Flixotide® mouthpiece), thus providing a greater surface for drug

deposition.

The lower throat deposition obtained with the Alvesco® mouthpiece might be due to the fact that big particles that would normally impact on the throat might instead remain trapped in the longer mouthpiece, therefore decreasing the amount of particles available for throat deposition.

The $\text{FPF}_{ED} \leq 5$ of the HEF formulation in Table 4.9 was compared to the theoretical $\text{FPF}_{ED} \leq 5$ obtained using Equation (4.13) discussed in Section 4.3.3.

Equation (4.13) developed by Lewis (2007) gives a theoretical $\text{FPF}_{ED} \leq 5$ of 14.58% with the Flixotide® mouthpiece of 0.50 mm nozzle orifice diameter. This value is close to the result of 13.51±2.47% reported in Table 4.9.

Equation (4.13) gives a theoretical $\text{FPF}_{ED} \leq 5$ of 54.22% with the Alvesco® mouthpiece of 0.20 mm nozzle orifice diameter. This value is comparable to the result of 46.98±1.28% found in Table 4.9.

The results are therefore in line with the work of Lewis (2007) and Clark (1991) who established that the FPF of a spray is inversely proportional to the diameter of the nozzle orifice.

The results are also in agreement with the findings of Brambilla *et al* (1999) who studied the effect of nozzle orifice diameters on fine particle fractions. They found that the FPF≤4.7 (%) almost tripled when using a nozzle orifice diameter of 0.25 mm compared to a nozzle orifice diameter of 0.42 mm. They mainly attributed this increase in the FPF value to a reduction of the throat deposition when using the smaller nozzle orifice. A smaller nozzle orifice may indeed lead to the formation of smaller initial droplets which might impact less on the throat as illustrated in Equation (4.11) developed by Stein et al (2012).

For a formulation containing HFA134a, ethanol, glycerol and API, Brambilla *et al* found a $FPF_{RD} \leq 4.7$ of 16% with a 0.42 mm nozzle orifice diameter compared with 42% with a 0.25 mm nozzle orifice diameter. Those percentages cannot be directly compared to the data in this work as the present formulation contains 5% w/w of PEG400 versus 1.3% w/w in Brambilla's formulations. The higher concentration of PEG400 in this work can explain the fact that the $FPF_{RD} \leq 5$ is smaller for the HPEF formulation compared to Brambilla's findings. However the nozzle orifice diameter effect was similar to the effect reported by Brambilla, as the $FPF_{RD} \leq 5$ also tripled from 4.90±0.45% with the Flixotide® mouthpiece of 0.50 mm nozzle orifice diameter to 15.71±1.66% with the Alvesco® mouthpiece of 0.20 mm nozzle orifice diameter.

For the HEF formulation, the $FPF_{RD} \leq 5$ also almost tripled from 13.51±2.47% for the Flixotide® mouthpiece versus 38.54±1.43% with the Alvesco® mouthpiece. Contrary to Brambilla *et al* (1999) who found that the MMAD was not significantly altered when decreasing the nozzle orifice from 0.42 mm to 0.25 mm in a HFA solution formulation, the MMAD decreased significantly for the HEF formulation when the diameter of the mouthpiece was decreased from 0.50 mm to 0.20 mm ($p<0.05$). The reduction in MMAD when using a mouthpiece with a smaller nozzle orifice diameter is consistent with the work of Polli *et al* (1969) who found that the MMAD decreased from 11 μm to 3.2 μm when using mouthpieces of nozzle orifice diameters of 0.61 mm and 0.46 mm respectively.

For the HPEF formulation, the MMAD was not altered by the type of mouthpiece used. This might be explained by the fact that the PEG400 is a viscous liquid which does not evaporate during the atomisation of the spray and therefore represents the main factor dictating the residual size of the droplets. This might also be due to the fact that even if the Flixotide® mouthpiece would aerosolise bigger particles than the Alvesco® mouthpiece, the higher throat deposition associated

with the HPEF formulation when using the Flixotide® mouthpiece would prevent the particles from reaching past the throat. As a result, they would not be included in the MMAD calculations.

When applying Equation (4.12) developed by Lewis (2007), to the HPEF formulation, a MMAD of 3.91 μm was calculated. This theoretical value is comparable to the 4.12±0.37 μm and 4.16±0.19 μm MMAD values obtained with the Alvesco® and Flixotide® mouthpieces respectively. This result is therefore in line with the findings of Lewis (2007) who reported that for HFA-based solution formulations, the MMAD is primarily influenced by the concentration of non-volatiles in the formulation.

The Flixotide® mouthpiece was associated with higher throat depositions for the HEF and HPEF formulations. As high throat depositions can be associated with decreased pMDIs efficiencies and increased risks of side effects, it was decided that the Alvesco® mouthpiece was more suitable for the delivery of both solution formulations and would therefore be used in this work.

4.5.4 Effect of actuation forces on spray characteristics

This work showed that the deposition patterns of sprays actuated at two different forces using a pneumatic piston were similar. The actuation of the canisters at 30 N and 50 N did not lead to any statistical difference in the percentage drug deposition on any stage of the NGI, in the FPFs or in the MMAD for any of the three formulations ($p>0.05$). This might be due to the fact that the effect of the forces provided by the pneumatic piston on the valve opening rate is non-significant.

Although the results were not significant due to the high standard deviation of the measurements conducted with the pneumatic piston, Figures 4.9 and 4.10 showed

that the manual actuation by the "healthy" female user led to increased throat depositions for the two most volatile formulations (HF and HEF). This difference might be explained by the gradual nature of the manual actuation compared to the automated actuation, which might influence the valve opening rate.

The automated actuation might lead to a more abrupt opening of the valve orifice due to the constant force of the pneumatic piston throughout the actuation. This could cause a higher pressure gradient across the nozzle orifice earlier in the aerosolisation process due to a more important propellant build up in the expansion chamber. As the pressure gradient provides the energy to aerosolise the droplets, the abrupt valve opening under automated actuations could lead to the aerosolisation of smaller droplets, which would cause a lower fraction of the spray to deposit on the throat.

On the contrary, the manual actuation could lead to a slower opening of the valve orifice, leading to a lower pressure gradient at the nozzle orifice and therefore to the aerosolisation of larger droplets, causing a higher percentage of the spray to deposit on the throat.

Once again, a strong difference in the throat depositions between the manual and automated actuations was not correlated with a high difference in the MMAD. This could be due the fact that the MMAD only takes into account the particles entering the NGI.

These results would suggest that the automated actuations might lead to different aerosolisation patterns compared to the manual actuations. For the HEF formulation, there was more variability in the data obtained with the piston actuation than with the manual actuation. It could be due to the fact that a higher pressure gradient causes more turbulence in the spray and therefore contributes to a less repeatable and stable deposition pattern.

The HPEF formulation was not affected by the type of actuation force used ($p>0.05$). This could be explained by the fact that the size of the particles was mostly dictated by the presence of PEG400, a viscous and non-volatile excipient. As the formulation is more viscous, even a more abrupt valve opening might not provide a sufficient amount of energy to aerosolise the spray into smaller droplets. The high variability associated with the automated actuations for the HF and HEF formulations was not observed for this formulation. This could be explained by the lower vapour pressure of the formulation, which might lead to a smaller level of turbulence and a more stable aerosolisation process. This is in line with the work of Ju *et al.* (2012) who showed that formulations containing a higher concentration of non-volatile components tend to produce more steady puffs than more volatile formulations.

4.6 Summary

The aim of this chapter was to study the deposition patterns of three pMDI formulations depending on several parameters. The type of formulation used was shown to affect the spray characteristics, with the less volatile formulations leading to the aerosolisation of bigger droplets and increased throat depositions.

The device design was also shown to affect the deposition pattern of the aerosols as a larger nozzle orifice was shown to accentuate the throat deposition and to reduce the amount of fine particles.

Finally, the varying types of actuation tested showed that the magnitude of the automated actuation forces did not have a significant effect on the deposition patterns of any of the formulations. However, the manual actuation provided by a "healthy" female user was shown to accentuate the throat deposition, especially

for the most volatile formulations. The deposition profiles of the two most volatile formulations may have been influenced by the abrupt nature of the automated actuation which could increase the pressure gradient across the nozzle orifice and lead to the aerosolisation of smaller droplets.

Further work is needed to understand which mechanisms of the actuation process lead to the observed difference in the deposition patterns for the two most volatile formulations. The automated actuations could then be modified to better mimic manual actuations when conducting preliminary tests in pMDI development.

This chapter also highlighted a lack of correlation between a high MMAD and a high throat deposition. The MMAD, although it represents a measure of the particle size distribution, does not give information on particles impacting on the throat as it only takes into account particles entering the NGI. As the efficiency of a pMDI is directly linked to its throat deposition, another size parameter assessing the size of particles deposited in the throat and in the NGI might be useful.

Chapter 5

Experimental validation of the one-dimensional computational model of metered dose inhaler discharge

5.1 Introduction

5.1.1 Droplet diameter and oropharyngeal deposition

The efficiency of inhaled drug delivery is limited by its oropharyngeal deposition. Kleinstreuer *et al* (2007) presented a summary of early modelling of throat deposition obtained by Cheng *et al* (1999, 2003) to validate their computer simulation. A graph showing the relationship between the impaction parameter (IP) and the percentage deposition in the mouth and throat regions using Cheng's data and Kleinstreuer's computational results is shown in Figure 5.1 where IP is defined by

Equation (5.1) (Kleinstreuer *et al.*, 2007).

$$IP = d_p^2 Q \tag{5.1}$$

where d_p is the particle diameter in μm and Q is the patient's inhalation flow rate in L·min^{-1}.

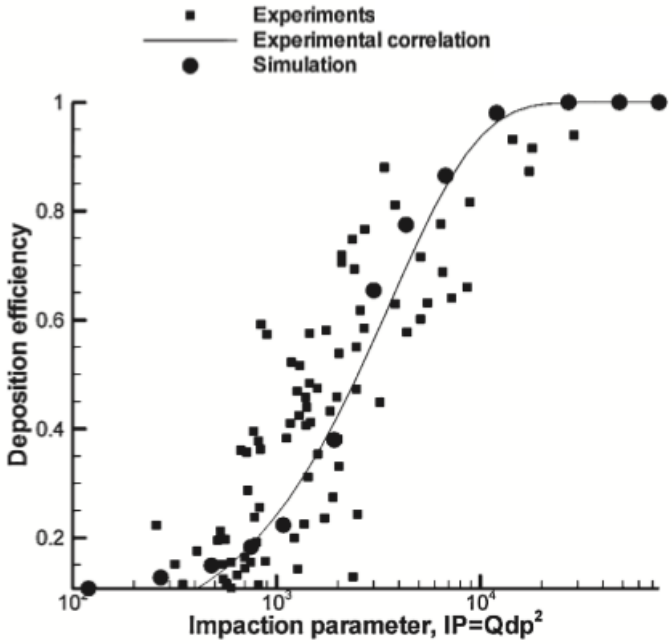

Figure 5.1: Deposition efficiency in the human upper airway, plotted as a function of the inertial parameter $d_p^2 Q$ as cited by Kleinstreuer *et al* (2007).

Figure 5.1 shows that the upper airway depositions increase with the inertial parameter IP. As at a given flow rate, IP is proportional to the square of the diameter of the particle, it can be concluded that the particle size is a major factor governing the deposition in the upper airways.

The results obtained from simulations studying the particles deposition in two human mouth-throat models developed by Jayaraju *et al.* (2008) show that larger particles lead to an increased amount of particles depositing in the mouth and throat regions. *In vivo* experiments by Ehtezazi *et al.* (2010) and clinical data

gathered by Buhl (2006) also showed that a higher particles size leads to an increased oropharyngeal deposition.

The primary atomisation of the spray, which describes the breaking up of the flow into droplets inside the pMDI, was studied in chapters 2 and 3. It is of interest to measure the particles size at several distances from the nozzle orifice in order to understand the evolution of the particles dimensions from the nozzle orifice to the respiratory system.

In this chapter, the velocity and size of the droplets were measured during their atomisation downstream of the nozzle orifice, also referred to as secondary atomisation. Secondary atomisation occurs after the primary atomisation which corresponds to the boiling and evaporating of the formulation inside the device (Versteeg *et al.*, 2006). The velocity and size of the droplets during their transportation from the nozzle orifice to the patient's throat are of interest and were measured experimentally using several laser techniques, at distances relevant to human oropharyngeal anatomy.

5.1.2 Droplets velocity and oropharyngeal deposition

Droplets velocity also increases the percentage deposition in the throat region (Stein and Myrdal, 2006). This is illustrated by Equation (1.3), discussed in Chapter 1,

$$S = B\, m_p\, U_p$$

which shows that the stopping distance of a particle increases when its velocity increases.

Droplet velocity is governed by properties of the formulation such as its vapour

pressure, which controls the velocity at which the formulation is discharged from the expansion chamber. It is also influenced by the patient's inspiratory flow rate which affects significantly the aerosol velocity in the patient's airways. The velocity of the spray issued from a pMDI decreases rapidly from approximately $60\,\mathrm{m{\cdot}s^{-1}}$ when exiting the device to a few meters per second (corresponding to the patient's inspiratory flow velocity) upon reaching the throat (Stein and Myrdal, 2006). This is mainly due to the particles mass loss through their evaporation, making them slow down upon interaction with the quiescent air (Hochrainer *et al.*, 2005). As particles velocity affects the efficiency of pMDIs by altering the amount of drug impacting on the back of the throat, it was also of interest to study this parameter. The velocity of several formulations was measured using a laser technique at several distances, up to 10 cm away from the nozzle orifice.

Applications of laser techniques to measure the velocity of pMDI sprays

Laser Doppler anemometry (LDA) was used by Lee *et al* (1991) to calculate the droplets velocity of pMDI sprays as a function of the distance from the orifice and as a function of the aerosolisation time. Their results are discussed later in the chapter. To the best knowledge of the author, no other work used LDA to obtain velocity measurements from pMDI sprays.

LDA assumes all particles are spherical which represents a shortcoming of this method for the measurements of particles issued from pMDIs as they might not all be spherical (Versteeg and Hargrave, 2002). LDA is a suitable method for the calculation of particles velocity at one point in the spray but cannot calculate droplets velocities on an entire plane. This type of measurement is not optimal for the study of pMDI sprays as it was shown that droplet velocities are lower on the edges of the sprays compared to the centre (Crosland *et al.*, 2009).

Dunbar *et al* (1996, 1997) conducted experiments to measure the velocity of a

HFA134a spray 25 mm downstream of the nozzle orifice using phase Doppler particle analysis (PDPA) and high-speed photography; they reported maximum velocities of 60 $m \cdot s^{-1}$.

Wigley *et al* (2002) assessed droplets velocities at a distance of 2.6 mm from the nozzle orifice using phase Doppler anemometry (PDA); they measured a velocity peak of approximately 90 $m \cdot s^{-1}$. As PDA can only assess the velocity of droplets at one point, many researchers have chosen to use particle image velocimetry (PIV) as it can assess particles velocity over entire areas.

Work on the characterisation of aerosol sprays using PIV have been conducted by Han *et al.* (2002) who investigated the effect of different airflow rates on particles velocity inside the mouthpiece of a DPI and observed a highly turbulent flow at all flow rates.

Crosland *et al* (2009) investigated the effect of a spacer on the velocity of pMDI sprays using PIV. Their results revealed that the spacer did not have a strong impact on the spray velocity and that the pMDI sprays had a higher velocity at the positions located closer to the extremity of the mouthpiece. The effect of several time delays after the actuation on the flow velocity was investigated by Crosland *et al* (2009). Their results are shown in Figure 5.2.

Figure 5.2 shows that the spray velocity decreases between 2 ms and 10 ms delays but increases between 10 ms and 40 ms delays. The effect of delays was further studied in this work to understand better their influence on the exiting spray velocity. Figure 5.2 also showed that an airflow of 30 $L \cdot min^{-1}$ did not affect strongly the velocity profile of the spray. This shows that the recommended advice to breath in a pMDI at a flow rate of 30 $L \cdot min^{-1}$ may not alter the spray velocity and its potential impact on throat deposition (Keller, 1999).

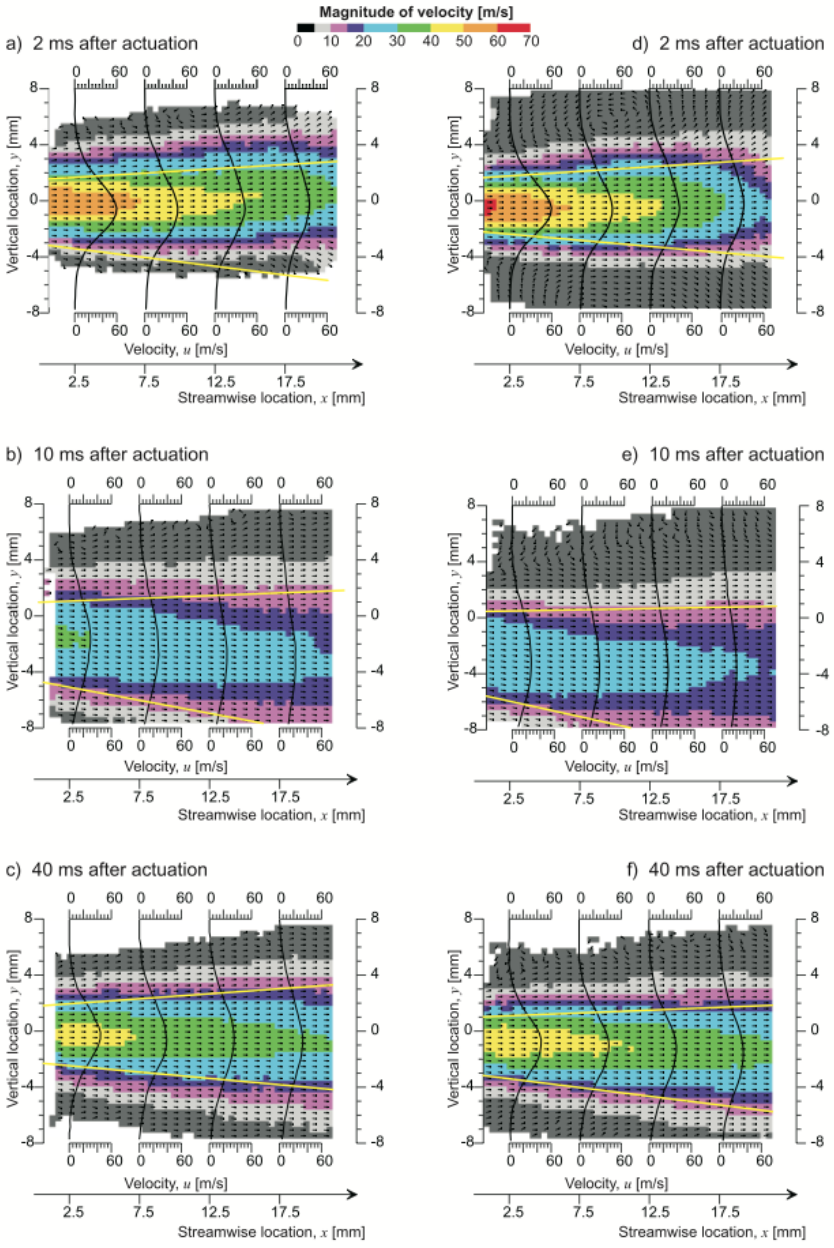

Figure 5.2: The vector velocity flow field and selected radial (vertical) profiles of axial velocity for three time delays actuated into quiescent air (a to c) and with a 30 L·min^{-1} coflow (d to f) (Crosland *et al.*, 2009).

When converting the mass flow rate to a velocity using Equation (5.2), a $30\,\mathrm{L{\cdot}min^{-1}}$ flow rate leads to a velocity of approximately $2\,\mathrm{m{\cdot}s^{-1}}$ at the oropharynx. The low air velocity might be the reason why the flow rate does not significantly affect the aerosol velocity.

$$U_{air} = \frac{Q}{A_{trachea}} \tag{5.2}$$

where U_{air} is the velocity of air in $\mathrm{m{\cdot}s^{-1}}$, Q is the volumetric flow rate of air in $\mathrm{m^3{\cdot}s^{-1}}$ and $A_{trachea}$ is the area of the trachea in $\mathrm{m^2}$ (Ali, 2008).

The recommended $30\,\mathrm{L{\cdot}min^{-1}}$ flow rate might be aimed at directing the aerosol through the respiratory tract. It might also affect the particles size and therefore the particles deposition location within the respiratory tract. In order to understand whether the flow rate has an effect on the size of particles aerosolised, particle size measurements are carried later in the chapter at several flow rates. The effect of the number of actuations on the performance of HFA-based salbutamol sulfate sprays was also analysed by Crosland *et al* (2009) and it was shown that the velocity profile did not change over the canister lifetime.

5.1.3 Particle size measurements

Particles size can be assessed using laser diffraction. As the angle of diffraction of a laser upon contact with a particle is inversely proportional to the size of the particle, laser diffraction uses diffraction angles to assess particles size.

The advantage of this method is that it can provide real-time and in-situ analysis of aerosol droplets. This allows investigations on the dynamic character of the aerosol. However, because the laser light is only scattered from the surface of the droplets, laser diffraction cannot differentiate drug-containing particles from the rest of the sample (Pu *et al.*, 2011). Laser diffraction instruments can also suffer

from beam steering, a phenomenon due to the change in refractive index caused by the evaporation of the propellant which can create large phantom droplets that are non existent in the spray. Laser diffraction assumes that particles are spherical which might not be the case in all sprays (Mitchell *et al.*, 2006), (Versteeg and Hargrave, 2002).

Several instruments use laser diffraction to assess particles size. In this chapter, the Helos from Sympatec® and the Malvern Spraytec® were employed.

Sympatec®

The particle analyser Helos was developed by Sympatec® GmbH (Clausthal-Zellerfeld, Germany) in 1983 to measure particles of diameters 0.1 μm to 8750 μm (Sympatec, 2010). It was used by Pu *et al* (2011) to investigate the effect of different temperatures and formulations on the particles sizes of HFA aerosols. Their results showed that the droplets size decreased at increasing temperatures. This could be explained by the fact that at higher temperatures, a formulation has a higher vapour pressure and therefore a stronger evaporative power.

Pu *et al* (2011) also investigated the effect of non-volatiles on the size of particles by comparing a formulation containing 0.2% w/w of a non-volatile component and 5% w/w of ethanol with a 100% HFA formulation. The results show that the presence of non-volatiles leads to an increase in particles size. The use of the Sprayer unit from Sympatec allowed Pu *et al* to measure the spray at distances of 8 cm, 12 cm and 18 cm from the mouthpiece. The sprays contained more fine particles at 18 cm than at 12 cm from the mouthpiece, it can thus be assumed that the particles measured at 8 cm and 12 cm from the mouthpiece had not yet reached their residual size. The latter results show that the Helos particle sizer from Sympatec® can be used successfully to assess the intermediate size of particles issued from pMDIs.

The effect of varying flow rates on sprays issued from pMDIs and DPIs on the residual size of particles has been studied using impaction instruments. However, as their cut-off diameters generally depend on the flow rate at which they are used, impaction devices are not ideal to study the effect of flow rate on particles size (Feddah *et al.*, 2000). The effect of several flow rates on the intermediate size of pMDIs sprays has to the best knowledge of the author never been studied although it could give valuable information on the probability of particles reaching the respiratory system. For this reason, the effect of several flow rates on the size of particles issued from three different formulations was studied using the Helos from Sympatec®.

Malvern Spraytec®

The Malvern Spraytec® can measure particles with a diameter ranging from 0.1 μm to 2000 μm (malvern.com, 2012). This covers the range required for the characterisation of pMDIs' sprays. Malvern developed a multiple scattering analysis algorithm, allowing the measurement of particles in higher concentration sprays than traditional laser diffraction techniques. As a result, the Malvern Spraytec® is able measure sprays obscuring up to 98% of the laser intensity and could therefore be used to measure particles closer to the nozzle orifice.

The Malvern Spraytec® can also measure the particles size as a function of the distance from the nozzle orifice. This is of interest as the particle size distribution of pMDI sprays varies with this distance. This represents the main advantage of the Malvern Spraytec® over the Helos from Sympatec® and impaction devices.

The Malvern Spraytec® was used by Haynes *et al* (2004) to study the effect of temperature on pMDIs sprays. Their results showed that the particles size of the spray decreased at increasing temperatures.

According to Haynes *et al* (2004), the Malvern Spraytec® overestimates the particles size of HFA-based aerosols compared to the Andersen cascade impactors (ACI). This could be due to the fact than when entering the laser measurement zone, the spray is not yet fully evaporated and might lead to the measurement of droplets which contain propellant. In comparison, the ACI only assesses the particle size distribution of the drug particles. Inhalation cells can be used to reduce this effect as they allow the spray to evaporate more completely before entering the measuring zone. However, measurements with an inhalation cell do not give information on the size of particles as they enter the throat, but rather on the particles residual size. In order to assess the chance of impaction on the throat based on particles size, it might be more relevant to measure particles as they would behave in real life (i.e. without inhalation cells).

The oversizing of the Malvern Spraytec® might also be due to the fact that impactors do not measure the particle size distribution of all droplets but only of those able to get past the induction port which might also contribute to the difference in particle size distribution obtained with both methods.

The variation of the refractive index in the aerosol cloud might affect the Malvern Spraytec® results. When measuring particle size near the nozzle orifice (closer than 10 cm), the evaporation of the liquid phase might erratically alter the path of the laser beam, leading to the creation of large "phantom" droplets (malvern.com, 2007). In order to reduce the laser light refraction due to the high vapour mass near the orifice, one can remove the "phantom" droplets by "killing" the detector channels measuring the largest droplets. However, when doing this, large droplets present in the spray might not be detected (Dunbar, 1996).

Application to pMDI sprays

Laser diffraction is not highly recommended for the characterisation of suspension

formulations because it cannot differentiate between drug-containing and drug-free particles, which are both present in suspensions sprays (Pu *et al.*, 2011). Therefore, the measurements might not characterise drug particles but pure propellant particles. In order to get an even number of API droplets when measuring suspension formulations, the pMDI can be shaken before each measurement.

The results obtained with laser diffraction on suspension sprays cannot be directly compared to impaction measurements as impactors measure only the size of drug-containing droplets. However, Pilcer *et al* showed a good correlation in the particles size obtained by impaction and laser diffraction when testing formulations issued from DPIs (Pilcer *et al.*, 2008).

As the active pharmaceutical ingredient (API) is assumed to be homogeneously dissolved into solution formulations, the fact that laser diffraction devices do not perceive the difference between drug-containing and drug free droplets would not represent an issue for those formulation types (Pu *et al.*, 2011). In solution formulations, laser diffraction has be shown to be an efficient tool to characterise the particles size change depending on the formulations and solvents employed.

Although laser diffraction instruments might be less accurate and consistent than impaction instruments, they represent a much faster alternative to particle sizing and can therefore be used when screening many formulations at early stages in product development.

Pu *et al* (2011) used the Helos from Sympatec® to assess the particle size distribution of pMDIs sprays obtained under different conditions. As the Helos does not allow the measurement of particles size as a function of the distance from the nozzle orifice, in this work it was decided to use the Helos as well as the Malvern Spraytec® to obtain more comprehensive data on the spray development.

In their experiments, Clark (1996) as well as Smyth and Hickey (2003) used the Malvern 2600 launched in 1980 (Vines, 2010). The Malvern 2600 employed the Fraunhofer analysis to assess particles size. This method gives less accurate results than the Mie theory used in the Malvern Spraytec® when studying particles smaller than 25 μm which corresponds to the particles size measured by Clark (1996) as well as Smyth and Hickey (2003) (Mitchell *et al.*, 2006). In their data, Smyth and Hickey (2003) observed a multimodal particle size distribution. As Fraunhofer theory has been reported to bias results in the presence of multimodal distributions towards the mode with the most significant peak, the results of Smyth and Hickey might have been affected (Mitchell *et al.*, 2006).

The Malvern Spraytec® operates with a laser twice more powerful than the Malvern 2600 and can capture more data at a faster rate (malvern.com, 2012). The Malvern Spraytec® can also operate at lower transmissions than the Malvern 2600 which might give a better accuracy for the measurements of high density flows such as pMDI sprays near the nozzle orifice (Strakey, 2003).

5.1.4 Aims and objectives

In Chapter 4, the effect of the actuation force on the aerodynamic size distribution of the droplets was studied. In the current chapter its influence on both the size and velocity of the droplets was investigated using laser diffraction and PIV respectively. It was of interest to capture those properties at several distances and times in the aerosolisation process in order to understand the spatial and temporal development of pMDIs sprays.

The aim of this chapter was to characterise the effect of several actuation forces, formulations and device parameters on the velocity and size of particles issued from pMDIs using laser-based analytical techniques.

The objectives to address this aim were:
- the investigation of the effect of the formulation on the velocity and size of the aerosolised particles using PIV, the Malvern Spraytec® and the Sympatec®.
-the study of the influence of the environmental temperature on spray characteristics using the Malvern Spraytec®.

5.2 Materials and equipment

The equipment used in this chapter included:

- a filling crimping machine (Pamasol, Switzerland)
- aluminium canisters from Valois (Marly Le Roi, France)
- 50 μL non-continuous valves from Valois (Marly Le Roi, France)
- an experimental aluminium rig connected to a switch providing automated actuation of the canisters (see Section 4.2.7 in Chapter 4)
- a Flixotide® mouthpiece (Allen and Hanburys Ltd, Middlesex, UK)
- an Alvesco® mouthpiece (Takeda Pharmaceuticals International GmbH, Zurich, Switzerland)
- a 36 cm/14.5" high gauge (Rabone Chesterman, Sheffield, UK)
- an electrical trigger (built and designed in-house from De Montfort University)

The equipment used for the PIV measurements were:

- a Dantec PCO Camera equipped with a green filter (Dantec, Massachusetts, USA)
- a FlowManager software version 4.5 (Dantec, Massachusetts, USA)
- a Flowmap system HUB (Dantec, Massachusetts, USA)
- a Peltier device (Dantec, Massachusetts, USA)
- a NewWave Solo laser of wavelength 532 nm (New Wave Research ESI, Portland, Oregon)

The equipment used for the Sympatec® measurements were:

- a Sympatec® LD particle-sizer and its Windox 5 software (HELOS Compact, Model KA), (Sympatec GmBH, Clausthal-Zellerfeld, Germany)
- a wash bottle (HELOS Compact, Model KA), (Sympatec GmBH, Clausthal-Zellerfeld, Germany)
- Whatman lens cleaning tissue (Whatman, Kent, UK)
- acetone analytical reagent (Fisher Scientific, Loughborough, UK)

The equipment used for the Malvern Spraytec® measurements were:

- a Malvern Spraytec® 97 and its software RTSizer version 5.41 (Malvern, Worcestershire, UK)
- a drying oven Type VT6 (Thermo Fisher Scientific, MA, United States)

The equipment used to measure the velocity of the canister during actuations were:

- a linear variable differential transformer (LVDT) Solartron Metrology DC25 (West Sussex, UK)
- a USB 6211 analog to digital converter (National Instrument, Berkshire, UK)

5.3 Device design

In order to measure the spray velocity at the nozzle orifice, a transparent mouthpiece in plastic was designed with a 3D printer to let the laser illuminate the flow. However, it was found that it was not sufficiently transparent to allow the laser to penetrate sufficiently. It was thus decided to measure the particles velocities outside the mouthpiece.

For the PIV measurements, all formulations were tested with the Flixotide® mouthpiece as the stem of Valois 50 μL valves could not fit in the Alvesco® mouthpiece. Although this did not represent an issue in the previous chapter in which a few actuations were required for each test, it was problematic in the PIV experiments as the canister was displaced during the multiple measurements required in PIV measurements and could not be repositioned for fear of disturbing the alignment of the whole system.

The closest location from the nozzle orifice for the velocity measurements therefore corresponded to the distance between the nozzle orifice and the extremity of the Flixotide® mouthpiece, which was 25 mm. For the particle size measurements with the Sympatec® and the Malvern Spraytec®, the Flixotide® mouthpiece with a nozzle orifice diameter of 0.50 mm was used for the suspension formulation. For the two solution formulations, the Alvesco® mouthpiece with a length of 37 mm and a nozzle orifice diameter of 0.20 mm was used.

5.4 Manufacture of formulations

The pure propellant formulations were manufactured by crimping the canisters with the Valois 50 μL valves and forcing approximately 20 g of HFA134a under pressure in each canister using the filling crimping machine (Pamasol, Switzerland).

The HF, HEF and HPEF formulations were prepared as described in Section 4.2.2 of Chapter 4. Table 5.1 shows the composition of the formulations studied in this chapter.

	Names of the formulations			
	HFA134a	HF	HEF	HPEF
FP	-	0.05%	0.05%	0.05%
HFA134a	100%	$\simeq$ 99.95%	$\simeq$ 84.95%	$\simeq$ 84.95%
Ethanol	-	-	15%	10%
PEG400	-	-	-	5%

Table 5.1: Percentage by weight of each component of the studied formulations.

5.5 Experimental method

5.5.1 PIV measurements of sprays issued from pMDIs

An experimental analysis based on 2D-PIV data was performed. The canister support was painted in matt black to minimise any potential light reflection. The measurements were performed using a Dantec Dynamics PIV system. The laser used was a pulsed Nd:YAG laser, emitting light at 532 nm with a maximum frequency of 15 Hz. The images were recorded using a Dantec PCO Camera with a 1280×1024 pixel CCD cooled by a Peltier module to improve the signal-to-noise ratio. The laser control, the laser/camera synchronisation, the data acquisition and processing were handled by a hardware module (FlowMap System Hub) and

a software (FlowManager) installed on a PC.

The actuation of the canister by pneumatic cylinder and the PIV system recording were coordinated using a purpose-built electrical trigger. The PIV was set up to receive a signal from this external trigger. A delay could be implemented in order to record the images at a specific delay after the actuation. Figure 5.3 represents a schematic of the PIV setup.

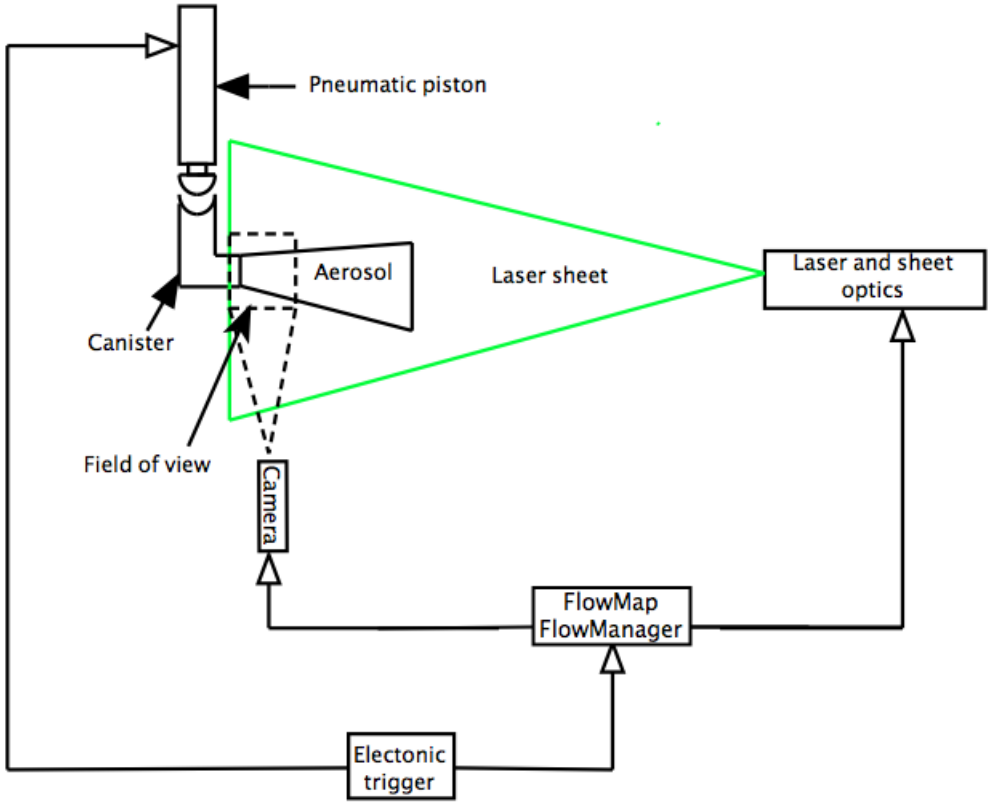

Figure 5.3: Schematic of the PIV setup.

The 2D instantaneous velocity vectors were determined on a vertical plane crossing the pMDI's plane of symmetry. At least 250 instantaneous measurements were performed for each experimental condition. A period of 10 s separated each canister actuation.

The velocity was measured at the extremity of the mouthpiece located at a dis-

tance of 25 mm from the nozzle orifice. However due to intense scattering of the mouthpiece, the measurements in the area were deemed unreliable. It was decided to only use data at a distance of 10 mm from the mouthpiece extremity (35 mm from the nozzle orifice).

The time between two consecutive laser pulses, the interrogation area size and the characteristics of the data analysis were carefully selected after preliminary tests in order to maximise the measurements accuracy. For each actuation, two frames separated by a 10 μs delay were recorded using one laser pulse per frame. Each pulse had a duration of 0.01 μs.

Each time the canister was replaced within one set of measurements, the camera image was closely studied to ensure the measurement zone had not been modified. Between each test, a new calibration was done in order to obtain well-focused measurements and to calculate the scale at which the measurements were conducted. A typical frame obtained when calibrating the system is shown in Figure 5.4.

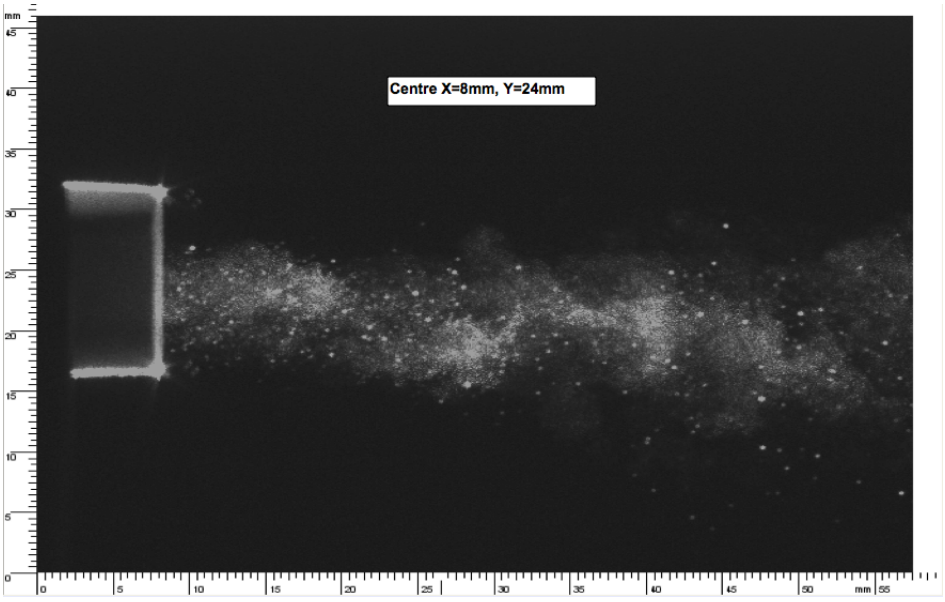

Figure 5.4: Picture of a HFA134a spray allowing the calibration of the system.

A FlowManager tool referred to as a mask was applied to all images to remove

any noise related to the canister and its mouthpiece. A cross-correlation algorithm was then applied to the masked images to extract meaningful velocities. It was performed on a rectangular grid with 50% overlap between adjacent cells; the final interrogation area was set at 32×32 pixels which corresponded to a dimension of 1.5 mm×1.5 mm and gave a spatial resolution of 0.75 mm.

5.5.2 Sympatec® measurements of sprays issued from pMDIs

The Helos device operates with a HeNe-laser of 632.8 nm wavelength. An inhaler cell that increased the distance from the nozzle orifice to the measuring zone to approximately 6 cm was used. The measurements were triggered at an optical concentration of 1%. The flow rate through the metering device was monitored using a Venturi meter. A wash bottle collected the fine particles and prevented them from entering the vacuum pump of the Sympatec®.

Before each measurement the pMDI was shaken for 10 s before being fired in the central adapter. For each set of experiments, a minimum of three replicates samples was tested. The background was checked before each pMDI actuation, and every five actuations, the inhaler cell was cleaned with a Whatman lens cleaning tissue (Whatman, Kent, UK) and acetone (Fisher Scientific, Loughborough, UK). A delay of 10 s was used between each shot to avoid cooling of the metering chamber. In each plot obtained with the Windox software, the 10th (D_{10}), 50th (D_{50}) and 90th (D_{90}) percentile of the cumulative particle under-size frequency distribution were presented. This set of experiments was conducted on an open bench in a temperature-controlled room.

5.5.3 Malvern Spraytec® measurements of sprays issued from pMDIs

The Malvern Spraytec® 97 and its software RTSizer version 5.41 configured for a measurement frequency of 2.5 kHz was used, giving the measurements a time resolution of 400 μs. The laser used was a 5 mW HeNe laser of 632.8 nm wavelength. The data acquisition system contained 36 light detectors, each capturing the light diffracted from particles of different sizes.

As the particles in the centre of the spray have a higher velocity and undergo less turbulence than the peripheral droplets, the canister was placed so that the laser measuring zone was located at the centre of the plume (Liu *et al.*, 2012). The size of particles was measured at two locations:

- close from the end of the mouthpiece (4 cm from the nozzle orifice)
- 7.5 cm from the nozzle orifice (which would represent approximately the location of the throat when the pMDI is used by a patient)

The standard operating procedure (SOP) defining measurement parameters such as the hardware configuration, the triggering mechanisms and the type of recording method is described below.

The 100 mm focal lens which has a particle size range between 0.5 μm and 200 μm was chosen for this experiment.

The Mie theory of light used by the Malvern technology requires data such as the refractive indexes of the media and measured sample. The media refractive index was the air refractive index (1.00+0.00i) and the particulate refractive index was set to the value of the refractive index of HFA134a (1.17+0.00i) (Stone and Zimmerman, 2011), (Solvay, 2008).

The duration of the measurement was set to 2 s and the measurement was triggered manually with the canister actuation.

The instrument was set to flash mode and a frequency of 2.5 kHz was used.

For each measurement, all the frames of the spray were averaged and the mean particle size distribution was used to determine the D_{50}.

The noise level was recorded before each set of experiment. The alignment and background of the system were checked prior each measurement by running a background measurement to ensure that the optics had not been contaminated during previous measurement.

For each set of experiments, a minimum of three measurements was conducted.

When studying the effect of temperature, the canister was heated by storing it in a drying oven (Thermo Fisher Scientific, MA, United States) one hour before the experiment. As the room was kept at 20 °C, the experiments were conducted quickly in order for the canister to remain at constant temperature.

The data were reduced in all measurements by removing the detector channels that might have been affected by beam steering. As the first 8 detectors measure particles with a diameter greater than 76.56 μm, it was decided not to take them into account in order to "kill" the large "phantom" droplets. This procedure should not affect the results as particles issued from pMDIs have a diameter lower than 76.56 μm at the distances studied (further than 4 cm from the nozzle orifice) (Clark, 1991).

5.6 Results

5.6.1 PIV measurements of sprays issued from pMDIs

Influence of formulation design on spray characteristics

The axial velocity of two formulations is shown in Figure 5.5. The velocity values were selected at different vertical coordinates depending on the distance from the mouthpiece in order to follow the downward shape of the spray.

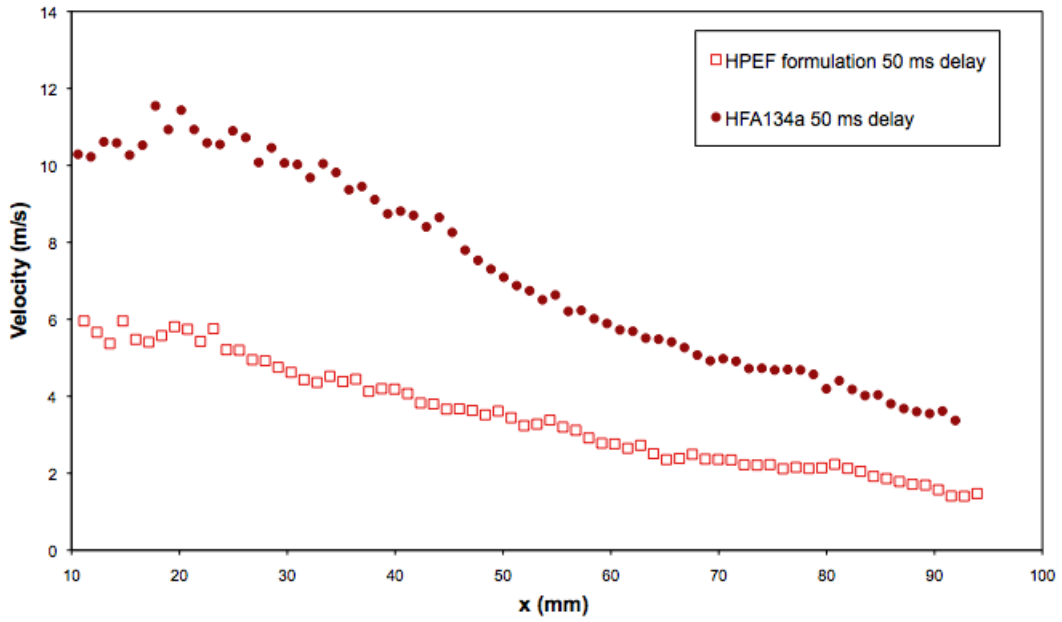

Figure 5.5: Velocity of two formulations as a function of the distance from the end of the mouthpiece. Each data point represents a mean of n≥250 determinations.

Figure 5.5 shows that for both formulations, the velocity of the droplets decreases significantly as they travel away from the mouthpiece. The HFA134a formulation was faster, with a velocity ranging from 12 $m \cdot s^{-1}$ to 4 $m \cdot s^{-1}$ compared to a velocity of 6 $m \cdot s^{-1}$ to 2 $m \cdot s^{-1}$ for the HPEF formulation.

The turbulence level of the spray U' is defined as the variation of each velocity

measurement away from the mean velocity and calculated using Equation (5.3).

$$U' = \sqrt{\frac{\sum(U_n - \bar{U})}{N}} \tag{5.3}$$

where U' is the turbulence of the spray in $\mathrm{m.s^{-1}}$, U_n represents each individual velocity value in $\mathrm{m.s^{-1}}$ and $\bar{U}$ is the mean velocity of all measurements in $\mathrm{m.s^{-1}}$. The turbulence level of the spray is plotted in Figure 5.6.

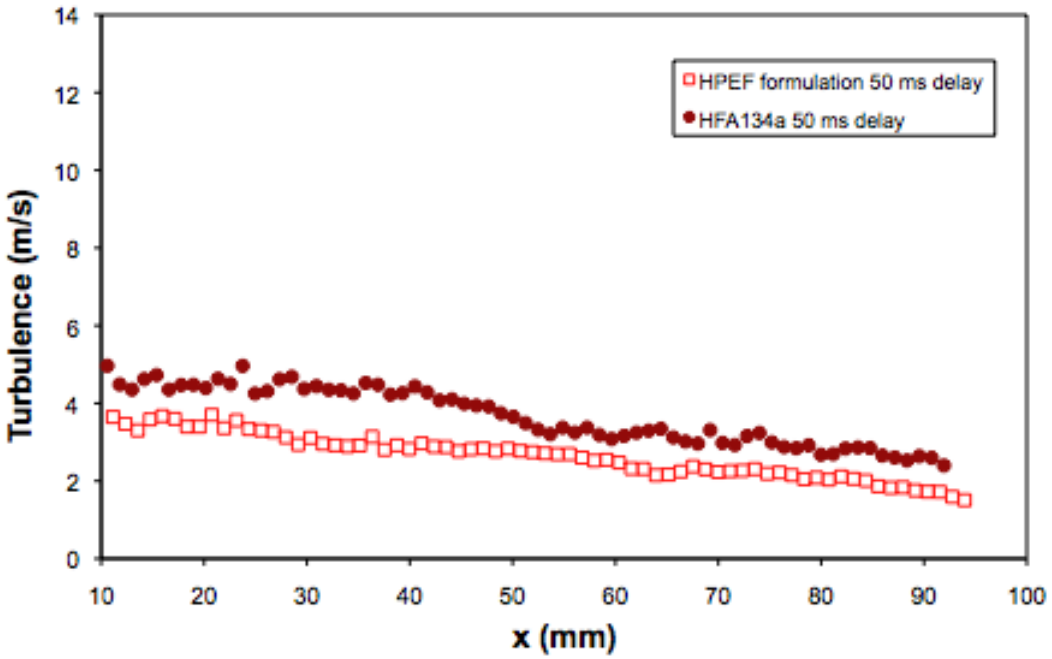

Figure 5.6: Turbulence of the spray as a function of the distance from the end of the mouthpiece for a pure HFA134a and a HPEF sprays. Each data point represents a mean of n≥250 determinations.

The HFA134a formulation had a turbulence ranging from approximately $3\,\mathrm{m{\cdot}s^{-1}}$ to $5\,\mathrm{m{\cdot}s^{-1}}$ compared to the HPEF formulation which had a turbulence of approximately $2\,\mathrm{m{\cdot}s^{-1}}$ to $4\,\mathrm{m{\cdot}s^{-1}}$.

Influence of actuating forces on spray velocity

Figure 5.7 shows the resulting vector velocity flow field obtained after data analysis.

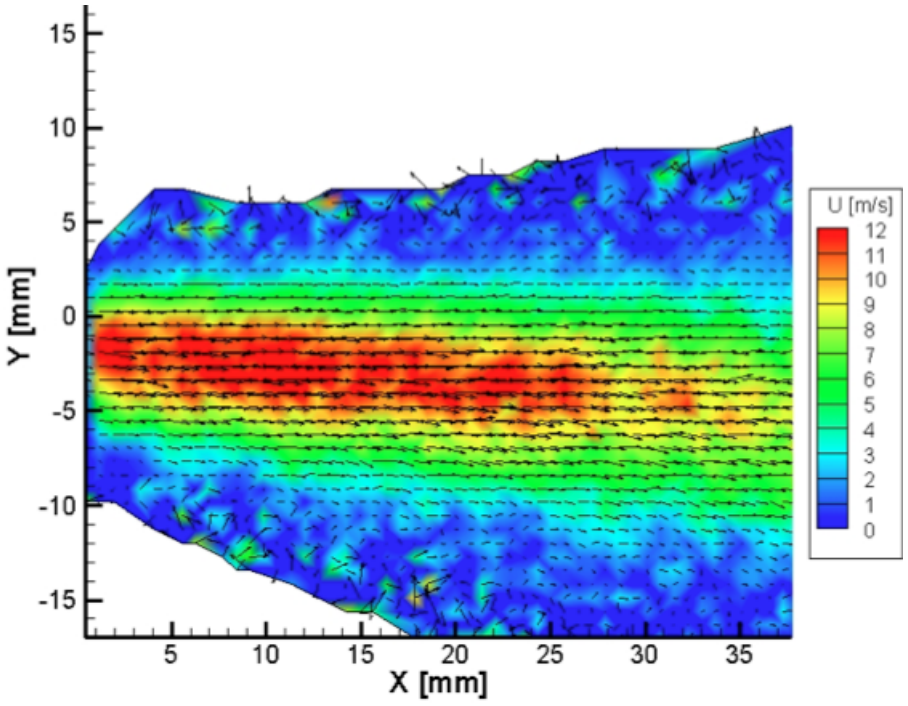

Figure 5.7: The vector velocity flow field of axial velocity for a HFA134a spray at the extremity of a Flixotide® mouthpiece after the mask and the cross-correlation were applied. Mean of n≥250 determinations.

Figure 5.7 shows velocities ranging from 12 m·s^{-1} to 7 m·s^{-1} from the extremity of the mouthpiece to a distance of 35 mm from the mouthpiece respectively. Crosland *et al* (2009) obtained velocities in the range of 60 m·s^{-1} to 20 m·s^{-1} at 2.5 mm and 17.5 mm from the extremity of the mouthpiece respectively for a HFA134-based formulation. The field of view in Crosland's work is significantly lower than the one used in the current work, which could explain the difference between the results obtained in both experiments. Crosland *et al* measured the exit velocities of the spray close to the extremity of the mouthpiece whereas in the current work, the development of the spray over a typical pMDI/back of the throat distance was captured.

Figure 5.7 also reveals a slight downward slope of the spray in line with Crosland *et al* (2009) who reported a spray direction ranging from 0.2° to 5.8° below horizontal. The effect of varying the actuation forces was tested on pure HFA134a canisters and can be seen in Figure 5.8. Forces of 30 N, 40 N and 50 N were studied. The velocity profiles as a function of the actuation force were obtained by spatially bin averaging the data over zones of 2 mm on the entire measurement region. The velocity values were selected at different vertical coordinates depending on the distance from the mouthpiece in order to follow the downward shape of the spray.

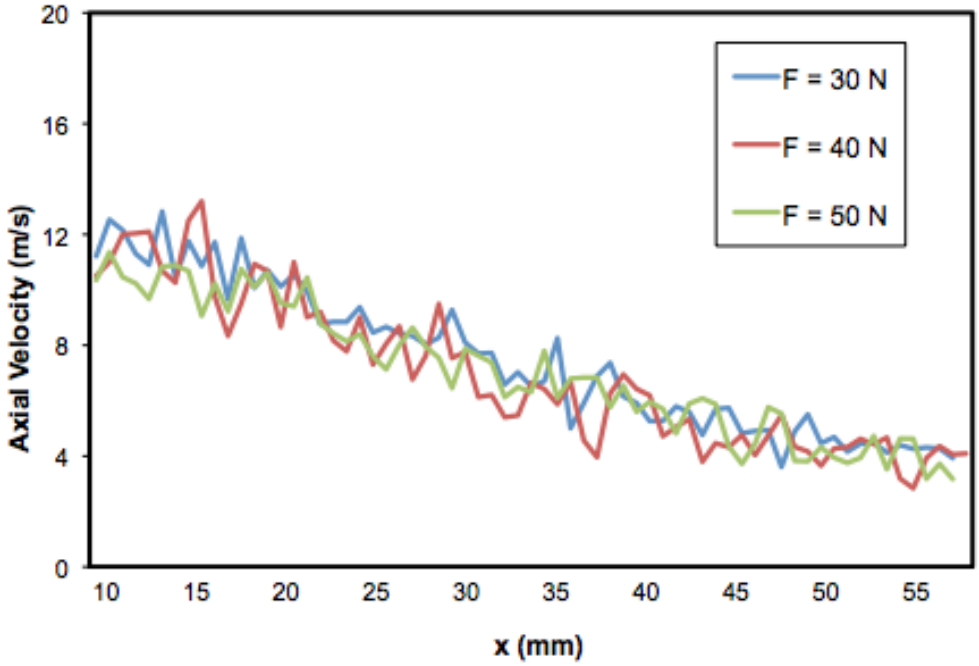

Figure 5.8: Particles velocity as a function of the distance from the end of the mouthpiece for 3 actuation forces for a HFA134a aerosol. Each data point represents a mean of n≥250 determinations.

Figure 5.8 shows that the actuation force did not affect the particles velocity. All forces led to a spray velocity of around 12 $m \cdot s^{-1}$ at a distance of 1 cm from the mouthpiece and approximately 4 $m \cdot s^{-1}$, 5 cm from the mouthpiece.

Influence of delays on spray velocity

The influence of the time interval between the actuation and the measurement of the spray velocity was studied. The measurements were realised with no delay, 50 ms, 100 ms and 200 ms delays. The effect of the delays on the spray velocity along the spray trajectory can be seen in Figure 5.9.

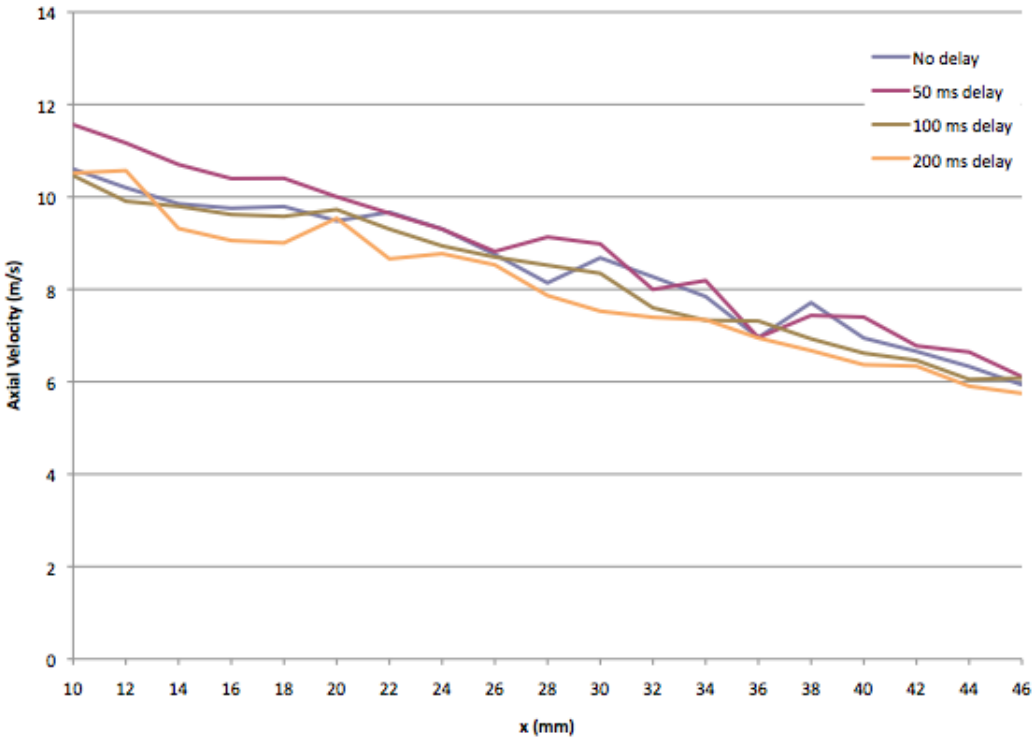

Figure 5.9: Effect of time delays on mean axial velocity for a HFA134a aerosol. Each data point represents a mean of n≥250 determinations.

The velocity values were again selected at different vertical coordinates depending on the distance from the mouthpiece in order to follow the downward shape of the spray. The average of all velocities along the spray trajectory was then calculated for each delay and the time-resolved velocity profile of the spray shown in Figure 5.10 was plotted.

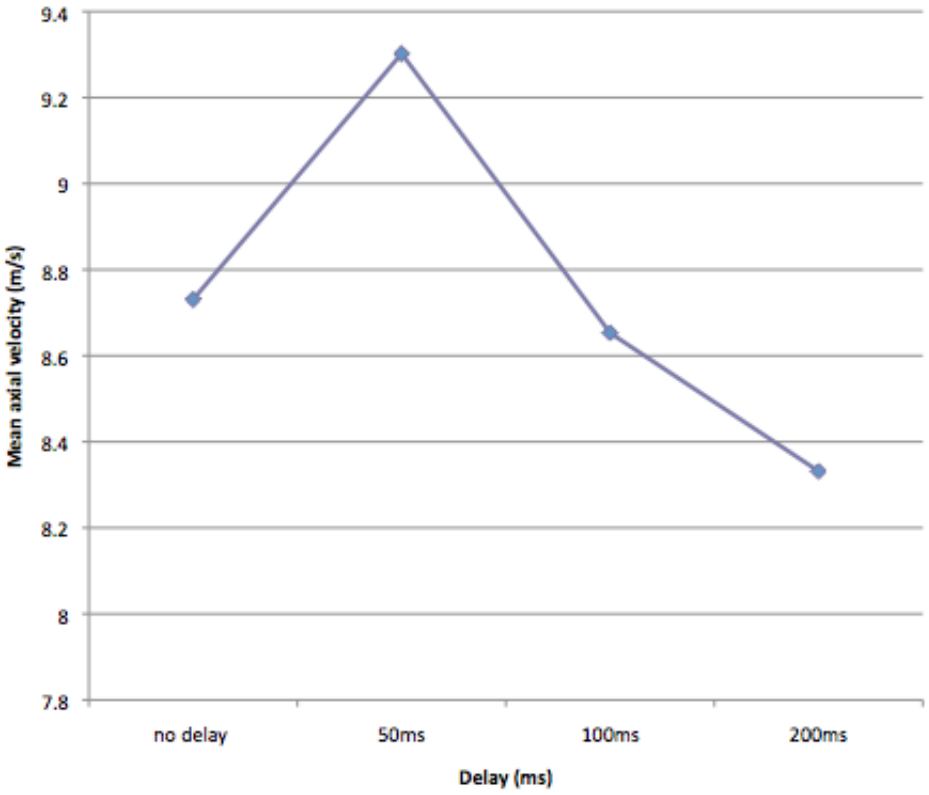

Figure 5.10: Temporal profile of a HFA134a spray at several time delays over the whole spray trajectory. Each data point represents a mean of n≥250 determinations.

It can be seen that the spray reached its maximum velocity 50 ms after its actuation. Its velocity then decreases as the delay increases. However, as the turbulence level of HFA134a aerosols is ranging from 1.5 $m \cdot s^{-1}$ to 4 $m \cdot s^{-1}$, the observed effect of delays on the velocity of the spray might not be significant and the experiments would need to be repeated to confirm this trend.

5.6.2 Sympatec® measurements of sprays issued from pMDIs

Effect of formulation design on spray characteristics

The HF, HEF and HPEF sprays were compared when actuated by hand at a flow rate of 30 $L \cdot min^{-1}$. This flow rate was chosen as it was used in the next generation

impactor (NGI) measurements in Chapter 4 and could therefore allow a better comparison of the results obtained with the NGI and the Sympatec®. However, the latter measured the spray at a distance of 6 cm from the nozzle orifice, assessing the intermediate size of the particles whereas the NGI measured their residual size. The D_{50} of the three formulations can be seen in Table 5.2.

	HF	HEF	HPEF
	Mean±SD	Mean±SD	Mean±SD
D_{50} (μm)	3.78±0.14	2.49±0.13	4.14±0.10

Table 5.2: D_{50} values of the three formulations obtained with the Sympatec® when actuated by a "healthy" female user at a flow rate of 30 L·min^{-1}. Mean of n=3 determinations for each formulation.

The average D_{50} of particles issued from the suspension formulation containing drug particles of 2.76±0.03 μm diameter was 3.78±0.14 μm. The percentage of particles of diameter ≤5 μm was approximately 87.7±2.7%.

The average D_{50} of the HEF formulation for the three measurements was 2.49±0.13 μm, which is significantly lower than the D_{50} value of the suspension formulation ($p<0.05$). For the HEF formulation, the percentage of particles of diameter ≤5 μm varied between 95% and 100%, which is significantly higher than the value obtained for the suspension formulation ($p<0.05$).

The HPEF formulation, with a D_{50} of 4.14±0.10 μm aerosolised significantly larger particles than the HF and the HEF formulations ($p<0.05$). The percentage of particles of diameter ≤5 μm for the HPEF formulation was 62.3±1.2 %, which is significantly lower than the percentages of particle of diameter ≤5 μm obtained for the HF and HEF formulations ($p<0.05$).

The D_{50} of both solution formulations cannot be directly compared to the D_{50} of the suspension formulation as both solution formulations were aerosolised using the Alvesco® mouthpiece of nozzle orifice diameter 0.20 mm whereas the suspen-

sion formulation was aerosolised using the Flixotide® mouthpiece of nozzle orifice diameter 0.50 mm.

Effect of airflow rate on spray characteristics

The effect of the flow rate on the particle size distribution of the HF, HEF and HPEF formulations was also studied using the Sympatec®. The effect of a 30 L·min^{-1} and a 60 L·min^{-1} flow rates on the HF formulation can be seen in Figure 5.11.

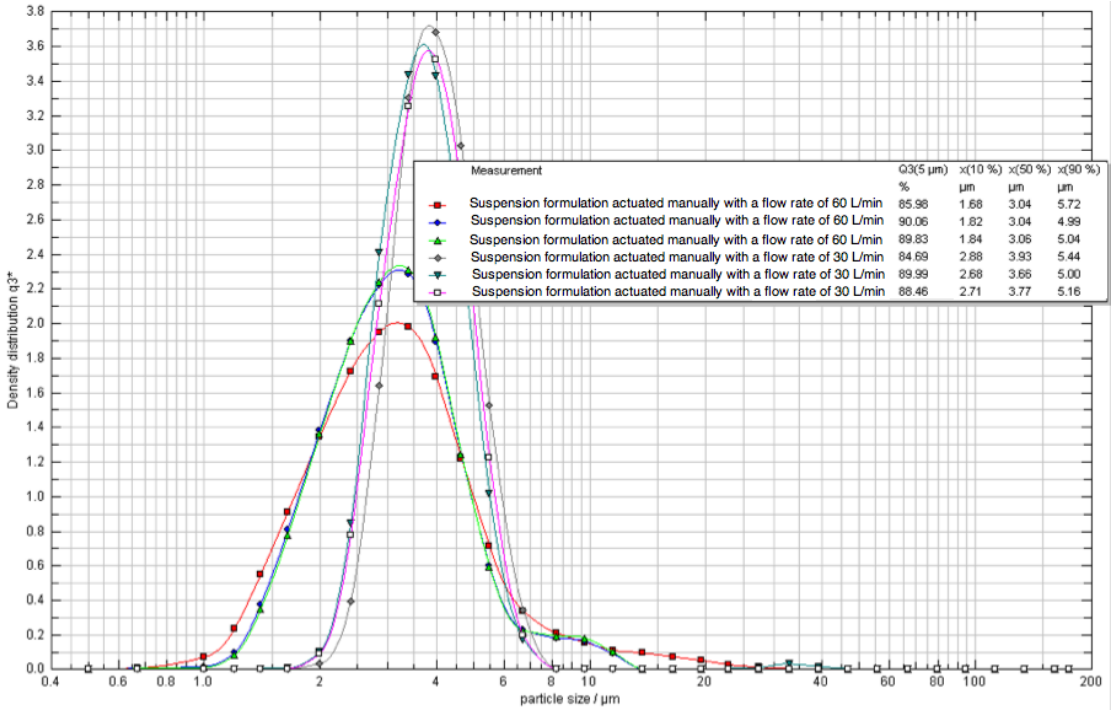

Figure 5.11: Particle size distribution of the HF formulation actuated by hand at flow rates of 30 L·min^{-1} and 60 L·min^{-1}.

Figure 5.11 shows that both flow rates result in varying particle size distribution curves. The 60 L·min^{-1} flow rate results in a shift of the particle size distribution curve towards the left, signalling a higher percentage of fine particles when the higher flow rate is used. The average of the D_{50} for the three measurements was 3.05±0.01 μm for the 60 L·min^{-1} flow rate and 3.79±0.14 μm for the 30 L·min^{-1} flow rate.

This effect was also observed with the HEF and HPEF formulations as shown in

Figures 5.12 and 5.13 respectively. The average of the D_{50} for the three measurements of the HEF aerosol was 2.49±0.13 μm at the 30 L·min^{-1} flow rate and 1.28±0.08 μm at the 60 L·min^{-1} flow rate. A higher percentage of particles smaller than 1 μm can be observed at the 60 L·min^{-1} flow rate in Figure 5.12.

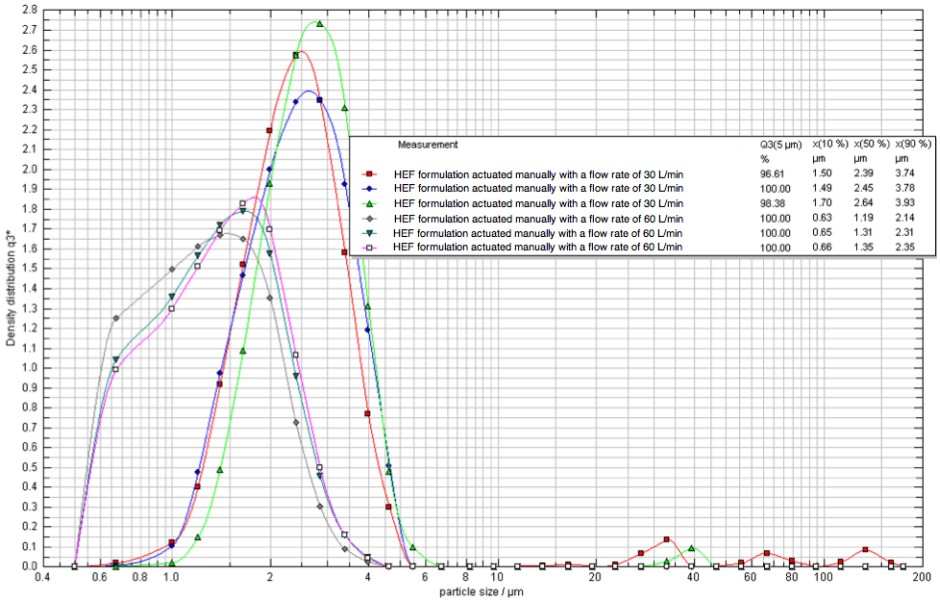

Figure 5.12: Particle size distribution of the HEF formulation actuated by hand at flow rates of 30 L·min^{-1} and 60 L·min^{-1}.

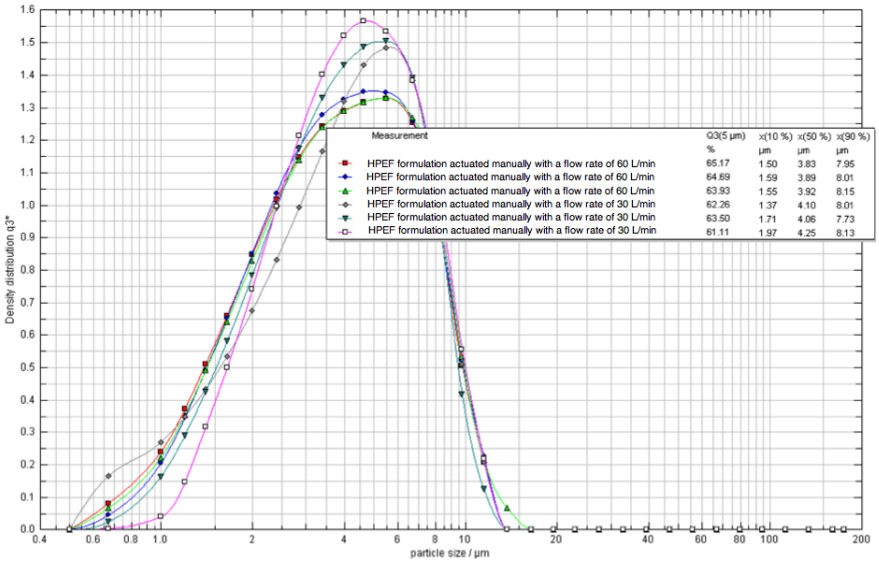

Figure 5.13: Particle size distribution of the HPEF formulation actuated by hand at flow rates of 30 L·min^{-1} and 60 L·min^{-1}.

The average of the D_{50} for the three measurements of the HPEF formulation was 3.88±0.05 μm at a flow rate of 60 L·min^{-1} and 4.14±0.10 μm at a flow rate of 30 L·min^{-1}.

For the three formulations, the 60 L·min^{-1} flow rate led to significantly smaller D_{50} values ($p<0.05$). The uniformity index is a measure ranging from 1 to 100 used to characterise the homogeneity of particle sizes (Hanna and York, 1998). It was calculated for each formulation at both flow rates using Equation (5.4).

$$UI = \frac{D_{10}}{D_{90}} \times 100 \tag{5.4}$$

where UI corresponds to the uniformity index (Hanna and York, 1998).

The D_{50} and uniformity index values of the three formulations at both flow rates are shown in Table 5.3.

	HF		HEF		HPEF	
Flow rate (L·min^{-1})	30	60	30	60	30	60
D_{50} (μm)	3.79	3.05	2.49	1.28	4.14	3.88
UI	53.02	34.11	40.93	28.55	21.15	19.25

Table 5.3: D_{50} and uniformity index values of the three formulations obtained with the Sympatec® when actuated by a "healthy" female user at flow rates of 30 L·min^{-1} and 60 L·min^{-1}. Mean of n=3 determinations at each flow rate.

Table 5.3 shows that the uniformity index significantly decreases at the higher flow rate for the HF and HEF formulations ($p<0.05$) and slightly decreases for the HPEF formulation. It also shows that at the recommended flow rate of 30 L·min^{-1}, the uniformity index is significantly lower for the HPEF formulation compared to the HF and HEF formulations and is significantly higher for the HF formulation compared to the HEF and HPEF formulations ($p<0.05$).

Effect of actuation force on spray characteristics

The effect of two actuation forces provided by a pneumatic piston on the particle size distribution of the HEF formulation can be seen in Figure 5.14.

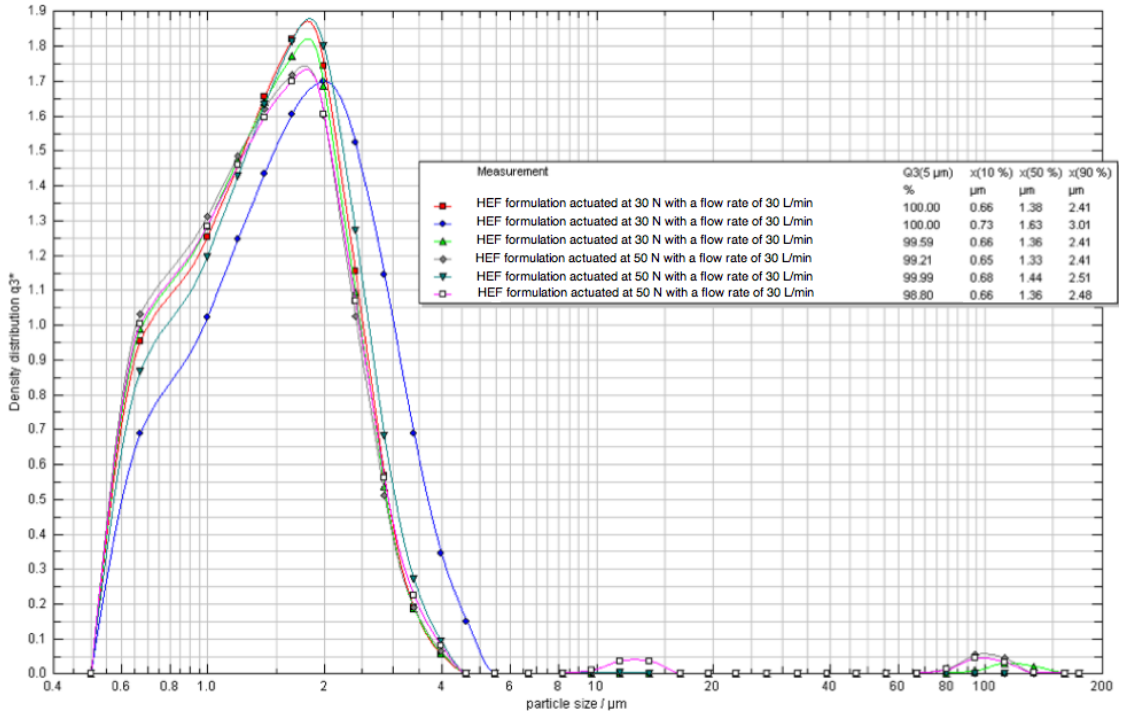

Figure 5.14: Particle size distribution of the HEF formulation actuated by a pneumatic piston at 30 N and 50 N at a flow rate of 30 L·min^{-1}.

Figure 5.14 shows that the actuation force delivered by the pneumatic piston had no significant effect on the particle size distribution of the aerosols. The average of the D_{50} for the three measurements of the HEF formulation actuated at 30 N was 1.46±0.15 μm and 1.38±0.06 μm at 50 N.

However, it can be seen in Figure 5.15 that the manual actuation provided by the "healthy" female user led to the aerosolisation of coarser particles compared to automated actuations. The uniformity index had a value of 27.39% and 26.97% for the 30 N and 50 N actuations respectively compared to a significantly higher value of 60.82% for the actuation of the "healthy" female user ($p<0.05$).

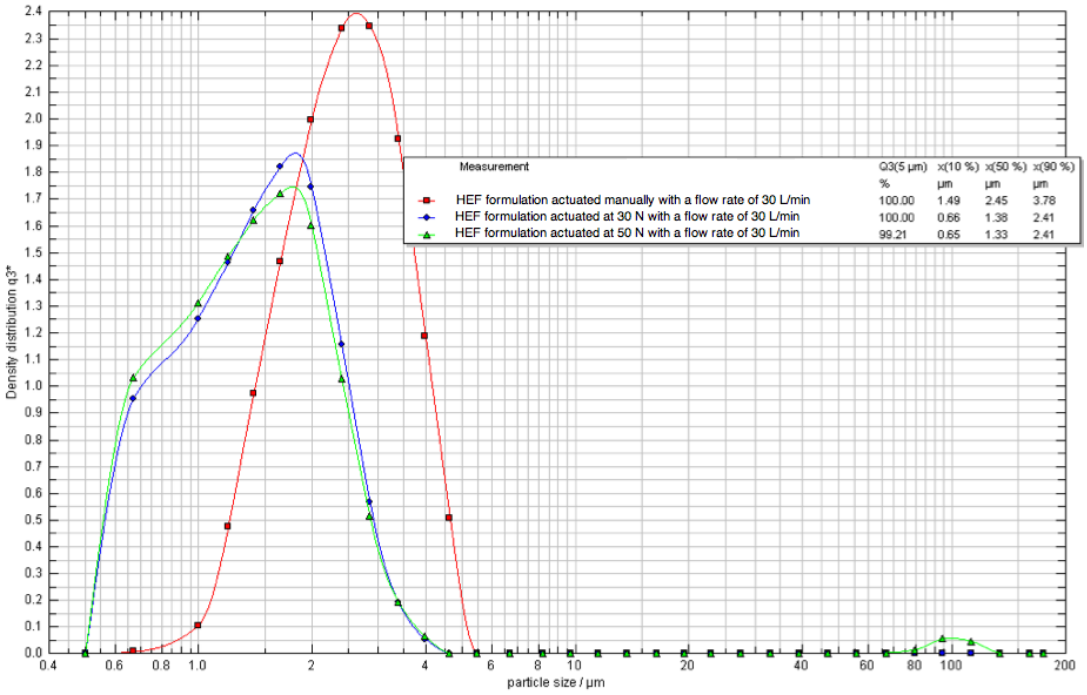

Figure 5.15: Particle size distribution of the HEF formulation at a flow rate of 30 L·min^{-1} actuated by a "healthy" female user and by a pneumatic piston at 30 N and 50 N.

5.6.3 Malvern Spraytec® measurements of sprays issued from pMDIs

Particle size measurements at 4 cm from the nozzle orifice

The data measured at 4 cm from the nozzle orifice for the three formulations and three types of actuations at two temperatures are shown in Table 5.4 which reveals that the D_{90} of the HF formulation for all experiments was significantly larger than the D_{90} of the HEF and HPEF formulations ($p<0.05$).

		HF Mean±SD	HEF Mean±SD	HPEF Mean±SD
30 N actuation at 20 °C	D_{10} (μm)	2.04±0.44	1.99±0.36	2.85±0.81
	D_{50} (μm)	10.84±1.75	6.86±0.68	11.41±4.53
	D_{90} (μm)	72.14±0.86	20.44±9.76	41.30±25.89
50 N actuation at 20 °C	D_{10} (μm)	1.46±0.18	1.82±0.51	2.59±0.71
	D_{50} (μm)	8.87±1.13	6.14±0.53	9.23±2.45
	D_{90} (μm)	72.41±0.32	13.91±1.91	29.84±16.96
Manual actuation at 20 °C	D_{10} (μm)	3.85±0.05	3.09±0.40	4.14±0.39
	D_{50} (μm)	11.71±0.25	8.29±0.42	10.87±1.09
	D_{90} (μm)	73.39±0.23	28.12±11.76	30.66±11.25
Manual actuation at 40 °C	D_{10} (μm)	3.28±0.28	2.26±0.61	2.72±0.53
	D_{50} (μm)	55.73±19.67	4.93±0.17	6.96±0.90
	D_{90} (μm)	74.56±0.70	20.17±5.82	18.59±7.06

Table 5.4: D_{50} obtained using the Malvern Spraytec® at 4 cm from the nozzle orifice. Manual actuations provided by a "healthy" female user. Mean of n≥3 determinations for each data.

As the two solution formulations were tested using the same mouthpiece, a direct comparison of those formulations was possible. Table 5.4 shows that the diameters of particles issued from the HEF formulation were consistently lower than those issued from the HPEF formulation. In all experimental conditions, the D_{50} values were lower for the HEF formulation compared to the HPEF formulation.

It is suggested that the high variability of the results observed in Table 5.4 might be due to the close distance of the measurement zone to the nozzle orifice. As a result, a new set of experiments was realised at 7.5 cm from the nozzle orifice.

Particle size measurements at 7.5 cm from the nozzle orifice

Although it is difficult to find a value for the nozzle orifice to back of the throat distance, it was possible to estimate it based on several articles (Finlay, 2001), (Battagel *et al.*, 2002), (Kim and Park, 2011). It was assumed that the distance from the nozzle orifice to the back of the throat was approximately 7.5 cm and that this distance could be used to describe the properties of the droplets as they penetrate the respiratory system.

The data obtained at 7.5 cm from the nozzle orifice for the three formulations and three types of actuations at two temperatures are shown in Table 5.5. It reveals that most D_{50} values were significantly smaller when the spray was measured at 7.5 cm from the nozzle orifice compared to when it was measured at 4 cm from the nozzle orifice ($p<0.05$).

		HF Mean±SD	HEF Mean±SD	HPEF Mean±SD
30 N actuation at 20 °C	D_{10} (μm)	0.94±0.01	2.31±0.57	1.48±0.39
	D_{50} (μm)	2.53±0.04	6.53±1.06	6.38±0.56
	D_{90} (μm)	5.85±1.11	19.84±3.59	16.70±1.36
50 N actuation at 20 °C	D_{10} (μm)	1.06±0.12	1.48±0.26	1.43±0.15
	D_{50} (μm)	2.65±0.10	5.42±0.35	6.01±0.32
	D_{90} (μm)	7.31±0.65	13.13±0.81	15.30±0.71
Manual actuation at 20 °C	D_{10} (μm)	0.84±0.18	3.35±0.13	3.55±0.03
	D_{50} (μm)	2.71±0.22	7.83±0.19	9.74±0.29
	D_{90} (μm)	12.89±5.54	16.57±0.51	21.05±1.07
Manual actuation at 40 °C	D_{10} (μm)	2.30±0.46	2.09±0.62	3.17±0.49
	D_{50} (μm)	3.19±0.29	4.57±0.98	5.42±0.68
	D_{90} (μm)	4.18±0.45	14.04±3.21	17.09±4.21

Table 5.5: D_{50} obtained using the Malvern Spraytec® at 7.5 cm from the nozzle orifice. Manual actuations provided by a "healthy" female user. Mean of $n\geq3$ determinations for each data.

It can be seen that the D_{50} of the spray was influenced by the formulation components. For all measurements, the D_{50} values of the HF formulation were significantly smaller than the D_{50} values of the HEF formulation ($p<0.05$) and the D_{50} values of the HEF formulation were in almost all cases slightly smaller than the D_{50} values of the HPEF formulation.

Table 5.5 also shows that both solution formulations had significantly lower D_{50} values when the canisters were heated at 40 °C compared to when they were kept at 20 °C ($p<0.05$).

Finally, the manual actuation provided by the "healthy" female user was shown to lead to higher D_{50} values than both automated actuations.

Evaluation of the spray duration using the Malvern Spraytec®

The spray duration issued from the three formulations was measured. It was defined as the lapse of time during which the intensity of the laser signal was lower than 98% of its initial value. This intensity threshold might explain the shorter duration observed with the Malvern Spraytec® for the HF formulation compared to the PIV set up which continued measuring particles after a delay of 200 ms after the actuation. The duration of the three formulations can be seen in Table 5.6.

	HF	HEF	HPEF
	Mean±SD	Mean±SD	Mean±SD
Duration (s)	0.06±0.02	0.21±0.005	0.26±0.010

Table 5.6: Sprays duration measured at a distance of 7.5 cm from the nozzle orifice at 20 °C. Mean of n≥3 determinations for each formulation.

Table 5.6 shows that the duration of the plume is significantly affected by the type of formulation aerosolised ($p<0.05$). The suspension formulation has a significantly lower duration than both solution formulations and the HPEF formulation produces sprays with the longest durations compared to the HF and HEF formulations ($p<0.05$).

5.7 Discussion

5.7.1 PIV measurements of sprays issued from pMDIs

Comparison to other works

The velocity profiles obtained in Figure 5.8 were higher than the LDA results obtained by Lee *et al* (1991) when measuring a mixture of CFC-11 and CFC-12 (30/70% w/w) with a ratio of surfactant to drug of 1/10. They found a velocity of

7.5 m·s^{-1} to 5 m·s^{-1} at a distance of 30 mm from the nozzle orifice (Lee *et al.*, 1991). The lower velocity measured by Lee *et al* (1991) can be explained by the fact that propellants CFC-11 and CFC-12 have a vapour pressure of 89 kPa and 580 kPa respectively whereas HFA134a used in the present work has a vapour pressure of 590 kPa (Smyth and Hickey, 2011). Although CFC sprays are expected to have a lower initial velocity due to their lower vapour pressure, the velocity of HFA aerosols might reduce more as the spray travels away from the nozzle as they are made of smaller droplets which would decelerate more in contact with air than bigger CFC droplets. This might explain that CFC sprays are found to be approximately twice faster as HFA sprays at a distance of 10 cm from the nozzle (Hochrainer *et al.*, 2005).

The present findings were in line with the high-speed photography results of Dhand *et al* (1988) who calculated a spray exit velocity in the range of 13 m·s^{-1} to 15 m·s^{-1} for four commercial CFC-based pMDIs (Dunbar, 1996).

However, the present PIV results were not in line with Clark's PDA velocity data of 35 m·s^{-1} at a distance of 5 cm from the nozzle orifice with a formulation containing CFC-12 and 1% sorbitan trioleate. The velocity difference could be explained by the fact that Clark used 100 μL valves compared to the 50 μL valves used in this work. Higher metering volumes were shown to lead to bigger droplets and might therefore allow, due to higher mass conservation of big droplets, to better maintain the droplets velocity throughout their trajectory. This could contribute to explain the high velocity profiles obtained by Clark a few centimetres downstream of the nozzle orifice (Newman *et al.*, 1982).

However, the 35 m·s^{-1} velocity reported by Clark at a distance of 5 cm from the nozzle orifice remains higher than velocities reported in sprays studies at similar distances from the nozzle orifice. For example, Crosland *et al* found velocities of

$20\,\mathrm{m{\cdot}s^{-1}}$ to $30\,\mathrm{m{\cdot}s^{-1}}$ when measuring a HFA134a formulation at a distance of 1.5 cm from the extremity of the mouthpiece corresponding to a distance of approximately 4 cm from the nozzle orifice (Crosland *et al.*, 2009).

Hochrainer *et al* (2005) also found considerably lower velocities than Clark when testing formulations with similar vapour pressures. While Clark reports a velocity of approximately $18\,\mathrm{m{\cdot}s^{-1}}$ at a distance of 10 cm from the nozzle orifice, Hochrainer found velocities of $5.6\,\mathrm{m{\cdot}s^{-1}}$ to $6.3\,\mathrm{m{\cdot}s^{-1}}$ for varying CFC-based formulations at the same location (Hochrainer *et al.*, 2005).

Although CFC-based formulations have been shown to have a velocity approximately twice higher compared to their equivalent HFA-based formulations at distances of 10 cm from the nozzle, this still does not explain the much higher velocity values found by Clark compared to authors who also measured CFC-based formulations (Hochrainer *et al.*, 2005). The experimental method of Clark was not sufficiently detailed to enable any conclusion to be drawn (Clark, 1996).

As PIV measurements are thought to measure the velocity of liquid droplets, the velocities measured using PIV should correspond to the velocity of the liquid phase calculated in the simulation in Chapter 3 using a similar nozzle orifice diameter. The $17\,\mathrm{m{\cdot}s^{-1}}$ maximum liquid phase velocity calculated at the nozzle orifice in Chapter 3 is in line with the $12\,\mathrm{m{\cdot}s^{-1}}$ maximum velocity measured approximately 25 mm downstream of the nozzle orifice using PIV.

Influence of formulation design on spray characteristics

The difference of velocities observed in Figure 5.5 between the two formulations can be explained by the higher vapour pressure of the pure propellant formulation compared to the HPEF formulation.

The velocities follow the same trend as the PDA velocity measurements of Liu *et al*

(2012) at a distance of 2 cm from the end of the mouthpiece (approximately 5 cm from the nozzle orifice) although they are slightly lower in magnitude (Dunbar, 1996). When measuring several suspension formulations containing only drug and HFA134a whose vapour pressures should be similar to the pure HFA134a formulations measured in Figure 5.5, Liu *et al* found velocities in the range of $10\,\mathrm{m{\cdot}s^{-1}}$ to $20\,\mathrm{m{\cdot}s^{-1}}$ compared to the $8\,\mathrm{m{\cdot}s^{-1}}$ velocity obtained with the pure HFA134a formulation at the same location in the present work.

The formulation most similar to HPEF that Liu *et al* studied is Proventil HFA which contains HFA134a, ethanol and oleic acid. When measuring the velocity of a Proventil spray, Liu *et al* found a velocity of $6.5\,\mathrm{m{\cdot}s^{-1}}$ compared to the $4\,\mathrm{m{\cdot}s^{-1}}$ velocity obtained with the HPEF formulation at the same location in the present work.

The HFA134a formulation which has a higher vapour than the HPEF formulation, has the highest turbulence level. This can be explained by the fact that a higher vapour pressure leads to a higher velocity. For both formulations, the turbulence level decreased as the distance from the nozzle orifice increased. This can be explained by the fact that at longer distances from the nozzle orifice, the spray velocity decreases, leading to a lower level of turbulence.

Influence of actuating forces on spray velocity

In Chapter 4, the manual actuations provided by a "healthy" female user led to an increased throat deposition compared to two automated actuations forces of varying magnitudes. No effect was reported between the automated actuation forces of varying magnitudes. In the PIV experiments, the manual actuation could not be tested so that the results are not comparable to the ones obtained in Chapter 4.

In this chapter, the magnitude of the three automated actuation forces had no discernible effect on the spray velocity. This might be due to the fact that although the magnitude of actuating forces could theoretically have an effect on the valve opening rate, this effect was not significant in reality or too small to be detected in the PIV measurements.

The velocities for the three actuation forces ranged from $12\,\mathrm{m{\cdot}s^{-1}}$ to $4\,\mathrm{m{\cdot}s^{-1}}$ at 35 mm and 90 mm from the nozzle orifice respectively. As a typical flow rate recommended for pMDI is $30\,\mathrm{L{\cdot}min^{-1}}$ which corresponds to a velocity of approximately $2\,\mathrm{m{\cdot}s^{-1}}$ at the oropharynx, the flow rate might have an effect on the velocity of the particles when the latter reach the throat (Keller, 1999). The flow rate did not have an effect in Crosland's work captured at the extremity of the mouthpiece where the spray velocity was significantly higher than the velocity of air through the trachea (Crosland *et al.*, 2009). However, it might have an effect nearer the patient's throat where the spray and user airflow velocities are comparable.

Influence of delays on spray velocity

The peak velocity observed 50 ms after the onset of actuation in Figures 5.9 and 5.10 could be due to a change of flow regime during the aerosolisation process. At the nozzle orifice, the spray is first critical due to the high pressure gradient between the metering chamber and atmospheric pressure. After this initial velocity peak, the flow becomes subcritical as a higher fraction of liquid builds up in the expansion chamber. As the flow starts evaporating in the expansion chamber, the pressure builds up, leading to a critical flow and higher spray velocity (Wigley *et al.*, 2002).

After it reaches its maximal pressure, the pressure in the expansion chamber decreases as the metering chamber empties. As a result, the spray velocity decreases once more.

The 50 ms delay could therefore represent the time needed for the flow to reach a sonic state for a HFA134a spray. The peak velocity delay would depend on several factors such as the expansion chamber volume, the nozzle to valve orifice ratio and the vapour pressure of the formulation. This finding is in agreement with Crosland's PIV measurements in which a peak velocity was found approximately 60 ms after the actuation of the canister (Crosland *et al.*, 2009).

In their computational model and PDA work on HFA134a-based formulations shown in Figure 3.22 in Chapter 3, Wigley *et al* (2002) found velocity peaks 50 ms and 70 ms after the actuation respectively. However, the magnitude of the velocity was much higher in their work. This could be due to the fact that they measured the velocity at the nozzle orifice whereas the velocity in the current study was measured 35 mm downstream of the nozzle orifice.

Lee *et al* (1991) also found a peak velocity approximately 70 ms after the actuation in their time-resolved LDA measurements of a CFC-11 and CFC-12 mixture.

According to Dunbar's PDA work, a first velocity peak occurs upon actuation of the canister and a second peak occurs approximately 0.07 s later. Although the first peak was not identified in this work, the timing of the peak observed seem to be in line with the second peak described by Dunbar (Dunbar, 1996).

5.7.2 Sympatec® measurements of sprays issued from pMDIs

Effect of formulation design on particle size distribution

The results shown in Table 5.2 are in line with the results of Pu *et al* (2011) obtained with a Helos from Sympatec®. When measuring the size of particles issued from a suspension formulation containing API of median diameter 1.77 μm, they obtained a D_{50} of 3.61±0.04 μm compared to the value of 3.78±0.14 μm obtained in this

work.

In their Sympatec Inhaler 2000® measurements, Jones *et al.* (2005) found that approximately 78% of particles had a diameter $\leq$6.4 μm when measuring a suspension formulation containing FP with an initial D_{50} of 4.07$\pm$0.29 μm. In this work the micronised FP had a D_{50} of 2.76$\pm$0.03 μm and 88% of particles had a diameter $\leq$5 μm. The higher percentage of fine particles in this work can be explained by the lower size of FP particles used compared to the size of FP particles used in Jones's work. It also shows that aggregation of the drug particles in the formulation occurred only to an insignificant level, which might be due to the extremely low concentration of FP in the formulation.

The lower D_{50} of the HEF formulation compared to the suspension formulation could be due to the fact that the HEF formulation is a solution formulation in which drug particles are completely dissolved contrary to suspension formulations in which drug particles stay intact and might therefore contribute to higher D_{50} values. It could also be due to the use of mouthpieces of different nozzle orifice diameters for each formulation. The HEF formulation was aerosolised using the Alvesco® mouthpiece which has a nozzle orifice diameter of 0.20 mm in comparison with the Flixotide® mouthpiece used to aerosolise the suspension mouthpiece which has a nozzle orifice of 0.50 mm and might therefore have led to the aerosolisation of coarser droplets.

The HPEF had a significantly higher D_{50} than the HEF formulation. This is to be expected as the HPEF formulation contained 5% w/w of PEG400 which can be used to control the size of particles issued from pMDIs by increasing the viscosity and reducing the volatility of formulations (Ash and Ash, 2004).

The low uniformity index of the HPEF formulation compared to the HF formulation observed in Table 5.3 could be due to the fact that the HF formulation only contains

drug particles and propellant so that once the propellant has evaporated, the size of the droplets would be relatively uniform whereas the HPEF formulations contains components such as ethanol and PEG400. As those components have varying rates of evaporation, the Sympatec® might measure different particles size, leading to a less uniform particle size distribution (Stein and Myrdal, 2006).

Effect of airflow rate on the particle size distribution of the HEF and HPEF formulations

The aerosolisation of smaller droplets at the higher flow rate can be explained by the fact that it might increase the level of turbulence in the spray. This would in turn increase the amount of energy available for evaporative mass transfer, resulting into finer particles. The evaporation of the droplets to form fine particles could explain the lower uniformity index observed at the higher flow rate. This phenomenon was negligible for the HPEF formulation; as HPEF droplets contain the viscous and non-volatile component PEG400, they might not be able to aerosolise in smaller droplets, even at an increased flow rate.

The effect of the flow rate on the particle size distribution is in agreement with Jones's findings. However, the increase in the D_{50} values obtained at the low flow rate in Jones's work was less significant than in the present work. This might be due to the fact that the difference between the high and low flow rates tested in Jones' work was only approximately $10\,L{\cdot}min^{-1}$ compared to $30\,L{\cdot}min^{-1}$ in this work.

Effect of actuation force on the particle size distribution of the HEF formulation

The fact that the manual actuations provided by a "healthy" female user led to the aerosolisation of coarser particles compared to the automated actuations is

similar to the NGI findings in Chapter 4. Manual and automated actuations have different characteristics such as the high velocity of the automated piston believed to lead to a faster opening of the metering valve. It was decided to investigate the characteristics of the manual and automated actuations in order to understand what might cause the differences in the aerosolisation process observed throughout this work.

Comparison of the NGI and the Sympatec® results

The D_{50} of 3.79 μm obtained with the Sympatec® for the HF formulation was higher than the MMAD of 2.09 μm obtained with the NGI in Chapter 4.

The D_{50} of 2.49 μm obtained with the Sympatec® for the HEF formulation was also higher than the MMAD of 0.74 μm obtained with the NGI.

The D_{50} of 4.14 μm obtained with the Sympatec® was however in line with the MMAD value of 4.16 μm obtained for the HPEF formulation with the NGI.

The Sympatec® overestimated the size of the particles issued from the two most evaporative formulations. This could be due to the fact that the Sympatec® measures the size of the entire droplets including volatile and semi-volatile components, whereas NGIs only assess the residual size of the particle. As a result, the Sympatec® measured the particles before the volatile components had time to fully evaporate. On the contrary, due to the presence of the viscous PEG400 in the HPEF formulation, HPEF particles might not further evaporate downstream of the Sympatec® measurement zone and might therefore retain their large size when being measured with the NGI.

To limit the overestimation of particles size in the Sympatec® measurements, the distance between the nozzle orifice and the measurement zone could be increased. Sympatec® has developed a simulation throat that can be placed between the

mouthpiece and the laser measurement zone. This would allow to measure the particle size distribution of a formulation as it enters the throat which would provide measurements comparable to the NGI.

The Malvern Spraytec® is able to measure sprays at different distances from the nozzle orifice. As the aim of this work was to understand the evolution of particles characteristics from the nozzle orifice to the throat of a potential user, the Malvern Spraytec® was used in the next series of experiments.

5.7.3 Malvern Spraytec® measurements of sprays issued from pMDIs

Particle size measurements at 4 cm and 7.5 cm from the nozzle orifice

In Stein and Myrdal's work, the size of the initial droplets was calculated based on the residual or intermediate droplets size with the help of Equations (5.5) and (5.6) developed for solution formulations (Stein and Myrdal, 2006), (Stein *et al.*, 2012).

$$MMD_{in} = MMD_{re} \frac{\rho_{in} C_{NV}}{\rho_{re}}^{\frac{-1}{3}} \tag{5.5}$$

$$MMD_{inter} = MMD_{in} \left(\frac{\rho_{in} \times (C_{NV} + C_{Cosol})}{\rho_{inter}} \right)^{\frac{1}{3}} \tag{5.6}$$

where MMD_{in}, MMD_{inter} and MMD_{re} are respectively the initial, intermediate and residual mass median diameters (MMDs) in μm, ρ_{in}, ρ_{inter} and ρ_{re} are respectively the densities of initial, intermediate and residual droplets in kg·m^{-3} and C_{NV} and C_{cosol} are respectively the percentages by weight of non-volatiles and cosolvents in the formulation.

As Equations (5.5) and (5.6) only take into account the rate of evaporation due

to the evaporative nature of a component and not the evaporation due to the turbulence of the flow, they represent only an approximation of initial droplet sizes. The aim of this work was to provide empirical data on the spray at several locations in its trajectory, which is the reason why the Malvern Spraytec® was used.

In the present work, the two solution formulations were tested using the same mouthpiece, which makes a direct comparison of those formulations possible. It can be seen in Table 5.4 that the HPEF formulation led to significantly higher D_{50} values than the HEF formulation for all experiments ($p<0.05$). This agrees with Equation (5.6), developed by Stein *et al*, which shows that the intermediate size of droplets increases at increasing non-volatiles concentrations (Stein and Myrdal, 2006), (Stein *et al.*, 2012).

The data in Table 5.4 were measured at a distance of 4 cm from the nozzle orifice and might not all be relevant due to their high standard deviations. This is in agreement with the findings of Moren and Hathaway who measured the particle size distribution of a commercial pMDI using laser holographic microscopy 3 cm downstream from the nozzle orifice (Dunbar, 1996). They measured a D_{50} of 36 μm and observed a large standard deviation. They attributed the large range of particle sizes to the fact that at a small distance from the nozzle orifice, some droplets containing multiple drug particles as well as large quantities of propellant and surfactant might have a significant effect on the D_{50}.

The high standard deviations in Table 5.4 could be attributed to the same reason. This would be particularly the case for the HF formulation being issued from the Flixotide® mouthpiece which has a higher nozzle orifice diameter than the Alvesco® mouthpiece used for the HEF and HPEF formulations and could therefore lead to the aerosolisation of bigger droplets near the nozzle orifice. This could

explain the significantly higher D_{90} of the HF formulation compared to the D_{90} of both solution formulations. This finding would tend to show that the diameter of the nozzle orifice has an impact on the initial particle size distribution of aerosols.

Errors in the D_{90} might also be due the variation of the refractive index in the aerosol cloud caused by the evaporation of the liquid phase, which erratically alters the path of the laser beams, particularly for measurements close to the nozzle orifice. This effect would be particularly pronounced for the HF formulation. As it is the most volatile formulation, it could have undergone a more intense flashing at the nozzle orifice during primary atomisation and a more intense evaporation during the secondary atomisation when the particles were measured.

This in line with the findings of Clark (1996) who observed beam steering effects and therefore did not use particle sizing results obtained closer than 5 cm from the nozzle orifice when using a Malvern 2600 laser diffraction sizer with a 100 mm focal length lens. Clark stated that measurements with a Malvern 2600 should only be conducted 8 cm to 24 cm from the nozzle orifice. It has been reported that the Malvern 2600 can give accurate measurements at transmissions of 2.5% compared to the Malvern Spraytec® which is said to be accurate at transmissions as low as 2%. This means that the Spraytec® can analyse sprays of higher concentration and can therefore measure particles closer to the nozzle orifice than the Malvern 2600 (Strakey, 2003).

Other errors could be due to the presence of irregular-shaped particles such as shear ribbons. The latter are droplets created during primary atomisation when the liquid phase covering the walls of the expansion chamber and nozzle orifice breaks up in ligaments before being aerosolised in droplets (Versteeg and Hargrave, 2002). The ligaments and ribbons can cause deviations in the scattering profiles recorded in the region near the nozzle orifice and may lead to errors in particle size

distributions (Haynes *et al.*, 2004).

The high variability of the measurements might also be caused by the high concentration of droplets so close from the nozzle orifice, which might have prevented accurate laser measurements (Wigley *et al.*, 2002). For this reason, the next set of measurements was realised at a distance of 7.5 cm from the nozzle orifice.

Table 5.4 and 5.5 show that particles measured 7.5 cm away from the nozzle orifice tend to be smaller than particles measured 4 cm from the nozzle orifice. This is expected, as the sprays should have evaporated more completely when measured further from the nozzle orifice. Liu *et al* (2012) observed a similar trend when measuring pMDIs sprays using PDA at 3 cm and 6 cm from the nozzle orifice. For all 9 pMDIs sprays measured, the droplets were smaller when the spray was measured at a distance of 6 cm from the nozzle orifice (Liu *et al.*, 2012).

Those results are also in line with the data obtained by Haynes *et al* (2004) with the Malvern Spraytec®. It was found that aerosols measured using a USP throat combined with a 20 cm extension contained smaller droplets compared to aerosols measured using solely a USP throat. Haynes *et al* attributed this change to a more complete evaporation of the spray when the extension was used.

The present work differed from Haynes *et al*'s work as the evolution of the droplets size from the extremity of the mouthpiece to a typical back of the throat distance was investigated. The size of particles potentially entering the throat of a user was therefore determined.

At 7.5 cm from the nozzle orifice, the D_{50} of the HEF solution at 20 °C was 7.83±0.19 μm when the pMDI was actuated manually. Haynes *et al* found a D_{50} of 3.64±0.12 μm when measuring a placebo formulation with HFA134a and 15% ethanol. The lower values of Haynes *et al* might be due to the fact that when con-

ducting the measurements, they used a USP throat in which the biggest particles impacted prior the Malvern Spraytec® measurements. In this work, however, the particles were measured directly after exiting the pMDI. The difference in the D_{50} agrees with the Malvern Mastersizer results of Ding *et al* (2000) who found that the size of particles issued from various CFC-based pMDI sprays decreased when using a USP throat compared to the measurements without a USP throat (Haynes *et al.*, 2004).

Clark (1996) was the first to measure experimentally the size of particles issued from pMDIs. After modifying a metering valve to obtain continuous sprays, he measured the size of particles issued from those sprays using a Malvern 2600 and found D_{50} values of 6.5 μm (for a pure CFC-12 formulation) and 9 μm (for a formulation containing 2% surfactant) at a distance of approximately 8 cm from the nozzle orifice. The present results follow the same trend as Clark's results as at a distance of 7.5 cm from the nozzle orifice, the HF formulation containing only drug and propellant had a D_{50} of 2.71 ± 0.22 μm compared to a D_{50} of 9.74 ± 0.29 μm for the HPEF formulation containing 5% of PEG400. The higher D_{50} of the HPEF formulation compared to the formulation with the highest surfactant concentration in Clark's work might be explained by the fact that the formulation in the present work contains 5% of non-volatiles compared to 2% in Clark's work. The lower D_{50} obtained for the HF formulation could be due to the fact that Clark used CFC-12 known to issue bigger particles than HFA134a (Smyth, 2003). It could also be due to the smaller nozzle orifice diameter used in the present work compared to Clark's work (i.e. 0.50 mm compared to 0.60 mm) (Clark, 1996).

Effect of actuation force on the particle size distribution of the three formulations

Table 5.5 showed that the change in the automated actuation forces did not affect the size of the particles. However, it can be noticed that at the higher actuation force, the standard deviation was smaller. This might be because the canister was not always properly actuated at 30 N as it represents the minimum force that could actuate the canister. This would mean that the deposition process was more repeatable at 50 N compared to 30 N. This was however not the case in Chapter 4, in which both automated actuations were associated with high standard deviations. However, the measurements are slightly different in this chapter; the NGI, an impaction device, tests the size as well as the velocity of the particles whereas the Malvern Spraytec® measures only particles size. This could mean that although the velocity was constant at both forces (resulting in similar deposition in the NGI), the size of the particles was less variable at the highest actuation force. This would agree with the PIV measurements in which a constant velocity was observed at the three actuation forces tested.

The manual actuation provided by a "healthy" female user led to the aerosolisation of coarser droplets compared to both automated actuations although the type of actuation had no significant effect on the suspension formulation ($p>0.05$). This is in agreement with the results obtained with the NGI shown in Figures 4.9 and 4.10 in Chapter 4, and with the Sympatec® in Figure 5.15.

The characteristics of the actuation stroke are believed to be responsible for the aerosolisation of sprays with different particle size distributions. This finding is of interest as it suggests that by actuating the spray in a different manner, the emitted particles could be smaller and the throat deposition could be decreased. Different types of automated and manual actuations should be analysed in order to identify

what led to the difference between the manual and the automated actuations.

Effect of temperature on the particle size distribution of the three formulations

The fact that the higher temperature led to a decrease of the particle sizes of both solution formulations is in line with the results of Polli *et al* (1969) that were shown in Chapter 3 and with the results of Haynes *et al* (2004).

Haynes and coworkers (2004) investigated the effects of temperature and non-volatiles concentration on the residual size of the droplets using a Malvern Spraytec®.

They found that equilibrating the Qvar 50 and Proventil HFA pMDIs at 40 °C and 55 °C led to a reduction of the D_{50} compared to when the formulations were maintained at room temperature.

As Haynes *et al* (2004) measured the effect of temperature on the size of particles which reached past a throat extension, they could not assess the potential effect of temperature on throat deposition itself. In this chapter, the effect of temperature on the size of particles was studied at the supposed throat location. As a result, the present work might be more informative on the potential amount of drug that could deposit in the throat.

The observed effect of temperature on particles size is also in line with the work of Pu *et al* (2011) using a Sympatec® discussed earlier in this chapter. They showed that the size of the particles issued from a pMDI decreased as the temperature increased from 15 °C to 30 °C when measured at 8 cm and 12 cm from the extremity of the mouthpiece (Pu *et al.*, 2011).

The change in temperature had no significant effect on the suspension formulation. This might be due to the fact that the HF, as the most volatile formulation, had

already completely evaporated at 7.5 cm from the nozzle orifice. The remaining particles measured would correspond to the micronised drug particles; the size of which is determined by the primary particles in the formulation and would therefore not be affected by temperature changes.

The 2.71±0.22 μm D_{50} of the suspension formulation was in the same range as the value of 2.76±0.03 μm obtained when the FP particles were measured by laser diffraction as described in Section 4.2.2 in Chapter 4 (Jaffari *et al.*, 2013). This would mean that at 7.5 cm from the nozzle orifice, the HFA134a in the suspension formulation had completely evaporated and the aerosol was composed solely of FP particles.

However, the initial MMD might be affected by temperature change at the nozzle orifice where the formulation has not yet evaporated. This was shown in the simulation which calculated a MMD of 85 μm at 293 K compared with 45 μm at 313 K at the nozzle orifice.

Duration of the sprays issued from the three formulations

The short duration of the suspension formulation compared to the two solution formulations in Table 5.6 can be explained by the nozzle orifice diameter of the Flixotide® mouthpiece. As it is more than twice the size of the nozzle orifice diameter of the Alvesco® mouthpiece used for the two solution formulations, the suspension formulation is discharged significantly faster than the other two formulations.

The simulation discharge time shown in Figure 3.4 is longer compared to the discharge of the suspension formulation obtained with the Malvern Spraytec®. This might be due to the fact that the metering valve had a volume of 63 μL in the simulation compared to 50 μL in the present chapter.

However, it is also a possibility that the Malvern Spraytec® might not be able to record all droplets from the most evaporative HF formulation, as they would evaporate faster than the two formulations containing semi-volatile or non-volatile components. This could also explain the difference in durations observed between the simulation developed in Chapter 3 and the durations shown in Table 5.6. The simulation duration of approximately 0.17 s is more in line with the duration of the two less evaporative HEF and HPEF formulations.

Dhand *et al* (1988) measured the duration of the sprays issued from four commercially available CFC-based pMDIs using high-speed photography. They found that the sprays lasted between 0.065 s and 0.095 s depending on the pMDI tested (Dunbar, 1996).

These short durations could be due to the fact that the camera used by Dhand *et al* (1988) might not be able to perceive the particles towards the end of the aerosolisation process at which point the aerosol would be almost completely evaporated. In comparison, the plumes measured in the current work corresponded to the time during which the sprays obscure more than 2% of the laser intensity.

Hochrainer *et al* (2005) found spray durations in the range of 0.15 s to 0.36 s depending on the type of pMDI studied using a video recording method. Gabrio found spray durations of between 0.16 s and 0.51 s when investigating several marketed pMDIs using a quick-response thermocouple (Gabrio *et al.*, 1999).

As the HPEF formulation is less evaporative than the HEF formulation, it could have obscured the laser path for a longer period, contributing to the significantly longer duration of the HPEF spray compared to the HEF spray ($p<0.05$). As the HEF formulation results in the aerosolisation of smaller droplets than the HPEF formulation and that smaller droplets do not always scatter a sufficient amount of light to be recognised as a valid signal, the HEF spray might not be properly

measured towards the end of the aerosolisation when particles reach small sizes (Liu *et al.*, 2012). This could also contribute to the smaller duration of the HEF formulation compared to the HPEF formulation.

5.7.4 Comparison of the measurements using the Sympatec®, Malvern Spraytec® and the Next Generation Impactor

Malvern Spraytec® is believed to overestimate the particle size distribution of HFA-based pMDIs (Haynes *et al.*, 2004). Haynes *et al* (2004) found that for a given formulation, the D_{50} (obtained from the Malvern Spraytec®) was significantly larger than the MMAD (obtained from the NGI).

This might be due to the fact that during the laser measurements, components less volatile than propellants such as ethanol are still evaporating (their evaporation could last approximately 2 s as suggested by Haynes *et al* (2004)). This results in the measurements of droplets bigger than the residual droplets measured with the NGI. This is in agreement with the results of this work. Table 5.7 compares the data obtained with the NGI in Chapter 4 with the data obtained with the Malvern Spraytec® and the Sympatec® for all formulations actuated by hand.

	HF	HEF	HPEF
	Mean ± SD	Mean ±SD	Mean± SD
Sympatec® - D_{50} (μm) 30 L·min^{-1} airflow, no throat	3.78±0.14	2.49±0.13	4.14±0.10
Malvern Spraytec® - D_{50} (μm) No airflow, no throat	2.71±0.22	7.83±0.19	9.74±0.29
NGI - MMAD (μm) 30 L·min^{-1} airflow, throat	2.09±0.07	1.29±0.22	4.16±0.19

Table 5.7: Summary of the D_{50} and MMAD obtained for the HF, HEF and HPEF formulations with manually actuated pMDIs - HF formulation aerosolised using the Flixotide® mouthpiece, HEF and HPEF formulations aerosolised using the Alvesco® mouthpiece. Mean of n≥3 determinations for each data.

The differences shown in Table 5.7 between the MMAD and the D_{50} values have also been reported by Smyth and Hickey (2003) when they compared D_{50} values obtained from a Malvern 2600 instrument with the MMAD values obtained with an ACI. They found that the MMAD values were several factors lower than the D_{50} values. This might be explained by the fact that they did not insert a throat between the nozzle orifice and the measurement zone when using the Malvern 2600. As a result the biggest particles in the spray were included in the Malvern particle size distribution.

When using a NGI, the biggest particles tend to deposit in the throat and this phenomenon is accentuated by the 30 L·min^{-1} entraining flow drawn through the apparatus. The particles depositing in the throat are not included in the calculation of the MMAD. The biggest particles than can enter the NGI apparatus and subsequently be included in the MMAD calculation have a diameter of 11.72 μm which corresponds to the cut-off diameter of the first stage of the NGI at 30 L·min^{-1} flow rate.

Although, the MMAD and the D_{50} obtained from the Malvern Spraytec® were comparable for the suspension formulation, the D_{50} was higher than the MMAD for both solution formulations. This could be due to the fact that at 7.5 cm away

from the nozzle orifice, which corresponds approximately to the distance to a user's throat, the particles issued from the less volatile formulations (both solution formulations) were not completely evaporated and thus had not yet reached their residual size.

The high particle size of both solution formulations obtained with the Malvern Spraytec® at 7.5 cm from the nozzle orifice could also be observed in the NGI experiments by considering the throat deposition associated with each formulation. The high particle size distribution and high momentum of particles issued from both solution formulations before entering the NGI was illustrated in Chapter 4 by their high throat deposition (77.04±3.17% for the HEF formulation and 86.38±1.02% for the HPEF formulation as shown in Table 4.8 in Chapter 4).

On the contrary, the particles issued from the suspension formulation were suspected to have completely evaporated and to have reached their residual size upon entering the laser measurement zone due to their higher vapour pressure. This is illustrated by the comparatively lower throat deposition of the HF formulation observed in the NGI experiments in Chapter 4 (38.69±2.50%), and by the resultant observation that the HF formulation had comparable MMAD and D_{50} values from the Malvern Spraytec®.

A closer agreement between those two techniques might be achieved if the evaporation of all volatile components of the spray is complete by the time the spray enters the laser measurement zone (Haynes *et al.*, 2004). However, the most crucial experimental set up to modify in order to obtain comparable sizes across the different techniques would be the use of a throat similar to the one used in the NGI measurements in both laser diffraction methods. The laser measurements would therefore only include the particles exiting the throat in the particle size distribution of the aerosol, as the NGI does.

Table 5.7 shows that the results obtained with the Sympatec® and the NGI were comparable. This could be due to the fact that a 30 L·min^{-1} flow rate was used in both methods whereas it was not used in the Malvern Spraytec®. As seen in Figure 5.11 in this chapter, a high flow rate could contribute to a more intense evaporation of particles. This is explained by the fact that a high flow rate provides a greater energy to the aerosol to evaporate during the secondary atomisation of the formulation. The presence of a flow rate in both the Sympatec® and the NGI could therefore contribute to the smaller particles sizes measured with those apparatus.

The highest D_{50} value measured by the Sympatec® for the suspension formulation might be due to the fact that it was measured closer to the nozzle orifice (6 cm) than in both the NGI and Malvern Spraytec® measurements. The suspension formulation was aerosolised with the Flixotide® mouthpiece which, with its large orifice diameter, could increase the initial particle size distribution of a formulation close to the nozzle orifice.

The oversizing of the particles using the laser diffraction methods might also be due to the fact that large particles always scatter a sufficient amount of light. On the contrary, smaller droplets might not always scatter a sufficient amount of light to be recognised as valid signals. This might result in a fraction of the smaller droplets in the spray not being taken into account in the assessment of the particle size distribution (Liu *et al.*, 2012).

Due to fundamental differences in the measuring principles behind each technique, it is not possible to directly compare the sizes of particles measured with the different methods. However, the particle sizes determined using all techniques are relevant and give different information which can be combined to assess the characteristics of the formulations over their entire aerosolisation process. The NGI provides information on the characteristics of the spray most likely to enter

the respiratory system based on both size and velocity of particles whereas the laser methods can give information on the size and velocity of particles at different times and locations in the aerosolisation process.

5.8 Piston behaviour in manual and automated actuation

In order to understand what caused the different aerosolisation patterns between the manual and automated actuations in the NGI, Malvern® and Sympatec® measurements, the velocity of the canister when actuated with the pneumatic piston and manually was studied throughout the actuation event. As in Chapter 3, the displacement of the pneumatic piston was measured using a linear variable differential transformer (LVDT) whose output was captured on a computer by means of a USB 6211 analog to digital converter (National Instrument, Berkshiron the spray as for all e, UK) at a sampling frequency of 1 kHz. The distance travelled by the stem when it was fully actuated was found to be approximately 3.5 mm which is in the same order of magnitude as the value of 5 mm found by Pu *et al* (2011) when using the Sprayer device from Sympatec® in their experiments. The actuations provided by the "healthy" female adult and by the automated piston are shown in Figure 5.16.

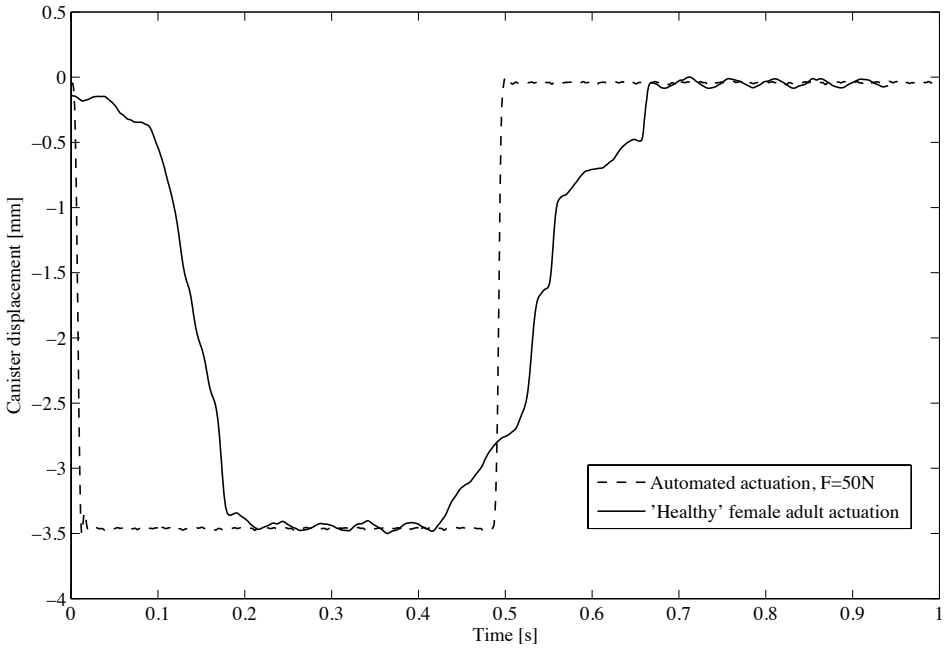

Figure 5.16: Displacement of the canister as a function of time during an automated actuation and a "healthy" female adult actuation.

Figure 5.16 shows that the automated actuation led to a faster displacement of the canister, translating into a faster opening of the metering valve compared to the actuation provided by the "healthy" adult female user. In Chapter 3, the period during which the valve remains fully open was assumed not to have an effect on the spray as for all actuations, the valve orifice remained open for a longer time than the entire aerosolisation duration. This is also the case in Figure 5.16 which shows that the automated actuation and the actuation provided by the female user have comparable durations that are both longer than the discharge of the formulation.

The velocity of the canister during its actuation was calculated for the 30 N, 50 N and manual actuations. The results can be seen in Table 5.8.

	30 N actuation	50 N actuation	"Healthy" female adult*	"Weak" inexperienced female adult*
Canister velocity ($m \cdot s^{-1}$)	0.17	0.28	0.023	0.0018

Table 5.8: Canister velocity during the 30 N, 50 N and manual actuations. Mean of n≥3 determinations for each actuation type. *both adults were part of the research team.

The automated actuation using a Sprayer device from Sympatec® in Pu *et al*'s work had a maximum velocity of $0.125\,m \cdot s^{-1}$ which is lower than the velocity of the automated actuations in this work but much higher than the velocity of both types of manual actuations (Pu *et al.*, 2011). In Liu *et al*'s work, the automated actuation was provided using the SprayVIEW MDx automated actuator (Proveris Scientific Corporation, Marlborough, MA). The piston had a velocity of $0.050\,m \cdot s^{-1}$, which is comparable, although still approximately twice the velocity of the actuation provided by the "healthy" female adult in the present work (Liu *et al.*, 2012).

Table 5.8 shows that both manual actuations led to significantly slower displacements of the canister than the 30 N and 50 N actuations, causing a slower opening of the valve orifice area ($p<0.05$). The difference was less pronounced between the two automated actuations although the 50 N force led to a significantly faster opening of the valve orifice area than the 30 N force ($p<0.05$).

This difference in canister velocity could be due to the fact that the component of the force along the axis of the canister might change during the manual actuation process. On the contrary, the automated actuations were provided by the pneumatic piston which was perfectly aligned with the axis of the canister during the entire duration of the actuation.

The faster opening of the pMDI valve with the automated actuations could lead to a greater discharge from the metering chamber into the expansion chamber earlier

in the aerosolisation process. As a result, the pressure build up in the expansion chamber might be greater, leading to a more intense flashing at the nozzle orifice and to the aerosolisation of smaller particles. This could be the reason for the lower throat deposition and smaller particle size observed with the automated actuations in the experiments throughout this work. Equation (2.53) presented in Chapter 2, indeed showed an inversely proportional relationship between the pressure build up in the expansion chamber and the size of the aerosolised droplets (Dunbar, 1996). Those experimental results are in line with the simulation results in which a higher valve opening rate led to the formation of smaller droplets at the nozzle orifice due to a higher pressure build up in the expansion chamber.

5.9 Summary

This chapter investigated the velocity and size of droplets issued from pMDIs when modifying several parameters such as formulation design, mouthpiece design, actuation force and temperature.

When comparing two formulations, the PIV measurements showed that the initial velocity was higher for the formulation with the highest vapour pressure.

The Malvern Spraytec® showed that the formulations with the lowest vapour pressures remained suspended in the air for a longer time.

Changes in formulations influenced the particle size distributions in measurements obtained with both laser diffraction instruments. The particle size distribution of the three formulations obtained using the Malvern Spraytec® and the Sympatec® were in the same order of magnitude as the NGI results obtained in Chapter 4 but could not be directly compared as each instrument measured the sprays using specific settings.

The Malvern Spraytec® measurements provided evidence that smaller nozzle orifices diameters lead to longer spray durations. This finding is of interest as a longer spray duration could help certain pMDI users synchronising the actuation of their device with their inhalation.

The effect of temperature on the size of the droplets was assessed using the Malvern Spraytec® and agrees with the simulation results in Chapter 3. The fact that higher temperatures might lead to smaller droplets being aerosolised is of foremost importance as users in different environments might not all benefit from the same device efficiency.

Measurements with both the Malvern Spraytec® and the Sympatec® showed that the type of actuation (manual versus automated) had an effect on the particle size distribution of the aerosols confirming the simulation and NGI results. This is explained by the fact that the valve opening rate was lower with the manual actuations compared with the automated actuations.

Chapter 6

Summary of thesis and conclusion

6.1 Findings of the present investigation

This thesis investigated the aerosolisation process of sprays issued from pMDIs. The initial, intermediate and residual properties of the droplets were determined using a simulation and several experimental methods. The aim of the thesis was to uncover factors that might influence the efficiency of pMDIs by studying their effect on the characteristics of the aerosolised sprays.

Although it is known that a significant fraction of the geriatric population has trouble to generate the minimum force to actuate their pMDIs correctly (Armitage and Williams, 1988), the effect of the actuation forces on device efficiency has to the best knowledge of the author received little study. It was therefore decided to investigate their effects on the valve orifice opening rate and ultimately on the properties of the aerosolised spray.

It was found that a "healthy" female adult actuation was associated with a fast displacement of the canister. This translated in a significantly faster opening rate

of the valve orifice (approximately ten times higher) than when a "weak" and inexperienced female research team member actuated the canister.

It was found that automated actuation forces led to a valve orifice opening rate significantly higher than the valve opening rate of the "healthy" female user. This is relevant as in some studies using automated actuations, the velocity of the canister was significantly higher than for both "healthy" and "weak" female adults. When conducting studies using automated actuations, scientists should be cautious to use canister displacement velocities that match those of real pMDI users. Although apparatus such as the SprayVIEW MDx automated actuator and Sprayer device from Sympatec® allowing modifications of the actuation characteristics, have been used in works such as Liu *et al*'s and Pu *et al*'s respectively, both works used highly different actuation profiles. This suggests a standardised method to optimally simulate user actuation has yet to be developed. A one-dimensional model was developed to study the properties of the spray at the nozzle orifice where experimental measurements are difficult to conduct. The exit velocity and mass median diameter (MMD) of the spray, the two factors most affecting the efficiency of pMDIs, were studied. When implementing the valve opening rate of a "healthy" female in the simulation, lower MMD values were obtained than at the lower rate of valve opening of the "weak" and inexperienced female user. This finding is critical as pMDI users with a lower actuation force such as geriatric or paediatric populations as well as users affected by arthritis might aerosolise sprays formed of bigger particles than healthy adults users, increasing drug deposition on the throat and therefore reducing their device efficiency.

An increase in temperature led to the formation of sprays of higher velocities with lower MMD values at the nozzle orifice and to a lower residual mass of the formulation in the metering chamber. The calculation of residual mass after each actuation was of interest as they might prevent pMDI users from getting accurate doses of

API at the target locations. This effect of temperature on the spray may be an issue as patients using their pMDIs in varying environments or in environments with high differences between outdoor and indoor temperatures might not benefit from the same device efficiency.

The computational model was modified in order to simulate the discharge of suspension formulations. The results were in line with the literature, which suggests that the simulation could be used to investigate suspension formulations.

In all the results obtained from the simulation, the main factor affecting the size and velocity of the droplets was the expansion chamber pressure which could be modified by manipulating the nozzle to valve orifice diameter ratio. Lower nozzle to valve orifice diameter ratios increased the expansion chamber pressure, therefore decreased the MMD values and increased the exit velocity of the spray. This is relevant as devices with varying valve to nozzle orifice diameter ratios could be designed to fit the needs of different types of users and environments in order to optimise the performance of pMDIs.

In this thesis, the effect of certain parameters on the spray characteristics could be assessed on the spray's entire trajectory using several experimental techniques. Laser techniques were used to measure the intermediate properties of the droplets while the NGI determined the residual size of the droplets. Both methods are important as they give information on the size the drug particles might have upon reaching the throat and the target site.

The effect of actuation forces reported in the simulation was also observed in the NGI experiments in which the automated actuations reduced the throat deposition compared to the manual actuation of the "healthy" female. This might be due to the fact that the automated actuation, with a significantly higher valve opening rate than the manual actuation, led to a higher pressure gradient at the nozzle

orifice, causing the aerosolisation of smaller particles.

A mouthpiece with a high nozzle orifice diameter and a short length led to an increased throat deposition for both solution formulations compared to a mouthpiece with a lower nozzle orifice diameter and longer length. This shows that varying the mouthpiece design could be used to obtain different spray deposition patterns. Longer mouthpieces could contribute to reduce the throat deposition. This is in line with the simulation results in which a smaller orifice diameter led to the aerosolisation of smaller droplets at the nozzle orifice.

When comparing three formulations, the formulation containing PEG400 was less affected by the different actuation forces. It might mean that formulations containing viscous and non-volatile components have a more stable aerosolisation process due to their lower evaporation rate and are less influenced by a change in experimental conditions such as the valve orifice opening rate.

After calculating the initial properties of the droplets by means of a computational simulation and measuring their residual properties with a NGI, the characteristics of the intermediate droplets were assessed using diverse laser methods. The velocities measured with the particle image velocimetry (PIV) were in line with the liquid phase velocities calculated in the simulation. The PIV work on several formulations showed that the pure propellant formulation had a faster initial velocity than the HPEF formulation, which can be explained by the lower vapour pressure of the latter.

In the Malvern Spraytec® measurements, it was found that increasing the temperature from 20 °C to 40 °C decreased the particle size distribution for the HEF and HPEF formulations which is in line with the simulation results in which the MMD values at the nozzle orifice decreased at higher temperatures. The Sympatec® and Malvern Spraytec® measurements concurred with the NGI results, revealing bigger

particles aerosolised with the HPEF formulation compared with the HF and HEF formulations.

The effect of the valve opening rate was similar with the Sympatec®, Malvern Spraytec®, NGI and simulation results. The Sympatec® measured bigger particles in the HEF formulation with the manual actuation of the "healthy" female compared to automated actuations. This coincides with the higher NGI throat deposition measurements obtained with the manual actuation; this is also in line with the high MMD values obtained at low valve orifice opening rates (such as those provided by manual actuations) in the simulation. When using the Malvern Spraytec®, the manual force with a low valve opening rate also tended to lead to the aerosolisation of bigger droplets compared to the automated actuations although the trend was weaker than with the NGI and the Sympatec® measurements.

It was found that, although giving results in the the same order of magnitude, the three particle sizing methods could not be directly compared as they each use different operating principles.

6.2 Recommendations for future work

The computational model has several limitations, including the assumption that the propellant vapour behaves as an idea gas in the expansion chamber. This might not be accurate as the pressure in the expansion chamber is relatively high and the vapour phase is not dry. The pressure in the expansion chamber could instead be measured using a pressure sensor. An empirical equation correlating the expansion chamber pressure to diverse parameters such as the nozzle orifice diameter to valve diameter ratio could be developed.

The residual mass of propellant in the metering chamber at the end of the simulated

formulation discharge was very high in the present work. This might be explained by the fact that the evaporation of the propellant due to heat transfer with the surroundings at the end of the discharge was not taken into account. In future works, the evaporation of the remaining propellant could be simulated. This would increase the pressure in the metering chamber, allowing a longer discharge of the formulation, which would in turn reduce the residual mass in the metering chamber.

In the simulation of suspension formulations, the equation used to calculate the MMD could be improved in order to take into account the size and agglomeration of particles in the formulation.

Although, the present model can take into account the presence of FP, it cannot simulate the discharge of formulations containing components that dissolve in HFA134a. This limitation is due to the fact that the model only uses the equations of state of pure HFA134a which could not be applied to mixtures of components dissolved in HFA134a. The model could therefore be improved to simulate the discharge of several types of formulations such as solution formulations.

In the current literature the velocities at the nozzle orifice obtained from models range from $19\,\mathrm{m{\cdot}s^{-1}}$ to $225\,\mathrm{m{\cdot}s^{-1}}$ (Ju *et al.*, 2010), (Dunbar, 1996). The velocity measurements inside or at the extremity of the mouthpiece are not reliable and values ranging from $60\,\mathrm{m{\cdot}s^{-1}}$ (Crosland *et al.*, 2009) to $90\,\mathrm{m{\cdot}s^{-1}}$ have been reported (Wigley *et al.*, 2002).

A computational fluid dynamics (CFD) model could be developed to give a more detailed analysis of the discharge through the device. It could be combined with the present model, using its outputs as boundary conditions, to simulate the flow between the nozzle orifice and the extremity of the mouthpiece where experimental measurements are difficult to conduct.

As actuation profiles and velocities of the valve opening have never been extensively investigated, it would be of interest to study the actuation profiles of several patient populations using a linear variable differential transformer (LVDT) in order to assess the variations in the actuation process according to the type of population studied. Automated actuations if used in *in vitro* studies could thus be set up to better mimic the hand actuation of diverse users.

The actuation of "weak" pMDI users should be studied to determine whether they can achieve a sufficient expansion chamber pressure to aerosolise the spray in fine particles and thus benefit from an optimal efficiency of their device.

The MMAD values commonly used in impaction works can sometimes be misleading as they only take into consideration the size of particles depositing within the NGI. It might thus be helpful to create another size parameter taking into account all droplets emitted from the device, as it would give a better insight on potential throat depositions. In order to compare the velocities of several formulations using PIV, a time-resolved analysis should be implemented as the time needed for the flow to reach its sonic regime varies with the vapour pressure of each formulation. The phase Doppler anemometry (PDA) technique could therefore be used. A larger measuring zone should be studied to capture the velocity profile of the spray upon reaching the patients' throat as this velocity represents one of the main factor determining the amount of drug depositing on the back of the throat. It would also be of interest to compare the manual and automated actuations using PIV to understand the role of the valve opening rate on the velocity of the aerosolised droplets.

A second camera would allow measurements of the size of droplets issued from the spray, using droplet imaging velocimeter and sizer (DIVAS). Those measurements would be of interest as they could provide information on the size of the droplets

from the extremity of the mouthpiece to the back of the throat. This method could validate the particle sizing results obtained with the NGI, the Sympatec® and the Malvern Spraytec®.

Finally, the Malvern Spraytec® and PIV measurements should be made with an accompanying co-current airflow to represent more realistically the conditions under which pMDIs are used instead of being conducted in quiescent air as was done in this work. Certain laser measurements apparatus such as the Malvern Spraytec® could also be used in combination with an impactor to combine information on the size of the particles during their trajectory with their deposition location.

6.3 Personal contribution to the field

This thesis provides an extensive range of experimental measurements, using and comparing results obtained from three particle sizing methods, including one impaction technique and two laser-based techniques. Those three methods have never been combined in a single piece of work. This thesis could therefore represents a good literature review for future studies on aerosol particle sizing.

To the best knowledge of the author, the simulation developed in Chapter 2 represents the first modelling work simulating the rate of opening of the valve orifice. The simulation was also modified to model the discharge of suspension formulations and could be further improved to model any formulation design, including solution formulations. This model also provides the boundary conditions required in computational fluid dynamics works modelling the behaviour of the aerosol near the nozzle orifice where experimental measurements are difficult to obtain.

The temperature at which the inhaler is kept and used was shown to influence the spray characteristics, with low temperatures leading to the aerosolisation of larger

droplets. Although, the effect of temperature was reported in the literature, it has not been previously incorporated into a model. The effect of temperature is not taken into account when prescribing inhalers in diverse environments although this work shows that pMDIs might need to be designed for a specific range of temperatures in order to maximise their performance.

This work has demonstrated that actuation forces might affect the size of the droplets aerosolised from a pMDI, with low actuation forces producing significantly larger droplets. This represents a novel and critical finding that needs to be considered, as weak patients might represent a large part of pMDI users and may not be able to benefit from an optimal device efficiency.

Those factors might not be critical for the delivery of drugs to the lungs. However, with pMDIs evolving towards the delivery of more expensive drugs with stronger side effects to the systemic circulation, the devices will need to deliver drugs more accurately in order to limit the risk of side effects and reduce the cost of therapy. Appropriate forces of actuation and temperature ranges might help pMDI drug delivery to be more reliable and accurate and therefore need to be investigated further.

The effect of different formulations and device parameters were investigated computationally and experimentally. To the best knowledge of the author, the effect of several types of cosolvents had never been previously studied while keeping the other formulation components at constant concentrations. It was seen that each excipient produced aerosols with different characteristics. As a result, different formulation designs might be used to improve aerosol properties according to the temperature at which it is used and the actuation force of the user.

The effect of device design on the spray characteristics was also studied. The role of the valve opening rate, investigated for the first time in this work, and the ratio

of the nozzle to valve orifice diameter affect the size distribution of the aerosol through the modification of the pressure gradients across both orifices. As a result, it is thought that device designs could also be manipulated in order to yield certain spray properties for specific types of users under different environmental conditions.

In conclusion, this thesis has investigated the applicability of a new computational approach which can successfully predict the aerosolisation performance of pMDIs. This represents a potentially successful tool for widespread application to aid in silico formulation and device engineering. One particularly novel aspect has been the incorporation of patient use factors, in term of device handling competencies.

References

Aamir, M. A. and Watkins, A. P. Numerical analysis of highly pressurised liquid propane. *International Journal of Heat and Fluid Flow*, **21**:420–431 (2000).

Adrian, R. J. Particle-imaging techniques for experimental fluid mechanics. *Annual Reviews of Fluid Mechanics*, **23**:261–304 (1991).

Agnew, J. E. *Physical properties and mechanisms of deposition of aerosols* (1984).

Ali, M. *Physical and computational models of human lung for optimizing respiratory drug delivery*. Ph.D. thesis, Donaghey College of Engineering and Information Technology (2008).

Andersen, S., Cermak, R., Clodic, D., Hickman, K., Keller, F., Koehler, J., McInerney, E., Pearson, A., Tope, H. and Yamabe, M. Technology and Economic Assessment Panel (2010).

Anderson, P. J. History of aerosol therapy: Liquid nebulization to MDIs to DPIs. *Respiratory Care*, **50**(9):1139–1150 (2005).

Armitage, J. M. and Williams, S. J. Inhaler technique in the elderly. *Age and Ageing*, **17**:275–278 (1988).

Ash, M. and Ash, I. *Handbook of preservatives*. Synapse Information Resources Inc., New York (2004).

Ashworth, H. L., Wilson, C. G., Sims, E. E., Wotton, P. K. and Hardy, J. G. Delivery of propellant soluble drug from a metered dose inhaler. *Thorax*, **46**:245–247 (1991).

AstraZeneca. Annual report. Technical report, AstraZeneca (2011).

Bar-Kohany, T. and Sher, E. Effervescent atomization under sub-sonic and choked conditions - a theoretical approach. *Chemical Engineering Science*, **59**:5987–5995 (2004).

Barnes, P. J. and Godfrey, S. *Asthma Therapy*. M. Dunitz, The Livery House, 7-9 Pratt Street, London NW1 (1998).

Bastiaans, R. J. M. Cross-correlation PIV; theory, implementation and accuracy. Technical report, Eindhoven University of Technology (2000).

Bateman, E. and Fitzgerald, M. Global strategy for asthma management and prevention. Technical report, Global Initiative for Asthma (2011).

Battagel, J. M., Johal, A., Smith, A. and Kotecha, B. Postural variation in oropharyngeal dimensions in subjects with sleep disordered breathing: A cephalometric study. *European Journal of Orthodontics*, **24**:263–276 (2002).

BBC Research. Global market for pulmonary drug delivery. Technical report, BBC research (2012).

Berlin, C. M. and McCarver, D. G. "Inactive" ingredients in pharmaceutical products. *Pediatrics*, **99**(2):267–278 (1997).

Berry, J., Heimbecher, S., Hart, J. L. and Sequeira, J. Influence of the metering chamber volume and actuator design on the aerodynamic particle size of a metered dose inhaler. *Drug Development and Industrial Pharmacy*, **29**(8):865–876 (2003).

Beychok, M. R. Calculating accidental release flow rates from pressurized gas systems. *Air Dispersion* (1998).

Bisgaard, H., Klug, B., Sumby, B. S. and Burnell, P. K. P. Fine particle mass from the Diskus inhaler and Turbuhaler inhaler in children with asthma. *European Respiratory Journal*, **11**:1111–1115 (1998).

Braman, S. S. Chronic cough due to chronic bronchitis: ACCP evidence-based clinical practice guidelines. *Chest*, **129**(1):104–115 (2006).

Brambilla, G., Ganderton, D., Garzia, R., Lewis, D., Meakin, B. and Ventura, P. Modulation of aerosol clouds produced by pressurised inhalation aerosols. *International Journal of Pharmaceutics*, **186**:53–61 (1999).

Brennen, C. E. Bubble growth and collapse. Technical report, Caltech University (2005).

Buhl, R. Local oropharyngeal side effects of inhaled corticosteroids in patients with asthma. *Allergy*, **61**:518–526 (2006).

Burnell, P. K. P., Small, T., Doig, S., Johal, B., Jenkins, R. and Gibson, G. J. *Ex-vivo* product performance of Diskus and Turbuhaler inhalers using inhalation profiles from patients with severe chronic obstructive pulmonary diseases. *Respiratory Medicine*, **95**:324–330 (2001).

Cassell, J. Education is the key to success in the nebulisers market (2012).

Chan, H. K., Young, P. M., Traini, D. and Coates, M. Dry powder inhalers: Challenges and goals for next generation therapies. *Pharmaceutical Technology Europe*, **19**(4):19–26 (2007).

chemicalbook.com. Fluticasone propionate (80474-14-2) (2008).

Clark, A. R. *Metered atomisation for respiratory drug delivery*. Ph.D. thesis, Loughbourough University, UK (1991).

Clark, A. R. Medical aerosol inhalers-past, present, and future. *Aerosol Science and Technology*, **22**(4):374–391 (1995).

Clark, A. R. MDIs: Physics of aerosol formation. *Journal of Aerosol Medecine*, **9**(S1):19–26 (1996).

Clark, M. *Transport modelling for environmental engineers and scientists*. 469. John Wiley and Sons, New Jersey, second edition (2009).

Clarke, S. W. and Newman, S. P. Therapeutic aerosols. 2. drugs available by the inhaled route. *Thorax*, **39**(1):1–7 (1984).

Clarke, S. W. and Pavia, D. Lung mucus production and mucociliary clearance - methods of assessment. *British Journal of Clinical Pharmacology*, **9**(6):537–546 (1980).

Clayborough, R. and Simpson, I. DPI Technologies: Time for a rethink. Technical report, Sagentia (2010).

Copley. Quality solutions for inhaler testing. Technical report, Copley Scientific, Nottingham, NG4 2JY, United Kingdom (2012).

Copley, M. The complexities of DPI testing. *Manufacturing Chemist*, pp. 45–47 (2009).

Covar, R. A. and Gelfand, E. W. Pressurized metered-dose inhalers versus dry-powder inhalers, advantages and disadvantages (2008).

Cripps, A., Riebe, M., Schulze, M. and Woodhouse, R. Pharmaceutical transition to non-CFC pressurized metered dose inhalers. *Respiratory Medicine*, **94**:S3–S9 (2000).

Crosland, B. M., Johnson, M. R. and Matida, E. A. Characterization of the spray velocities from a pressurized metered-dose inhaler. *Journal of aerosol Medicine and Pulmonary Drug Delivery*, **22**(2):85–97 (2009).

Cumming, B. Human anatomy and physiology (2001).

Devenport, W. J. Laser Doppler anemometry (2006).

Dhand, R. New nebuliser technology – aerosol generation by using a vibrating mesh or plate with multiple apertures (2003).

Dolovich, M. Measurement of particle-size characteristics of metered dose inhaler (MDI) aerosols. *Journal of Aerosol Medecine-Deposition Clearance and Effects in the Lung*, **4**(3):251–263 (1991).

drugs.com. Albuterol (2009).

Dunbar, C. A. *An experimental investigation of the spray issued from a pMDI*. Ph.D. thesis, Manchester, UK (1996).

Dunbar, C. A. Atomization mechanisms of the pressurized metered dose inhalers. *Particulate science and technology*, **15**(3):195–216 (1997).

Dunbar, C. A., Watkins, A. P. and Miller, J. F. *Theoretical investigation of the spray from a pressurized metered-dose inhaler*, volume 7. Begell House, Redding CT (1997).

Dupont. Thermodynamic properties of hfc-134a. Technical report, Dupont Suva, Geneva, Switzerland (2004).

Ehtezazi, T., Saleem, I., Shrubb, I., Allanson, D. R., Jenkinson, I. D. and O'Callaghan, C. The interaction between the oropharyngeal geometry and aerosols via pressurised metered dose inhalers. *Pharmaceutical Research*, **27**(1):175–186 (2010).

Elias, E. and Lellouche, G. S. Two-phase critical flow. *International Journal of Multiphase Flow*, **20**:91–168 (1994).

Fadl, A., Wang, J. and Zhang, Z. Metered-dose inhaler efficiency enhancement: A case study and novel design. *Inhalation Technology*, **22**(7):601–609 (2010).

Fadl, A., Wang, J., Zhang, Z. and Cheng, Y. S. Effects of MDI spray angle on aerosol penetration efficiency through an oral airway cast. *Journal of Aerosol Science*, **38**(8):853–864 (2007).

Feddah, M. R., Brown, K. F., Gipps, E. M. and Davies, N. M. *In-vitro* characterisation of metered dose inhaler versus dry powder inhaler glucocorticoid products: Influence of inspiratory flow rates. *Journal of Pharmaceutical Sciences*, **3**(3):317–324 (2000).

Ferron, G. A. Aerosol properties and lung deposition. *European Respiratory Journal*, **7**(8):1392–1394 (1994).

Fincham, A. M. and Spedding, G. R. Low cost, high resolution DPIV for measurement of turbulent fluid flow. *Experiments in Fluid*, **23**:449–462 (1997).

Fink, J. B. Metered-dose inhalers, dry powder inhalers , and transitions. *Respiratory Care*, **45**(6):623–635 (2000).

Finlay, W. H. *The mechanics of inhaled pharmaceutical aerosols*. Academic Press, Harcourt Place, 32 Jamestown Road, London NW1 7BY,UK (2001).

Fradley, G. Fifty years of the pressurised metered dose inhaler - building on a golden heritage. Technical report, 3M Drug Delivery Systems, Loughborough, UK (2006).

Furness, G. Innovative technologies breathing new life into inhalable therapeutics. ondrugdelivery.com (2006).

Gabrio, B. J., Stein, S. W. and Velasquez, D. J. A new method to evaluate plume characteristics of hydrofluoroalkane and chlorofluorocarbon metered dose inhalers. *International Journal of Pharmaceutics*, **186**:3–12 (1999).

Ganderton, D., Lewis, D., Davies, R., Meakin, B. and Church, T. The formulation and evaluation of a CFC-free budesonide pressurised metered dose inhaler. *Respiratory Medicine*, **97**(Suppl. D):S4–S9 (2003).

Gharib, M., Pereira, F., Dabiri, D., Hove, J. R. and Modarress, D. Quantitative flow visualization: Toward a comprehensive flow diagnostic tool. *Integr. Comp. Biol.*, **42**:964–970 (2002).

Global initiative for chronic obstructive lung diseases. Technical report (2011).

Gorokhovski, M. and Herrmann, M. Modeling primary atomization. *Annual Reviews of Fluid Mechanics*, **40**:343–366 (2008).

Gray, S. L., Williams, D. M., Pulliam, C. C., Sirgo, M. A., Bishop, A. L. and Donohue, J. F. Characteristics predicting incorrect metered-dose inhaler technique in older subjects. *Archives of Internal Medicine*, **156**(9):984 (1996).

Gupta, A., Stein, S. W. and Myrdal, P. B. Balancing ethanol cosolvent concentration with product performance in 134-a based pressurized metered dose inhalers. *Journal of Aerosol Medecine Deposition Clearance and Effects in the Lung*, **16**(2):167–174 (2003).

Han, R., Papadopoulos, G. and Greenspan, B. Flow field measurement inside the mouthpiece of the spiros inhaler using particle image velocimetry. *Aerosol Science and Technology*, **36**:329–341 (2002).

Hanna, M. and York, P. Salmeterol xinafoate with controlled particle size. Technical report, Glaxo Group Limited (1998).

Haynes, A., Shaik, M. S. and Singh, M. Evaluation of the Malvern Spraytec with inhalation cell for the measurement of particle size distribution from metered dose inhalers. *Journal of Pharmaceutical Sciences*, **93**(2):349–363 (2004).

Heyder, J. Deposition of inhaled particles in the human respiratory tract and consequences for regional targeting in respiratory drug delivery. *Proceedings of the American Thoracic Society*, **1**:315–320 (2004).

Hickey, A. J. *Pharmaceutical inhalation aerosol technology*, volume 134. Marcel Dekker, USA, second edition (2004).

Hochrainer, D., Holz, H., Kreher, C., Scaffidi, L., Spallek, M. and Wachtel, H. Comparison of the aerosol velocity and spray duration of Respimat Soft Mist and pressurized metered dose inhalers. *Journal of Aerosol Medecine*, **18**(3):273–282 (2005).

Huang, H., Dabiri, D. and Gharib, M. On errors of digital particle image velocimetry. *Measurement Science and Technology*, **8**:1427–1440 (1997).

ICH. Validation of analytical procedures: Text and methodology. International Conference of Harmonisation of Technical Requirements for Registration of Pharmaceuticals for Human Use (2005).

Ingenito, E. P., Evans, R. B., Loring, S. H., Kaczka, D. W., Rodenhouse, J. D., Body, S. C., Sugarbaker, D. J., Mentzer, S. J., DeCamp, M. M. and Reilly, J. J. Relation between preoperative inspiratory lung resistance and the outcome of lung-volume-reduction surgery for emphysema. *New England Journal of Medecine*, **338**(17):1181–1185 (1998).

Inhalation Report. Battle of the MDI and DPI patent trends (2009).

Inthavong, K., Tu, J., Ye, Y., Ding, S., Subic, A. and Thien, F. Effects of airway

obstruction induced by asthma attack on particle deposition. *Journal of Aerosol Science*, **41**:587–601 (2010).

Irwin, R. S. and Rippe, J. M. *Intensive care medecine*. Wolters Kluwer Health, sixth edition (2008).

Jaffari, S., Forbes, B., Collins, E., Barlow, D. J., Martin, G. P. and Murnane, D. Rapid characterisation of the inherent dispersibility of respirable powders using dry dispersion laser diffraction. *International Journal of Pharmaceutics*, **447**(1–2):124–131 (2013).

Jahanmiri, M. Particle image velocimetry: Fundamentals and its applications. Technical report, Chalmers University of Technology, Goeteborg, Sweden (2011).

Jayaraju, S. T., Brouns, M., Lacor, C., Belkassem, B. and Verbanck, S. Large eddy and detached eddy simulations of fluid flow particle deposition in a human mouth-throat. *Journal of Aerosol Science*, **39**:862–875 (2008).

Jones, S. A., Martin, G. P. and Brown, M. B. High-pressure aerosol suspension-a novel laser diffraction particle sizing system for hydrofluoroalkane pressurised metered dose inhalers. *International Journal of Pharmaceutics*, **302**:154–165 (2005).

Ju, D., Shrimpton, J., Bowdrey, M. and Hearn, A. Effect of expansion chamber geometry on atomization and spray dispersion characters of a flashing mixture containing inerts. Part 1. Numerical predictions and dual laser measurements. *International Journal of Pharmaceutics*, pp. 23–31 (2012).

Ju, D., Shrimpton, J. and Hearn, A. The effect of reduction of propellant mass fraction on the injection profile of metered dose inhalers. *International Journal of Pharmaceutics*, **391**:221–229 (2010).

Keller, M. Innovations and perspectives of metered dose inhalers in pulmonary drug delivery. *International Journal of Pharmaceutics*, **186**(1):81–90 (1999).

Kim, J. E. and Park, W. K. Determination of the proper size of oropharyngeal airway: Correlation with external body measurements. *European Journal of Anaesthesiology*, **28**:228 (2011).

Klea134a. Thermodynamic property data (2011).

Kleinstreuer, C., Shi, H. and Zhang, Z. Computational analyses of a pressurized metered dose inhaler and a new drug-aerosol targeting methodology. *Journal of Aerosol Medecine*, **20**(3):294–309 (2007).

Kleinstreuer, C. and Zhang, Z. Optimal drug-aerosol delivery to predetermined lung sites. *Journal of Heat Transfer*, **133**(1):1–12 (2011).

Kleinstreuer, C., Zhang, Z. and Donohue, J. F. Targeted drug-aerosol delivery in the human respiratory system. *Annual Reviews of Biomedical Engineering*, **10**:195–220 (2008).

Labiris, N. R. and Dolovich, M. B. Pulmonary drug delivery. Part 1: Physiological factors affecting therapeutic effectiveness of aerosolized medications. *Journal of Clinical Pharmacology*, **56**:588–599 (2003).

Lambert, A. R., Shaughnessy, P. O., Tawhai, M. H., Hoffman, E. A. and Lin, C. Regional deposition of particles in an image-based airway model: Large-eddy simulation and left-right lung ventilation asymmetry. *Aerosol Science and Technology*, **45**(1):11–25 (2011).

Laube, B. L. The expanding role of aerosols in systemic drug delivery, gene therapy, and vaccination. *Respir Care*, **50**(9):1161–1174 (2005).

Leach, C. L. Approaches and challenges to use Freon propellants replacements. *Aerosol Science and Technology*, **22**(4):328–334 (1995).

Leach, C. L. The CFC to HFA transition and its impact on pulmonary drug development. *Respir Care*, **50**(9):1201–1206 (2005).

Leach, C. L., Davidson, P. J., Hasselquist, B. E. and Boudreau, R. J. Lung deposition of hydrofluoroalkane-134a beclamethasone is greater than that of chrofluorocarbon fluticasone and chlorofluorocarbon beclomethasone. *Chest*, **122**(2):510–516 (2002).

Lee, K. C., Suen, K. O. and Yianneskis, M. Characterisation of evaporating sprays from metered-dose inhalers by LDA. In Dybbs, A. and Ghorashy, B., editors, *Laser Doppler Anemometry—Advances and Applications 1991*, volume 2, pp. 563–570. New York (1991).

Lee, S. L. Scientific and regulatory considerations for bioequivalence (BE) of dry powder inhalers (DPIs). GPha/FDA Fall Technical Conference, US Food and Drug Administration (2011).

Lewis, D. Metered-dose inhalers: Actuators old and new. *Expert Opinion Drug Delivery*, **4**(3):235–245 (2007).

Lipworth, B. J. Systemic adverse effects of inhaled corticosteroid therapy. *Archives of Internal Medicine*, **159**:941–955 (1999).

Liu, X., Doub, W. H. and Guo, C. Evaluation of metered dose inhaler spray velocities using phase Doppler anemometry (PDA). *International Journal of Pharmaceutics*, **423**:235–239 (2012).

Loh, L. C., Teng, C. L., Teh, P. N., Koh, C. N., Vijayasingham, P. and Thayaparan, T. Metered-dose inhaler technique in asthmatic patients. *Med J Malaysia*, **59**(3):335–341 (2004).

Luo, H. Y., Liu, Y. and Yang, X. L. Particle deposition in obstructed airways. *Journal of biomechanics*, **40**:3096–3104 (2007).

Lyons, H. A. and Tanner, R. W. Total lung volume and its subdivisions in children: Normal standards. *Journal of Applied Physiology*, **17**(4):601–604 (1962).

MacMichael, D. B. A. and Hearne, D. J. Us patents 6405727 and international patent WO 0193933 (2002).

malvern.com. Measuring sprays containing propellants or volatile components. malvern.com (2007).

malvern.com (2012).

Mannkind Corporation. Product pipeline. mannkindcorp.com (2013).

Marshall, H. How to use your metered dose inhaler (2010).

Merck. Proventil® HFA (albuterol sulfate) inhalation aerosol. merck.com (2012).

Michael, Y., Snowden, M. J., Chowdhry, B. Z., Ashurst, I. C., Davies-Cutting, C. J. and Riley, T. Characterisation of the aggregation behaviour in a salmeterol and fluticasone propionate inhalation aerosol system. *International Journal of Pharmaceutics*, **221**:165–174 (2001).

Milner, A. D. Bronchodilator drugs in childhood asthma. *Archives of Disease in Childhood*, **56**:84–85 (1981).

Mitchell, J. P. and Nagel, M. W. Particle size analysis of aerosols from medicinal inhalers. *Kona*, **22**:32–65 (2004).

Mitchell, J. P., Nagel, M. W., Nichols, S. and Nerbrink, O. Laser diffractometry as a technique for the rapid assessment of aerosol particle size from inhalers. *Journal of Aerosol Medecine*, **19**(4):409–433 (2006).

Mitchell, J. P., Nagel, M. W., Wiersema, K. J. and Doyle, C. C. Aerodynamic particle size analysis of aerosols from pressurised metered dose inhalers: Comparison

of Anderson 8-stage cascade impactor, next generation pharmaceutical impactor, and model 3321 Aerodynamic Particle Sizer aerosol spectrometer. *AAPS PharmSciTech*, **4**(4):1–9 (2003).

van der Molen, T., Foster, J. M., Caeser, M., Mueller, T. and Postma, D. S. Difference between patient-reported side effects of ciclesonide versus fluticasone propionate. *Respiratory Medicine*, **104**:1825–1833 (2010).

Morén, F. and Andersson, J. Fraction of dose exhaled after administration of pressurized inhalation aerosols. *International Journal of Pharmaceutics*, **6**:295–300 (1980).

Muramatsu, K., Yukitake, K., Nakamura, M., Matsumoto, I. and Motohiro, Y. Monitoring of nonlinear respiratory elastance using a multiple linear regression analysis. *European Respiratory Journal*, **17**:1158–1166 (2001).

Murnane, D., Martin, G. P. and Marriott, C. Investigations into the formulation of metered dose inhalers of salmeterol xinafoate and fluticasone propionate microcrystals. *Pharmaceutical Research*, **25**(10):2283–2291 (2008).

Newman, S. P. Aerosol deposition considerations in inhalation therapy. *Chest*, **88**(2):152S–160S (1985).

Newman, S. P. Principles of metered-dose inhaler design. *Respir Care*, **50**(9):1177–1190 (2005).

Newman, S. P. and Busse, W. W. Evolution of dry powder inhaler design, formulation, and performance. *Respiratory Medicine*, **96**:293–304 (2002).

Newman, S. P., Morén, F., Pavia, D., Corrado, O. and Clarke, S. W. The effects of changes in metered volume and propellant vapour pressure on the deposition of pressurized inhalation aerosols. *International Journal of Pharmaceutics*, **11**:337–344 (1982).

O'Brien, J. M. Airflow, lung volumes, and flow-volume loop (2012).

Ochs, M., Nyengaard, L. R., Lung, A., Knudsen, L., Voigt, M., Wahlers, T., Richter, J. and Gundersen, H. J. G. The number of alveoli in the human lung. *American Journal of Respiratory and Critical Care Medicine*, **169**(1):120–124 (2004).

O'Donnell, D. E. and Laveneziana, P. Physiology and consequences of lung hyperinflation in COPD. *European Respiratory Review*, **15**(100):61–67 (2006).

Oliveira, R. F., Teixeira, S., Silva, L. F., Teixeira, J. C. and Antunes, H. Study of a pressurized metered-dose inhaler spray parameters in Fluent. *Proceedings of the World Congress on Engineering*, **2** (2010).

Oliveira, R. F., Teixeira, S., Teixeira, J. C., Silva, L. F. and Antunes, H. *PMDI sprays: Theory, experiment and numerical simulation*. InTech - Open Science (2012).

O'Riordan, T. G. Formulations and nebulizer performance. *Respiratory Care*, **47**(11):1305–1312 (2002).

Pilcer, G., Vanderbist, F. and Amighi, K. Correlations between cascade impactor analysis and laser diffraction techniques for the determination of the particle size of aerosolised powder formulations. *International Journal of Pharmaceutics*, **358**:75–81 (2008).

Polli, G. P., Grim, W. M., Bacher, F. A. and Yunker, M. H. Influence of formulation on aerosol particle size. *Journal of Pharmaceutical Sciences*, **58**(4):484–486 (1969).

Prasad, A. K. Particle image velocimetry. *Current Science*, **79**(1):51–60 (2000).

Pu, Y., Kline, L. C. and Berry, J. The application of "in-flight" laser diffraction to the particle size characterization of a model suspension metered dose inhaler. *Drug Development and Industrial Pharmacy*, **37**(5):552–558 (2011).

Purewal, T. S. *Metered Dose Inhaler Technology*. CRC Press LLC, Florida (1997).

Pust, O. PIV: Direct cross-correlation compared with FFT-based cross-correlation. Lisbon (2000).

Rogers, G. F. C. and Mayhew, Y. R. *Thermodynamic and Transport Properties of Fluid*. Blackwell, Oxford, UK, fifth edition (1995).

Rubin, B. K. Physiology of airway mucus clearance. *Respir Care*, **47**(7):761–768 (2002).

Rubin, B. K. and Fink, J. B. The delivery of inhaled medication to the young child. *Pediatric Clinics of North America*, pp. 717–731 (2003).

Saleem, I. and Smyth, H. Influence of surfactant (pluronic L81) and cosolvent ethanol on their ability to modulate particle size distribution and lung deposition of pressurised metered dose inhalers. *Journal of Pharmacy and Pharmacology*, **61**(Suppl. 1):A119–A120 (2009).

Sanders, M. Inhalation therapy: An historical review. *Primary Care Respiratory Journal*, **16**(2):71–81 (2007).

Sanders, P. A. *Valves and actuators*. Van Nostrand Reinhold Co., USA (1979).

Schayck, C. P. V. and Donnell, D. The efficacy and safety of QVAR (hydrofluoroalkane-beclometasone diproprionate extrafine aerosol) in asthma (part 2): Clinical experience in children. *International Journal of Clinical Practice*, **58**(8):786–794 (2004).

Schuepp, K. G., Straub, D., Moller, A. and Wildhaber, J. H. Deposition of aerosols in infants and children. *Journal of Aerosol Medecine-Deposition Clearance and Effects in the Lung*, **17**(2):153–156 (2004).

Serras-Pereira, J., van Romunde, Z., Aleiferis, P. G., Richardson, D., Wallace, S. and Cracknell, R. F. Cavitation, primary break-up and flash boiling of gasoline, iso-octane and n-pentane with a real-size optical direct-injection nozzle. *Fuel*, **89**:2592–2607 (2010).

Shaik, A. Q. *Numerical modeling of two-phase flashing propellant flow inside the twin-orifice system of pressurised metered dose inhalers (pMDIs)*. Ph.D. thesis, Loughborough University, Loughborough, UK (2009).

Shaik, A. Q. and Versteeg, H. K. Model for the prediction of internal flow conditions in pressurised metered dose inhalers (pMDIs) (2008).

Sheffer, A. L. Partners® Healthcare – Asthma center grand rounds. asthma.partners.org (2005).

Sher, E., Bar-Kohany, T. and Rashkovan, A. Flash-boiling atomization. *Progress in Energy and Combustion Science*, **34**:417–439 (2008).

Siekmeier, R. and Scheuch, G. Systemic treatment by inhalation of macromolecules - principles, problems and examples. *Journal of Physiology and Pharmacology*, **59**(Part 1 Suppl. 6):53–79 (2008).

Smaldone, G. C., Foster, W. M., O'Riordan, T. G., Messina, M. S., Perry, R. J. and Langenback, E. G. Regional impairment of mucociliary clearance in chronic obstructive pulmonary disease. *Chest*, **103**:1390–1396 (1993).

Smyth, H. *Excipient Development for Pharmaceutical, Biotechnology, and Drug Delivery Systems*. Informa Healthcare (2006).

Smyth, H. D. C. The influence of formulation variables on the performance of alternative propellant-driven metered dose inhalers. *Aerosol Delivery and Asthma Therapy*, **55**(7):807–828 (2003).

Smyth, H. D. C. and Hickey, A. J. *Controlled Pulmonary Drug Delivery*. Springer (2011).

Solvay. Solkane 227 pharma and Solkane 134a pharma. Technical report, Solvay Fluor, Hannover, Deutschland (2008).

Stein, S. W. and Myrdal, P. B. A theoretical and experimental analysis of formulation and device parameters affecting solution MDI size distributions. *Journal of Pharmaceutical Sciences*, **93**(8):2158–2175 (2004).

Stein, S. W. and Myrdal, P. B. The relative influence of atomization and evaporation on metered dose inhaler drug delivery efficiency. *Aerosol Science and Technology*, **40**(5):335–347 (2006).

Stein, S. W., Sheth, P. and Myrdal, P. B. A model for predicting size distributions delivered from pMDIs with suspended drug. *International Journal of Pharmaceutics*, **422**:101–115 (2012).

Stone, J. A. and Zimmerman, J. H. Index of refraction of air (2011).

Storey, R. and Ymén, I. *Solid State Characterization of Pharmaceuticals*. 418–419. John Wiley and Sons (2011).

Strakey, P. A. Assessment of multiple scattering errors of laser diffraction instruments. Technical report, Air Force Research Laboratory, CA (2003).

Sveum, R., Bergstrom, J., Brottman, G., Hanson, M., Heiman, M., Johns, K., Malkiewicz, J., Manney, S., Moyer, L., Myers, C., Myers, N., O'Brien, M., Rethwill, M., Schaefer, K. and Uden, D. Diagnosis and management of asthma. *Insitute for Clinical Systems Improvement.*, pp. 1–86 (2012).

Swarbrick, J. *Encyclopaedia of pharmaceutical technology*, volume 4. Informa Healthcare, USA, third edition (2007).

Sympatec. Sprayer. sympatec.com (2010).

Tan, F. L. and Shua, P. S. K. Java applet on computation of thermodynamic properties of steam and r134a refrigerant. *Computer Applications in Engineering Education*, **11**(4):211–225 (2003).

Telko, M. and Hickey, A. J. Dry powder inhaler formulation. *Respir Care*, **50**(9):1209–1227 (2005).

Terzano, C. Metered dose inhalers and spacer devices. *European Review for Medical and Pharmacological Sciences*, **3**:159–169 (1999).

Tiddens, H. Matching the device to the patient. *Pediatric Pulmonology*, **37**(Suppl. 26):26–29 (2004).

Tillner-Roth, R. and Baehr, H. D. An international standard formulation for the thermodynamic properties of 1,1,1,2-tetrafluoroethane (HFC-134a) for temperatures from 170k to 455k and pressure up to 70mpa. *Journal of Physical and Chemical Reference Data*, **23**(5):657–729 (1994).

Tiwari, D., Goldman, D., Malick, W. and Madan, P. Formulation and evaluation of albuterol metered dose inhalers containing tetrafluoroethane (p134a), a non-cfc propellant anon-cfcpropellant. *Pharmaceutical Development and Technology*, **3**:163–174 (1998).

Tobin, M. J., Chadha, T. S., Jenouri, G., Birch, S. J., Gazeroglu, H. B. and Sackner, M. A. Breathing patterns. *Chest*, **84**(2):202–205 (1983).

Toogood, J. H. Side effects of inhaled corticosteroids. *The Journal of Allergy and Clinical Immunology*, **102**(5):705–713 (1998).

Usmani, O. S., Biddiscombe, M. F., Nightingale, J. A., Underwood, S. R. and Barnes, P. J. Effects of bronchodilator particle size in asthmatic patients using monodisperse aerosols. *Journal of Applied Physiology*, **95**:2106–2112 (2003).

Vacek, V. and Vins, V. Two-phase flow analyses during throttling processes. *International Journal of Thermophysics*, **30**:1179–1196 (2009).

Versteeg, H. K. and Hargrave, G. K. *Near-orifice spray and valve flow regime of a pharmaceutical pressurised metered dose inhaler* (2002).

Versteeg, H. K., Hargrave, G. K. and Kirby, M. Internal flow and near-orifice spray visualisations of a model pharmaceutical pressurised metered dose inhaler. *Journal of Physics*, **45**:207–213 (2006).

Vincken, W., Dekhuijzen, R. and Barnes, P. The ADMIT series – Issues in inhalation therapy. 4) how to choose inhaler devices for the treatment of COPD. *Primary Care Respiratory Journal*, **19**(1):10–20 (2010).

Vines, A. Calling all Malvern 2600 users! Bring your photos to ILASS Americas 2010. Technical report, Malvern, Worcestershire UK (2010).

Waechter, J. Obstructive and restrictive lung mechanics (2005).

Weibel, E. R. and Gomez, D. M. Architecture of the human lung. *Science*, **137**(3530):577–585 (1962).

Weng, W., Jaw, S., Chen, J. and Hwang, R. Optimization of particle image distortion for PIV measurements. *9th International Conference on Hydrodynamics* (2010).

Wernet, M. P. *Optical metrology for fluids, combustion and solids*. Kluwer Academic Publishers (2003).

Wigley, G., Versteeg, H. K. and Hodson, D. Near-orifice PDA measurements and atomisation mechanism of a pharmaceutical pressurised metered dose inhaler. In *ILASS-Europe 2002* (2002).

William, I. R. O. and Liu, J. Influence of formulation additives on the vapor pressure of hydrofluoroalkane propellants. *International Journal of Pharmaceutics*, **166**:99–103 (1998).

World Health Organization. Chronic obstructive pulmonary disease (COPD) (2012).

Xu, R. *Particle characterization: Light scattering methods*. Kluwer Academic Publishers, Netherlands (2001).

Yeh, Y. and Cummins, H. Localized fluid flow measurements with an HeNe laser spectrometer. *Applied Physics Letters*, **4**(10) (1964).

Yuan, G., Drost, N. A. and Mclvor, R. A. Respiratory rate and breathing pattern. *McMaster University Medical Journal*, **10**(1):23–25 (2013).

Zhang, Y., Finlay, W. H. and Matida, E. A. Particle deposition measurements and numerical simulation in a highly idealized mouth-throat. *Journal of Aerosol Science*, **35**:789–803 (2003).

Appendix

Density of air (Rogers and Mayhew, 1995)

$$\rho_a = 1.6665 \times 10^{-5} \times T^2 - 0.013864 \times T + 3.8351 \tag{A.1}$$

where T is the temperature in K.

Density of liquid HFA134a (Klea134a, 2011)

$$\rho_l = 89.838713\,u^4 + 79.877831\,u^3 + 298.02172\,u^2 + 967.57693\,u + 508 \tag{A.2}$$

where $u = \left(1 - \dfrac{T}{T_{crit}}\right)^{\frac{1}{3}}$ with $T_{crit} = 374.18\,\mathrm{K}$.

Density of vapour HFA134a (Klea134a, 2011)

$$\rho_v = -5583.8\,u^4 + 13688.75\,u^3 - 11368.8\,u^2 + 3335.18\,u - 113.501 \tag{A.3}$$

for $223\,\mathrm{K} < T < 273\,\mathrm{K}$, where $u = \left(1 - \dfrac{T}{T_{crit}}\right)^{\frac{1}{3}}$.

$$\rho_v = -2202.55\,u^4 + 5252.284\,u^3 - 3500.71\,u^2 + 84.07428\,u + 388.752 \tag{A.4}$$

for $273\,\mathrm{K} < T < 353\,\mathrm{K}$, where $u = \left(1 - \dfrac{T}{T_{crit}}\right)^{\frac{1}{3}}$.

Specific enthalpy of liquid HFA134a (Klea134a, 2011)

$$h_{lp} = -157.687\,u^4 + 261.1633\,u^3 - 753.47\,u^2 + 189.8021\,u + 249.0896 \qquad \text{(A.5)}$$

where $u = \left(1 - \frac{T}{T_{crit}}\right)^{\frac{1}{3}}$.

Specific enthalpy of vaporisation of HFA134a (Klea134a, 2011)

$$h_{lvp} = 219.1886\,u^4 - 510.952\,u^3 + 460.3925\,u^2 + 163.7313\,u \qquad \text{(A.6)}$$

where $u = \left(1 - \frac{T}{T_{crit}}\right)^{\frac{1}{3}}$.

Specific enthalpy of vapour HFA134a (Klea134a, 2011)

$$h_{vp} = 61.5016\,u^4 - 249.7887\,u^3 - 293.0775\,u^2 + 353.5334\,u + 249.0896 \qquad \text{(A.7)}$$

where $u = \left(1 - \frac{T}{T_{crit}}\right)^{\frac{1}{3}}$.

Vapour pressure of HFA134a (Tillner-Roth and Baehr, 1994)

$$P = P_{crit} \exp\left(\frac{T_{crit}}{T}(-7.686556\,v + 2.311791\,v^{\frac{3}{2}} - 2.039554\,v^2 - 3.583758\,v^4)\right) \qquad \text{(A.8)}$$

for $180\,\mathrm{K} < T < 374.15\,\mathrm{K}$, where $v = 1 - \frac{T}{T_{crit}}$ and $P_{crit} = 4.056\,29 \times 10^6\,\mathrm{Pa}$

Specific heat capacity of the gas phase of HFA134a at constant pressure (Dunbar, 1996)

$$C_{pg} = 1.7812 \times 10^{-6} \times T^3 - 2.8662 \times 10^{-3} \times T^2 + 3.005 \times T + 143.897 \qquad \text{(A.9)}$$

for $223\,\mathrm{K} < T < 353\,\mathrm{K}$.